Master thesis

Joining techniques for internal bonding of components into carbon fibre-reinforced polymer structures with limited access.

Thom van der Starre

Delft University of Technology, Hall Spars



TU Delft

Master thesis

by

Thom van der Starre

Student number: 4586158
Graduation date: 27 March 2023
Chair Holder: Dr. ir. M. J. M. Hermans
Committee members: Dr. ir. M. J. M. Hermans
Prof. CA Dransfeld
Dr. S. Kumar

Instructor: Prof. CA Dransfeld, Dr. S. Kumar, D. Morris, T. Gielleit.
Faculty: 3mE, Mechanical, Maritime and Materials Engineering

TU Delft

Preface

This report shows the final product of my master of science thesis. I would start by thanking Hall Spars and Southern Spars for providing me with a challenging thesis topic and my supervisors from these companies, Dale Morris and Thijs Geilliet, for their trust and support throughout the project.

In particular, I would like to thank Clemens Dransfeld, my daily supervisor, for making me feel welcome since I started this thesis. And creating a healthy work environment, giving me enthusiastic support and giving me the guidance I needed. His feedback and expertise where were extremely valuable during this research. Lastly, I am grateful to my supervisor Sid Kumar for his trust and support throughout my project.

In this master's thesis, I tried to apply all the knowledge I gained throughout my Bachelor's in mechanical engineering and Master's in Material Science. I tried to combine this to gain insight into joining composites in the mast building industry. This research involved a wide range of tasks: performing mechanical, optical and thermal measurements, manufacturing composite samples and applying knowledge of coding in python. Due to corona, I missed a lot of hands-on experience. Therefore, I would like to entire staff of the DASML lab for helping and guiding me to create this experience to perform my experiments successfully.

I conducted this research at Aerospace faculty in the Structures department. I want to thank everyone in this group for their daily support and welcoming me. Especially Camill, Sian, Charlotte, Anup, Buse, Alberto, Idriss and Linde (thanks for all the coffee breaks). I also want to thank my friends and parents for listening to my endless stories about composites and supporting me.

Overall, I am pleased with the end result of this study. I hope my research will be valuable in the field of joining composite materials.

Thom van der Starre
Delft, March 2023

Abstract

Hall spars, a leading innovator in the composite mast-building industry with a long history of successful projects, provided a challenge which is the inspiration of this thesis. This thesis aims to contribute to the challenge: Joining techniques for the internal bonding of carbon fibre-reinforced polymer components into carbon fibre-reinforced polymer structures. ”Internal bonding” can also be called ”bonding with limited access”. This requires a deep understanding of the problem, materials and joining techniques. Due to confidentiality, the exact joining location will not be explained in this version. The exact material and material datasheets will not be mentioned in this version of the thesis.

Currently, the epoxy adhesive film is used for these types of joints. Adhesive co-bonding raises challenges due to the limited access to the mast. Challenges concerning surface preparation, low mechanical strength, reliability and labour intensity. Other techniques will be reviewed for the internally bonding limited access hollow tubes. The aim is that no new tooling is required, and the currently used materials and process parameters can be used. The thermoset resin used is an epoxy carbon fibre prepreg.
According to the literature study, potential joining techniques for this application are joining with partially cured thermosets and joining with fusion welding of thermoset composites. Differential scanning calorimetry measurements are performed to analyse the thermoset resin. Material characterisation is required to apply the joining methods with the currently used material and process parameters of Hall Spars. Process parameters for the curing model, and glass transition temperature model are derived. Using this material model allows creating the insight that partial cured joining with the thermoset resin of Hall Spars is not feasible. The structural integrity of the joined parts can not be guaranteed in the curing cycle.
Polyetherimide is used as thermoplastic material to apply the fusion welding technique on the thermoset. This thermoplastic film is co-cured with the thermoset and used as a coupling layer to join the two thermoset parts. Performing an interphase analysis with the scanning electron microscope indicates interphase formation at the PEI/epoxy interface. The higher the isothermal curing temperature, the thicker this interphase. Gelation causes the interphase formation to slow down.
The interphase formation at the interface is not been observed as expected based on the literature review. This required a test if the interphase formation would have occurred at a smaller scale than the scanning electron microscopy could observe. This can be achieved by performing single-lap shear experiments. These joints are processed according to Hall Spars process parameters. Joints created with the fusion coupling technique with the PEI film show promising results. However, due to high void content, a lower ultimate lap shear strength is observed. Therefore it is advised to investigate a curing cycle with a second dwell phase. This changes the viscosity profile of the resin. Therefore allows the trapped air at the PEI/epoxy interface to leave the joint. This could potentially lead to more reliable joints.

Contents

Preface i

Summary ii

1 Introduction 1

2 Literature review 2
2.1 Background of the mast . . . 2
2.2 Material aspects . . . 3
2.3 Secondary joining . . . 5
2.4 Surface preparation . . . 6
2.5 Current technique . . . 7
2.6 B-staging joining of thermoset composites . . . 7
2.6.1 Cure characteristics . . . 8
2.6.2 Mechanical performance of the joint . . . 12
2.7 Fusion bonding of thermoset composites . . . 15
2.7.1 Interdiffusion thermoset and thermoplastic . . . 15
2.7.2 Fusion welding process . . . 18
2.7.3 Mechanical performance characteristics . . . 19
2.7.4 Thermal degradation . . . 20
2.8 Industrialization . . . 21
2.8.1 B-staging joining of thermoset composites . . . 21
2.8.2 Fusion bonding of thermoset composites . . . 22
2.8.3 Comparison of the joining methods . . . 23
2.9 Conclusion . . . 24

3 Research framework 25
3.1 Research gaps and objectives . . . 25
3.2 Framework . . . 26
3.3 Research questions . . . 27
3.4 Hypothesis . . . 27

4 Resin characterisation 28
4.1 Methodology . . . 28
4.2 Sample preparation and material definition . . . 29
4.3 Measurements . . . 31
4.3.1 Temperature modulated DSC . . . 31
4.3.2 Determination of ΔH_{ult} and analysis of ramp cure at different heating rates . . . 32
4.3.3 Cure kinetic model . . . 34
4.3.4 Avrami analysis . . . 43
4.4 Results and discussion . . . 44
4.4.1 Di Benedetto . . . 45
4.4.2 Model maximum degree of cure . . . 45
4.4.3 Curing model . . . 46
4.4.4 Avrami Analysis . . . 50
4.4.5 Gel point . . . 51
4.5 Concluding remarks . . . 53

5 Interphase analysis 54
5.1 Methodology . . . 54
5.2 Sample preparation and material definitions . . . 54
5.3 Results and discussion . . . 58

5.3.1 Laser confocal microscopy of cross sections . . . 62
5.3.2 Scanning electron microscopy of cross sections . . . 62
5.4 Concluding remarks . . . 66

6 Mechanical strength 68
6.1 Methodology . . . 68
6.2 Sample preparation and material definition . . . 69
6.3 Measurements . . . 75
6.4 Results and discussion . . . 78
6.4.1 Fracture surface . . . 78
6.4.2 Shear strength . . . 85
6.5 Concluding remarks . . . 89

7 Applicability from lab scale to industrial scale 91
7.1 Free standing patch . . . 91
7.2 Capillary flow . . . 93
7.2.1 Results from new designs to avoid capillary flow. . . . 93

8 Conclusions and recommendations 94
8.1 Conclusions . . . 94
8.2 Recommendations . . . 95

A Appendix: Literature study, curing history impact on material parameters, partially cured resin 102

B Appendix: Literature study, fusion welding methods 104

C Appendix: Literature study, results measurements 106
C.1 Results TMDSC . . . 107
C.2 Results dynamic DSC . . . 108
C.3 Isothermal DSC . . . 109
C.4 Second measurement, dynamic DSC . . . 109
C.5 Results derivation Kamal model parameters, graphical analytical method . . . 110
C.6 Results derivation Kamal model parameters, curve fit method . . . 114
C.7 Gelpoint for dynamic heating rates . . . 114
C.8 Thickness of PEI film measured with the SEM . . . 115
C.9 ABD matrix . . . 116

D Appendix: Literature study, grinding and polishing 117

E Appendix: Literature study, glass transition temperature co-curing, partially cured samples 118

F Appendix: Literature study, dimensions lap shear joints 120

G Appendix: Literature study, python codes 122
G.1 Dynamic DSC measurements . . . 122
G.2 Isothermal measurements . . . 127
G.3 DiBenedetto python code . . . 137
G.4 Second DSC measurement, dynamic . . . 137
G.5 Bailleul model . . . 140
G.6 Kamal model graphical -analytical . . . 146
G.7 Gel point . . . 146

List of Figures

2.1 Illustration of shrouds, spreaders and stays. [1] . . . 2
2.2 The resin and fibres forming a composite[2] . . . 3
2.3 Joining of thermoplastic polymers. Heat and pressure are being applied, which causes the chain mobility to increase. The interface disappears, and chains entangle. . . . 3
2.4 Co-curing, heat and pressure is are applied. Cross-links form between the two parts. . . . 4
2.5 Adhesive co-bonding. The adhesive layer is shown in green, light green before, and dark green after curing. . . . 4
2.6 Thermoset joining, one part is uncured, and the other is partially cured. After the heat and pressure, both parts are cross-linked . . . 5
2.7 Fusion bonding of thermoset composites: First step, joining a thermoplastic film with a thermoset. The thermoplastic chains diffuse into the thermoset. Meanwhile, the thermoset cures by the applied heat and pressure. . . . 5
2.8 Fusion bonding of thermoset composites: Second step, both parts are welded together via the chain entanglement of the thermoplastic layer. . . . 5
2.9 Two numerical solutions . . . 6
2.10 Contaminated surface after removal of the peel ply. Contaminations are marked in green [3] . 7
2.11 Two numerical solutions . . . 8
2.12 Systematic overview approach modelling b-staging. DOC: degree of cure, DSC: Differential scanning calorimetry, MDSC: Temperature modulated DSC, Tg: Glass transition temperature. For other definitions see the nomenclature [4],[5] . . . 9
2.14 Correlation between degree of cure and glass transition temperature, measurements are obtained with a DSC, and T_g model is the DiBenedetto model. An increase in the degree of cure results in an increase in Glass transition temperature. [5] . . . 10
2.15 CCT diagram to illustrate isothermal and dynamical cure, note DOC means the degree of cure and p represents α. [6] . . . 11
2.16 Illustration of two types of parts which will be B-staged and co-cured together [4] . . . 12
2.17 Left the normalized interlaminar shear strength, at the right normalized interlaminar fracture toughness energy,G_{ic}. In C1, stack A is uncured, and the degree of cure increases up to a fully cured C5. [7] . . . 13
2.18 Cross-sectional image of the interface between a partially and fully cured laminate after the final curing step. The cure rate of the partially cured part in the left image is 60%, and a homogeneous interface region is visible. At the right image, the rate of cure is 70%, and a ripple-like non-homogeneous interface region is visible [8] . . . 14
2.19 Fracture surface for different types of curing combinations [9] . . . 14
2.20 Physical state dependent on the degree of cure and temperature [10] . . . 14
2.21 Typical where thermoset prepreg is co-cured with a thermoplastic film [11] . . . 15
2.22 The schematic formation of a semi-interpenetrating network (IPN) where network A is a thermoset polymeric system and network B is a thermoplastic polymeric system [12]. . . . 16
2.23 At the left pure epoxy, the right, pure thermoplastic (PEI). Epoxy-rich particles in PEI-rich matrix. Epoxy particles are reducing in size towards pure thermoplastic region [12] . . . 17
2.24 Upper critical solution temperature and lower critical solution temperature shown in a phase diagram. [13] . . . 17
2.25 Phase diagram of epoxy/PES mixture [14] . . . 18
2.26 Classification of fusion techniques [15] . . . 19
2.27 Comparison between thermoset fusion welded joints (blue) and adhesive co-bonded joints (green) at various temperatures [11] . . . 20
2.28 Micrographs of a thermoset composite fusion bond. Left thermal degradation is present, in the right graph a good weld is shown without thermal degradation [16] . . . 20

2.29 Long-term stability for different partially cured parts. Note that the T_g is directly proportional to the degree of cure. Storage is at room temperature [6] . . . 22
2.30 left: Schematic representation of the resistance welding setup. [17]. Right: a: before joining, b: thermoplastic film softens due to heat, c:the soft thermoplastic material fuses into the mesh. This is due to the applied pressure. Mesh stays in the joint [18] . . . 23
2.31 Two heating mechanisms. [19] . . . 23

3.1 Frame work illustrated in a sketch. . . . 26

4.1 A typical result of temperature modulated DSC measurements analysed with the TRIOS software. Glass transition is determined with the reversing, and the exothermic heat flow is determined with the non-reversing heat flow. The start of the exothermic peak is close to the glass transition temperature. . . . 32
4.2 Measurements temperature modulated DSC. The glass transition temperature and the measured degree of cure are reported for the samples. . . . 32
4.3 Normalized heat flow. This sample is heated with 5 °C /min. The blue-shaded area between the curve and baseline is the normalized heat of the reaction. . . . 33
4.4 Dynamical measurements, the average and standard deviation for each heating rate. The higher the heating rate, the shorter the curing time and the higher the peak of the heat flow. The blue arrow shows this trend. . . . 33
4.5 Dynamical measurements, evolution degree of cure over time, the average and standard deviation for each heating rate. The higher the heating rate, the sooner the heating occurs. The blue arrow shows this trend. . . . 34
4.6 Normalized heat flow. Isothermal measurement at 105 °C. The blue-shaded area between the curve and baseline is the normalized heat of the reaction. . . . 35
4.7 Results of isothermal curing at 105,115,125 and 135 °C. For each temperature, four samples are made and measured. The mean heat flow at each isothermal heat flow is shown. The blue arrow indicates the trend. The higher the isothermal curing temperature, the higher the heat flow peak and the shorter the curing time. . . . 35
4.8 Evolution of the degree of cure over time. The mean of each isothermal temperature is shown. The blue arrow indicates the trend. The higher the isothermal curing temperature, the sooner the reaction occurs and the higher the final degree of cure. . . . 36
4.9 Normalized residual heat of a sample initially isothermal cured at 105 °C. The area determines the heat in between the curve and the baseline. . . . 37
4.10 Linear slope to characterise parameters for K(T). Equation 4.15 fitted through the measurement points. . . . 38
4.11 The polynomial term for each isothermal curing temperature as a function of the degree of cure 39
4.12 Derived polynomial term in python based on the measured data points at each degree of cure 39
4.13 The intercept of the reaction rate with the y-axis for each curing temperature results in K_1, indicated with the dots. . . . 40
4.14 Temperature dependency of the parameters n&m, parameters of graphical-analytical and curve fitting method are displayed . . . 42
4.15 Temperature dependency of the parameters n&m, parameters of graphical-analytical and curve fitting method are displayed . . . 43
4.16 Avrami plot of the curing data for the isothermal curing temperatures 105,115,125 and 134 °C. 44
4.17 Result DiBenedetto model, lambda parameter is determined based on the least square method with the measurement points in the MTDSC. The model shows a good fit with the measurement points. . . . 45
4.18 Result model for the maximum degree of cure, mu parameter is determined based on the least square method with the experimental data from isothermal curing. The mean of each T_c is used. 46
4.19 Result of the Bailleul model compared with experimental data at isothermal curing temperatures. The shaded area indicates the standard deviation of the experimental data. . . . 46
4.20 Result of the Bailleul model compared with experimental data at dynamical curing rates. The shaded area indicates the standard deviation of the experimental data. . . . 47
4.21 Zoomed-in representation of the unexpected behaviour with dynamical heating rates. The area of interest is marked in red. . . . 47

4.22 The vertical line represents α_{max} for 135 degrees. The function increases above this α. 48
4.23 Result of the Kamal model using the curve fitting method compared with experimental data at isothermal curing temperatures. The shaded area indicates the standard deviation. 48
4.24 Result of the Kamal model compared with experimental data at dynamical curing rates. The shaded area indicates the standard deviation of the experimental data. The curve fitting method is used to derive parameters Kamal model 49
4.25 Result of the Kamal model using the curve fitting method compared with experimental data at isothermal curing temperatures. The shaded area indicates the standard deviation. 49
4.26 Result of the Kamal model compared with experimental data at dynamical curing rates. The shaded area indicates the standard deviation of the experimental data. The graphical-analytical method is used to derive parameters Kamal model 50
4.27 The avrami plot of the experimental curing data for the isothermal curing temperatures 105,115,125 and 135 °C. Two straight lines are fitted for each curing temperature 50
4.28 The isothermal curing temperatures 105,115,125 and 135 °C. The transition points are indicated. After these points, the curing rate decreases significantly due to the change from a chemical to a diffusion-controlled reaction. 51
4.29 The red line is the data based on the data sheets. The gel time is plotted over the inverse of the isothermal curing temperature. The gel times according to the curing model are compared via the R2 method to find the actual gel point. 51
4.30 Viscosity profile for dynamic heating rates according to the datasheet (not available in this version). The yellow marked area shows the zone where the viscosity increases significantly. This indicates the gel point. 52
4.31 Curing behaviour for dynamic heating rate 1 °C, according to python script. The temperature at gelation is marked with a black cross, degree of cure at gelation is marked with a blue cross. 52

5.1 Molecule structure polyetherimide. [20] 55
5.2 Schematic build up parts for autoclave. PEI film was placed on top of the prepregs. Including legend. 55
5.3 Autoclave setup 56
5.4 Schematic build-up parts for the hot press including the legend. 56
5.5 Hot press setup 57
5.6 The four autoclave curing cycles. First, dwell at 105,115,125 or 135 °C, second at 135 °C. The cycle with the first dwell at 135 °C has no second dwell. 57
5.7 The two hotpress curing cycles. First, dwell at 135 and 149 °C. Instant heating, so no heating ramp. 58
5.8 The cure kinetic model, in combination with the datasheet, is used to estimate the gel points. Gel points for the samples are indicated with the cross. 59
5.9 The curing process with the unintended capillary flow. Process displayed in four steps. Steps 2 and 3 happen simultaneously. However, for clarification, these are split up into two figures. . 60
5.10 Diffusion towards the PEI film. Comparison of the travelled path for epoxy particles around the fibres and epoxy particles through the bulk resin. 61
5.11 Cros-section view of the epoxy/PEI interface, laser + optical microscope used with 50x zoom. CF/EP: carbon fibre epoxy, PEI: PEI film, EP: bulk epoxy, Embedding resin embeds the samples. The difference before and after NMP treatment is visible in the PEI film. 61
5.12 Samples cured in the autoclave, 50x magnification is used to create the images. The red box indicates the interface between the PEI and the bulk epoxy. A dark wavy pattern is visible. The orange boxes indicate the carbon fibre /PEI interface. A straight interface is visible. No difference between the samples is visible in the laser confocal microscope. 62
5.13 Cross-sectional 63
5.14 Bulk epoxy - PEI interphase, SEM images Interphase between PEI and bulk epoxy is indicated with the orange box. The higher the curing temperature of the first dwell, the less straight (wavier) the interphase is. Indicating higher activity at the interphase during co-curing. 64
5.15 SEM figures from the samples cured with the hot press at (1) 135 °C and (2) 149 °C. 65
5.16 Diffusion length in microns 66

6.1 Schematic figure, ultimate strength is the top of the curve 68

6.2 250 kN Zwick tensile testing machine in the DASML lab . . . 69
6.3 Dimensions lap shear joint according to the D5868 standard [21] . . . 70
6.4 Support parts supporting the sample during curing. The black lines are the part, (cured carbon fibre epoxy prepreg) and in the blue, the support samples are indicated. . . . 70
6.5 Schematic illustration of the layup . . . 70
6.6 Benchmark sample, parts joined with epoxy adhesive film . . . 71
6.7 Partially cured sample . . . 71
6.8 PEI film as adhesive coupling layer . . . 71
6.9 Illustration of two types of parts which will be B-staged and co-cured together [4] . . . 71
6.10 Build up bottom part, configuration with adhesive film, including the legend. . . . 72
6.11 Build up bottom part, configuration with partial cure, including the legend. . . . 72
6.12 Build up bottom part, configuration with PEI film, including the legend. . . . 73
6.13 Build up bottom part, configuration with PEI film and interlayer, including the legend. . . . 73
6.14 Curing temperature, calculated degree of cure and calculated glass transition temperature. . . . 73
6.15 Curing temperature, calculated degree of cure and calculated glass transition temperature. Cure cycle for the partially cured sample with DOC of 0.7. . . . 74
6.16 Curing temperature, calculated degree of cure and calculated glass transition temperature. Cure cycle for the partially cured sample with DOC of 0.5. . . . 74
6.17 Build up the top part, configuration with adhesive film, including the legend. . . . 74
6.18 Build up the top part, configuration with partial cure, including the legend. . . . 75
6.19 Build up the top part, configuration with PEI film, including the legend. . . . 75
6.20 Build up the top part, configuration with PEI film and PEI interlayer, including the legend. . . . 75
6.21 The results of the lap shear tests. The shear stress is displayed over the strain. Each colour indicates a sample. The ultimate shear stress of each sample is indicated with the cross. The results of the lap shear tests. The shear stress is displayed over the strain. Each colour indicates a sample. The ultimate shear stress of each sample is indicated with the cross. . . . 77
6.22 Measured ultimate lap shear strength of each configuration. Data is represented in a box chart. This data will be discussed in section 6.4 . . . 78
6.23 Acceptable and unacceptable failure modes [21] . . . 79
6.24 Top view fracture surface. Fracture surface in red . . . 79
6.25 Height image of the fracture surface of the adhesive joint with epoxy film adhesive. The failure mode is the cohesive failure of the adhesive. . . . 80
6.26 Height image of the fracture surface of the joint with the partially cured bottom part after the first curing cycle. DOC=0.5. . . . 81
6.27 Height image of the fracture surface of the joint with the partially cured bottom part after the first curing cycle. DOC=0.7. . . . 81
6.28 C-scan cross-sectional samples which are joined. The bottom part was partially cured. The interface is indicated with red lines. . . . 82
6.29 Height image of the fracture surface of the joint with 60 microns PEI film as coupling. . . . 82
6.30 Height image of the fracture surface of the joint with 60 microns PEI film as coupling and 60 microns of PEI between each ply. . . . 83
6.31 Height image of the fracture surface of the joint with 120 microns PEI film as coupling and 60 microns of PEI between each ply. This is the image of the positive outlier. No voids are spotted, which indicates adhesive failure of the PEI and epoxy. . . . 83
6.32 Height image of the fracture surface of the joint with 120 microns PEI film as coupling and 60 microns of PEI between each ply. This is the image of the sample with voids, which indicates adhesion failure of the PEI and epoxy. . . . 84
6.33 Two figures show the voids formed between the PEI and CF/EP interface. (1) a laser confocal microscopiy figure. (2) a picture was taken in the lab with an iPhone. . . . 85
6.34 Stress strain curves. A brittle material has little to no strain in the plastic regime. A ductile material has a lot of strain in the plastic regime. . . . 86
6.35 Stepwise change in the stress-strain curve, indicated with the black arrows. . . . 86
6.36 (1) Unloaded single lap shear joint. Loading the single lap shear joint (2) causes the adherends and, therefore, the adhesive to strain. Resulting in the shear stress profile shown in (2) . . . 87
6.37 The redistribution of the shear stress of a ductile joint. This occurs in the plastic regime, after reaching the Yield point. In blue indicated the ultimate shear stress and in red the shear stress. 87

6.38 This sample is not debulked. This results in adhesive failure as the main failure mode. Additionally, some ply delaminations are visible. . . . 89
6.39 Lap shear strength of not debulked samples with a 60 micron PEI film a 60 microns PEI interlayer. . . . 89
6.40 Bending moment due to sample asymmetry can cause peel stresses in the joint. . . . 89

7.1 Simplified illustration, the Glass transition temperature is ”being pushed up” by the curing temperature. This is in the co-curing cycle. In the first cycle, the part is cured to the degree of cure 'Y'. . . . 92
7.2 Cure kinetic model simulates the two curing cycles. The first is the b-stage cycle (in green); the degree of cure after this cycle is 0.5. And the second cycle after assembly is the co-cure cycle (in blue). (1) shows the scenario where the curing temperature remains below the glass transition temperature, (2) shows the opposite scenario. . . . 92
7.3 The PEI film is directly positioned onto the mould in this method. It is presupposed that no resin flow will occur between the PEI film and the mould . . . 93
7.4 No epoxy resin flowed on top of the PEI film. The PEI film is free of epoxy resin. No capillary flow occurred during curing, causing the PEI interface to be free and ready to be used for a joint. 93

8.1 A comparison of the currently used and advised type of curing cycle for PEI/epoxy joining. The difference is the added dwell phase for the advised curing cycle. Resulting in a different viscosity profile. . . . 95

A.1 Left: Relationship between curing degree and density, right: the relationship between curing degree and modulus [10] . . . 102

C.1 Results temperature modulated DSC measurements. . . . 107
C.2 Results the heating rates 1,2.5,5 and 10 °C / minute . . . 108
C.3 Isothermal measurements at 105,115,125 and 135 °C . . . 109
C.4 Normalized residual heat of all the samples sample initially isothermally. The area determines the heat in between the curve and the baseline with the python code. . . . 110
C.5 Graphic representations of Equation 4.19,Equation 4.23 and Equation 4.24 for the isothermal DSC results obtained at 105°C. Slope is represented by the red dotted line. . . . 110
C.6 Graphic representations of Equation 4.19,Equation 4.23 and Equation 4.24 for the isothermal DSC results obtained at 115°C. Slope is represented by the red dotted line. . . . 111
C.7 Graphic representations of Equation 4.19,Equation 4.23 and Equation 4.24 for the isothermal DSC results obtained at 125°C. Slope is represented by the red dotted line . . . 111
C.8 Graphic representations of Equation 4.19,Equation 4.23 and Equation 4.24 for the isothermal DSC results obtained at 135°C. Slope is represented by the red dotted line. . . . 112
C.9 Result of the parameters n and m after each iteration for curing temperature = 105 °C . . . 112
C.10 Result of the parameters n and m after each iteration for curing temperature = 115 °C . . . 113
C.11 Result of the parameters n and m after each iteration for curing temperature = 125 °C . . . 113
C.12 Result of the parameters n and m after each iteration for curing temperature = 135 °C . . . 113
C.13 Isothermal measurements at 105,115,125 and 135 °C, with the curve fits for the Kamal model . 114
C.14 Viscosity profile for dynamic heating rate 2 °C, according to python script. The curing temperature at the gel point is: 118 °C. . . . 114
C.15 Viscosity profile for dynamic heating rate 3 °C, according to python script. The curing temperature at the gel point is:123 °C. . . . 115
C.16 Thickness of PEI film measured with the SEM for a sample cured at 105 °C. . . . 115

E.1 Cure kinetic model simulates the two curing cycles. The first is the b-stage cycle (in green); the degree of cure after this cycle is 0.3. And the second cycle after assembly is the co-cure cycle (in blue). (1) shows the scenario where the curing temperature remains below the glass transition temperature, (2) shows the opposite scenario. . . . 118
E.2 Cure kinetic model simulates the two curing cycles. The first is the b-stage cycle (in green); the degree of cure after this cycle is 0.7. And the second cycle after assembly is the co-cure cycle (in blue). (1) shows the scenario where the curing temperature remains below the glass transition temperature, (2) shows the opposite scenario. . . . 118

E.3 Cure kinetic model simulates the two curing cycles. The first is the b-stage cycle (in green); the degree of cure after this cycle is 0.9. And the second cycle after assembly is the co-cure cycle (in blue). (1) shows the scenario where the curing temperature remains below the glass transition temperature, (2) shows the opposite scenario. 119

List of Tables

2.1 Joining steps of a partially cured thermoset with an uncured thermoset composite, illustrated in Figure 2.13 [22] . . . 8
2.2 Guidelines for the homogeneous degree of cure of a part [6] . . . 21
2.3 Comparative table of the joining methods . . . 24

4.1 Reaction enthalpy, mean and standard deviation . . . 33
4.2 Maximum degree of cure at each isothermal temperature, reaction enthalpy and residual reaction heat. Average and standard deviation. . . . 37
4.3 Parameters kamal model obtained with the graphical-analytical from isothermal cure performed with DSC. . . . 41
4.4 Parameters kamal model obtained with curve fitting from isothermal cure performed with DSC. 42
4.5 Values for linear relationships n and m with the curing temperature, temperature in Kelvin. . . . 42
4.6 Values for linear relationships n and m with the curing temperature [K] . . . 43
4.7 Parameters derived in section 4.3 . . . 44
4.8 R^2 of the Bailleul model for the measured isothermal curing temperatures and different heating rates. . . . 47
4.9 R^2 of the Kamal model with the curve fitting method . . . 49
4.10 R^2 of the Kamal model with the graphical-analytical method . . . 50

5.1 Properties of polyetherimide [20] . . . 55
5.2 Comparative tables of the results of the interphase analysis in this section. . . . 66

B.1 Bulk heating . . . 104
B.2 Two-stage techniques . . . 104
B.3 Frictional heating . . . 105
B.4 Electromagnetic heating . . . 105

C.1 Residual heat flow, maximum degree of cure and reaction enthalpy of the samples . . . 109

D.1 Grinding and polishing procedure. . . . 117

1

Introduction

The practice of sailing dates back to ancient civilizations, with the earliest recorded evidence of its use dating back to 3500 BC in Egypt. The design of sailing boats has evolved significantly throughout the centuries, yet one component remained the same, the mast. It is one of the most important components of a sailing boat as it keeps the sail upright, even in the most challenging weather conditions. Nowadays, sailing is a popular sport pushing athletes and engineers to their limits. World's best sailors and engineers are brought together in competitions like America's cup or sailGP to achieve the highest performance. This sets the standard for the rest of the sailing industry. This has driven engineers to incorporate composite materials into the designs. Composite materials have many advantages over conventional materials such as metals. A main driver for using composites is their strength over-weight ratio. Using composites in a design brings several challenges, particularly concerning joining composite parts. This process can be labour-intensive, increase weight, and decrease strength or reliability. Finding effective solutions to these challenges is essential to continue the advanced development in the sailing industry.
Hall spars, a leading innovator in the composite mast-building industry with a long history of successful projects, provided a challenge which is the inspiration of this thesis. For a specific type of mast, it is necessary to bond a part into the mast internally. This is challenging since masts can be tens of meters in length. This makes it difficult to access the inside of the mast to join the component. Conventional joining techniques have proved effective, and there is a desire to improve efficiency and consistency in the process. and must therefore be studied and potentially replaced to find more effective solutions. This thesis aims to contribute to the challenge: Joining techniques for the internal bonding of carbon fibre-reinforced polymer components into carbon fibre-reinforced polymer structures. "Internal bonding" can also be called "bonding with limited access". This requires a deep understanding of the problem, materials and joining techniques.

First, in chapter 2 the literature review is presented. Here, the importance of this study is explained. Based on the research gaps in this study, the research objectives and the framework are identified in chapter 3, which are translated into research questions with the hypothesis. chapter 4 describes the resin characterisation. Thermal measurements are performed, and these results are used to create the curing model. This curing model will be used throughout this study and forms the basis for the first alternative joining method, partially cured composites. The second alternative joining method in the literature is the fusion welding joining of thermoset composites. chapter 5 The interphase between the thermoplastic and thermoset film is study to test the applicability of fusion welding joining. In chapter 6, explains the mechanical testing phase of this study. chapter 7 studies the applicability from lab-scale to the mast-building industry. This research will be concluded in chapter 8. Suggestions for improvement of the current study and future perspectives on this topic will be made in the second part of chapter 8.

2

Literature review

A literature study has been performed based on the research topic given by Hall Spars. The parts which are relevant to this study are presented in this chapter. Firstly, a brief introduction to masts. Secondly, an introduction to composites and joining of composites. Followed by a description of the currently used joining method. Two alternatives to this joining method are found in the literature and described in this chapter. Lastly, this literature study will be concluded. This conclusion forms the start of this thesis.

2.1. Background of the mast

First, this section introduces the essential functions and engineering of the mast. Starting with the functions of a mast. Secondly, the manufacturing aspect is reviewed. The mast can be divided into different parts. The mast and booms are the so-called ”spars”. Together with the stays and shrouds, this forms the mast’s standing rigging; they work as truss elements, see Figure 2.1. The running rigging is the halyards and sheets. This study is focused on the standing rigging and, in particular, the mast [23]. The standing rig is referred to as the rig.

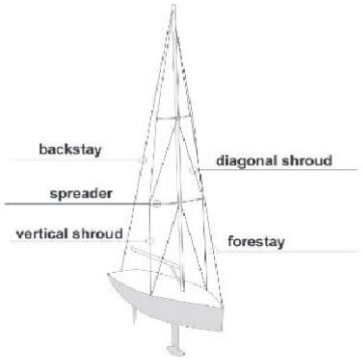


Figure 2.1: Illustration of shrouds, spreaders and stays. [1]

The sails generate the aerodynamic forces, pushing the boat forwards. Hydrodynamic forces work on the boat’s hull; the hydrodynamic and aerodynamic forces should be balanced for a boat to sail. The primary function of the mast is to support the sails; it provides a way to convert the aerodynamic forces into a force which works on the hull. The mast should have sufficient vertical stiffness to keep the sails in place; however, slight vertical bending of the mast is desired to provide the ideal shape for the sails. This shape depends on the weather conditions. Therefore, sail-makers and rig designers work closely together to optimise the stiffness of the rig for the sails. The sails are designed to have low aerodynamic resistance, so the same must apply to the shape of the mast. The cross-section of the mast should be small, and the shape should be optimised to disturb the aerodynamic flow into the sail as little as possible but still be able to offer a sufficient stiffness [24].

Besides supporting the sails, the rig should also be able to be handled by the crew. An example of this is a racing-leisure hybrid boat. The rig needs to change between a racing setup and leisure efficiently. To fulfil the functions above, a structure is needed which can do this in all weather conditions. During sailing, several types of structural loads are applied to the mast. These loads can vary significantly and over a few seconds. Peak loads can occur during a manoeuvre or be caused by human error. To make sure the structure will not fail, design guides are created, such as the DNVGL guide [25].

Due to confidentiality, the exact part and joining location method won't be described in this version of this study. However, it concerns internal joining into a structure with limited access. For more information, ask for the confidential version.

2.2. Material aspects

This chapter explains different joint configurations from a material aspect. In carbon fibre-reinforced polymers, the resin functions as a matrix for the carbon fibre. In masts, epoxy is a commonly used resin. As mentioned, a resin can be a thermoset or a thermoplastic polymer. Epoxy is a thermoset resin. In Figure 2.2, it is shown that the resin and fibres together form the composite.

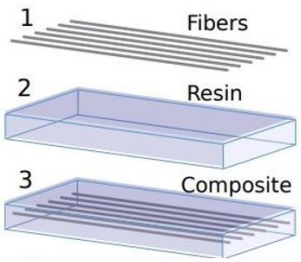
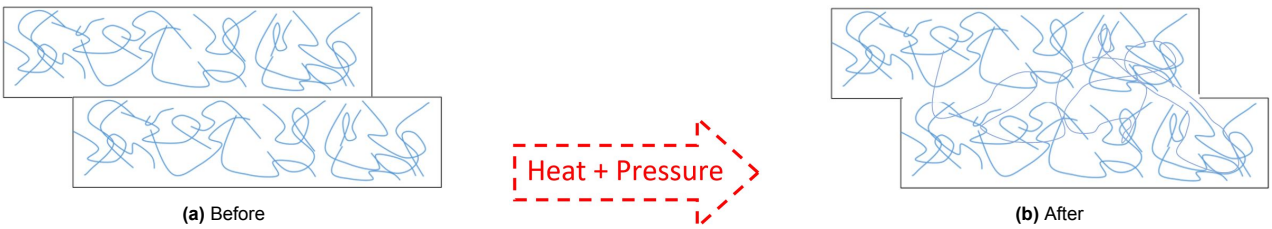


Figure 2.2: The resin and fibres forming a composite[2]

A thermoset resin consists of monomers in the uncured state. During processing, cross-links will form, and all these monomers will form an interconnected 3d network. This is an irreversible process [10]. This is not the case with thermoplastic resin. Here long polymer chains have increasing mobility when the temperature increases. From a material perspective, there are several joining configurations possible. It is essential to understand the material science behind these joints to implement them later in the manufacturing process.

Thermoplastic joining

A thermoplastic polymer exists out of long polymer chains entangled around each other in a glassy state. These polymers have a high molecular weight, meaning the chains are long. The fusion bonding process, also called joining, occurs in four steps. In the first step, heat is applied; this causes the chain mobility of the polymer to increase. Secondly, the applied pressure an intimate interface creates between the two parts. Thirdly, due to time and pressure, inter-diffusion occurs, and new entanglements are created. Lastly, the part cools down, the mobility increases, and the entanglements remain. An interface-free joint is created where reversible chain entanglements form the basis of this joint. This is visualized in Figure 2.3, chains re-entangle, and no bond line is visible [26] [27].



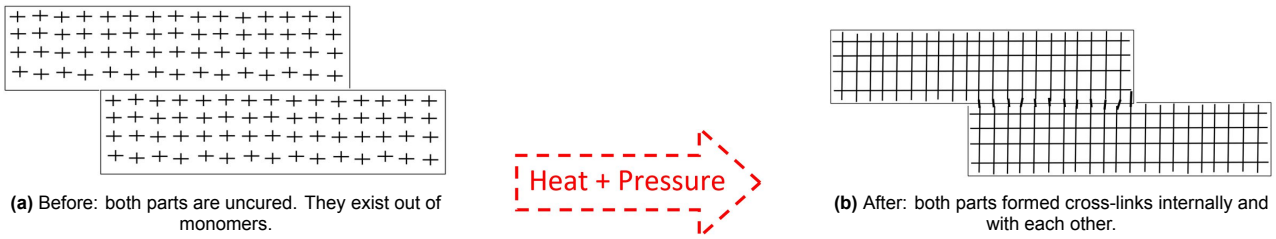
(a) Before **(b)** After

Figure 2.3: Joining of thermoplastic polymers. Heat and pressure are being applied, which causes the chain mobility to increase. The interface disappears, and chains entangle.

Thermoset joining

A thermoset polymer is built from monomers that cross-link into a polymer during curing. Thermoset bonding can be classified into different categories. The degree of cure of the adherents determines the category. The bonding method greatly influences the bonded structure's performance since the failure mode, and joint strength are influenced by the bonding method [28] [29].

In Figure 2.4 joining of two uncured thermoset parts is shown. This is also called co-curing. Both adherents are uncured, so they exist out of monomers [30]. In the curing step, heat and pressure are applied. The cross-links form between monomers and both parts cure. The joint between the parts is built up out of cross-links. This is a chemical bonding mechanism [31]. Technically co-cure joining does not form a joint. Since the cross-links cause a new complete part to form and the joint interface will disappear after curing.

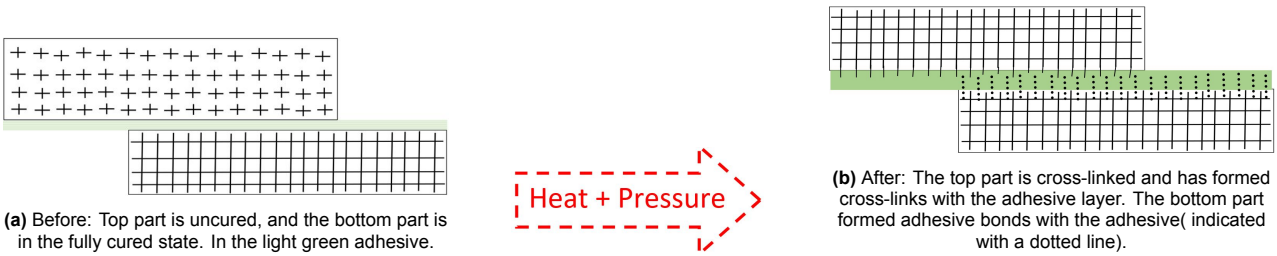


(a) Before: both parts are uncured. They exist out of monomers.

(b) After: both parts formed cross-links internally and with each other.

Figure 2.4: Co-curing, heat and pressure is are applied. Cross-links form between the two parts.

The second configuration of thermoset joining is adhesive co-bonding. This configuration is schematically shown in Figure 2.5. In this scenario, an uncured part is joined with a cured part. An adhesive layer (shown in green) increases the bond strength. The uncured part and the adhesive layer form cross-links during curing. The adhesive bond forms secondary adhesive bonds with the cured part [32]. No cross-links are formed between the green adhesive film and the cured part. Using adhesive co-bonding raises certification issues in applications such as aviation [33]. Secondary bonding is the scenario where both parts are already cured before bonding. Secondary bonds are formed with the adhesive. These are weaker than the co-curing and co-bonding configurations and will therefore not further be reviewed in this report [30].

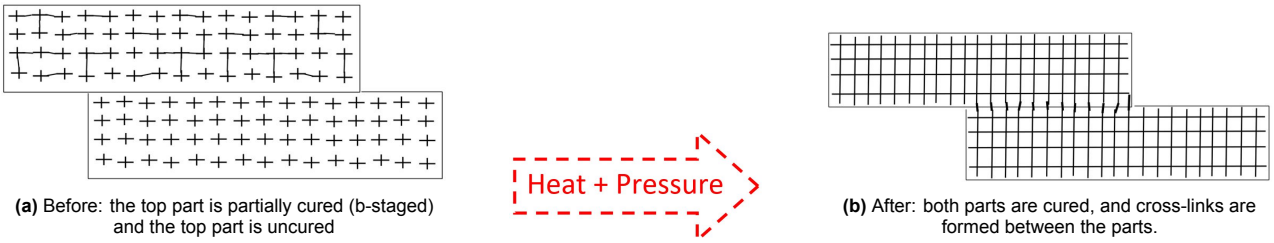


(a) Before: Top part is uncured, and the bottom part is in the fully cured state. In the light green adhesive.

(b) After: The top part is cross-linked and has formed cross-links with the adhesive layer. The bottom part formed adhesive bonds with the adhesive(indicated with a dotted line).

Figure 2.5: Adhesive co-bonding. The adhesive layer is shown in green, light green before, and dark green after curing.

In the literature, a relatively new method is described. This joining technology is a variation of the co-curing joining method. The joining mechanism of this technology is chemical-cross linking [32]. This method is called B-staging. In this new method, the curing reaction of an adherent will be slowed down. The slowing down of the reaction will occur before all the cross-links are formed. The reaction has to be slowed down by an external means, such as by cooling the part [34]. By doing this, cross-links will still be available at a later stage. In the second step, the B-staged epoxy will be cured with an uncured part, chemical cross-links will form, and the bond will form. In Figure 2.6, an illustration of a B-staged thermoset is shown. Some cross-links are formed between the monomers; however, there are still cross-links available. In this specific example, the other part is uncured. After applying heat and pressure, final cross-linking will happen, and both parts will cure. Cross-links will form between the two parts. The advantage of this method will be explained in section 2.6

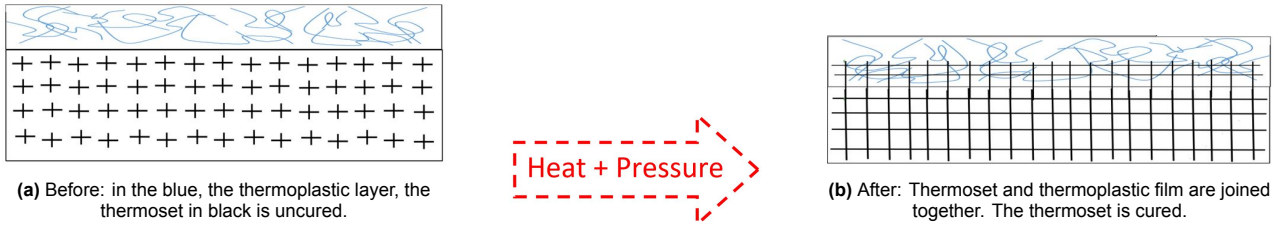


(a) Before: the top part is partially cured (b-staged) and the top part is uncured

(b) After: both parts are cured, and cross-links are formed between the parts.

Figure 2.6: Thermoset joining, one part is uncured, and the other is partially cured. After the heat and pressure, both parts are cross-linked

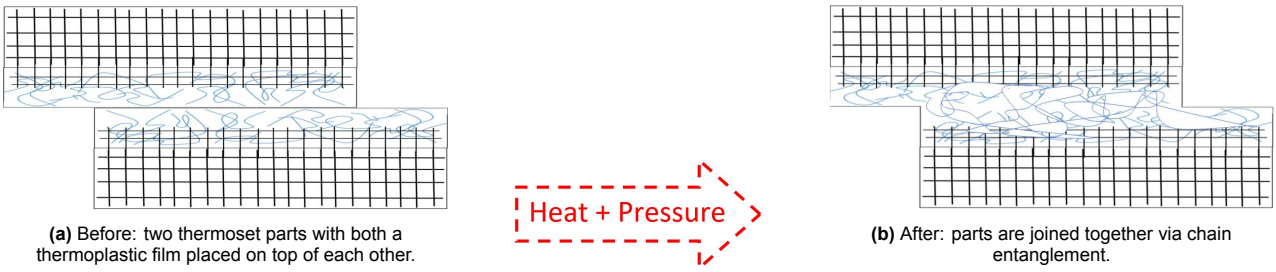
Another configuration to join thermoset parts together is using a thermoplastic coupling. This fusion bonding of thermoplastics in thermoset polymers is called the fusion bonding of thermoset composites. This is a two-step process. In Figure 2.7, the first step is shown, and a thermoplastic layer is joined with the thermoset. Initially, the thermoset is uncured. After applying heat and pressure, the thermoset cures, and the thermoplastic chains diffuse into the thermoset. At the cooling stage, the chain mobility decreases, and the chains are mechanically interlocked into the thermoset. The second joining step is shown in Figure 2.8. Both parts are placed on top of each other, with the thermoplastic films facing each other. Heat is applied, and the thermoplastic chains fuse. This welding of the thermoplastic chains occurs in the same manner described in Figure 2.3. The usage of several techniques can achieve both steps. The exact details of this process will be explained in section 2.7



(a) Before: in the blue, the thermoplastic layer, the thermoset in black is uncured.

(b) After: Thermoset and thermoplastic film are joined together. The thermoset is cured.

Figure 2.7: Fusion bonding of thermoset composites: First step, joining a thermoplastic film with a thermoset. The thermoplastic chains diffuse into the thermoset. Meanwhile, the thermoset cures by the applied heat and pressure.



(a) Before: two thermoset parts with both a thermoplastic film placed on top of each other.

(b) After: parts are joined together via chain entanglement.

Figure 2.8: Fusion bonding of thermoset composites: Second step, both parts are welded together via the chain entanglement of the thermoplastic layer.

2.3. Secondary joining

As mentioned earlier, the exact location and joining technique will not be mentioned. The following can be mentioned: The carbon fibre-reinforced polymer part needs to be placed into the hollow closed-section tube, which also can be described as a limited access hollow tube. Using this technique causes two geometrical limitations. Firstly it excludes the possibility of the part being in the same curing cycle as the mast. This causes the need for a joining method.

A significant difference between metals and CFRP is that metal is isotropic, and CFRP is anisotropic. A second big difference is the low plasticity of CFRP in comparison to higher plasticity in metals [33]. A joining method which is being used for metals is mechanical fastening. This joining method in CFRP results in stress concentration around the holes and cutouts. These stress concentrations occur due to a lack of plasticity. Around these holes, local delaminations could originate. Additionally, these mechanical fasteners will add

extra weight to the structure. Thermoplastic materials have a wide range of reliable joining technologies since the bonding surface disappears, and the pats fuse into one new part. However, fusion welding is impossible since this study will focus on using thermoset polymers. A thermoplastic is based on a reversible joint, but a thermoset exists of a non-reversible bond. Once the cross-links are formed, they can not break open again. A commonly used method to join CFRP parts is adhesive joining, which will be discussed later. A geometric limitation is limited access to the hollow structure. The inside of the structure tube can only be accessed via the bottom or the top. This complicates the surface preparation.

2.4. Surface preparation

A parameter for the bond quality and strength is surface preparation. The function of surface treatment is to remove all contaminants and to create a good surface wet-ability [1]. The surface treatments mentioned below are peel ply and sanding. These both have the role of improving mechanical locking, and chemical bonding [31]. It has been tried to treat the surface of the tubular mast with abrasives. This is been done by using sanding paper and a sander. However, due to a high workload and limited access, this method will not be considered relevant.

Peel ply

One of the few available options is a peel-ply treatment. Due to its low cost and ease of use, peel ply is widely used as a surface treatment in the composite industry [36]. The peel is attached as the outermost layer at a prepreg and removed before bonding. It functions as a protection layer against contaminations in later process steps. Once the peel ply gets removed, the matrix bonds break and leave a fractured surface behind [9], [31]. There are two types of peel ply, dry peel ply and wet peel ply. The wet peel ply forms a textured surface and creates a resin-rich layer. However, this can lead to a decrease in the bending stiffness, and after removal, there is a high risk of matrix damage [37]. Using a wet peel ply requires using a wet peel ply. The matrix must be more brittle than the matrix used in the prepreg. Dry peel ply is more prevalently used in the industry, according to [31]. The topology of the fibres or fabric determines the topology that the peel ply will leave behind [38]. A schematic overview of the usage of the peel ply is shown in Figure 2.9. In Figure 2.9a, a side view of uncured prepreg is shown. In Figure 2.9b, a peel ply is placed on top of the uncured prepreg. In Figure 2.9c, the peel ply lays on top of the cured resin. It is visible that the resin impregnates the prepreg. Once the peel ply gets removed, the increased surface area and rough topology are created. This is shown in Figure 2.9d

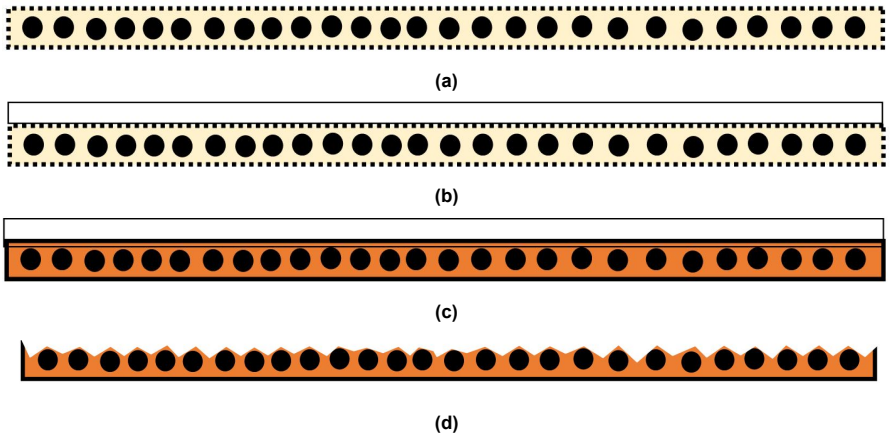


Figure 2.9: Simplified visualization of the usage of peel ply. A side view of the prepreg is shown. In a and b, the resin is uncured; in c and d, the resin is cured. In d, the increased surface area is visible. [22]

Limitation of peel ply

Dry peel plies are often coated with a release agent to ensure peel ply removal. These release agents are detected as a contaminant after removal on the laminate surface [3]. These contaminations reduce the bond

[1] Meaning: "Wettability is the ability of a liquid to maintain contact with a solid surface, and it is controlled by the balance between the intermolecular interactions of the adhesive type (liquid to the surface) and cohesive type (liquid to liquid) "[35]

strength since they facilitate crack growth. A contaminated surface is shown in Figure 2.10. Therefore it is advised to use light grid blasting after the removal of the peel ply. However, the project scope focuses on limited access joints, which do not facilitate this [39]. Therefore it is advised to use a peel ply without a release agent in a non-accessible joint. When using a non-treated peel ply, care must be taken in removal; a higher force is needed, but this can potentially damage the underlying ply surface. When working in non-accessible structures, it could be harder to work with a cure and do a surface inspection after removal.



Figure 2.10: Contaminated surface after removal of the peel ply. Contaminations are marked in green [3]

2.5. Current technique

The source of the current technique used is based on conversations with engineers of Hall Spars. A condition for implementing the new joining technique is that current tooling must be used. This is the main reason there is no investigation into designing new moulds. As mentioned earlier, there is the possibility of using adhesive co-bonding. Hall Spars currently uses this method.

Based on several meetings with the engineers who are currently working on this project at Hall Spars, it has been decided that the main focus of this study will be on the improvement of the bond performance. Adhesive co-bonding for this limited access joint brings certification, reliability and labour-intensive challenges. In this literature review, other techniques will be reviewed for the internally bonding limited access hollow tubes. These techniques must integrate into the current manufacturing method. In other words, no new tooling must be needed. The autoclave and epoxy prepreg. The part must be joined in the conventional closed-section tubular structure. The quality of potential bonding performance of these will be reviewed and compared with the currently used adhesive co-bonding. Secondly, the possibility of using this method in the industry will be considered.

2.6. B-staging joining of thermoset composites

In section 2.2, the material principle of b-staging joining of thermoset composites is explained. Using partially cured epoxy, b-staging saves potential cross-links, which can be formed later in the final curing step. This method is described well in the literature. This joining technology is a variation of the co-curing joining method.

The desired degree of cure of thermoset composites made from epoxy depends on the design requirements. Uncured epoxy will not be rigid at room temperature. If the adherent needs to be rigid at room temperature, the glass transition temperature (T_g) must be above room temperature. The T_g depends on the degree of cure, which will be explained later.

In a study by Motsch-Eichmann et al. [22], a clear overview of the manufacturing steps is given when prepregs laminate and the autoclave is used. Here a composite part is made by combining two parts, A and B. Here A is partially cured, and B is uncured. In the final curing step, both parts get joined together. However, a detailed cure characteristics study of the resin is required to achieve this joining process successfully.

Table 2.1: Joining steps of a partially cured thermoset with an uncured thermoset composite, illustrated in Figure 2.13 [22]

Step	**Production partially cured part (part A)**
1	Cleaning the mould (in the blue) and covering it with release agent (in red)
2	Placing the prepreg (dashed line), peel ply (yellow) in the mould and prepare the vacuum bag,
3	Partially cure part A according to the curing cycle, then quickly cool down and place into the refrigerator (at -17°C [22])
	Production of the composite part (A and B)
4	Cleaning the mould and covering it with release agent
5	Take partially cured part A out of the refrigerator, remove the peel ply of part A
6	Place part A in the mould and place the prepregs of part B accordingly
7	Prepare the vacuum bag(s) and run the final curing step

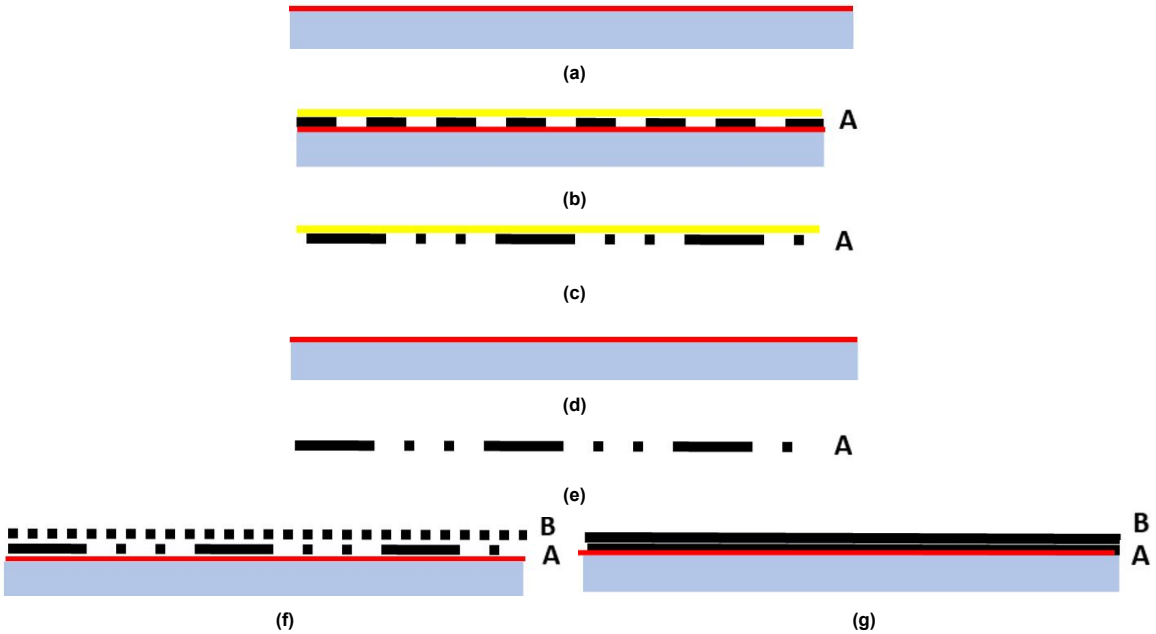


Figure 2.11: Simplified visualization of the joining process of two composite parts. A is first manufactured to the partially cured state and then joined with uncured part B. Description is given in Table 2.1 [22]

2.6.1. Cure characteristics

A successful approach is given in [4] and [5] to model the cure kinetics of the resin. This approach is simplified in a structured overview inFigure 2.12.

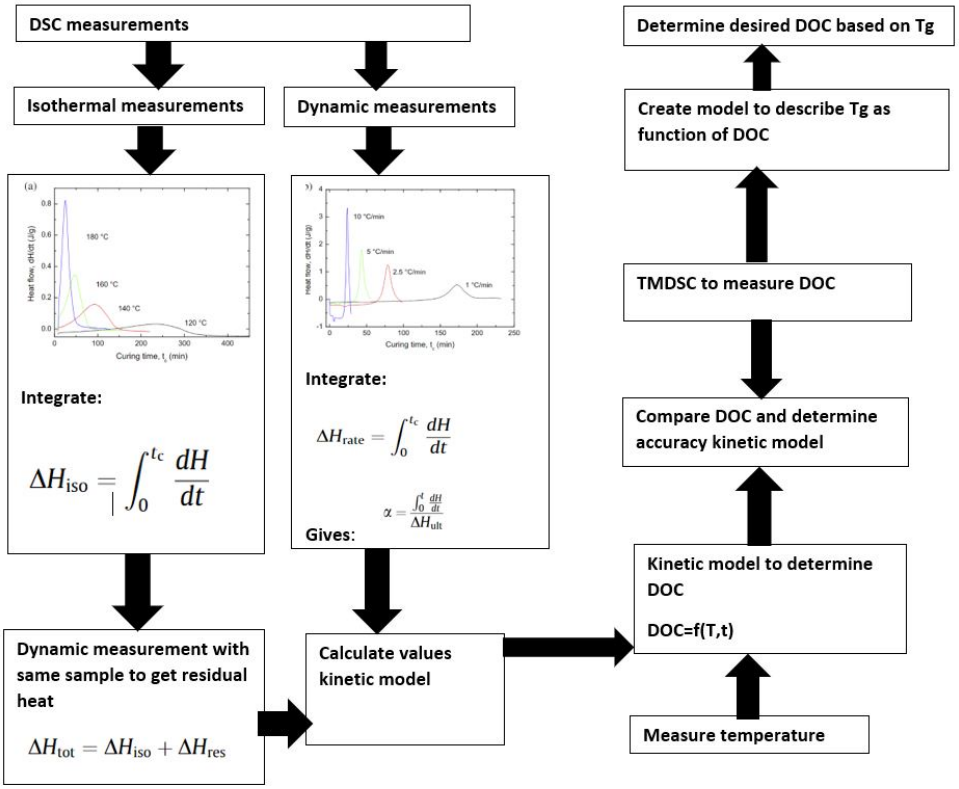
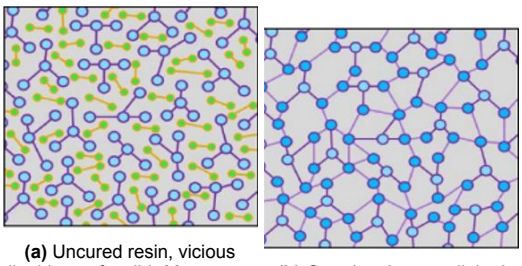


Figure 2.12: Systematic overview approach modelling b-staging. DOC: degree of cure, DSC: Differential scanning calorimetry, MDSC: Temperature modulated DSC, Tg: Glass transition temperature. For other definitions see the nomenclature [4],[5]



(a) Uncured resin, vicious liquid or soft solid. Monomers and hardener

(b) Cured resin, crosslinked polymer network

Figure 2.13: Curing of a thermoset resin [40]

Epoxy is a thermoset resin. In this thesis, the resin cures in a heat-induced irreversible reaction. Before curing, the resin exists of monomers and hardeners. In the curing reaction, covalent bonds are formed between the chains. This curing reaction is exothermic. Experimental data is gathered by performing Differential scanning calorimetry, DSC, and temperature-modulated DSC, TMDSC, measurements. With the DSC measurements and a method described in [41], the values of a kinetic model are determined. This kinetic model can be described as $\alpha = f(T, t)$. Another model describes the relationship between the convergence rate and the glass transition temperature, also $T_g = f(\alpha)$. With this model, the desired degree of cure can be determined.

Differential scanning Calorimetry

DSC is a thermal analysis technique. A small resin sample (2-3 mg) is placed in a temperature-controlled cell. A second empty cell is used as a reference. Both cells are exposed to heat. The heat flow coming out of the cells is measured. By comparing the sample cells versus the reference cell, the heat flow of the sample can be determined. This heat flow allows evaluating the material properties, which will be described in more detail in chapter 4. Dynamic DSC measurements will be used to determine the maximum heat of the reaction. In other words, how much heat will be released for a maximum degree of cure? For temperature-modulated

measurements, the temperature is varied with a sinusoidal frequency. Chemical cross-links from during the curing of a thermoset, in other words, $C = C$ links breaking open and forming a chain of $C - C$ links. This is the non-reversible portion of the reaction. However, different, reversible reactions take place as well. TMDSC can distinguish the difference. It can measure the part which belongs to a chemical reaction (loss of heat capacity, the heat consumed by the chemical reaction) and a storage heat capacity (reversible part) [42]. This temperature-modulating technique is used to determine the transitions for overlapping thermal events. The T_g is the inflexion point of the reversible heat flow versus the temperature. The exothermic peak δH_{res} of the non-reversible heat flow is used to measure the convergence rate.

DiBenedetto model

The glass transition temperature is a reversible polymer transition from the rubbery state into the glassy state. Sudden changes in viscosity, heat capacity and shear modulus can characterise this temperature. The glass transition temperature,T_g, depends on the convergence rate,α. The higher the rate of convergence, the higher the cross-linked network. This results in higher energy needed for molecular motions, translating into a higher T_g[10]. The literature studies that work with b-staging epoxies uses a model to describe this relationship. This model is called the DiBenedetto model [4], [33], [10], [5], [6]. The model is described in Equation 4.8:

$$T_g = T_{g0} + \frac{(T_{g_\infty} - T_{g0})\,\lambda\alpha}{1 - (1 - \lambda)\alpha} \tag{2.1}$$

$T_g - Glass\ transition\ temperature$
$\alpha - Rate\ of\ convergence$
$\lambda - Parameter$
$T_{g0} - T_g\ uncured\ resin$
$T_{g\infty} - T_g\ fully\ cured\ resin$

Two of these studies mention that the λ parameter will be found using the least-squares fit method with the measured data [33] [4]. In the other studies, the parameter is used according to the literature.

This model's importance is understanding which convergence rate is required to have a certain T_g. To get a strong chemical bond, a low rate of convergence is desirable. A low rate of convergence means that there are a lot of epoxy-amine groups left which still can react. These reactions result in covalent bonds, the most vital type of bond. When a part can be supported during the final curing step (for example, via the usage of vacuum bags), the T_g can be lower than the T_c. In other words, the resin can flow during this co-curing step. This resin flow will result in chemical adhesion between the bonded parts [4]. As mentioned earlier, the lower limit of the T_g is room temperature. However, if a part has to be free-standing while curing, the T_g has to be higher than the T_c. An illustration is shown in Figure 2.14. The measurements in this study are done by using a DSC. The DiBenedetto model shows the highest accuracy at a rate of convergence higher than 0.7. This is the region of interest for the application of this study according to [5].

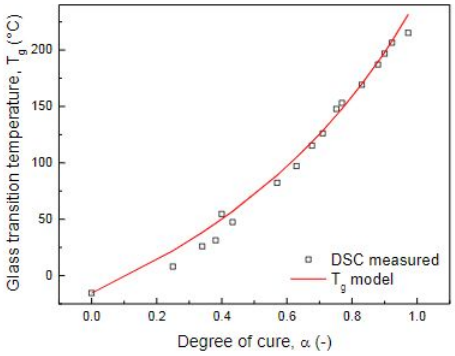


Figure 2.14: Correlation between degree of cure and glass transition temperature, measurements are obtained with a DSC, and T_g model is the DiBenedetto model. An increase in the degree of cure results in an increase in Glass transition temperature. [5]

Cure kinetic model

If the $T_c > T_g$, the resin is in the rubbery state. In this state, the reaction is chemically controlled. If the $T_c < T_g$ vitrification occurred, the reaction is diffusion controlled. This mechanism is slower than chemically controlled, and it may even cease to react [6]. An illustration is given by [6] and is shown in Figure 2.15. Low dynamical heating rates lead to vitrification, resulting in a highly controlled curing rate (due to the slower reaction mechanism). However, these low heating rates require a long period and are not practical. Another way to achieve a diffusion-controlled mechanism is by using a moderate isothermal cure temperature. This, therefore the practical way to achieve partial cure states[6].

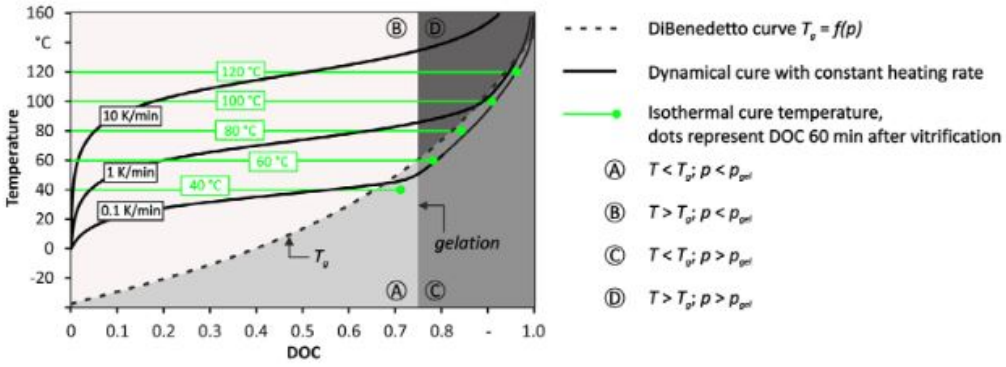


Figure 2.15: CCT diagram to illustrate isothermal and dynamical cure, note DOC means the degree of cure and p represents α. [6]

According to Mullet et al., it is crucial to make a difference in the curing model for diffusion or chemically controlled curing [6]. In [4], this effect is taken into account. A model mentioned in [43] is used; however, to take the impact of the curing mechanism into account, an adjustment is made. The original model expects the rate of convergence to be 1 for a fully cured sample. However, due to the slower curing mechanism at a high α, this 1 is replaced with $\alpha_{max}(T)$. The final kinetic model used in [4] is shown in Equation 4.14

$$\frac{d\alpha}{dt} = k_1 e^{-E_1\left(\frac{T_{ref}}{T}-1\right)} \cdot \sum_{i=0}^{n} a_1 \alpha^i \left(\alpha_{\mathsf{max}}(T) - \alpha\right)^n \tag{2.2}$$

$E_1 - Activation\ energy$
$T_{ref} - Arbitrary\ temperature\ in\ operating\ range$
$n - Reaction\ component$
$\frac{d\alpha}{dt} - Curing\ rate$
$k1 - Frequency\ Factor$
$\alpha_max(T) - Maximum\ degree\ of\ cure\ for\ the\ isothermal\ temperature\ T$
$a_1 - parameter$

In order to find the parameters $(k_1, E_1, T_{ref}$ and a) isothermal and dynamic measurements are done according to the method mentioned in [41]. The value n is found by using the least-squares fit method for the measured data.

In Equation 4.14 $\alpha_{max}(T)$ is used, in order to determine this both [5] and [4] used the same method. The DiBenedetto model is used, in Equation 4.8 the T_g is linked to the α, but now the $T_g = T_c$ and $\alpha_{max} = \alpha$. Instead of T_g being solved now α is being solved, this results in Equation 4.11. In both studies, the least squares fit method determines μ and $T_{g\infty}$.

$$\alpha_{\mathsf{max}} = \frac{(T_{\mathsf{c}} - T_{\mathsf{g0}})}{(T_{\mathsf{g}_\infty} - T_{\mathsf{g0}})\,\mu + (1-\mu)\,(T_{\mathsf{c}} - T_{\mathsf{g0}})} \tag{2.3}$$

$\mu - Adjustable\ parameter$
$T_c - Curing\ temperature$

The kinetic cure model described in Equation 4.14 is accurate for a rate of convergence between 0.3 and 0.9. Since this is the range of interest, this model is sufficient for the scope of this review. The inaccuracy outside this range can be explained by the fact that there are two hardeners in this study and that secondary reactions occur at a high α [5] [4].

The method described in [4] to use Equation 4.14 and Equation 4.11 shows accurate results for pure resin samples. However, applied to a composite part, it shows some inaccuracies. Inaccuracies are explained in the usage of their temperature-measuring tools. A second explanation is the relatively large variations in the curing temperature. The second measurement in a smaller range has been done, and this has been shown to improve the accuracy. The aim of the study to predict the α is achieved.

Curing profile
In Figure 2.6.1, the relationship between partial curing and the degree of cure is explained. This balances its rigidity (at room or curing temperature, depending on the manufacturing process) and a sufficient amount of chemical bonds. Studies show that higher curing temperature results in a higher curing rate and vice versa [44] [45] [5] [4] [43]. A lower cooling rate can lead to a higher controlled degree of curing. However, once this temperature is too low, the curing mechanism changes, and this could lead to different properties which are undesired [33]. In the studies [5] [4], a difference has been made between two types of parts. This is a part where the resin should be able to flow during curing, so here is the $\alpha < \alpha_{gel}$. However, the $T_g >$ room temperature makes it handleable. The T_g of this part stays during curing below the T_c to allow the resin to flow and avoid the formation of voids. The second type of part is a part where the $T_g > T_c$. The part stays rigid during curing. The T_g of this part determines the lower limit of the T_c. For the final curing step, the time and temperature are set accordingly to the manufacturer data sheets [33] [7] [9] [4] [5]. An illustration of these two types of parts is given in Figure 6.9, where (a) is the part which has to stay rigid during co-curing (therefore $T_g > T_c$) and for (b) $T_c > T_g$.

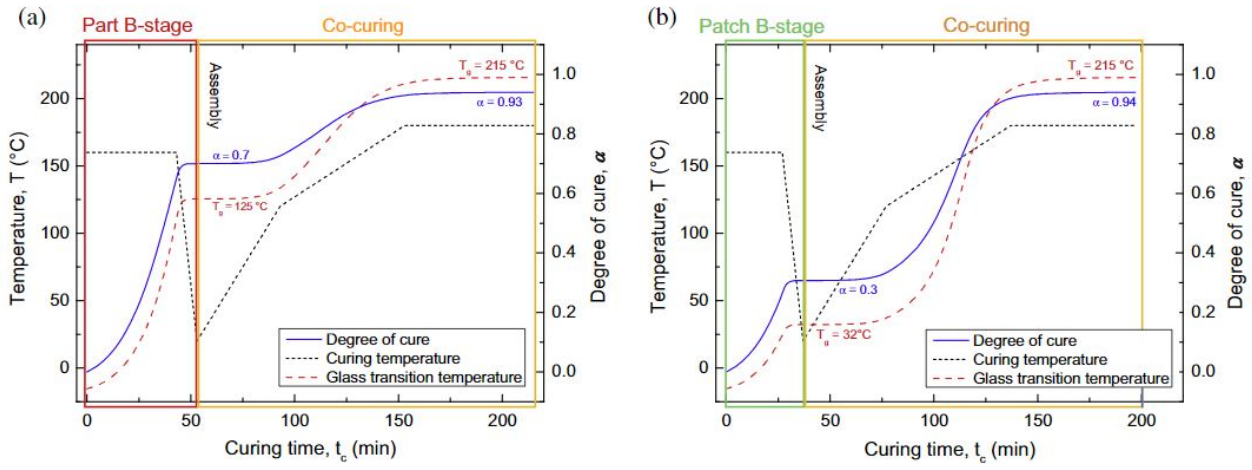


Figure 2.16: Illustration of two types of parts which will be B-staged and co-cured together [4]

2.6.2. Mechanical performance of the joint

In Figure 2.17, the mechanical performance of the conventional co-bonded adhesion joint is compared with the partially cured epoxy. It is shown that the partially cured epoxy joint shows higher performance. The lower the degree of cure, the higher the performance. In [4], it is shown that the method described in Figure 2.13 is an effective way of creating a bond without adhesives and a void-free interface. In the study, [7], the relationship between the bonding properties and the degree of cure has been researched using interlaminar shear strength and interlaminar fracture toughness. Several samples are made with an uncured stack B and a varying degree of cure of stack A. Varying from uncured to fully cured. So from co-curing to co-bonding with partial cure in between. An increase in the degree of cure of stack A decreases the shear strength. A critical note must be made on the interlaminar fracture toughness results of [7] shown in Figure 2.17. The interlaminar fracture toughness energy, the value C4, is not in trend with the other results. There is no clear hypothesis or explanation given for this outlier. [33] And [22] also prove the relationship between an increase in the degree

of cure and a decrease in the interlaminar fracture toughness. Although in the results of [22], the standard deviation increases of the partially cured samples compared to the standard deviation of the co-bonding and co-curing samples. Nevertheless, the trend of the mean is still as expected. [5] Shows that strength improvements are made when the b-stage method is used for local reinforcement. Weight savings can be made using this method instead of bolted structures. Both [5],[46] and [4] proved this strength improvement with the manufacturing technique ”resin transfer moulding”.

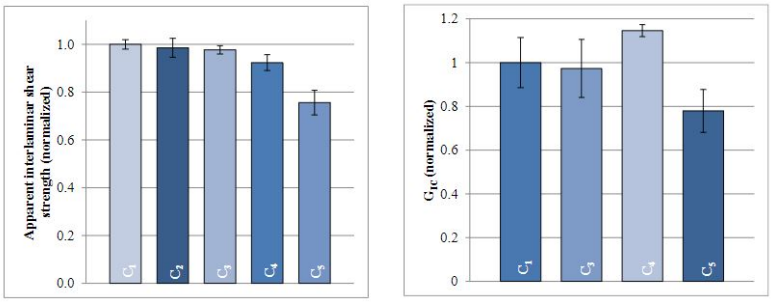


Figure 2.17: Left the normalized interlaminar shear strength, at the right normalized interlaminar fracture toughness energy,G_{ic}. In C1, stack A is uncured, and the degree of cure increases up to a fully cured C5. [7]

Interface of partially cured epoxy

In section 2.4, the negative effects of release agents in peel plies on the bond strength are mentioned. A study performed by [9] shows that these effects also occur for using partially cured epoxy. This is studied by reviewing the energy release rate of the peel ply. The worst type of peel ply even shows a 25% reduction in energy release rate compared to the reference peel ply. According to Motsch et al., the lower the energy release rate, the lower the effectiveness of the surface preparation. Grinding the surface after using a peel ply with a release agent improves the bond properties. It has not been studied whether grinding improves the bond properties when a peel ply without a release agent is used. An increasing degree of cure causes an increase in the number of residues or contamination left behind by the peel ply [9]

The surface treatment influences the bond performance. According to Moosburger et al., this is still valid for partially cured epoxy. A closer study done by Moosburger-Will [46] gives more insight into the microstructure of the interface. A resin-rich interface region will form between the parts. This region is homogeneous for co-bonding or low partially cured parts (<60%), which leads to homogeneous material properties. Since this area is homogeneous, crack propagation will occur, resulting in poor bonding quality. The peel ply produces an effective ripple-like surface for an intermediate curing degree (70%-80%), resulting in good mechanical interlocking and a high-contact surface. This has a positive effect on the bond performance. A follow-up study shows that these ripple-like surfaces remain after the final cure. They measured that this results in in-homogeneous surface morphology with significant differences in material properties [8]. It is reported that this is due to the limited mixing of the partially cured and fresh resin. The ripple-like structure is shown in Figure 2.18. They state that these mismatches do not affect the bulk properties. At the same time, it has a positive effect on the joining quality due to enhanced mode-1 fracture toughness and improved failure behaviour [8]. This improvement of the mode-1 performance for intermediate partially cured parts is shown in subsection 2.6.2.

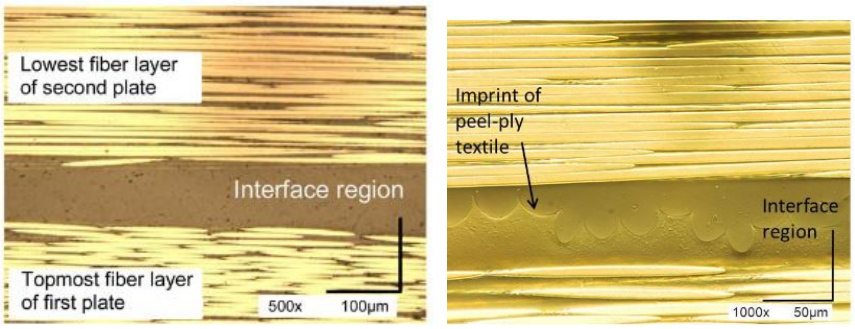


Figure 2.18: Cross-sectional image of the interface between a partially and fully cured laminate after the final curing step. The cure rate of the partially cured part in the left image is 60%, and a homogeneous interface region is visible. At the right image, the rate of cure is 70%, and a ripple-like non-homogeneous interface region is visible [8]

[9] And [33] show that for co-curing, the fibre matrix failure is the failure mode. An increasing degree of cure (towards co-bonding) shifts the failure occurs more in the bond zone. This effect is shown in Figure 2.19

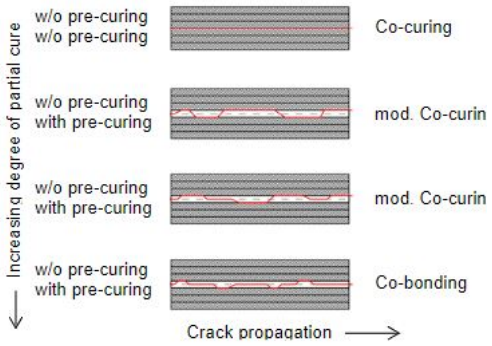


Figure 2.19: Fracture surface for different types of curing combinations [9]

Cure history

As mentioned in Figure 2.6.1, the T_g increases with an increasing degree of cure. If the $T_g < T_c$ the polymer is in the rubbery state, and the chain mobility is high. If the $T_g > T_c$ the polymer is in a glassy state. Here, the chain mobility is low. The region around $T_g = T_c$ is called the transition region. These physical states dependent on the degree of cure and temperature are shown in Figure 2.20. The impact of the curing history on material parameters such as density and hardness are described in Appendix A

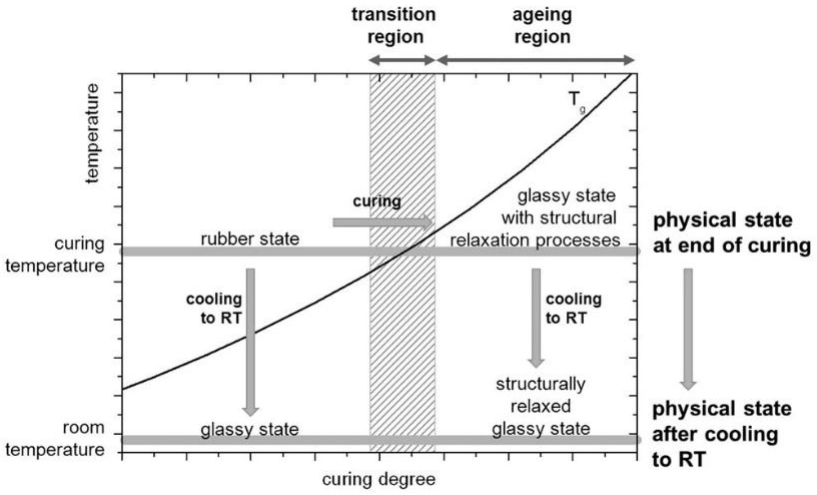


Figure 2.20: Physical state dependent on the degree of cure and temperature [10]

2.7. Fusion bonding of thermoset composites

Thermoplastics differ from thermosets; one of the critical differences is the joining mechanism. The difference in material aspect is explained in section 2.2. The joining steps of fusion bonding of thermoset composites are explained and illustrated in Figure 2.7a and Figure 2.7b. The advantage of using thermoplastic welding, also called fusion bonding, over mechanical fasteners is that it does not create stress concentrations. The advantage over thermoset adhesive bonding is that there is no need for surface preparation, and it reduces processing times [15].

A method described in the literature to use a thermoplastic film to join thermoset composites with a thermoplastic. A thermoplastic film will get co-cured with the thermoset. A thermoplastic film can be co-cured on top of the thermoset prepreg. This can be achieved in the autoclave or using a hot press. The thermoplastic film and the thermoset of the prepreg must be chemically compatible. Monnard et al. report two definitions of chemical compatibility. Firstly by having a (nearly) unique T_g. Secondly, by having spontaneous mixing by minimising the Gibbs free energy of mixing, ΔG_m. This can be achieved by minimising the enthalpy of mixing, δH_m [2]. Having (nearly) similar solubility parameters, δ minimizes the enthalpy of mixing [3][16]. However, if chemical compatibility can not be achieved, a second thermoplastic film can be added (a thermoplastic film which is chemically compatible with the thermoset adherent) [49]. A variety of potential thermoplastic materials are mentioned in the literature. Polysulfone shows potential in welding thermoplastic joints; this material is originally used as epoxy toughener [50], [51]. Polyethersulfone, PES, is successfully used as epoxy modified and shows good compatibility with epoxy [51]. Polyetherimide (PEI) shows a significant interdiffusion with epoxy, even with the presence of carbon fibres [52], [15], [53], [54]. Lastly, polyamide is mentioned in the literature as well. This material shows strong interactions with epoxy accordingly to [55]. A suitable thermoplastic should be studied for every type of thermoset and application. The interaction between a thermoplastic and a thermoset polymer can form a semi-interpenetrating polymer network, sIPN [56]. An illustration of the setup is given in Figure 2.21. Here, a thermoplastic film is placed as if it is just a thermoset prepreg ply. The thermoplastic layer will be placed at the mould, which will be the bonding surface for the joint. The cure cycle, as recommended by the prepreg manufacturer, can be used [11], [26].

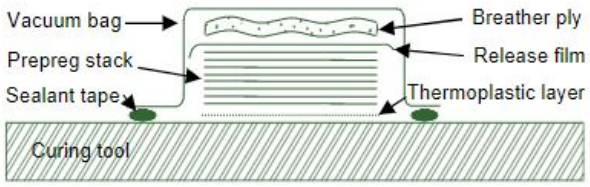


Figure 2.21: Typical where thermoset prepreg is co-cured with a thermoplastic film [11]

2.7.1. Interdiffusion thermoset and thermoplastic

Epoxy has a low fracture toughness at room temperature and tends to be very brittle. Toughening the joint with a thermoplastic could increase the ultimate shear strength [26]. To join the thermoplastic film on top of the thermoset, the film is placed on the top surface of the non-cured thermoset composite. The thermoset is in an uncured phase which means it will be liquid. The liquid reactive thermoset monomers will diffuse into the thermoplastic film, which is in a glassy state. The thermoplastic polymer will locally dissolute in the epoxy. According to Brauner et al., knowledge about the resin curing behaviour is required. This knowledge can be studied by DSC measurements[57] [44].

A semi-interpenetrating polymer network (IPN) is a polymeric system without covalent bonds between two (or more) polymeric networks; this network is formed between a linear (thermoplastic) and a cross-linked polymer (thermoset). [12]. The bonding between these two networks mostly occurs via interlocking on the molecular scale. This is also the case for the thermoplastic thermoset bond. However, in the diffusion of the thermoplastic and thermoset polymeric network, there is no complete interpenetration on the molecular scale, and bi-continuous morphologies are created. An example of a bi-continuos morphology is mentioned in [58]. Here a bi-continuous phase structure was found with a periodic distance of 20 nm. The formation of

[2] $G = H - T * S$, where T is temperature and S in entropy[47]

[3] $\Delta H_m = V(\delta_{TS} - \delta_{TP}) * 2 * fraction_{TS} * fraction_{TP}$, where V is volume and TP= thermoplastic, TS= thermoset [48].

a semi-interpenetrating network is shown in Figure 2.22. This semi-interpenetrating network will form at the thermoset/thermoplastic interphase, also called the interfacial region. This interfacial region lies in between the thermoset and thermoplastic. This interfacial region can be divided into three regions based on the amount of thermoplastic polymer. The first region is the liquid layer consisting of a diluted polymer solution with relatively free motions of entire polymer chains. Secondly, the gel layer is the swollen polymer in a rubbery state. Lastly, the infiltration layer, where the solvent molecules diffuse. The type of diffusion in the Fickian diffusion [44]. Fickian diffusion relates the diffusive flux to the gradient of the concentration. The flux goes from an area with a high towards an area with a low concentration.

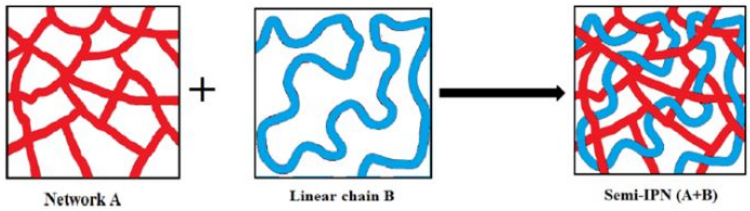


Figure 2.22: The schematic formation of a semi-interpenetrating network (IPN) where network A is a thermoset polymeric system and network B is a thermoplastic polymeric system [12].

The underlying mechanism behind the phase separation and mixing of the polymer blend is the physics behind the polymer blend. A blend can be miscible. Here, the individual components disappear, and a blend is formed on the molecular scale. Or a blend can be immiscible, so in the dispersion, both components retain their identity [59]. According to van der Vegt, a polymer blend is miscible when the Gibbs free energy of mixing is negative, shown in Equation 2.4.

$$\begin{aligned} \Delta G_m < 0, \text{ resulting in:} \\ \Delta H_m - T \cdot \Delta S_m < 0, \text{Where :} \\ \Delta H_m = V \cdot (\delta_1 - \delta_2)^2 \cdot \varphi_1 \cdot \varphi_2, \text{and} \\ \Delta S = k \ln \Omega \end{aligned} \tag{2.4}$$

$\Delta G_m - Gibbs\ free\ energy\ of\ mixing$
$\Delta H_m - Enthalpy\ of\ mixing$
$\delta_1, \delta_2 - Solubility\ parameters$
$\varphi_1, \varphi_2 - Volume\ fractions$
$k - The\ Boltzmann\ constant$
$\Delta S - gain\ in\ entropy\ upon\ mixing$
$\Omega - \ Number\ of\ arrangements$

In Equation 2.4 the enthalpy of mixing is governed by the interactions between the polymers. According to Vegt, a negative enthalpy can result in an exothermic reaction which can promote miscibility [59]. The gain in entropy will be a positive number since the amount of disorder increases upon mixing.

A morphology is formed in the interfacial region. This morphology depends on the competition between the cross-linking of the thermoset and the reaction-induced phase separation. This morphology changes in the interfacial region with the increasing size of epoxy droplets reducing in size towards the pure thermoplastic region. This phase morphology is shown in Figure 2.23. The increased toughness in the epoxy is due to the local ductile shear deformation of the thermoplastic polymer.

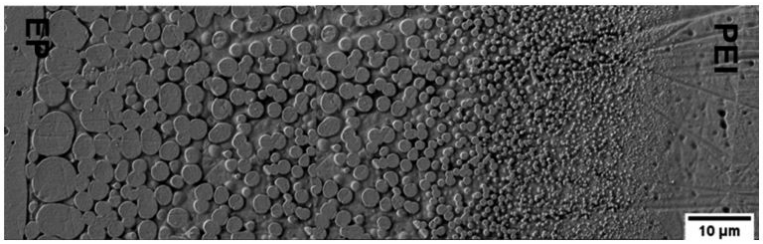


Figure 2.23: At the left pure epoxy, the right, pure thermoplastic (PEI). Epoxy-rich particles in PEI-rich matrix. Epoxy particles are reducing in size towards pure thermoplastic region [12]

The competition between the rate of phase separation and the cross-linking of the thermoset determines the final morphology. As soon as the T_g starts to exceed the curing temperature, the morphology gets frozen [14] The phase separation exists out of two mechanisms. The first mechanism is nucleation and growth, which results in spherical inclusions. A sphere or phase A develops over time in a phase B-rich region; over time, this sphere will grow. Secondly, a spinodal decomposition leads to co-continuous morphologies. For a spinodal decomposition, micro- or micro-separated domains are highly connected.

For a spinodal decomposition, the morphology can be adjusted by changing the thermoplastic concentration and the curing temperature. There are two types of phase behaviours between epoxy monomers and thermoplastic glassy polymers. Firstly, an upper critical solution temperature (UCST) (such as the thermoplastic PES). Secondly, lower critical solution temperature (LCST) (such as the thermoplastic PEI). For a thermoset/thermoplastic combination with a UCST, all temperatures above the UCST will lead to a homogeneous 1 phase, and for an LCST, vice versa. This is shown in Figure 2.24.

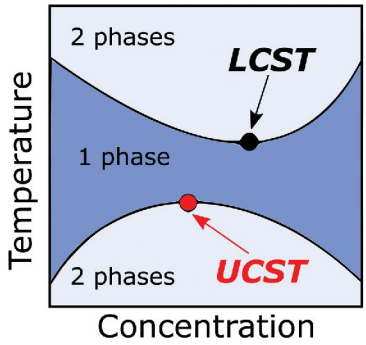


Figure 2.24: Upper critical solution temperature and lower critical solution temperature shown in a phase diagram. [13]

The morphology which is being formed depends on several parameters. In the literature, the following parameters are mentioned: the cure conditions, thermoplastic concentration, the molecular structure of the thermoplastic, solubility parameters of the components, dwell time, the stoichiometric ratio of curing agent to epoxy, type of accelerator and the molecular structure of the epoxy [44]. Mimura K. et al. show an example of how to control the morphology. The blend exists out of epoxy and PES, exhibiting an LCST phase behaviour. The phase diagram is shown in Figure 2.25 [14].

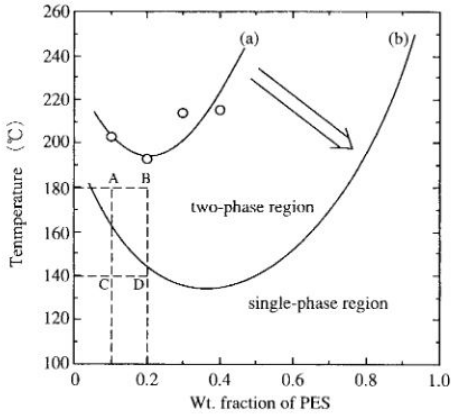


Figure 2.25: Phase diagram of epoxy/PES mixture [14]

Point C and D are moulded at 140 °C and have a homogeneous morphology. Both A and B are moulded at 180 °C and have a phase-separated morphology. In Figure 2.25, it becomes clear that an increase in PES content increases the temperature where phase separation will occur. In other words, more energy is needed for phase separation. This can be explained by increased viscosity due to increased PES content. The mobility decreases and, therefore, also the rate of phase separation [14]. This study also shows that the different morphologies have different fracture toughness. Therefore, it is important to clearly understand the influence of the process parameters on the morphology.

In the literature, higher fracture toughness is observed when the epoxy droplets are bigger. This bigger size of droplets is formed at higher dwell temperatures. The relationship between the interphase thickness and the fracture toughness is that higher temperatures lead to a higher interphase thickness which results in higher resultant fracture toughness. A study performed by Farooq et al. studied the relationship between the interdiffusion distance and the curing history. This study has two dwell phases. Two scenarios are studied. Firstly, they wait for the phase separation before moving into the second dwell. Secondly, they wait for 80% degree of cure to move in the second dwell phase. The interphase is studied using microscopy experiments and linked to the degree of cure via a kinetic model [44]. Via microscopy, the epoxy droplet size and the depth in the interphase can be determined. The reported outcome tells that the first option, waiting for the onset of phase separation, leads to a higher diffusion distance than the second option, 80% degree of cure. They hypothesise that the chain mobility is higher in the second dwell curing stage in the first scenario, and therefore a higher diffusion distance is reached. Secondly, it is reported that higher chain mobility results in smaller droplets. This could be explained by the fact that only the smaller droplets could diffuse deeper [44]. According to Harismendy et al., higher epoxy droplets will lead to higher fracture toughness and are formed at higher dwell temperatures [60]. Thicker films tend to ease the welding process [49]. According to Schieler et al., a thicker film also increases the shear strength [19]. According to Oyama et al., the interphase's thickness is the main factor influencing the mechanical performance and strength of the hybrid joint. They explain that by the load transfer, the thicker the interphase, the better the mechanical interlocking, which benefits the load transfer [61]. Initially, it has been thought that the diffusion process stops as soon as the phase separation starts. However According to Farooq et al., for both LCST and UST combinations, the diffusion continued after the onset of phase separation [44].

To summarize, the morphology depends on the competition between phase separation and the cross-linking of the thermoset. The process parameters and the concentrations can influence this morphology. Therefore the desired effects of modifying the epoxy with a thermoplastic (material properties and properties of the weld) can be influenced by the process parameters and the concentrations.

2.7.2. Fusion welding process

The thermoplastic films will be welded together in the fusion welding process step. Figure 2.3 shows this process step. The thermoplastic films are connected to the thermoset; therefore, the adherents are welded together via this fusion welding process step. Heat and pressure must be applied. The characteristics of the thermoplastic material determine the required temperature. The temperature must rise above the T_g for an

amorphous and above the T_m for a semi-crystalline polymer. This is required to soften the matrix so fusion bonding can occur. While softening the matrix, pressure needs to get applied. Once the entanglements are formed, the temperature must be cooled below the T_g or T_m respectively, while the pressure is still applied [19]. In Figure 2.26, a classification of all methods is given.

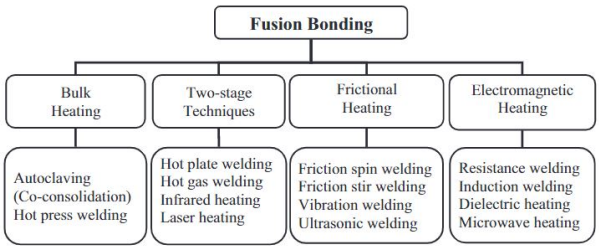


Figure 2.26: Classification of fusion techniques [15]

To select a fusion bonding method for joining into limited access hollow structures, the following criteria should be considered.

- Limited access to the joint, which is the inside of the structure.
- The joint is along the entire structure length, which can be up to 60 meters (both sides).
- Preferably, current tooling should be used.

The fusion bonding mechanism can be classified into bulk and local heating. The two-stage techniques, frictional heating and electromagnetic heating techniques, are local heating. All the methods are described in Table B.1,Table B.2, Table B.3 and Table B.4, which can be found in section 5.1.

2.7.3. Mechanical performance characteristics

A variety of welding techniques are found in the literature. The bond strength depends on various parameters such as the materials, diffusion depth and fusion welding technique. However, a trend is still visible. Various studies show that the joint's mechanical performance is equal to or higher than adhesive co-bonding. A comparative study is done by Ageorges et al., here this as well. However, they also conclude that the fusion technique highly influences bond strength. Xiong et al. overviewed the average bond strengths of several techniques. Here it is shown that welding strengths over 30 MPa can be achieved [18]. Ageroges et al. report that the adhesive co-bonds are within the same range or lower. This shows the potential of implementing thermoplastic films into thermoset joining.
Paton et al. compared the single lap shear strength at various temperatures. Adhesive co-bonding is being compared with thermoset composite fusion welds[11]. The results are shown in Figure 2.27. The mechanical strength of the thermoset fusion-welded joints is equal to or superior to the adhesively co-bonded joints. Smiley et al. report an increase of 25% increase in the bond strength of single lap joints between a co-consolidation fusion process compared to adhesive co-bonding. However, co-consolidation can lead to thermal degradation problems in the structure. This will be discussed further in this study [62].

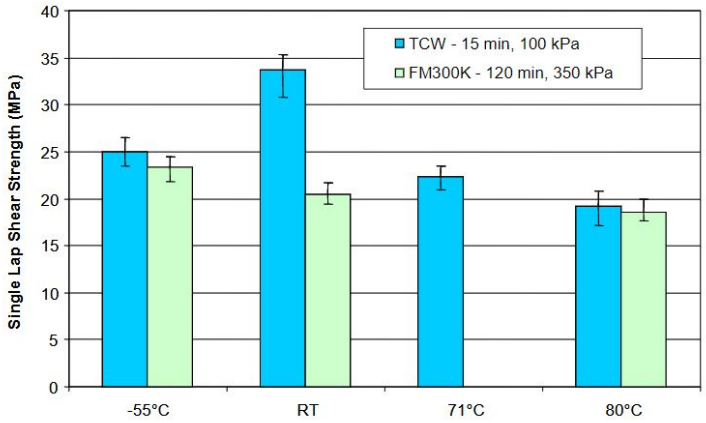


Figure 2.27: Comparison between thermoset fusion welded joints (blue) and adhesive co-bonded joints (green) at various temperatures [11]

2.7.4. Thermal degradation

High temperatures are generated during the adhesion process between the thermoset and thermoplastic film. This is achieved by either bulk heating or locally heating the thermoset/thermoplastic interface. The interlocking of the two materials occurs as a result, and a semi-interpenetrating network gets created. In it is mentioned that the temperature must rise above the T_g for an amorphous thermoplastic film and above the T_m for a semi-crystalline polymer. Thermoset composites exposed to temperatures much above the T_g of the resin can experience ageing. They were also referred to as thermal degradation. Tsotsis et al. show that an epoxy system exposed to a temperature at 177°C for 5000 hours is experiencing a decrease of 30% in compression strength. However, This thermal degradation also occurs at short timescales, according to Abouhamzeh et al. [63]. Mcknight et al. made micrographs of the good quality and degraded welds, shown in Figure 2.28.

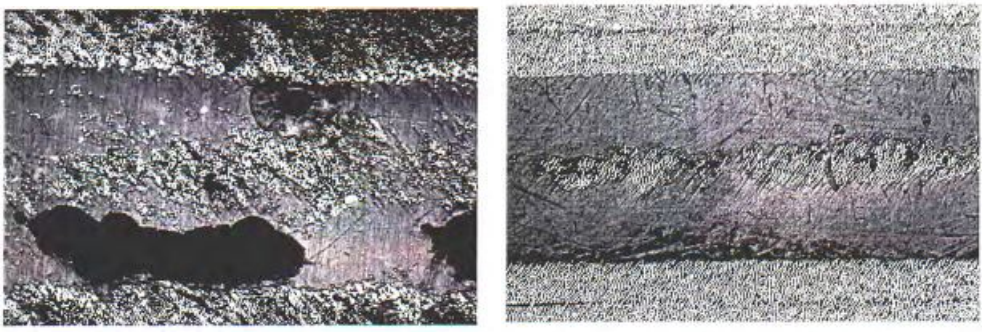


Figure 2.28: Micrographs of a thermoset composite fusion bond. Left thermal degradation is present, in the right graph a good weld is shown without thermal degradation [16]

The direct effects on mechanical material strength are measured. Measuring the mass loss is not relevant since the loss of mechanical performance can already occur when the chain starts breaking. This could be the point that mass loss is not relevant yet, translating into a loss of mechanical performance without mass loss. On the other hand, mass loss can occur due to moisture evaporation which does not affect the mechanical performance. Therefore, mass is not a good measure between thermal degradation and loss of mechanical performance [63]. Techniques such as TGA (thermo-gravimetric analysis), DSC and DMTA (dynamic mechanical thermal analysis) are relevant to measuring the effect of temperature exposure.

2.8. Industrialization

The applicability of the methods of b-stage joining of thermoset composites and fusion bonding of thermoset composites in mast manufacturing is reviewed in this chapter. This is done according to the challenges which are mentioned in the literature.

2.8.1. B-staging joining of thermoset composites

Bonding with partially cured parts does not require adhesives. Therefore it makes it possible to apply it without additional certification. In subsection 2.6.2, it is shown that due to the chemical reactivity of the partial cross-linked parts, this method positively affects the bonding performance. So the basic concept is proven to be effective. The biggest challenge is making this method feasible for the industry.

In [4] two challenges are mentioned are mentioned. The first challenge is monitoring the curing temperature; here, a small deviation in the temperature measurements has led to the inaccuracy of the kinetic model. Accurate temperature monitoring is suggested as a potential solution to overcome this inaccuracy. A second challenge addressed is the narrow window for the free-standing cure. However, for this problem, a solution is mentioned: Looking into other amine-curing epoxies with better suitability [5][4].

Ideally, a partially cured part has a low degree of cure. This increases the potential cross-links in the final bonding, resulting in low mechanical properties. In the studies in subsection 2.6.2, small patches with simple geometries are used. However, in the industry, the parts must have a certain rigidity in the partially cured state. This is to carry their weight and to make them handle-able[33].

In literature, one study is available that addresses the reproducibility and stability of partial cure epoxy matrix resin systems; this study is done by Müller et al. [6]. The studies mentioned above mainly focus on the basic concept of partially cured bonding; however, in the industry, geometric shapes will be more complex than just a flat plate, and higher thicknesses can be used. This has to take into account by designing the mould and cure cycle.

Reproducibility partial cure

Mullet et al. study the reproducibility of the partial degree of cure. This relates to a specific degree of cure and the capability to achieve a homogeneous degree of cure. This reproducibility gets complicated by thermal overshoots[6]. This overshoot occurs due to the exothermic reaction enthalpy. Müller et al. found that a reduced mould thickness has a more significant temperature overshoot [4].

Müllet et al. concluded that the formation of homogeneous partially cured parts is possible if a set of guidelines is followed. These guidelines are shown in Table 2.2.

Table 2.2: Guidelines for the homogeneous degree of cure of a part [6]

Validate and establish a reaction kinetic model to have a relevant cure cycle. This also allows for a reliable prediction of α and T_g for the partially cured part.
Avoid heat overshoot in the early stages of curing. Therefore the thickness of part must be selected with care.
Close attention must be paid to thermal boundaries in the design, such as mould design and material and ambient temperature. All these factors influence each other

Stability of partial cure states

Secondly, the stability of the degree of cure should be evaluated. Effects such as physical ageing (mentioned in Figure A), chemical ageing [5] or hydrothermal ageing [6]. It has been observed that a part with a low partial degree of cure tends to shift in T_g after being stored at room temperature for ten days. The higher the degree of cure, the longer it takes to reach this stable state, so the lower the shift in T_g over time. This is illustrated in

[4] Especially an overshoot at the beginning of the cure cycle has a high influence [6]

[5] Further formation of cross-links, irreversible process.

[6] Water uptake, however according to Müller et al. this process is reversible and therefore not considered in this study [6].

Figure 2.29. Müller et al. report that this increase of T_g is mainly caused by chemical ageing and is uncritical if the degree is sufficiently high. High temperatures cause the main risk to stability. However, not the degree of cure but the difference between the T_G (which is related to the degree of cure) and the exposure temperature is important for stability.

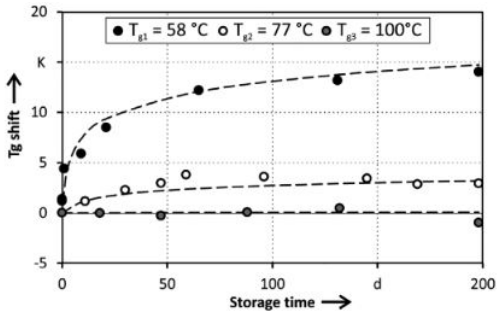


Figure 2.29: Long-term stability for different partially cured parts. Note that the T_g is directly proportional to the degree of cure. Storage is at room temperature [6]

2.8.2. Fusion bonding of thermoset composites

Thermal degradation of thermoset polymers

In subsection 2.7.4, thermal degradation is introduced. Thermal degradation results from the heating process. This process is required for the fusion of the thermoplastic film. Temperatures above 250 degrees for epoxy should be considered with thermal deg [63]. This thermal degradation can cause challenges in implementing fusion welding into the manufacturing process of masts. A setback in the mechanical properties of the epoxy is not desired. Therefore a careful study needs to be done into thermal degradation. Villegas et a. suggest that a possible solution could be to select a thermoset/thermoplastic combination where the welding temperature is below the T_g of the thermoset. However, the downside is that this limits the options of thermoplastic materials to be used [64]. A second alternative is to decrease the heating time for the degradation mechanisms to occur. However, more research must be done to achieve such a method in large structures. Chandran et al. report that a thicker thermoplastic layer in the co-curing method could potentially prevent the effect of thermal degradation. [17].

Fusion welding method

In subsection 2.7.4, the different fusion welding techniques are being compared. Due to the limited access and the geometrical shape of the mast, not all methods are suitable for manufacturing the mast. Autoclave heating, also called co-consolidation, Resistance welding, and induction welding, are the methods which are possible to implement based on the geometrics. However, as described in subsection 2.8.2 thermal degradation should be considered. Using the bulk heating method causes the entire structure to be heated for a significant time. This could lead to a lowering in mechanical properties due to thermal degradation. Therefore bulk heating is not suitable for application in the industry. Two-stage techniques are geometrical and not possible. Joining parts into a hollow structure causes a geometrical challenge. Ultrasonic welding shows promising results regarding thermal degradation; however, this method is not industrialized for continuous welding.

As explained in subsection 2.7.4 in resistance welding, the heat is generated by a heating element. A current flow through this heating element which generates the heat. At the same time, pressure is being applied. After the joining process, the heating element remains in the joint permanently. The setup is shown in Figure 2.30 [17]. The right figure shows that the mesh will remain in the joint.

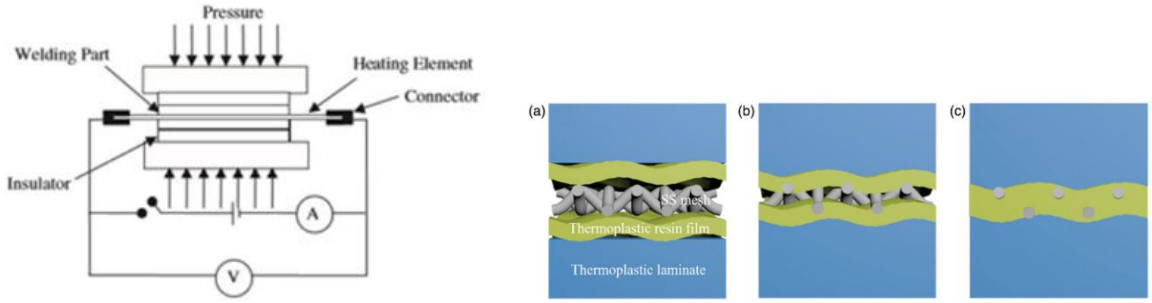


Figure 2.30: left: Schematic representation of the resistance welding setup. [17]. Right: a: before joining, b: thermoplastic film softens due to heat, c:the soft thermoplastic material fuses into the mesh. This is due to the applied pressure. Mesh stays in the joint [18]

Mcknight et al. studied the effect of thermal degradation, and resistance welding [16]. PSU is used as the thermoplastic film. They show promising results and a negligible loss in mechanical performance, which can be translated into a negligible effect of thermal degradation. However, they state that the correct parameters should be studied and used for each material. The dwell time, power and pressure. If this is not done correctly, a loss in shear strength is reported. Paton et al. successfully resistance welded on a curved section. Being able to weld on curved sections benefits the ease of implementing this welding method [11].

A second suitable method is induction welding. Schieler et al. successfully performed a study where induction welding was studied. The aim is to implement this method in Airbus helicopters [19]. An alternating magnetic field passes through a coil with a frequency. Two heating mechanisms occur in the carbon fibres. Heating by contact of the fibres and heating by dielectric hysteresis Figure 2.31. They showed that at a temperature above 250 °C, the mechanical performance started to decrease due to thermal degradation of the thermoset. This conclusion is based on the interlaminar shear strength. PEI and PES are used as thermoplastic materials. They conclude that it is possible to induction weld without a significant loss of mechanical performance. However, it is advised to investigate the usage of epoxies with a high degradation temperature. Secondly, they advise investigating weld-on temperatures lower or close to the thermal degradation temperature of the thermoset epoxy. Several thermoplastic films should be considered. But most importantly, it should be ideal to avoid the welding step.

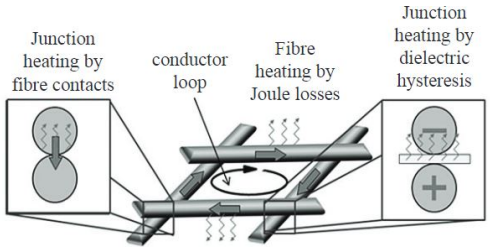


Figure 2.31: Two heating mechanisms. [19]

2.8.3. Comparison of the joining methods

Three joining methods are reviewed in this project. In Table 2.3, an overview of the methods is given based on the requirements. The requirements are discussed in this review. In chapter 8, a conclusion will be made based on Table 2.3. The first requirement is the ability to integrate into the current manufacturing process. In other words, are new tools required, and are their adjustments needed in the current process? The current process is joining with an epoxy adhesive secondary joint.

Table 2.3: Comparative table of the joining methods

Requirements:	Adhesive co-bonding	B-stage joining	Fusion bonding
Ability to integrate into current manufacturing process.	N/A	No new tooling is required besides temperature sensors.	New tooling is required for the fusion welding process step. Namely a heating element.
Required materials.	Current used epoxy prepreg.	Current used epoxy prepreg.	Current used epoxy prepreg + thermoplastic film.
Mechanical performance in comparison to adhesive co-bonding.	N/A	Higher interlaminar shear strength and higher fracture toughness.	Higher interlaminar shear strength and higher fracture toughness.
Surface preparation required and if yes which are possible.	Yes, peel ply. However, the usage is challenging due to limited access.	Yes, peel ply. However, the usage is challenging due to limited access.	No.
Challenges and potential limitations.	-Labour intensive -Low reliability -Lowest mechanical bond strength -Certifications are requiered	-The stability and reproducibility of the partially cured epoxy requires a thorough cure characteristics study. -The stability of the partially cured epoxy requires close temperature measurements -Prone to temperature overshoots,	-Implementing the heating element of the fusion welding step in the current manufacturing process. -Potential thermal degradation of the epoxy
Opportunities.	No new tooling is needed for this method.	The bonding mechanisms is based on chemical cross-links, this is more reliable than using an adhesive.	-Joining time is significantly lower than the other joining methods. -No surface preparation is required for the fusion welding step.

2.9. Conclusion

The challenge raised the need for a joining method to install a part inside a hollow tubular structure with limited access. This study reviews other suitable techniques to join parts inside a hollow carbon fibre-reinforced polymer tube. It must integrate into the current manufacturing method, and there must be the possibility of industrializing this method. Secondly, the bonding performance must improve compared to adhesive co-bonding.In the literature, no descriptions of joining parts into hollow limited-access tubular structures are available. However, new developments are being found which are used to join carbon fibre-reinforced polymers. These techniques are called b-stage joining and fusion bonding of thermoset composites. Both techniques are compared with adhesive co-bonding. The three methods are overviewed in Table 2.3.
The following key findings are formulated:

- Mechanical fasteners add weight to the structure, and stress concentrations result from the holes in the structure. Adhesive co-bonding arises challenges due to the limited access to the mast. Challenges concerning surface preparation, low mechanical strength, reliability and labour intensity. Due to these limitations, the adhesive co-bonding technique is unsuitable for industrialisation in the mast manufacturing industry.
- It can be concluded that both b-stage joining and fusion bonding can achieve a higher mechanical performance of the joint compared to adhesive co-bonding.
- Joining with partially cured epoxies needs the study of a thorough cure characteristic study to overcome problems with stability and reproducibility. Additionally, the cure history influences the mechanical properties of the partially cured epoxy. A good understanding is required to join this partially cured epoxy.
- The main concern of using fusion bonding of thermoset composites is selecting and implementing the fusion welding method into the manufacturing process. This is due to the limited access to the structure. Induction welding and resistance welding are successfully used as proof of concept in the literature.
- Fusion welding of thermoset composites allows for a shorter joining time than adhesive co-bonding or b-stage joining. However, thermal degradation can cause a decrease in the mechanical properties of the thermoset. In this specific study, this thermoset is epoxy.
- Fusion welding of thermoset composites does not require the usage of peel ply. This is an advantage over adhesive co-bonding and b-stage joining, which benefits the labour intensity.

3

Research framework

3.1. Research gaps and objectives

Based on the literature, it became evident that there are gaps in the literature concerning internal bonding in carbon fibre-reinforced polymer structures. These concepts are summarized below with additional comments.

- There are no studies available in the literature about internal bonding in the mast manufacturing industry in carbon fibre-reinforced polymer structures.
- There is no literature about the application of b-staging joining or fusion welding joining of thermoset composites in the mast manufacturing industry. Neither is their literature available about applying these methods for internal joining.
- There are a limited amount of studies about the reproducibility and stability of partially cured epoxies. Studies in literature are proof-of-concept studies on samples with square and thin geometrics. Therefore thermal effects are neglected.
- Studies concerning fusion welding of thermoset composites are mainly proof-of-concept studies. These studies are small-scale projects. More work needs to be done to gain knowledge about upscaling and industrializing.
- Thermal degradation is not studied broadly enough. This is often neglected due to the satisfactory mechanical performance. Although literature also shows that this thermal effect can not be neglected.
- Most of the literature studies into the field of joining with b-staged epoxy use the manufacturing process RTM. A limited amount of tests is performed using prepreg combined with the autoclave.

In the first stage of this study, conversations have taken place at Hall Spars. In these meetings between the engineers of Hall Spars, the project supervisor of the TU Delft, and the student, the requirements and scope of the study have been determined. Based on these ideas, the direction is chosen to look into the two alternative joining methods. These are discussed and reviewed in this study. Literature was found about these topics and used to create this review. Most relevant studies have been published within the last 15 years. Therefore, these joining methods are new topics; most of these studies were proof-of-concept studies. The aim was to include all the literature in this review. This was possible for the b-staging joining of thermoset composites since there was less literature available than for fusion joining. Based on the literature and the gaps in the literature study, the main research objective has been formulated based on the research gaps and Hall Spars' interest. To approach this main research objective, several sub-objectives are defined:

- Implement the joining techniques in mast manufacturing. In other words, joining high fibre volume unidirectional prepregs using these joining techniques. The autoclave will be used to apply the pressure and heat.
- Making a direct comparison of the mechanical performance of the joint by performing a lap shear test. These tests will be performed on the currently used adhesive co-bonding, b-staged epoxy composite and fusion welding of epoxy composite.

- Performing DSC measurements on the resin of the currently used composite. The data from these measurements will be used to determine the kinetic and Di Benedetto models. These models will create the autoclave's curing schedule (process parameters) based on the rigidity resulting from the $T_g >$ room temperature. And secondly, a part must maintain structural integrity during curing, so T_g>T_c must be valid for one part.
- To implement fusion welding of thermoset into mast manufacturing, a compatible thermoplastic film must be selected. To avoid thermal degradation in the welding step, the possibility of avoiding this step should be studied. This can be achieved by using the thermoplastic layer as a coupling term. Therefore, the effect of thermal degradation can be avoided.
- Current studies are performed with samples with small using square, thin and small geometrics. If joining with these two alternative methods proves efficient, different geometrics should be applied to the samples to study the thermal effects.

3.2. Framework

The approach of this thesis will be explained. A literature study is performed to understand the joining challenge, described in chapter 2. This study explains the need for this internal joint (not in the public version, this information can be found in the confidential version). Different joining methods for thermoset composites are reviewed and compared with the currently used method. Based on this review, two potential joining methods are chosen, joining with partially cured and fusion welding joining of thermoset composites. The study looks into the requirements to apply these joining techniques in the mast-building industry. Based on this conclusion, the research questions and the scope of this study are formed.

Secondly, an understanding of the characteristics of the resin is required. A model which predicts the degree of cure and the glass transition temperature will be needed to use this resin in the rest of this study. Differential scanning calorimetry measurements at different isothermal temperatures, heating rates and temperature-modulated runs are performed. This data is analysed with a python script. Different models are evaluated and eventually chosen. The resin characterisation and measurements are described in chapter 4.

Thirdly, for the joining method "fusion welding of thermoset composites", an interphase must be created between the thermoset epoxy and a thermoplastic film. Samples are manufactured to study this interphase formation and the impact of the process parameters on this formation. These samples are manufactured with the autoclave and the hot press. Cross-sectional images are made with the laser confocal microscope and the SEM after embedding, polishing and etching the samples. The description and results of this part can be found in chapter 5.
Joints are manufactured to test the proof-of-concept. The mentioned alternative joining methods, PEI film, Hall Spars's materials and curing conditions are used for these joints. These samples are manufactured in the composite lab at aerospace, cured in the autoclave, prepared with the Proth cutting machine, tested with the Zwick tensile machine and analysed with the laser confocal microscope. The description and results of this part can be found in chapter 6. Lastly, the applicability of the lab-scale joints to the industrial mast-building scale is reviewed in chapter 7. The joint processes will be reviewed according to the requirements found in the literature study. Additionally, shortcomings or findings about the joining methods will be described. In Figure 3.1, this framework is illustrated.

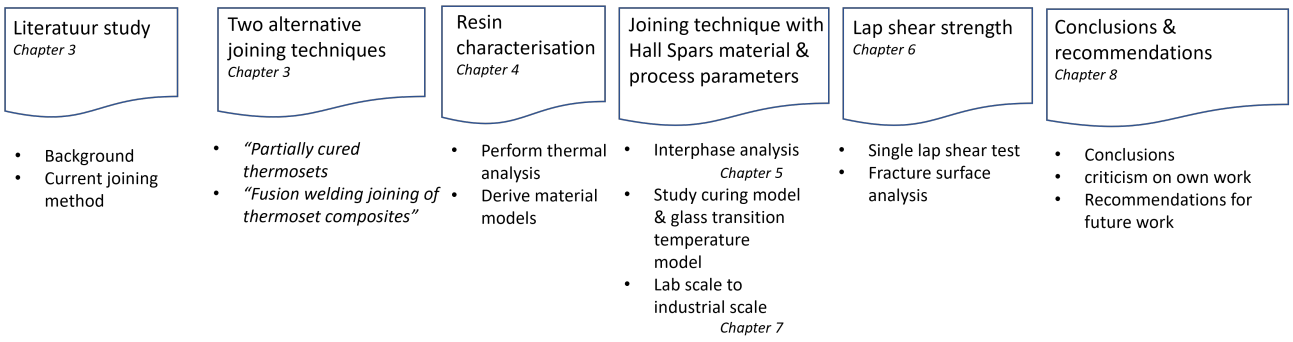


Figure 3.1: Frame work illustrated in a sketch.

3.3. Research questions

The research question for this study is to understand current materials and joining techniques for internal bonding of composites at Hall Spars, explore potential new joining methods, and study the requirements to implement these methods into the mast-building industry and mechanically test these joints. f

- **Research Question 1:**
  Are the Bailleul and the DiBenedetto models and the methods to derive the parameters described in the literature study applicable to the epoxy resin of Hall Spars? Can it directly be applied to understand and model the degree of cure and glass transition temperature in the relevant range (105-135°C and heating rates up to 2.5 °C / min), with a minimum R-squared value of 0.9? Or are model and method modifications required?
- **Research Question 2:**
  Does interphase formation between the selected thermoplastic polymer film and the epoxy resin of Hall spars occur at the relevant temperature range (105-135 °C)? If so: What is the impact of the temperature (heating rate and isothermal dwell temperature) on the interphase formation? Can this interphase formation be observed through cross-sectional optical microscopy and scanning electron microscopy imaging?
- **Research Question 3:**
  Is it feasible to manufacture samples on a lab scale with these alternative joining methods with Hall Spar's prepreg system and curing conditions? And how do these joints compare in terms of mechanical strength to the currently used epoxy adhesive film, benchmark, joints?
- **Research Question 4:**
  What is required to translate the lab-scale joining methods to the mast-building industry scale while considering Hall Spar's materials and curing conditions?

3.4. Hypothesis

- **Hypothesis 1:**
  Collecting material characteristic data using the isothermal, dynamic, and temperature-modulated DSC measurements allows for predicting the curing profile and the glass transition temperature. The Bailleul and the DiBenedetto models and the methods described in the literature allow deriving the parameters of the epoxy resin of Hall Spars. And therefore, predict this with a minimum R-squared value of 0.9 in the relevant range (105-135°C and heating rates up to 2.5 °C / min).
- **Hypothesis 2:**
  The interphase formation between the selected thermoplastic film and the epoxy resin at Hall spars will occur for isothermal curing temperatures above 120 °C. This can be observed through cross-sectional microscopy and scanning electron microscopy. The higher the isothermal curing temperature, the bigger the size of the interphase formation. The heating rate will have an impact if it is so low that gelation occurs during the ramp process. This gelation can potentially slow down interphase formation.
- **Hypothesis 3:**
  Manufacturing lab-scale samples with these alternative joining methods are feasible using Hall Spars's prepreg system and curing conditions. The mechanical strength of these joints will be in the same order as the benchmark samples.
- **Hypothesis 4:**
  To successfully apply partially cured joining in the mast industry, one part must maintain its structural integrity during the curing process. Therefore, the glass transition temperature of this part must remain above the curing temperature during curing. The required degree of cure must be found and applied to match this requirement. To implement fusion welding of thermoset joining, the thermoplastic film will be co-cured with the adherends in an autoclave, thus eliminating the difficulties associated with the welding step, as reported in the literature review. The thermoplastic film will be a so-called "coupling layer."

4

Resin characterisation

In this chapter, the models are described to determine the cure kinetics of the epoxy resin. section 4.1 describes the method used to determine the parameters of these models. The material used in this experiment and the sample preparation is described in section 4.2. The measurements and the determination of the parameters are presented in section 4.3. The determined models are presented and discussed in section 4.4. In section 4.5, concluding remarks on these models are provided. In this version, the material will not be called by name due to confidentiality. The data sheets will not be included. The epoxy thermoset resin used is called the epoxy thermoset.

4.1. Methodology

According to the literature study subsection 2.6.1, the joining methods ”B-staging joining of thermoset composites” and ”fusion bonding of thermoset composites” both require material models of the thermoset resin. These models provide information about the cure characteristics of the used thermoset. These cure characteristics are required to determine the suitable cure process parameters during this study. The literature study section 4.5 describes the suitable models. The DiBenedetto model is used to evaluate the evolution of the Glass transition temperature (T_g) to the degree of cure (α). The model to predict the maximum degree of cure, $\alpha_max(T)$, at each isothermal curing temperature,T_c, is derived from the Dibenedetto model. By relating $\alpha_max(T)$ with T_c instead of α with T_g in Equation 4.8. This lead to Equation 4.11. According to the literature study, the Bailleul model, described in Figure 2.6.1, is suitable to describe the cure kinetics of the thermoset epoxy resin system. A second cure kinetics model, which is not described in the literature study, will be used. This model is called the Kamal model and is described in section 4.5. A cure kinetics model is a simplification of reality. There is no ”one size fits all” solution. No cure kinetic models are available in the literature for the material used in this thesis. Therefore two models will be determined, and based on the least squares method, the most suitable cure kinetic model will be chosen for this thesis.

In the literature study subsection 2.6.1, a brief introduction to differential scanning calorimetry is provided. The parameters of these models are not provided by the supplier of the material and are unknown. These models are not made for the used material. However, these models are essential for this thesis. Differential scanning calorimetry experiments are performed in the Delft Aerospace Structures & Materials Laboratory (DASML) to gain more insight into these parameters. Isothermal, dynamic and temperature-modulated DSC measurements are performed. The isothermal measurements are performed according to ASTM E2070-13 [65]. The temperature-modulated DSC measurements are performed according to ASTM E2602-22 [66]. The dynamical measurements are performed according to ASTM 2160-04 [67]. This heat of the reaction is measured based on the linear baseline for integration. This measurement is performed in an analytical script in Python. The T_g is measured with the analytical tool of the software TRIOS. The details of these measurements are explained in section 4.3. The python script will determine the parameters of these models based on the measured data.

Kamal cure kinetics model

A curing model can describe the rate of cure. The cure rate is expressed as a product of a term depending on the temperature and a term depending on the degree of cure. This is shown in Equation 4.1.

$$\frac{d\alpha}{dt} = K(T) * G(\alpha) \tag{4.1}$$

One of the most widely used models is the so-called Kamal model [68]. This model is shown in Equation 4.2.

$$\frac{d\alpha}{dt} = (K_1 + K_2\alpha^m)(1-\alpha)^n \tag{4.2}$$

K_1 and K_2 are rate constants, and m and n are the reaction constants. There are multiple methods to determine the parameters of the Kamal model. Commonly used methods are curve fitting, and a graphic analytical method described by [69]. Both methods will be used in this thesis. The most accurate parameters are used in the next steps of this thesis.

Gelation
The gel point is the degree of cure, a point in the reaction where individual molecules form a single macroscopic molecule. This effect is caused by chemical crosslinking. In other words, the system loses its fluidity, and the viscosity becomes large. A sudden increase in viscosity can recognize this. The interdiffusion between a thermoset and thermoplastic polymer is described in the literature. During the curing, the liquid reactive thermoset monomers diffuse into the glassy thermoplastic polymer matrix. As a result of this process, the thermoplastic chains are dispersed into the thermoset resin. Once the gel point is reached, the mobility of the thermoset resin increases. Due to this limited mobility, the interdiffusion tends to slow down and stop around the gel point. However, a study by Farooq et al. reports a considerable diffusion distance at a degree of cure higher than the gelation point [44]. This is reported at temperatures +/- 180 °C.

The degree of cure where gelation occurs is not explicitly given by the manufacturer. However, the gel curve is given. The gel time for each isothermal curing temperature is given in the data sheets. This is used as input. A python script is written to analyse the gel point, found in the appendix section G.7. In this script, the cure kinetic model described in chapter 4 is used to analyse the gel point.

4.2. Sample preparation and material definition

In this section, the material is defined, and the sample preparation is described.

Material definition
In this version, the material will not be called by name due to confidentiality. The resin will be called the epoxy thermoset resin.

Sample preparation
This section describes the sample preparation for the DSC. The ASTM standards mentioned in section 4.1 are used as a guideline. The TA DSC250 is used for the DSC measurements. The nitrogen flow rate is 50 mL/min.

- Material is stored in the freezer in the DASML Lab at the aerospace faculty at -17 °C.
- Resin is scraped away from the edge of the bi-axe prepreg. At the edges, there is neat resin without fibres.
- TA standard sample plans and lids are being used.
- Weight of the test specimens is between 2-3 mg.
- Make an empty sample pan as a reference pan
- Open DSC Chamber and load the specimen and reference specimen.

When the sample pan is ready, the measurement can start. Three types of measurements will be performed. The procedure and goal of each measurement will be explained below. The results of the measurements will be discussed in section 4.3. Pre-heat the DSC chamber for the isothermal measurements. Via this manner, the chance of losing data in the first seconds of the measurement gets minimized.

Isothermal measurements
An isothermal measurement is where the test specimens are held at a constant temperature in a differential scanning calorimeter throughout an exothermic reaction. During this measurement, the heat of the reaction is measured over time. Integrating this heat flow as a function of time will result in the total heat of the reaction. For this isothermal measurement, ASTM E2070-13 is consulted [65]. The measurement analysis will be discussed in section 4.3.

- First an isothermal run at 105,115,125 and 135 °C. According to the datasheet, 60 minutes at 135°C leads to a fully cured sample. Every decrease of 10 degrees requires a doubling in curing time to ensure the exothermic reaction is finished. So for 125 °C 120 minutes, 115 °C 240 minutes and 105 °C 480 minutes.
- Plot the heat flow versus the reaction time and construct a baseline to get the exothermic heat of the reaction. Next is to integrate the area as a function of time, bounded by the base thermal curve and the baseline:

$$\Delta H_{\text{iso}} = \int_0^{t_c} \frac{dH}{dt} \tag{4.3}$$

- Perform a dynamical heat run with the same sample from 0-300 °C with 10 °C / min. The goal is to get the residual heat of the reaction: ΔH_{tot}
- Adding these two values gives the total heat of the reaction

$$\Delta H_{\text{tot}} = \Delta H_{\text{iso}} + \Delta H_{\text{res}} \tag{4.4}$$

Dynamical measurements
A dynamical measurement is a measurement where the test specimens are heated in a differential scanning calorimeter at a dynamic rate through a temperature region where a chemical reaction takes place. During this measurement, the heat of the reaction is measured over time. Integrating this heat flow as a function of time will result in the total heat of the reaction. This method is used to determine the degree of crystallization of the sample. The comparison will be made between a 100 % cured sample. The fraction of released heat will be compared to the ultimate heat of a fully cured sample to determine the degree of crystallization. For the dynamical measurements, ASTM 2160-04 is consulted [67].

- Set the temperature at -20 °C and hold isothermal for 1 minute to ensure the starting temperature is equal in the sample pan.
- Heat cycles from -20 °C to 300 °C are completed. With a heat rate of 1, 2.5, 5 and 10 °C / min.
- Python software measures the dynamic heat of the reaction. Construct a baseline to get the exothermic heat of the reaction. Next is to integrate the area as a function of time, bounded by the base thermal curve and the baseline

$$\Delta H = \int_0^{t_c} \frac{dH}{dt} \tag{4.5}$$

- Highest total will be used for ΔH_{ult}
- Make an evolution of the degree of cure

$$\alpha = \frac{\int_0^t \frac{dH}{dt}}{\Delta H_{\text{ult}}} \tag{4.6}$$

Temperature modulated measurements (MTDSC)
A temperature-modulated measurement is a variation of the regular DSC measurements. This type of measurement is used to determine the glass transition temperature. In a regular measurement, it is complicated to measure the glass transition when an exothermic reaction occurs near the glass transition. A temperature-modulated heat run modulates the temperature. For example, every 15 seconds with 0.5 degrees °Celcius while performing a regular dynamical heat rate of 10 °C / minute. In MTDSC, the measured heat flow can be separated into a non-reversing and reversing heat flow. The reversing heat flow is used to detect the glass transition temperature (due to a step-wise change in the heat capacity). The non-reversible heat flow allows measuring the exothermic heat of the reaction. The temperature-modulated DSC measurements are performed according to ASTM E2602-22. [66]. The MTDSC measures the glass transition temperature of the resin.

- Initiate the sample pan at -20 °C, isothermal for 1 minute. Heat to 300 °C with a heating rate of 5 °C / min with modulation of $\pm$ 0.3 °C every 15 seconds.
- Prepare a plot with the non-reversible and reversible heat flow versus the average sample temperature in the TRIOS software. The sigmoidal step change in the reversing heat flow signal can indicate the glass transition. The inflexion point on this curve can be taken as the Glass transition temperature.
- The exothermic peak of the non-reversible heat flow is measured. Construct a baseline to get the exothermic heat of the reaction. Next is to integrate the area as a function of time, bounded by the base thermal curve and the baseline

$$\alpha = 1 - \frac{\Delta H_{\text{res}}}{\Delta H_{\text{ult}}} \tag{4.7}$$

4.3. Measurements

The isothermal, dynamical and temperature-modulated measurements described in section 4.2 are performed. The data from these measurements are analysed in python and with the TRIOS software. This analysis and the parameters gained from these analyses are described in this chapter. The isothermal and dynamical heat measurements are used to determine the parameters for the cure kinetic model. During this study, the DSC machine broke down at the DASML lab. Therefore, not all measurements at 105 °C could have been performed. However, this is discussed with my daily supervisor.

4.3.1. Temperature modulated DSC

To find the optimum degree of cure for the partially cured samples, it is important to gain an insight into the evolution of the glass transition temperature,T_g, as a function of the degree of cure, α. A partially cured sample is free-standing when the curing temperature is lower than the glass transition temperature. If the glass transition temperature stays below the curing temperature, the resin can flow. According to the literature study, Figure 2.6.1, the DiBenedetto model gives an accurate representation of this evolution. In Figure 2.6.1, the physical reasoning behind this process is addressed. Due to the conversion, the mobility of the chains decreases, the more energy is needed to make the chains ”free to flow” Therefore, the glass transition temperature increases as a result of the increasing degree of cure. The model is described in Equation 4.8:

$$T_g = T_{g0} + \frac{(T_{g\infty} - T_{g0})\,\lambda\alpha}{1 - (1-\lambda)\alpha} \tag{4.8}$$

Lambda, λ, is the parameter determined using the least-squares fit method with measured data. T_{g0} is the glass transition temperature of the uncured resin and $T_{g\infty}$ is the glass transition temperature of fully cured resin. Both will be measured with the MTDSC measurements. The samples used for the input data are cured to various known degrees of cure.

In Figure 4.1, one of the analyses of a temperature-modulated measurement is shown. The glass transition temperature is (roughly) at the same point as where the exothermic heat reaction starts. This shows the need for a visualization of the non-reversing and reversing heat flow instead of a regular heat flow. The inflexion point at the reversing heat flow gives the glass transition temperature, indicated in green. The integration of the exothermic peak of the non-reversing heat flow gives the value of the residual heat, indicated in blue. Using Equation 4.7 will result in the actual degree of cure. The measured T_G and degree of cure are represented in Figure 4.2. The figures from these measurements can be found in appendix section C.1. The data in Figure 4.2 will be used in section 4.4 to derive the parameter λ for the DiBenedetto model.

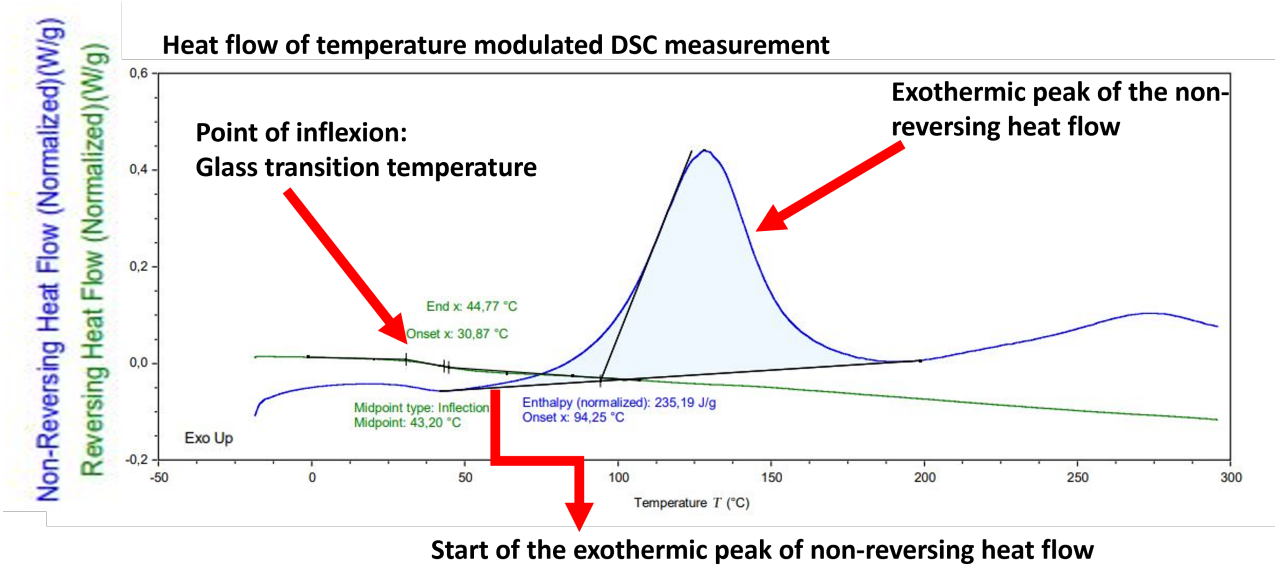


Figure 4.1: A typical result of temperature modulated DSC measurements analysed with the TRIOS software. Glass transition is determined with the reversing, and the exothermic heat flow is determined with the non-reversing heat flow. The start of the exothermic peak is close to the glass transition temperature.

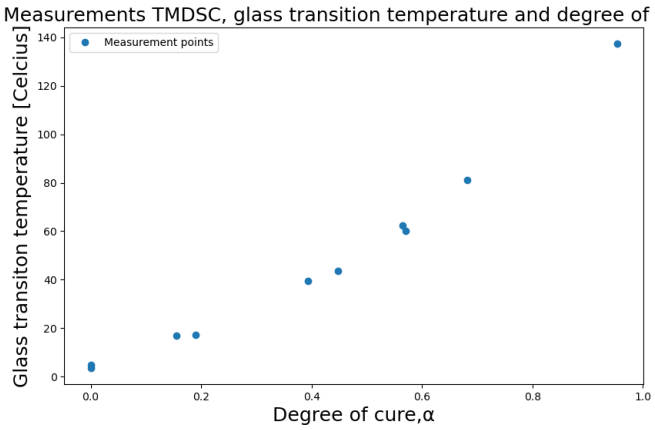


Figure 4.2: Measurements temperature modulated DSC. The glass transition temperature and the measured degree of cure are reported for the samples.

4.3.2. Determination of ΔH_{ult} and analysis of ramp cure at different heating rates

The dynamical measurements are performed with four different types of dynamical heating rates. 1, 2.5,5 and 10 °C/minute. This will be in the temperature range from -20 to 300 °C. The heat flow will be measured over time and imported into python. The analytical code will construct a baseline between the point before and after the exothermic reaction, according to section 9 of the ASTM standard [67]. This code can be found in appendix section G.1. The area bounded between the thermal curve, and the baseline can be recorded as the area of the heat of the reaction. The measured heat is normalized, which means the heat flow is divided by the weight of the sample. Three measurements are performed for each heating rate. The total heat of the exothermic reaction was the average value of the three highest measurements of ΔH. An illustration of the analysis of a sample is shown in Figure 4.3. This sample has a heating rate of 5 °C/min. The blue shaded between the curve, and the baseline is the normalized heat of the reaction. The results of all the other samples can be found in appendix section C.2.

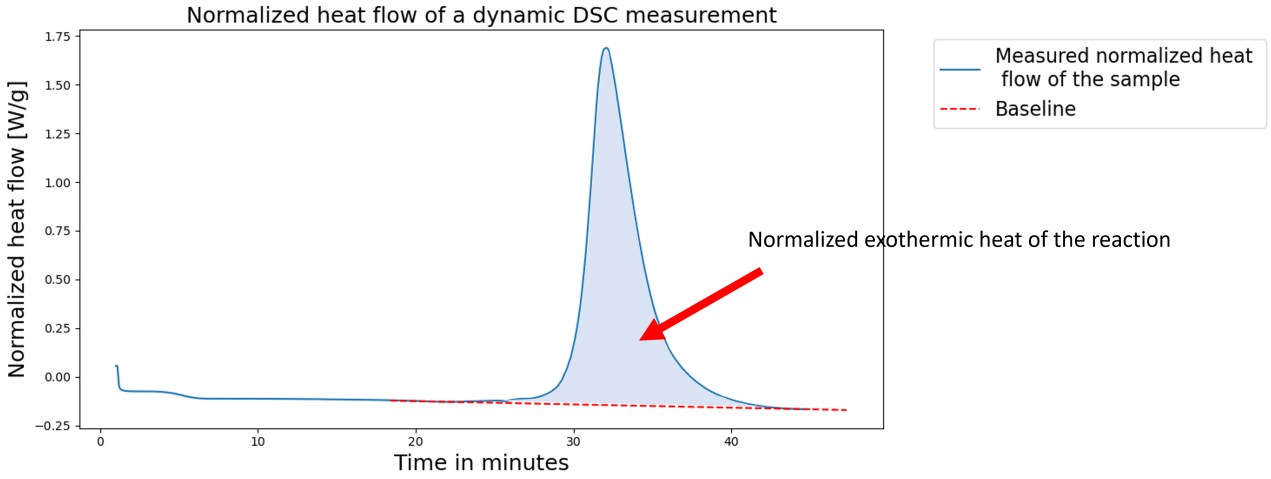


Figure 4.3: Normalized heat flow. This sample is heated with 5 °C /min. The blue-shaded area between the curve and baseline is the normalized heat of the reaction.

In Figure 4.4, each heating rate's average and standard deviation normalized heat flow is shown. The standard deviation is too small to observe at this scale. The arrow indicates the direction of the trend. The higher the heating rate, the shorter the curing time, and the higher the peak. The reactions with higher heating rates occur in a shorter time than the lower heat rates. The average and the standard deviation for each heating rate are represented in Table 4.1. The ultimate heating rate, ΔH_{ult}, is 426.5 J/g with a standard deviation of 0.70 J/g. The higher standard deviation for 2.5 °C/min can be explained by measuring inaccuracies of the weight: the samples weigh 2 and 3 mg. Human error can influence the normalized heat flow.

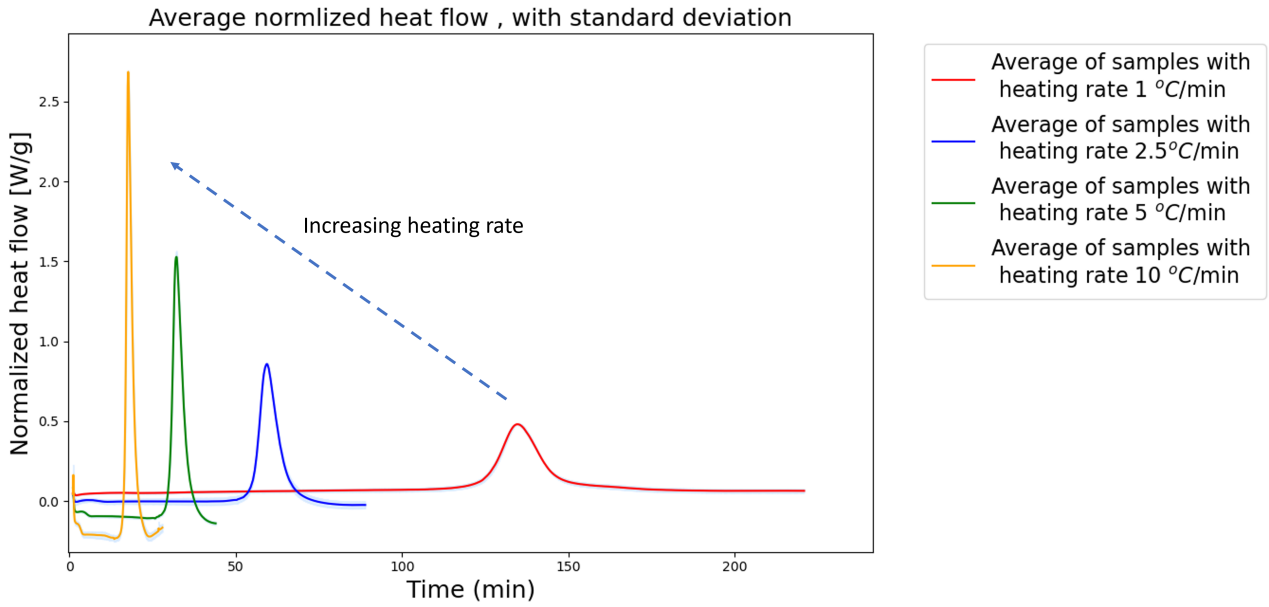


Figure 4.4: Dynamical measurements, the average and standard deviation for each heating rate. The higher the heating rate, the shorter the curing time and the higher the peak of the heat flow. The blue arrow shows this trend.

Table 4.1: Reaction enthalpy, mean and standard deviation

Heating Rate [°C/ min]	Reaction enthalpy, ΔH_{dyn} [J/g]
1	426.5 ± 0.7
2.5	387.3 ± 8.2
5	383.9 ± 2.2
10	377.6 ± 2.8

The evolution and the final degree of cure at each heating rate can be derived based on section 9 of ASTM standard 2160 [67].

$$\Delta H = \int_0^{t_c} \frac{dH}{dt} \tag{4.9}$$

Where the degree of cure is:

$$\alpha = \frac{\int_0^t \frac{dH}{dt}}{\Delta H_{\text{ult}}} \tag{4.10}$$

Applying Equation 4.10 on the measured data results in Figure 4.5. Here the average and standard deviation of the evaluation of each dynamic heating rate is displayed. An increased heating rate results in a sharper peak which occurs sooner than the slower heating rates. Therefore the trend is as expected. The higher the heating rate, the sooner the curing starts. To indicate this trend, a blue arrow is placed in Figure 4.5. At high heating rates, the reactions do not proceed to completion. The curing rate is too rapid, causing the mobility to be lost due to vitrification before all reactions occur. This results in fewer thermal effects and, therefore, less energy is released. Resulting in a lower enthalpy and a lower final degree of cure.

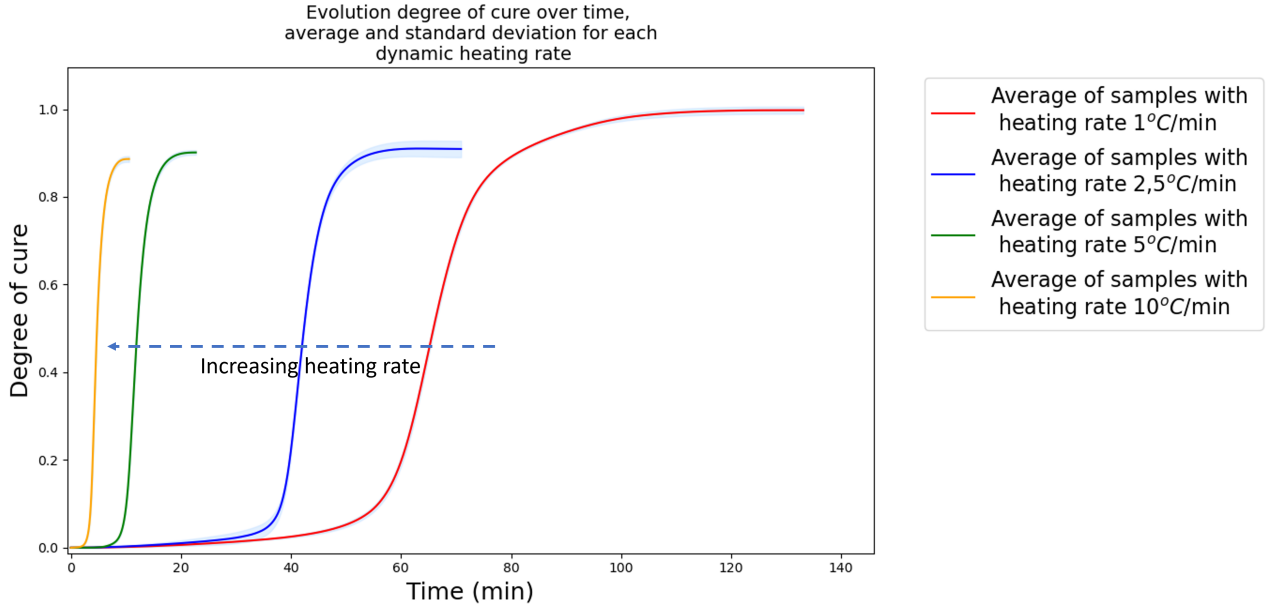


Figure 4.5: Dynamical measurements, evolution degree of cure over time, the average and standard deviation for each heating rate. The higher the heating rate, the sooner the heating occurs. The blue arrow shows this trend.

4.3.3. Cure kinetic model

Isothermal measurements are used to determine the parameters for the cure kinetics models. The furnace is preheated to avoid data loss during the DSC machine's stabilisation period. The prescribed isothermal curing temperature is 135 °C for 60 minutes. The samples are tested at 135,125,115 and 105 °C—four samples per isothermal temperature. At the end of each run, the sample is quenched to zero degrees Celcius. A second dynamical heat run from 0 to 300 °C with a heating rate of 10 °C is performed to obtain the residual heat of the reaction, ΔH_{res}. The procedure described in ASTM E2070 is consulted [65].

The heat flow of a sample cured at 105 °C is shown in Figure 4.7. The normalized heat flow of the curing reaction is indicated with the blue shaded area. This is the area between the curve and the baseline. A horizontal baseline is constructed between the start and end of the exothermic reaction. The end of the reaction is marked as the last measurement point. At this point, the baseline is horizontal. This concludes that the reaction is finished at this measurement point. The individual results of the other samples can be found in appendix section C.3.

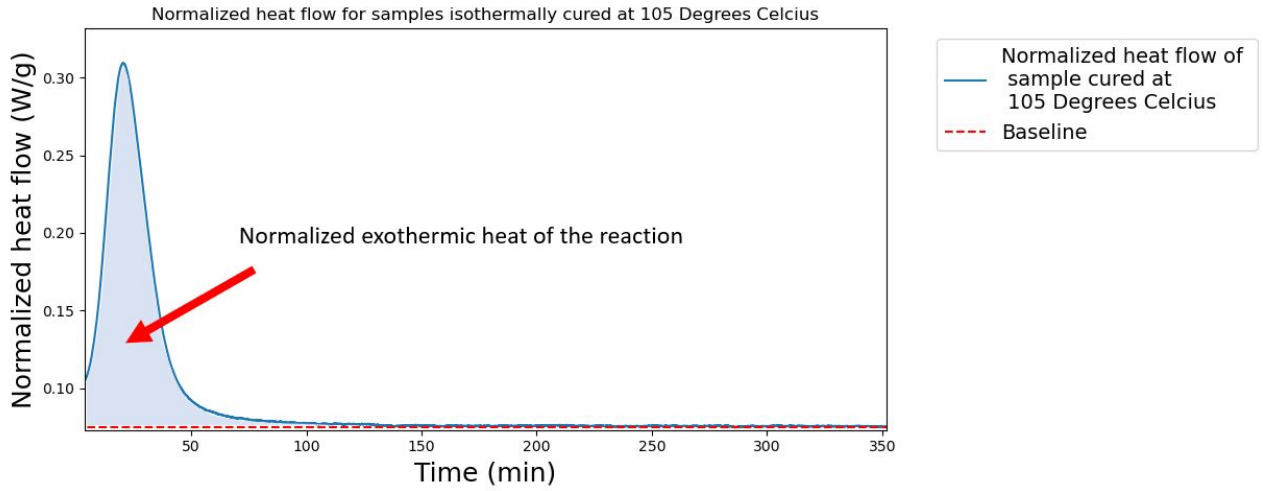


Figure 4.6: Normalized heat flow. Isothermal measurement at 105 °C. The blue-shaded area between the curve and baseline is the normalized heat of the reaction.

The average heat flow of the four measurements at each isothermal temperature are shown in Figure 4.7. A trend becomes visible, the higher the isothermal curing temperature, the higher the reaction rate. This results in a narrower reaction peak with a decreasing reaction time. This trend is indicated in the direction of the blue arrow. In Figure 4.7, the limit of the x-axis is from 0 to 7000 seconds, which is 115 minutes. In reality, the samples at 105 degrees require a longer time to end the reaction. However, with the x-axis on the full scale, the data will not be readable anymore and, therefore, will not be informative. The code used to analyse the data can be found in appendix section G.2, which is used to analyse the 135 temperature. The code for the different temperatures is identical.

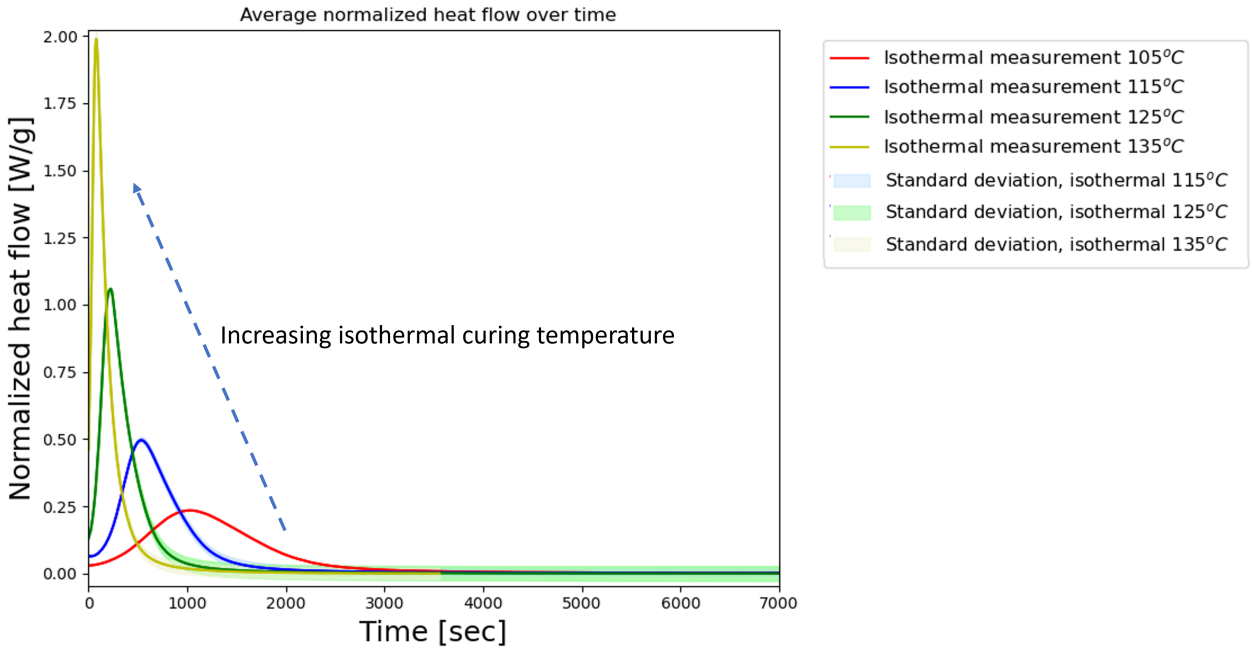


Figure 4.7: Results of isothermal curing at 105,115,125 and 135 °C. For each temperature, four samples are made and measured. The mean heat flow at each isothermal heat flow is shown. The blue arrow indicates the trend. The higher the isothermal curing temperature, the higher the heat flow peak and the shorter the curing time.

The total heat of the exothermic reaction is measured for each isothermal curing temperature. Equation 4.10 gives insight into the total degree of cure and the evolution of the degree of cure. The individual results of each measurement are used as input, Figure C.3. In Figure 4.8, this evolution is represented. This shows an

expected result, at each isothermal temperature, there is a convergence to a maximum degree of cure, α_{max}. The higher the curing temperature, the higher this degree of cure and the sooner the reaction occurs. This is indicated with the blue arrow. The glass transition temperature increases while the degree of cure increases. In other words, a growing polymer network causes the glass transition temperature to rise. When the glass transition temperature reaches the curing temperature, vitrification occurs in the vitrified state the reaction rate decreases. This is due to the change in reaction. Before vitrification occurs, the reaction is chemically controlled. This changes to diffusion controlled after vitrification. This causes the α_{max} to be lower at lower isothermal temperatures. The curing temperature is lower; therefore, the glass transition temperature reaches the curing temperature at a lower degree of cure than higher isothermal curing temperatures. This slows the reaction and makes the degree of cure converge to α_{max}, which does not allow for 100% curing.

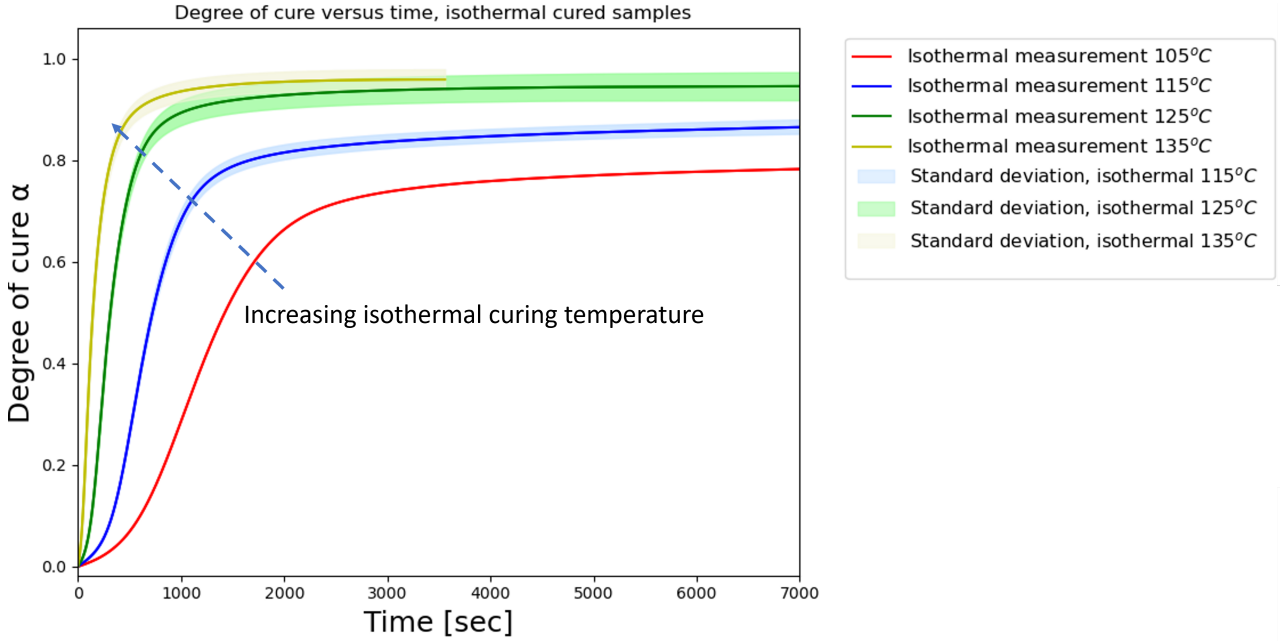


Figure 4.8: Evolution of the degree of cure over time. The mean of each isothermal temperature is shown. The blue arrow indicates the trend. The higher the isothermal curing temperature, the sooner the reaction occurs and the higher the final degree of cure.

The literature study concludes that there is a relationship between the maximum degree of cure and the curing temperature. $\alpha_max(T)$ can be written as a function of the Curing temperature T_c. The Dibenedetto model is used. Instead of relating T_g with α, T_c is related with α_{max}. This is achieved by solving α_{max}=α for $T_g = T_c$ in Equation 4.8. This results in Equation 4.11. The measured maximum degree of cure at each isothermal temperature is listed in Table 4.2. The parameter μ is fitted using a sum of least squares fit. The parameter μ is 0.547.

$$\alpha_{\text{max}}(T) = \frac{(T_{\text{c}} - T_{\text{g0}})}{(T_{\text{g}_\infty} - T_{\text{g0}})\,\mu + (1-\mu)\,(T_{\text{c}} - T_{\text{g0}})} \tag{4.11}$$

$$\mu - Adjustable\ parameter$$
$$T_c - Curing\ temperature$$

The samples of the isothermal measurements are cooled to 0 °, and a second measurement is performed. This is a dynamic measurement at 10 °C/min from 0 to 300 °C. This measurement obtains the residual heat of the reactions of the samples cured at isothermal temperatures. This residual heat is caused by the limited degree of cure due to vitrification, explained above. The total heat of the reaction is calculated using Equation 4.4. In Figure 4.9, a measurement is shown of a sample initially cured at 105 °C. The residual heat is released; this is the area between the curve and the baseline. The samples' measurements' results can be found in the appendix section C.4, and the python code used to analyse the data in appendix section G.4. The average residual heat of each isothermal curing temperature is listed in Table 4.2. The higher the initial curing temperature, the lower the residual heat.

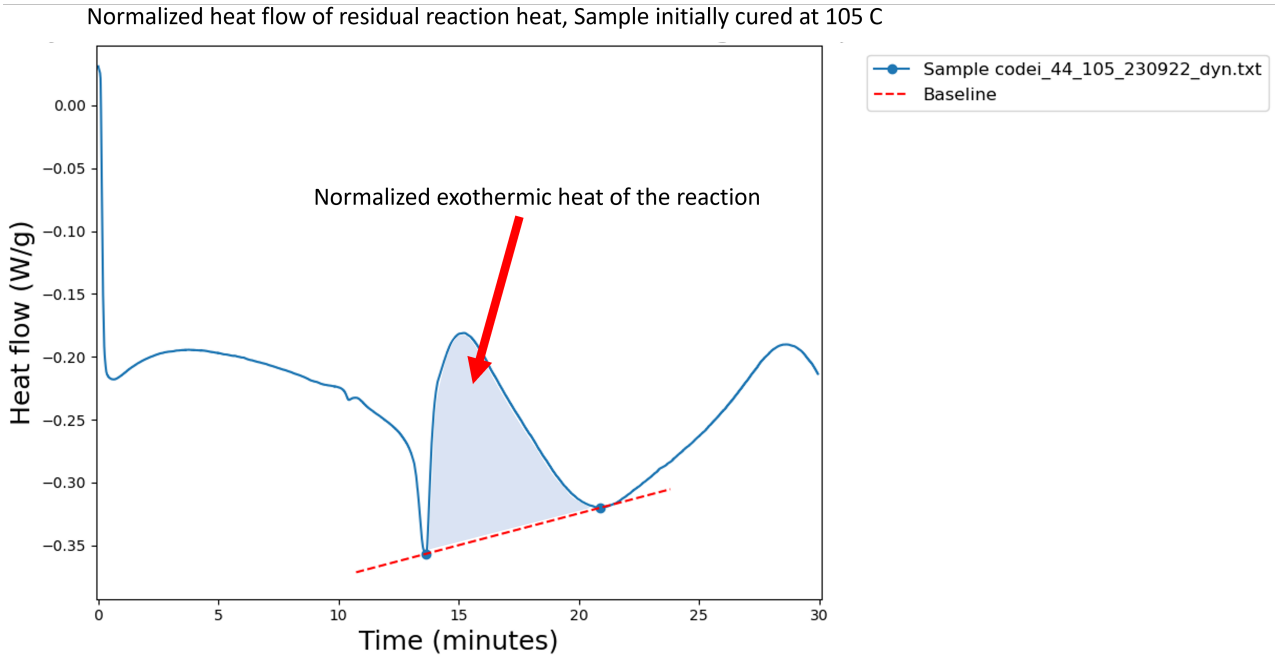


Figure 4.9: Normalized residual heat of a sample initially isothermal cured at 105 °C. The area determines the heat in between the curve and the baseline.

Table 4.2: Maximum degree of cure at each isothermal temperature, reaction enthalpy and residual reaction heat. Average and standard deviation.

T_c [°C]	degree of curemax	ΔH_{iso} [J/g]	ΔH_{res}[J/g]
135	0.97 $\pm$ 0.02	408.2 $\pm$ 7.3	0.2 $\pm$ 0.1
125	0.94 $\pm$0.02	397.8 $\pm$ 7.8	4.6 $\pm$ 3.9
115	0.90 $\pm$ 0.13	374.9 $\pm$ 6.5	13.9 $\pm$ 3.9
105	0.82 $\pm$ 0	350.6 $\pm$ 0	37.9 $\pm$ 0

The parameters of the cure kinetic model can be derived from the measurements described above. This is a model to describe the reaction rate as a function of the degree and cure.

$$\frac{d\alpha}{dt} = F(\alpha, T) \tag{4.12}$$

$F(\alpha, T)$ can be split up into two parts. A part "K" is a function of T, and a part "G" is a function of α. In other words, the rate of the degree of cure is dependent on a part which is variable to the temperature and a part which is variable to the degree of cure.

$$\frac{d\alpha}{dt} = K(T)G(\alpha) \tag{4.13}$$

Bailleul model

According to the literature review, Figure 2.6.1, the Bailleul model describes the cure kinetics of epoxy. The parameters of this model will be derived for the epoxy resin of Hall Spars. Bailleul et al. describe the reaction rate as a function of the temperature and degree of cure [70]. In the literature section, Figure 2.6.1, the model is explained in detail. The model is represented in Equation 4.14.

$$\frac{d\alpha}{dt} = k_1 e^{-E_1\left(\frac{T_{ref}}{T}-1\right)} \cdot \sum_{i=0}^{m} a_1 \alpha^i \left(\alpha_{\max}(T) - \alpha\right)^n \tag{4.14}$$

$E_1 - Activation\ energy$
$T_{ref} - Arbitrary\ temperature\ in\ operating\ range$
$n - Reaction\ component$
$\frac{d\alpha}{dt} - Curing\ rate$
$k1 - Frequency\ Factor$
$\alpha_max(T) - Maximum\ degree\ of\ cure\ for\ the\ isothermal\ temperature\ T$
$a_1 - parameter$

The parameters of the Bailleul model are derived by combining the methods described by Bailleul et al. and Keller et al. [70] [71]. $\alpha_{max}(T)$ is described with equation Equation 4.11 where μ is 0.614. $G(\alpha)$ is a polynomial function with an order m. The first step is normalising the polynomial term to 1 at the maximum reaction rate. The reaction rate at this point can be modelled by Equation 4.15. The reference temperature is set at 400 K. For this model, the mean of the data of each isothermal curing temperature is used.

$$\frac{d\alpha}{dt} = k_1 e^{-E_1\left(\frac{T_{ref}}{T}-1\right)} \cdot 1 \tag{4.15}$$

The natural logarithm of Equation 4.15 results in a linear function Equation 4.16. In other words: a straight line with the slope $-E_1$ with the origin $ln(k_{ref})$. For each isothermal curing temperature, the maximum $\frac{d\alpha}{dt}$ is measured. A plot of this maximum at each isothermal curing temperature is represented in Figure 4.10.

$$ln(K(T)) = ln(k_1) + -E_1 * \left(\frac{T_{ref}}{T} - 1\right) \tag{4.16}$$

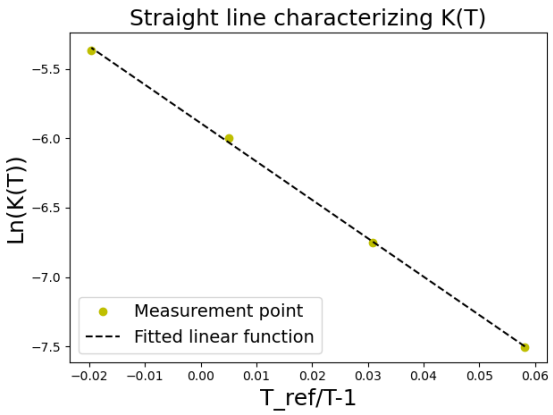


Figure 4.10: Linear slope to characterise parameters for K(T). Equation 4.15 fitted through the measurement points.

The temperature dependency kinetics can now be determined. This results in the following Arrhenius terms:

- k_1 = 0.00277 s^{-1}
- E_1 = 27.626

Combining the Arrhenius terms k_1 and E_1 with the measured $\frac{\mathrm{d}\alpha}{\mathrm{d}t}$ determines the polynomial term G. This is achieved with Equation 4.17. The term G is determined for each isothermal curing temperature; this is displayed in Figure 4.11.

$$\frac{\frac{\mathrm{d}\alpha}{\mathrm{d}t}}{k_1 \mathrm{e}^{\left(-E_1\left(\frac{T_{\mathrm{ref}}}{T}-1\right)\right)}} = \sum_{i=0}^{m} G_i \alpha^i \left(\alpha_{\mathrm{max}}(T) - \alpha\right)^n \tag{4.17}$$

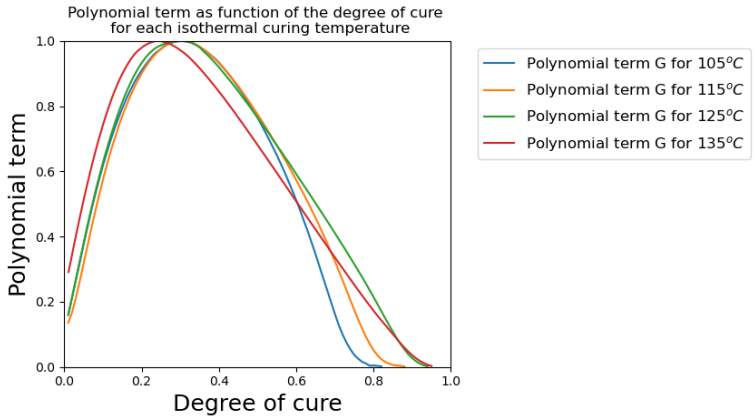


Figure 4.11: The polynomial term for each isothermal curing temperature as a function of the degree of cure

Combining the data of these four isothermal curing temperatures yields a value for G at each available point (at each degree of cure). A polynomial function with m=5 is created based on this data. Note: every isothermal data set temperature must provide equal data points. The lower temperatures would give more data points due to the longer curing time. This needs to be equalized before finding the polynomial terms. The polynomial function is displayed in Figure 4.12 with all the data points G at each degree of cure. The polynomial terms are:

- $G_1 = -1.600$
- $G_2 = 11.006$
- $G_3 = -16.460$
- $G_4 = 6.973$
- $G_5 = 0.0998$

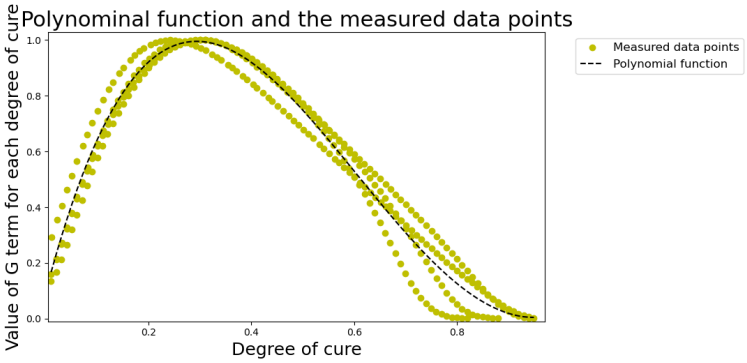


Figure 4.12: Derived polynomial term in python based on the measured data points at each degree of cure

The reaction component,n, in Equation 4.14 is optimized using a sum of least squares fit for the experimental measurements for each isothermal temperature. Analysing the optimised reaction component at each temperature shows that it is impossible to take n as a constant for all curing temperatures. Keller et al. solved this by making a linear relationship for n; this is shown in Equation 4.18 [71]. This results in n_s = -0.0164 and n_i = 2.163. The curing temperature is in Celcius in Equation 4.18. All the parameters for the Bailleul model are gathered. However, a cure kinetic model simplifies the real curing reaction. The cure kinetic model is the most important model in this study. A second common cure kinetic model will be evaluated. An educated guess for the most suitable model will be made later in this work. The python code for deriving the Bailleul model parameters can be found in Appendix section G.5.

$$n = n_s * T_c + n_i \tag{4.18}$$

Kamal model

A second curing model which will be evaluated for the currently used epoxy resin system for Hall spars is called the Kamal model. Among epoxy systems, the Kamal model is one of the most widely used curing models [68]. The model is represented at the beginning of this chapter in Equation 4.2. In this model, the rate of the curing of the reaction is expressed by two terms. A term dependent on the Temperature, $K(T)$, and a term dependent on the degree of cure, $f(\alpha)$. The Kamal model is repeated below in Equation 4.19

$$\frac{d\alpha}{dt} = (K_1 + K_2\alpha^m)(1-\alpha)^n \tag{4.19}$$

As stated before, K_1 and K_2 are temperature-dependent constants, and m and n are the reaction constants. The kamal model represented in Equation 4.19 will be adjusted. In the term $(1-\alpha)^n$ 1 will be replaced with $\alpha_{max}(T)$. This results in $(\alpha_{max}(T)-\alpha)^n$. Using $\alpha_{max}(T)$ considers the maximum achievable degree of cure at an isothermal cure temperature. This phenomenon is explained in Figure 2.6.1. This is shown in Equation 4.20.

$$\frac{d\alpha}{dt} = (K_1 + K_2\alpha^m)(\alpha_{max}(T)-\alpha)^n \tag{4.20}$$

The constants K_1 and K_2 in Equation 4.20 are Arrhenius temperature dependent. Combining this with Equation 4.20 results in Equation 4.21. Note that T is in Kelvin. The constant E is the activation energy divided by the gas constant; k_1 and k_2 are pre-exponential factors. [1/s]

$$\frac{d\alpha}{dt} = \left(k_1 \cdot e^{-\left(\frac{E_1}{T}\right)} + k_2 \cdot e^{-\left(\frac{E_2}{T}\right)} \cdot \alpha^m\right) \cdot (\alpha_{\text{max}}(T)-\alpha)^n \tag{4.21}$$

The aim is to determine the 6 Kamal model parameters: k_1, k_2, E_1, E_2, m and n and m combine this with the function for α_{max}. To determine these parameters, the temperature-dependent parameters $K1$ and $K2$ and n,m is needed for each measured isothermal curing temperature, 135,125,115 and 105 °C. According to the literature, there are several ways to determine these parameters. The most common methods are the curve fitting model, and a graphic analytical method described by [69]. Both methods will be used in this thesis, and the most accurate parameters will be used in the rest of this study.

Graphic-analytical method to derive parameters Kamal model

The first method used in this work is the graphic-analytical method. This method is described by Kenny et al. [69]. In this method, the constant, K_1, is assumed to be the initial reaction rate. This initial reaction rate is the reaction rate at $\alpha = 0$. This can be derived by taking the intercept of the reaction rate with the y-axis (at t=0) in Figure 4.13. These points are indicated with the dots in Figure 4.13. The K_1 parameters are listed in Table 4.3.

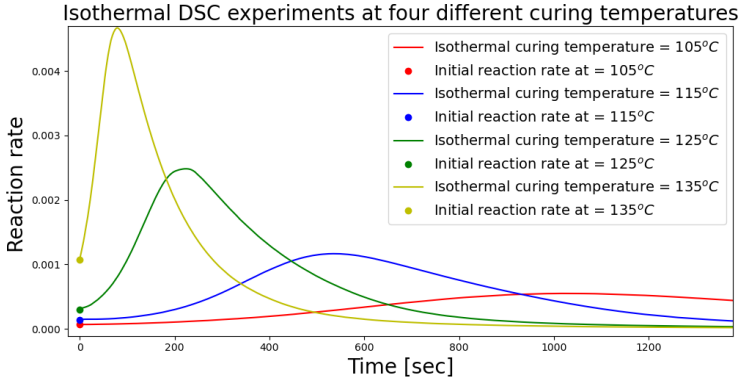


Figure 4.13: The intercept of the reaction rate with the y-axis for each curing temperature results in K_1, indicated with the dots.

Modifying Equation 4.19 results in Equation 4.22. This equation represents $ln(\frac{d\alpha}{dt})$ as function of $ln(1-\alpha)$ with the variable n and the constant $ln(K_1 + K_2 * \alpha^m)$. According to Kenny et al., a linear behaviour is observed when α approaches 1. **However, it is observed that the epoxy used in this study will not always reach a convergence of 1 at every isothermal temperature. Therefore, 1 is replaced by $\alpha_{max}(T)$.** The slope

of the linear behaviour equals the parameter n. This is shown in Figure C.5a,Figure C.6a,Figure C.7a and Figure C.8a.

$$\ln(d\alpha/dt) = \ln\left(K_1 + K_2\alpha^{\mathbf{m}}\right) + \mathbf{n}\ln(\alpha_{max}(T) - \alpha) \tag{4.22}$$

The next step is to rearrange Equation 4.2 to Equation 4.23. The previously derived parameters K_1, n and the experimental results are used. This is shown in Figure C.5b,Figure C.6b,Figure C.7b and Figure C.8b. In this figure, a linear behaviour is observed in nearly the entire range. This result was to be expected according to [69].

$$\ln\left\{[(d\alpha/dt)/(\alpha_{max}(T) - \alpha)^{\mathbf{n}}] - K_1]\right\} = \ln K_2 + \mathbf{m}\ln\alpha \tag{4.23}$$

To optimize the result, the obtained parameters are used. Rearranging Equation 4.2 in Equation 4.24 allows proceeding with an iteration. Via this formula, a new term for n can be derived. The parameters K_2 and m result from Equation 4.23.

$$\ln(d\alpha/dt) - \ln\left(K_2\alpha^{\mathbf{m}} + K_1\right) = \mathbf{n}\ln(\alpha_{max}(T) - \alpha) \tag{4.24}$$

After recalculating the new value for n by obtaining the slope with Equation 4.24, n can be used to re-obtain the values K_2 and m. This should be repeated until n and m convergences. If both values are within 1% of the subsequent calculation, the iteration is stopped. According to Kenny et al., this convergence occurs within 2 to 3 iteration steps. The value of the difference between the iterations is calculated according to Equation 4.25

$$|\frac{Value_{new} - Value_{old}}{Value_{old}}| * 100\% \tag{4.25}$$

The graphical representations of the results of this method can be found in the appendix section C.5. The result of each iteration step is shown in Figure C.5, Figure C.6, Figure C.7 and Figure C.8. Three iterations are required to obtain values less than 1% between two subsequent calculations for the value n. For m, fewer iterations are required. However, the three iterations are performed since this is needed for the parameter n. The graphical representation of the final iteration for parameter n is shown in the appendix: Figure C.5c, Figure C.6c, Figure C.7c, and Figure C.8c. The graphical representation of the final iteration of the parameters K_2 and m are displayed in the appendix: Figure C.5d, Figure C.6d, Figure C.7d, and Figure C.8d. Convergence is achieved for all parameters. The final parameters n, m, K_1 and K_2 of each isothermal curing temperature are listed in Table 4.3.

Table 4.3: Parameters kamal model obtained with the graphical-analytical from isothermal cure performed with DSC.

T(K)	$K_1[1/s]$	$K_2[1/s]$	**n**	**m**
378	0.6901e-06	0.0094	2.693	1.520
388	0.0001	0.0202	2.330	1.629
398	0.0003	0.0240	1.997	1.290
408	0.0011	0.0313	1.517	1.095

***Curve fitting** method to derive parameters Kamal model*

The curve fitting can be used to derive the parameters k_1, k_2, E_1, E_2, m and n and m of the Kamal model. This is a second method; the first was the graphical analytical method. As mentioned before, the cure rate can be expressed by a term dependent on the temperature and a term dependent on the degree of cure. The term dependent on the temperature follows the Arrhenius dependency. The Kamal model, which will be curve fitted for the mean of each isothermal temperature, is given in Equation 4.26.

$$\frac{d\alpha}{dt} = \left(K_1 + K_2\alpha^m\right)(\alpha_{max}(T) - \alpha)^n \tag{4.26}$$

The python software used to determine the curve fits can be found in the appendix section G.6. The figures of the results of these curve fits are shown in the appendix section C.6. The function $scipy.optimize.curvefit$ is used. This function used non-linear least squares to fit a function, f, to data. The function pcov is used to determine the standard deviation of each parameter determined with the curve fitting method. The standard deviation of the parameter K_1 is for all temperatures in the order of magnitude 10^{-6}, K_2 = 10^{-5}, n= 10^{-3} and m= 10^{-3}.

Table 4.4: Parameters kamal model obtained with curve fitting from isothermal cure performed with DSC.

T(K)	$K_1[s^-1]$	$K_2[s^-1]$	n	m
378	0.1515e-3	0.0147	2.545	1.496
388	0.1410e-3	0.0128	1.922	1.151
398	0.1625e-3	0.0140	1.732	0.862
408	0.5328e-3	0.0193	1.756	0.686

At this point, the parameters of isothermal cure in the Kamal model are obtained according to two methods, the graphical-analytical method and the curve fitting method. The parameters of both methods will be used. In section 4.4, the most suitable method will be picked based on the least square method, and therefore the most suitable set of parameters will be made. The rate constants K_1 and K_2 in Equation 4.26 are Arrhenius temperature dependent. See Equation 4.27 and Equation 4.28. Note that T is in Kelvin. The constant E is the activation energy divided by the gas constant.

$$K_1 = k_1 * exp(\frac{-E_{K_1}}{T}) \tag{4.27}$$

$$K_2 = k_2 * exp(\frac{-E_{K_2}}{T}) \tag{4.28}$$

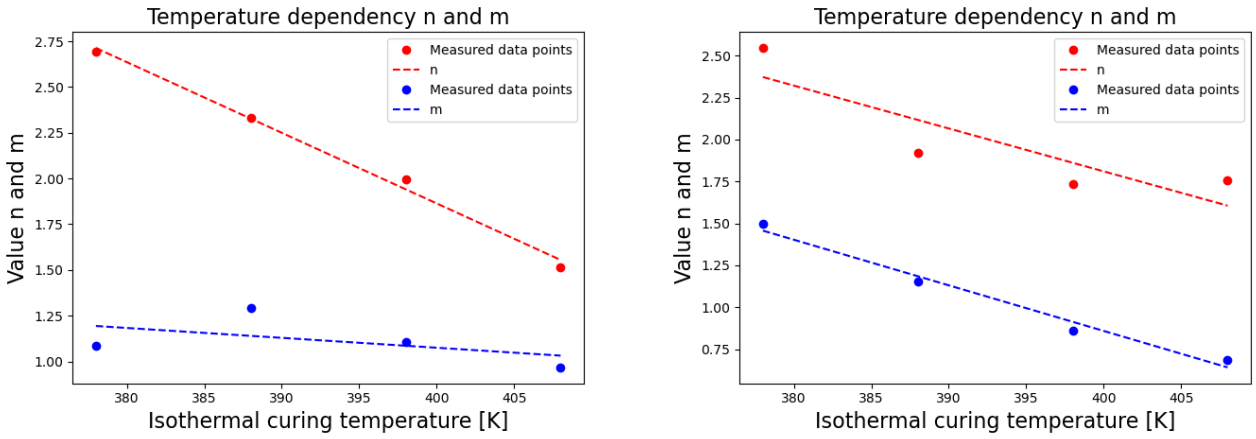
A temperature linear temperature dependency is observed for both n and m. n and m follow the relationships shown in Equation 4.29 and Equation 4.30. The values of these terms are summarised in Table 4.5. The graphical representation of these equations and the experimental data is displayed in Figure 4.14.

$$n = n_s * T_c + n_i \tag{4.29}$$

$$m = m_s * T_c + m_i \tag{4.30}$$

Table 4.5: Values for linear relationships n and m with the curing temperature, temperature in Kelvin.

Method	n_s	n_i	m_s	m_i
Graphical-analytical	-0.0386	17.310	-0.005	3.236
Curve fitting	-0.026	12.040	-0.027	11.730



(a) n and m of each isothermal curing temperature with parameters derived with graphical-analytical method

(b) n and m of each isothermal curing temperature with parameters derived with curve fitting method

Figure 4.14: Temperature dependency of the parameters n&m, parameters of graphical-analytical and curve fitting method are displayed. A linear relationship (dotted lines), Equation 4.29 and Equation 4.30 is fitted through the measurement points.

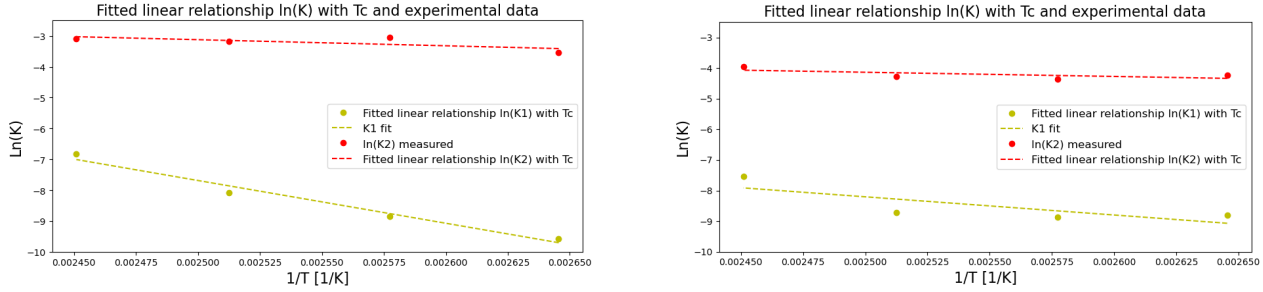
K_1 and K_2 were determined for each isothermal curing temperature based on the experimental data. Equation 4.27 and Equation 4.28 can be rewritten into Equation 4.31 and Equation 4.32. K_1 and K_2 are experimentally determined for each isothermal curing temperature via the two methods, graphical-analytical and curve fitting. The Kamal model parameters k_1 and E_1 are derived based on the linear relationships in Equation 4.31 and Equation 4.32 represented in Figure 4.15. The parameters are represented in Table 4.6

$$ln(K_1(T)) = ln(k_1) + -E_{K_1} * \left(\frac{1}{T}\right) \tag{4.31}$$

$$ln(K_2(T)) = ln(k_2) + -E_{K_2} * \left(\frac{1}{T}\right) \tag{4.32}$$

Table 4.6: Values for linear relationships n and m with the curing temperature [K]

Method	k_1	k_2	E_{K_1}	E_{K_2}
Graphical-analytical	524876603553.62445	6.193969249113078	13870.1198	5867.89
Curve fitting	767.1283	0.49434	5938.826	1372.481



(a) graphical-analytical method

(b) curve fitting method

Figure 4.15: Temperature dependency of the parameters n&m, parameters of graphical-analytical and curve fitting method are displayed

4.3.4. Avrami analysis

The change in kinetics from the chemically controlled to the diffusion-controlled stage explains why each isothermal curing temperature has a potential maximum degree of cure. The Avrami analysis provides useful information about these kinetics [68]. In the early curing stages, curing happens in a three-dimensional network. In other words, cross-links can form freely. This causes the crystallinity to increase. At some point, this increased crystallinity limits the growth of the cross-linked network, and cross-linking can only occur in restricted space. The Avrami equation can be used for isothermal curing and is given in Equation 4.33. The parameter b is a constant, and the parameter d is called the Avrami exponent. A change of the Avrami exponent, d, can be related to the change or reaction kinetics. In this study, this can be translated into the onset of the change from chemical to diffusion-controlled curing. To perform this analysis, Equation 4.33 needs to be rewritten into Equation 4.34. The Avrami plot is represented in Figure 4.16.

$$1 - \alpha = \exp\left(-bt^d\right) \tag{4.33}$$

$$\ln[-\ln(1-\alpha)] = \ln b + d \ln t \tag{4.34}$$

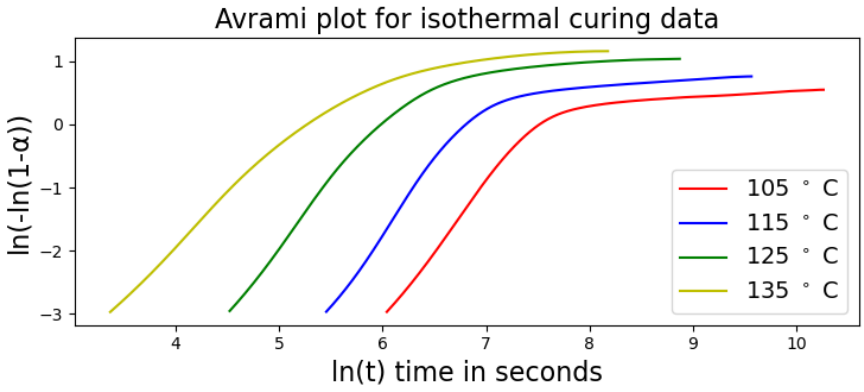


Figure 4.16: Avrami plot of the curing data for the isothermal curing temperatures 105,115,125 and 134 °C.

4.4. Results and discussion

In section 4.3 Isothermal, dynamical and temperature-modulated DSC measurements are performed. Based on these measurement parameters for the DiBenedetto, $\alpha_{max}(T)$ and cure kinetic models are derived. In this section, these models will be evaluated. All the derived parameters are listed in Table 4.7. The models will be evaluated based on the coefficient of determination. Also called R-squared R^2. This is a statistical measure to determine how well the model fits the data. This value ranges from 0-1. The closer to 1, the better the fit of the model.

Table 4.7: Parameters derived in section 4.3

Parameter	**Symbol**	**Unit**	**Value**
Di Benedetto			
Tg of uncured resin	T_{g0}	K	276.59
Tg of fully cured resin	$T_{g\,\text{inf}}$	K	411
Lambda	λ	-	0.5905
Alpha max			
Adjustable parameter	μ	-	0.547
Resin kinetics			
Reference temperature	T_{ref}	K	400
Ultimate reaction enthalpy	ΔH_{ult}	J/g	
Parameters Bailleul model:			
Activation energy	E_1	-	27.626
Frequency factor	k_1	s^-1	0.00277
Polynomial parameter	G_1	-	−1.584
Polynomial parameter	G_2	-	10.94
Polynomial parameter	G_3	-	−16.40
Polynomial parameter	G_4	-	6.962
Polynomial parameter	G_5	-	0.0998
Reaction exponent factor slope	n_s	-	-0.0164
Reaction exponent factor intercept	n_i	-	2.163
Parameters graphical-analytical for method Kamal model *:*			
Arrhenius term constant for K1	E_{K_1}	-	13870
Pre-exponential factor for K1	k_1	s^-1	524e9
Arrhenius term constant for K2	E_{K_2}	-	5867
Pre-exponential factor for K2	k_2	s^-1	6.19
Reaction n exponent factor slope	n_s	-	-0.0386
Reaction n exponent factor intercept	n_i	-	17.310
Reaction exponent m factor slope	m_s	-	-0.005

Reaction m exponent factor intercept	m_i	-	3.236
Parameters curve fitting for method Kamal model *:*			
Arrhenius term constant for K1	E_{K_1}	-	5938
Pre-exponential factor for K1	k_1	s^-1	767
Arrhenius term constant for K2	E_{K_2}	-	1372
Pre-exponential factor for K2	k_2	s^-1	0.49434
Reaction n exponent factor slope	n_s	-	-0.026
Reaction n exponent factor intercept	n_i	-	12.040
Reaction exponent m factor slope	m_s	-	-0.027
Reaction m exponent factor intercept	m_i	-	11.730

4.4.1. Di Benedetto

The Dibenedetto model is described with Equation 4.8. The parameter for the Dibenedetto model λ is 0.5905. This model is shown in Figure 4.17. The R^2 value of this model is 0.9918. This model agrees with the experimental data and will be used in this study.

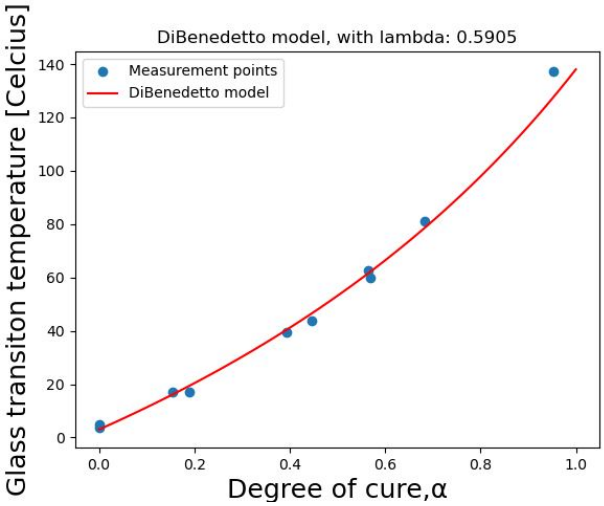


Figure 4.17: Result DiBenedetto model, lambda parameter is determined based on the least square method with the measurement points in the MTDSC. The model shows a good fit with the measurement points.

4.4.2. Model maximum degree of cure

The maximum degree of cure for an isothermal curing temperature is described with Equation 4.11 where μ is 0.547. This model is shown in Figure 4.18. The R^2 value of this model is 0.958. This model agrees with the experimental data and will therefore be used in this study. If the curing temperature reaches the glass transition temperature of the fully cured sample, the potential degree of cure reaches 1. For curing temperatures above $T_{g\infty}$ the maximum degree of cure remains 1. It physically is impossible to achieve $\alpha > 1$.

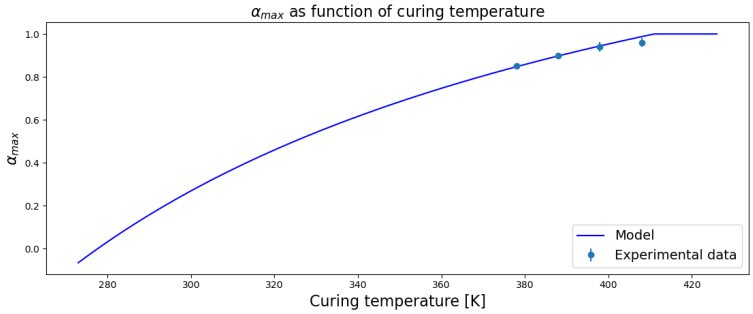


Figure 4.18: Result model for the maximum degree of cure, mu parameter is determined based on the least square method with the experimental data from isothermal curing. The mean of each T_c is used.

4.4.3. Curing model

Two curing models are introduced in this study, The Bailleul model and the Kamal model. The parameters are derived for both models in section 4.3. For the Kamal model, these parameters are derived in two methods. Therefore the Kamal model has two sets of parameters. In this section, these models will be evaluated to pick the most accurate curing model for the currently used resin.

Bailleul model

The first cure kinetic model is the Bailleul model. The parameters of this model are given in Table 4.7. In Figure 4.19, the results of the cure kinetic model for the isothermal curing temperatures are compared with the experimental data.

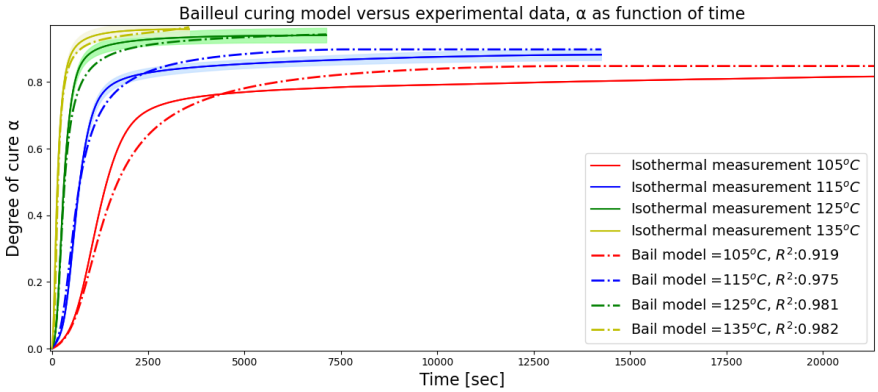


Figure 4.19: Result of the Bailleul model compared with experimental data at isothermal curing temperatures. The shaded area indicates the standard deviation of the experimental data. .

The results of the cure kinetic model for the dynamical curing rates are compared with the experimental data. This is shown in Figure 4.20.

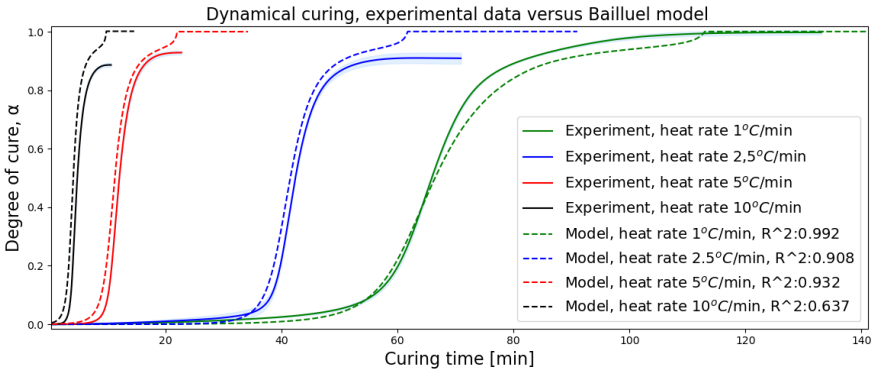


Figure 4.20: Result of the Bailleul model compared with experimental data at dynamical curing rates. The shaded area indicates the standard deviation of the experimental data.

Table 4.8: R^2 of the Bailleul model for the measured isothermal curing temperatures and different heating rates.

Isothermal temperature $[°C]$	R^2	**Dynamical heating rate** $[°C/min]$	R^2
105	0.919	1	0.992
115	0.975	2,5	0.908
125	0.981	5	0.932
135	0.982	10	0.637

- In Figure 4.20 an unexpected behaviour is spotted. In Figure 4.21, a zoomed-in representation of this effect is shown and marked in red Instead of converging to α_{max}, the degree of cure tends to increase. However, this effect can be explained by the method used to derive the Bailleul parameters.

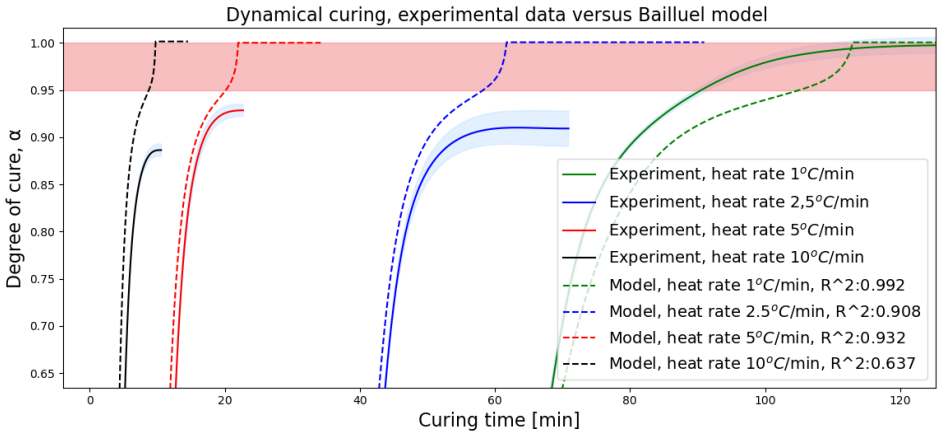


Figure 4.21: Zoomed-in representation of the unexpected behaviour with dynamical heating rates. The area of interest is marked in red.

- The Bailleul method has a polynomial term dependent on the degree of cure. The procedure of Bailleul et al. [70] has been followed. The isothermal curing data is used. However, the maximum measured degree of cure does not go to 1. There is no data available above α_{max} of 135 °C. In Figure 4.12 the polynomial as a function of the degree of cure in the range 0- α_{max} is given. In Figure 4.22 this effect is represented. The function increases once α exceeds α_{max} of 135 °C. This caused the deviation in Figure 4.21

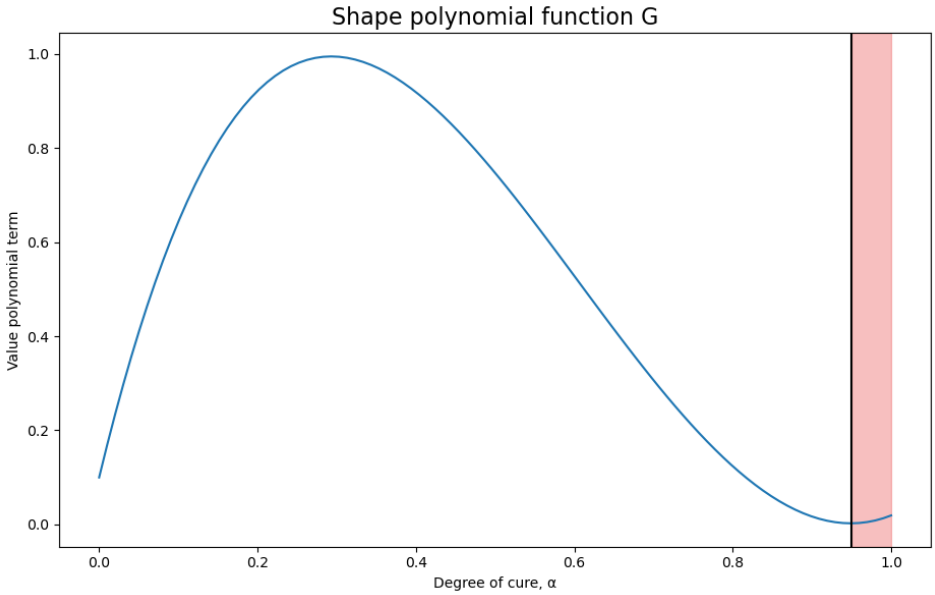


Figure 4.22: The vertical line represents α_{max} for 135 degrees. The function increases above this α.

- The main limitation of the Bailleul model, however, is that the area above the maximum measured degree of cure cannot be influenced. It is possible to fix this by setting a condition on the equation. For example: for a degree of cure higher than $\alpha_{maxmeasured}$ the function linearly slopes to 0. H

Kamal model

The second model is the Kamal model. The parameters of this model are given in Table 4.7. These parameters are derived according to two methods. The graphical-analytical method and the curve fitting method.

*Results of using the **curve fitting** method to derive parameters Kamal model*

First, the results using the curve fitting method. In Figure 4.23, the results of the cure kinetic model for the isothermal curing temperatures are compared with the experimental data.

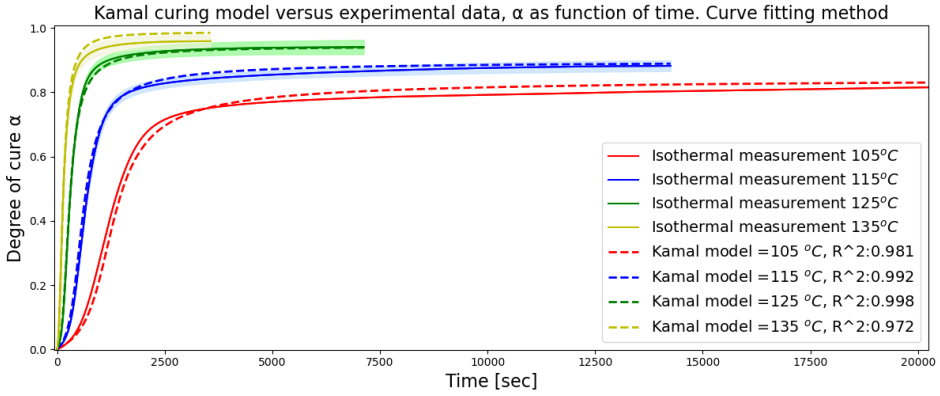


Figure 4.23: Result of the Kamal model using the curve fitting method compared with experimental data at isothermal curing temperatures. The shaded area indicates the standard deviation.

The results of the cure kinetic model for the dynamical curing rates are compared with the experimental data. This is shown in Figure 4.24.

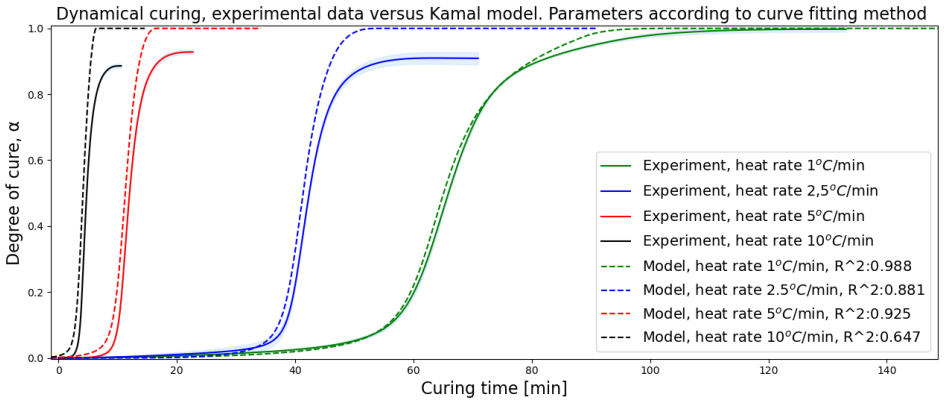


Figure 4.24: Result of the Kamal model compared with experimental data at dynamical curing rates. The shaded area indicates the standard deviation of the experimental data. The curve fitting method is used to derive parameters Kamal model

Table 4.9: R^2 of the Kamal model with the curve fitting method

Isothermal temperature $[°C]$	R^2	**Dynamical heating rate** $[°C/min]$	R^2
105	0.981	1	0.988
115	0.992	2,5	0.881
125	0.998	5	0.925
135	0.972	10	0.647

*Results of using the **graphical-analytical fitting** method to derive parameters Kamal model*
First, the results using the curve fitting method. In Figure 4.25, the results of the cure kinetic model for the isothermal curing temperatures are compared with the experimental data.

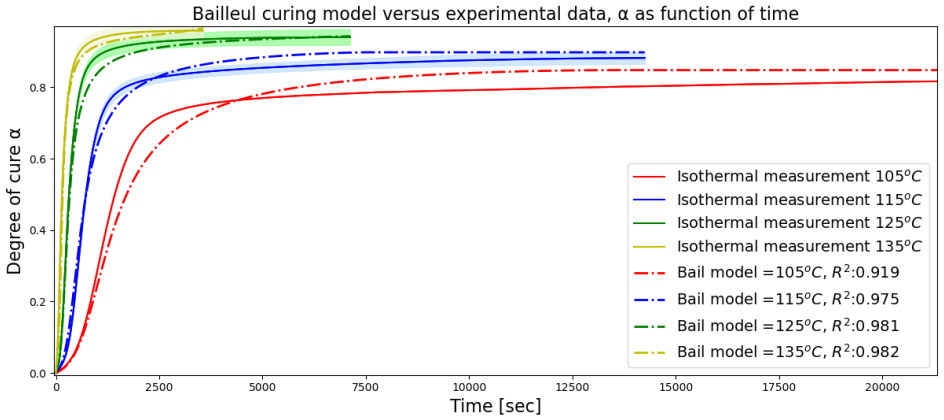


Figure 4.25: Result of the Kamal model using the curve fitting method compared with experimental data at isothermal curing temperatures. The shaded area indicates the standard deviation.

The results of the cure kinetic model for the dynamical curing rates are compared with the experimental data. This is shown in Figure 4.26.

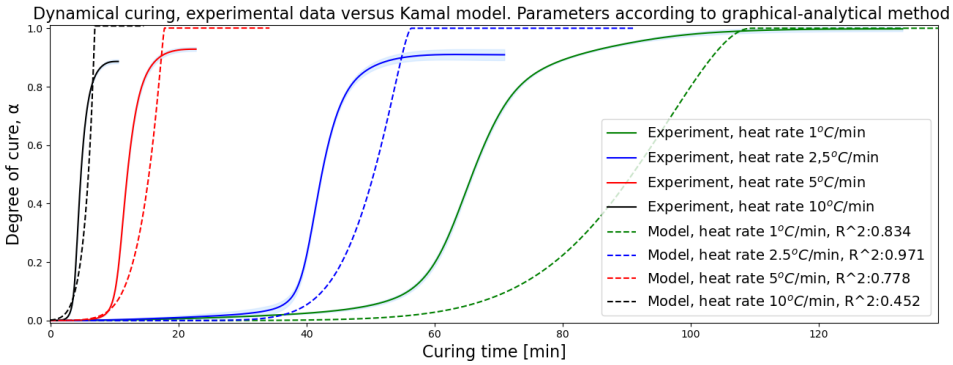


Figure 4.26: Result of the Kamal model compared with experimental data at dynamical curing rates. The shaded area indicates the standard deviation of the experimental data. The graphical-analytical method is used to derive parameters Kamal model

Table 4.10: R^2 of the Kamal model with the graphical-analytical method

Isothermal temperature $[°C]$	R^2	**Dynamical heating rate** $[°C/min]$	R^2
105	0.919	1	0.834
115	0.975	2,5	0.971
125	0.981	5	0.778
135	0.982	10	0.452

4.4.4. Avrami Analysis

In subsection 4.3.4 the Avrami plot is made. A decrease in the reaction component d is spotted. The Avrami plots for the different curing temperatures are shown in Figure 4.27. Two straight lines can be fitted for each curing temperature. The transition region between these two lines can be indicated as the transition region between the two reaction mechanisms. The intersection between the two lines can be related to the onset of the diffusion-controlled mechanism. However, this time point is, in reality, a region instead of a point. This can be observed in Figure 4.27. Combining these transition time points with the measured data results in Figure 4.28. This shows that the curing rate slows down significantly after this point.

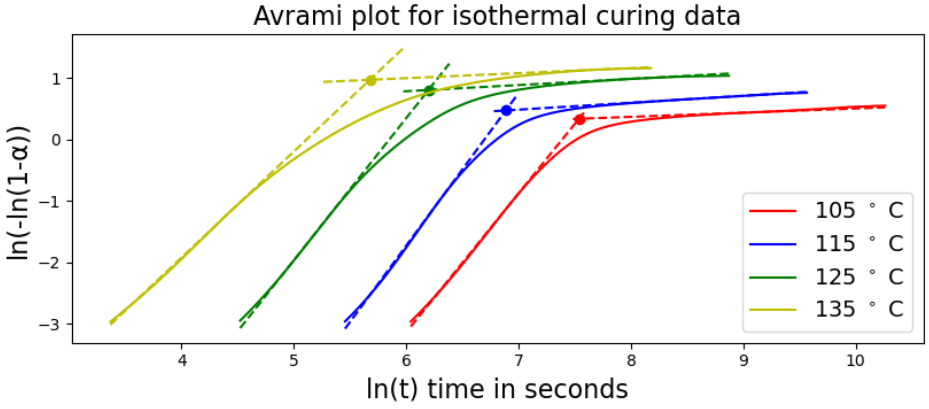


Figure 4.27: The avrami plot of the experimental curing data for the isothermal curing temperatures 105,115,125 and 135 °C. Two straight lines are fitted for each curing temperature

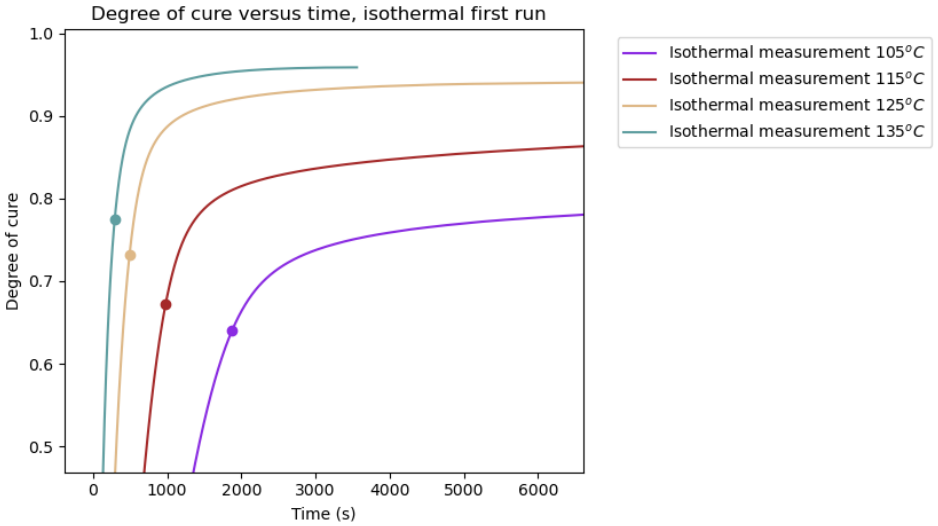


Figure 4.28: The isothermal curing temperatures 105,115,125 and 135 °C. The transition points are indicated. After these points, the curing rate decreases significantly due to the change from a chemical to a diffusion-controlled reaction.

4.4.5. Gel point

The cure kinetic model derived above is used to analyse the time it takes to reach the degree of cure X for isothermal curing temperature Y. This is done with a python code which can be found in appendix section G.7. This time data is stored. the stored data has an exponential decreasing curve. The Arrhenius equation has a relation of 1/T. Therefore, the time is plotted over the inverse of the isothermal curing temperature in Figure 4.29. The gel time, according to the data sheets, is also plotted over this inverse of the isothermal curing temperature. The R2 of the least squares regression, the gelation point, is determined. In other words, the cure kinetic model data is compared with the data sheets data to find the gel point. According to the least square, the gel point closest to the data sheets data is 0.28. R-squared is 0.99659. This is in the curing temperature range between 105 and 137 °C.

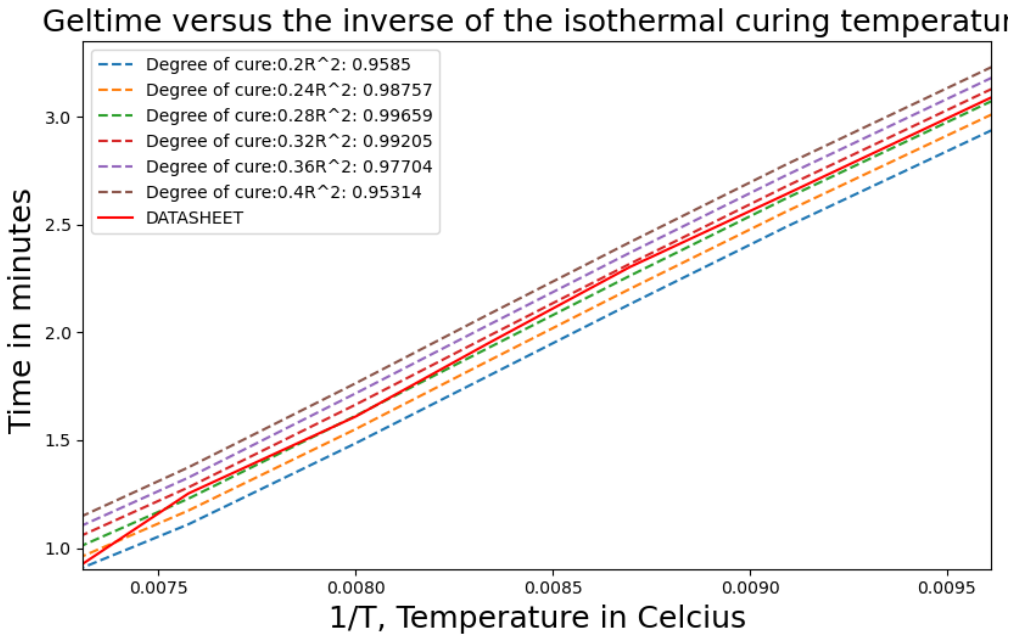


Figure 4.29: The red line is the data based on the data sheets. The gel time is plotted over the inverse of the isothermal curing temperature. The gel times according to the curing model are compared via the R2 method to find the actual gel point.

This can be verified by comparing this with the viscosity profile given in the datasheet. In the datasheet, the viscosity profile for the heating rates 1°C/min, 2 °C /min, and 3 °C/min are given; see Figure 4.30. The gelation occurs at 114 °/C, 109 °/C and °/C 100, respectively. It takes longer to reach the gel point at a lower heating rate than with a high heating rate. However, gelation occurs at a lower temperature for lower heating rates. The data sheets state that the calculated temperatures for gelation with these heating rates are 123 °C, 118 °C and 109 °C, respectively.

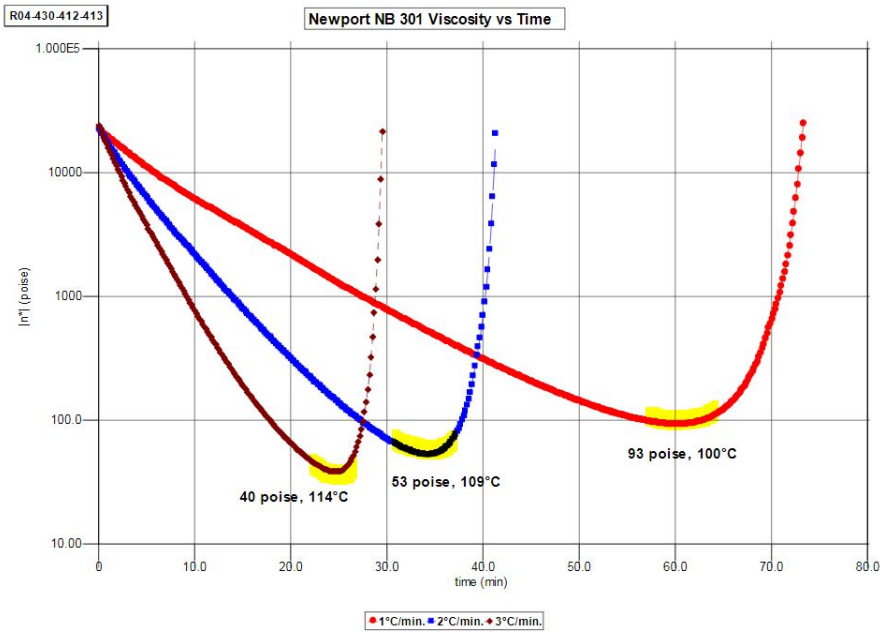


Figure 4.30: Viscosity profile for dynamic heating rates according to the datasheet (not available in this version). The yellow marked area shows the zone where the viscosity increases significantly. This indicates the gel point.

The estimated gelation point for the heating rate 1 °C is displayed in Figure 4.31. The other heating rates are in Appendix section C.7. The model suggests a curing temperature at the gel point of 110 °, the data sheets 100, for 1 °C/min. For 2 °C/min 118 °C and the data sheets 109 °C. And lastly, for 3 °C/min, the model suggests 123 °C and the data sheets 114 °C. The cure kinetics model combined with the result from Figure 4.29 predicts the gel point within 10% accuracy. Additionally, Figure C.14 shows that the gel point is in the steepest part of the degree of cure. A small difference in degree of cure has a big impact on the curing temperature. The model and the transition region show accurate agreement in Figure 4.30; therefore, the model will be used to estimate the gel point.

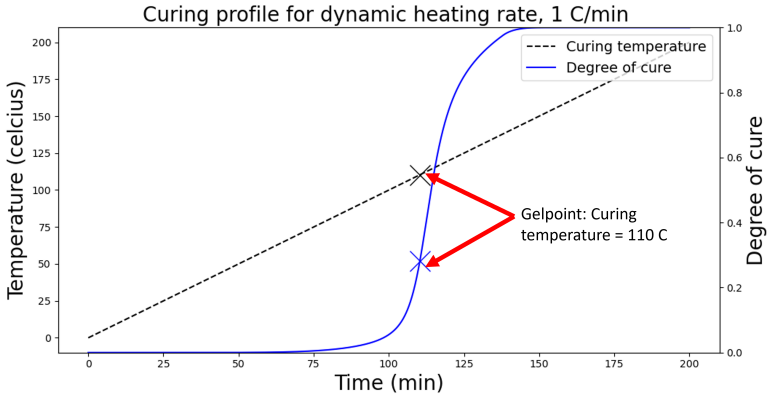


Figure 4.31: Curing behaviour for dynamic heating rate 1 °C, according to python script. The temperature at gelation is marked with a black cross, degree of cure at gelation is marked with a blue cross.

4.5. Concluding remarks

- The isothermal, dynamical and temperature-modulated DSC measurements are successfully performed. ASTM standards are followed to ensure reliable data analysis with a python script.
- The data is processed according to the described method in the literature to derive the Bailleul model. Testing this model with isothermal temperatures results in an R-squared of 0.919 and higher. Testing for dynamical heating rates, the R-squared value for 1- 2.5 °C / min was 0.908 and higher.
- The main limitation of the Bailleul model is the systematic deviation at the end of the dynamical heating rates. This is caused by the method to derive the polynomial function. the ”kink” formed at the end of the dynamical curve is not in trend with the expected curve. Therefore, this data is not reliable.
- To improve the cure kinetic modelling, a second model is introduced, the Kamal model. Two methods to derive the parameters are used and tested with the R-squared method.
- The method to derive the parameters of this model is adjusted to increase the accuracy of this model. A linear relationship is made for the parameters n and m.
- To get the model parameters, the graphical-analytical and the curve-fitting method are used. The graphical-analytical had an R-squared of minimal 0.919 for isothermal curing, and the R-squared value for 1- 2.5 °C / min was 0.834 and higher. The curve-fitting method had an R-squared of minimal 0.972 for isothermal curing, and the R-squared value for 1- 2.5 °C / min was 0.881 and higher
- The Kamal Model combined with the graphical-analytical method provides the most accurate results within the operating range. Although the R-squared value of 0.881 for a heating rate of 2.5°C per minute may not be perfect, a visual inspection of the results suggests that the Kamal Model offers the best predictions compared to other models.
- The model for the maximum degree of cure was required for the Kamal model and the Bailleul model. This model is derived from the measured data and verified with an R-squared of 0.958.
- The Di Benedetto model is derived with the measured data and verified with an R-squared of 0.9918.
- To understand the resin behaviour during curing, an Avrami analysis is performed. This allows for explaining the decrease in reaction rate by predicting the transition from a chemical to a diffusion-controlled curing mechanism.

5

Interphase analysis

In this chapter, the interphase will be analysed. This is achieved by studying the interdiffusion between the epoxy resin and the thermoplastic. This thermoplastic will function as a coupling layer for the fusion welding joints. In section 5.1, the methodology is explained. In section 5.2, the used materials are introduced together with the sample preparation. The results will be presented and discussed in section 5.3. In section 5.4, concluding remarks on these models are provided.

5.1. Methodology

The literature study describes a technique called fusion bonding of thermoset composites. A thin thermoplastic layer is used to join two thermoset composites. The thermoplastic film can be co-cured with the epoxy, allowing it to join the two thermoset parts. When co-curing the thermoset epoxy resin, particles can locally diffuse into the thermoplastic matrix. This diffusion is followed by reaction-induced phase separation. Resulting in a thermoset/thermoplastic interphase. This interphase allows for load transfer and can therefore function as a joint. The physics behind this process is explained in depth in the literature study subsection 2.7.1. This chapter aims to investigate this interphase formation between the thermoset and the thermoplastic polymer. The influence of the dwell temperature, heating ramp and gelation point on the size of the interphase will be studied.

According to the literature study, polyetherimide (PEI) shows a significant interdiffusion with epoxy, even with the presence of carbon fibres. This, in combination with the availability of PEI in the composite lab at the Aerospace faculty, is the reason for choosing PEI to investigate this joining concept. The first step is identifying the penetration between the epoxy and the PEI. This penetration will be studied for the manufacturer's prescribed heating rate to the isothermal temperatures 105,115,120,125 and 135 °C in the autoclave. Secondly, instant heating to 135 and 149 °C in the hot press. This allows studying the effect of the heating rate and the effect of the isothermal curing temperatures on the interphase formation and morphology. These samples will be analysed using the Keyence VK-X1000 3D laser scanning confocal microscope and the Jeol JSM-7500F scanning electron microscope. **optical, and laser and C is used in 20 and 50x zoom**
The literature study, subsection 2.7.1 describes the impact of the gelation point. The thermoset resin loses mobility after reaching the gelation point. This loss of mobility has an impact on interdiffusion. The interdiffusion slows down and stops after the epoxy reaches its gelation point. The gel point is studied in subsection 4.4.5

5.2. Sample preparation and material definitions

In this section, the material and sample preparation is described.

Material definition
The carbon fibre epoxy prepreg is mentioned and described in section 4.1. The thermoplastic polymer used in this experiment is polyetherimide (PEI). See Figure 5.1. The material properties are given in Table 5.1. The thickness of the thermoplastic film is 60 microns, provided by SABIC Saudi Arabia.

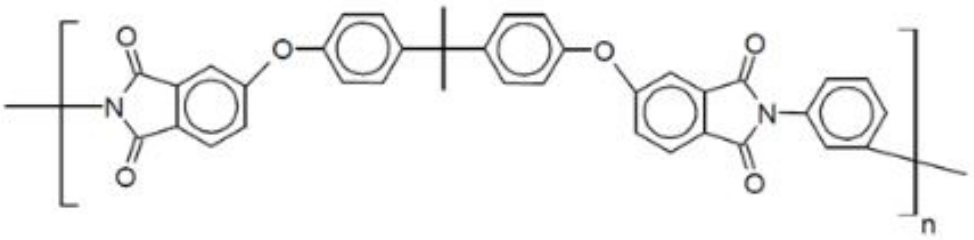


Figure 5.1: Molecule structure polyetherimide. [20]

Table 5.1: Properties of polyetherimide [20]

Material Property	Value & Unit
T_g	217 °C
Specific gravity	1.27 g/cm3

Sample preparation

Two types of samples are prepared for the interphase analysis. Samples will be cured in the autoclave, and samples will be cured with the hot press. The hot press avoids the temperature ramp; instant isothermal curing temperatures can be applied to the sample. The manufacturing process is listed below. Different steps are required for the autoclave and the hot press. This will be reported. Note scale of the schematic illustrations is not correct.

1. **Defrost:** The carbon fibre epoxy prepreg is taken out of the freezer. Wait till the temperature of the material reaches room temperature.
2. **Mold preparation:** The sides are sanded so the sealant tape will stick. Secondly, the mould is cleaned with isopropanol, and the sides are taped off to keep the surface clean for the sealant tape. Mould is treated with Marbocote. This should be rubbed onto the mould at least four times, separated by at least five minutes.
3. **Cutting:** Once the prepreg is up to room temperature, the prepreg is cut by hand with a rotary cutter. Covers with the required size are 3D printed and placed on top of the prepreg to increase the accuracy of the cutting. The PEI, adhesive, and release film are cut with a Stanley knife. Lastly, the vacuum bag and breather are cut with scissors.
4. **Building up laminate:** The build-up of each configuration is different. They will be explained separately. The breather and peel ply should stick out the sides for all samples and create a path to the vacuum connection. This allows the air to flow out and create a vacuum.

    - **Autoclave samples:** Peel ply is placed at the mould to create a path for the excess resin and the air to flow. The prepreg is placed. At the top comes the PEI film, peel ply, release film, breather and vacuum bag are placed. The PEI film is cleaned with isopropanol to remove contamination. The vacuum bag is stuck onto the sealant tape. The peel ply and the breather create a path for the air to flow out and create a vacuum. This is shown and illustrated in Figure 5.3a. The sample is placed on a rack, allowing air to flow underneath the sample. Therefore the sample will be heated and cooled via the bottom and top. This is shown in Figure 5.3b.

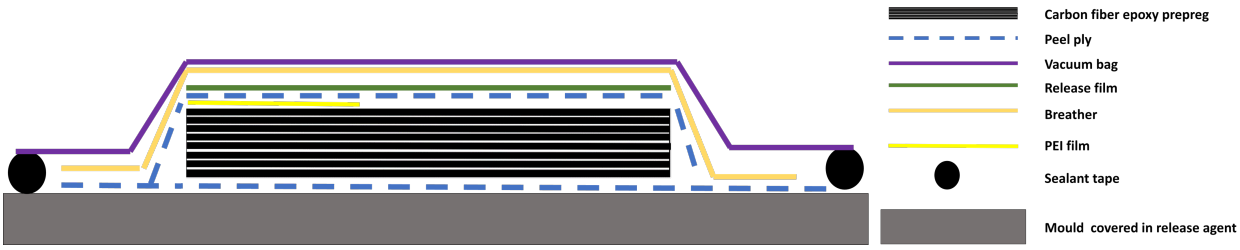
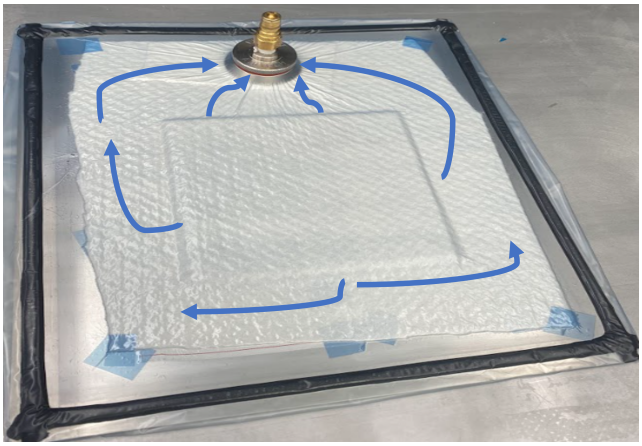
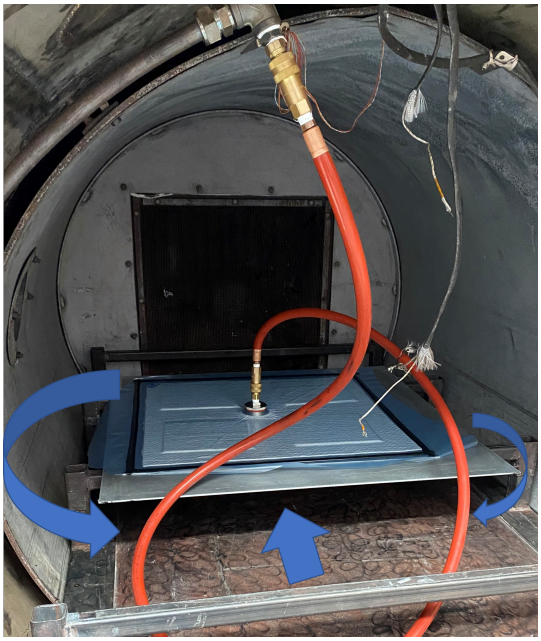


Figure 5.2: Schematic build up parts for autoclave. PEI film was placed on top of the prepregs. Including legend.



(a) Breather sticking out of the sample and creating a path for the air to the vacuum connection/ outlet.



(b) Sample placed on a rack to allow the air to flow underneath the sample.

Figure 5.3: Autoclave setup, (1) the sample is prepared on the mould in the vacuum bag, ready to be placed in the autoclave. Here the blue arrows indicate the path for the air to flow out of the sample and vacuum bag. (2) the sample is placed in the autoclave and connected to the vacuum. The blue arrows indicate for the air flowing in the oven to heat the part from two sides.

- **Hot press samples:** In the hot press, the pressure is applied by a press which closes. Therefore, the sample must be higher than the sealant tape. Two aluminium parts are placed under the sample to increase the height of the sample. This is shown in Figure 5.4. Peel-ply is placed at the mould to create a path for the excess resin and the air to flow. The carbon fibre epoxy prepregs and PEI are placed. The PEI film is cleaned with isopropanol to remove contamination. At the top comes the peel ply, release film, breather and vacuum bag are placed. The vacuum bag is stuck onto the sealant tape. The peel-ply and breather must be long enough to stick out of the press. The part that sticks out is connected to a hose. This hose is connected to a vacuum pump. This setup is displayed in Figure 5.5.

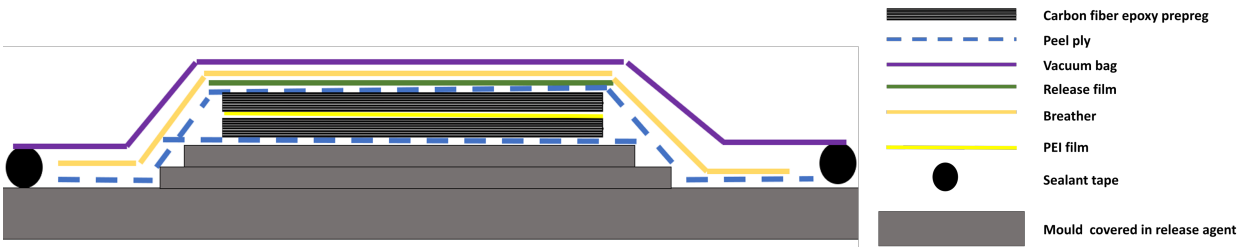
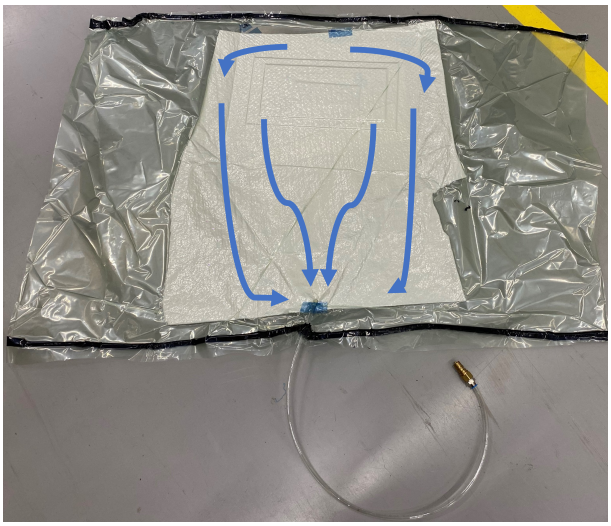


Figure 5.4: Schematic build-up parts for the hot press including the legend.



(a) The breather and peel-ply create a path for the air from to sample to the vacuum hose.



(b) The hose connection sticks out of the press, together with the breather and peel-ply. This ensures the sample is under vacuum while pressing.

Figure 5.5: Hot press setup, in (1) the sample is prepared in the vacuum bag. (2) the sample in the closed hot press. The blue arrows indicate the path of the air to flow out of the sample and the vacuum bag

5. **Curing**

(a) **Autoclave:** The four parts cured in the autoclave have a heating rate of 1.7 °C / min. This is the pre-described heating rate in the datasheets. The first dwell is at 105 °C, 115 °C, 125 °C and 135 °C for 60 minutes. The second dwell is at 135 °C for 60 minutes to ensure the same degree of cure for all parts. During the entire process, the pressure in the autoclave is 3.45 bar. The pressure inside the vacuum bag remains during the entire cycle. The curing temperatures are illustrated in Figure 5.6. All parts get a second dwell at 135 °C to ensure the same degree of cure. The part cured at 135 °C does not get a second dwell since the first dwell is at 135 °C.

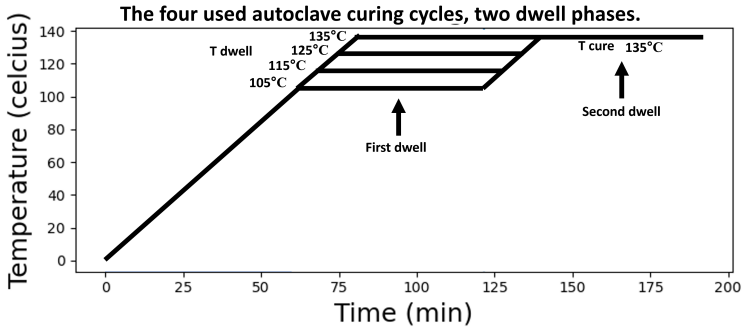


Figure 5.6: The four autoclave curing cycles. First, dwell at 105,115,125 or 135 °C, second at 135 °C. The cycle with the first dwell at 135 °C has no second dwell.

(b) **Hot press:** Two parts are cured in the Hot press. The hot press is preheated to 135 °C and 149 °C. The isothermal hold (dwell) is kept for 60 minutes. The pressure on the sample is 3.45 bar. The contact area is calculated, and the load divided by the contact area gives the required pressure. The pressure inside the vacuum bag remains vacuum during the entire curing cycle. The curing cycles are shown in Figure 5.7.

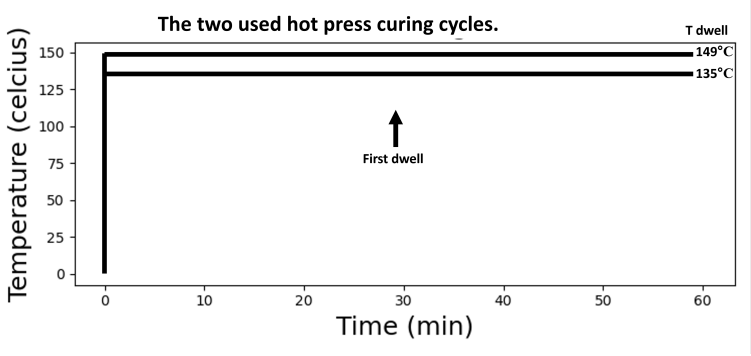


Figure 5.7: The two hotpress curing cycles. First, dwell at 135 and 149 °C. Instant heating, so no heating ramp.

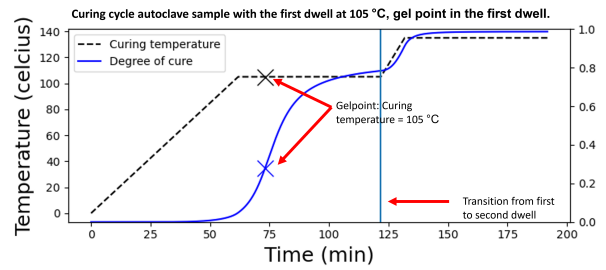
The samples need to be prepared for cross-sectional microscopy. The following steps are taken:

- **Cutting:** The cross-sectional cuts are made with the digitally automatable Proth column cutter. This cutter has a diamond-coated circular blade, which is 2 mm thick. The Proth removes 100 microns per horizontal movement. The samples are cut perpendicular to the fibre direction. Therefore the behaviour of the epoxy and PEI around the fibres become visible.
- **Resin embedding:** The samples are mounted in a plastic Struers clip. The samples are placed so that the epoxy prepreg neighbouring the PEI film has the zero direction perpendicular to the cross-section. The Struers clip with the samples is placed into a mould and embedded with Struers EpoFix. The curing occurs at room temperature in atmospheric pressure. The EpoxFix is mixed according to the datasheet. The resin is carefully poured into the mould to reduce the air bubbles in the resin.
- **polish and grinding:**The samples are polished and ground with a manual polishing machine. The aim is to create a smooth surface finish without scratches. The grinding and polishing procedure is described in the appendix Appendix D Table D.1. In between every step, the sample is rinsed with water and ethanol.
- **Etching:** The polished surfaces of the samples are etched with N-methyl-2-pyrrolidone (NMP). 1 ml of NMP is dripped on the surface for 10 seconds. This is followed by rinsing with ethanol and distilled water. Lastly, the surface is dried with compressed air. NMP should be handled with care due to health risks. A risk report is made and discussed with a lab worker before using the NMP. NMP is a solvent which dissolves the PEI. Therefore, it is possible to distinguish the PEI and the epoxy particles at the interphase.
- **Keyence microscopy and Scanning electron microscopy:** The samples can be used directly for optical microscopy. However, for Scanning electron microscopy, the samples need to be gold coated using a sputter coater.

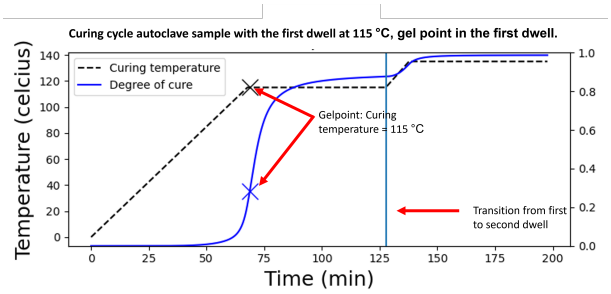
5.3. Results and discussion

Results gelation

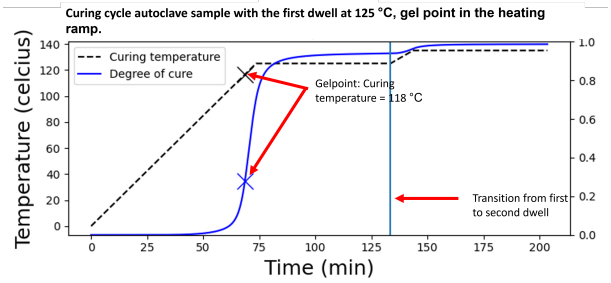
The gel point is set to 0.28, which is explained in section 4.1. Combining this with the cure kinetic model derived in chapter 4, and the applied cure cycles result in Figure 5.12. The gel point is indicated with the cross. The sample cured in the autoclave with the heating ramp and the isothermal dwell at 105 °C has the gel point in the temperature ramp, also called the first dwell. This is also the case for the part cured at 115°C, see Figure 5.8a and Figure 5.8b. The other two parts with the ramp, 125 °C and 135 °C, have the gelation point in the heating ramp. In other words, gelation occurs before the isothermal dwell temperature is reached, see Figure 5.8c and Figure 5.8d. This information will be used to study the impact of gelation. The parts manufactured in the hot press did not have the temperature ramp. Here the gelation occurred for both parts at the isothermal temperature; see the black cross in Figure 5.8e and Figure 5.8f.



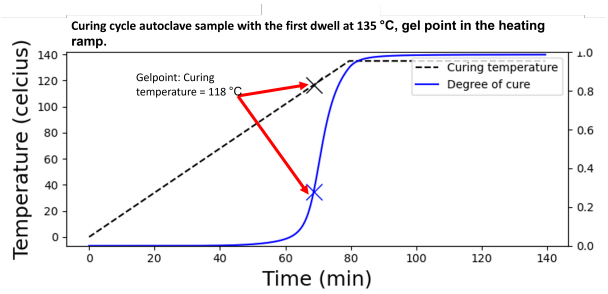
(a) Gel point for the sample with the first dwell at 105 °C. Curing temperature at the moment of reaching the gel point is 105°C, the temperature of the first dwell.



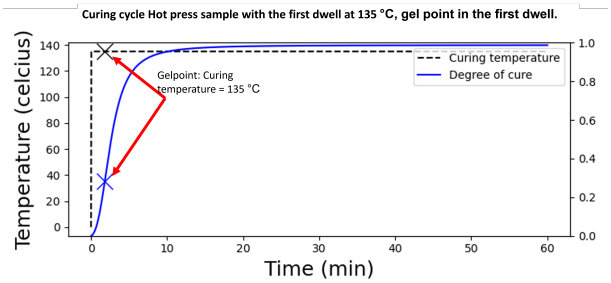
(b) Gel point for the sample with the first dwell at 115 °C.Curing temperature at the moment of reaching the gel point is 115°C, the temperature of the first dwell.



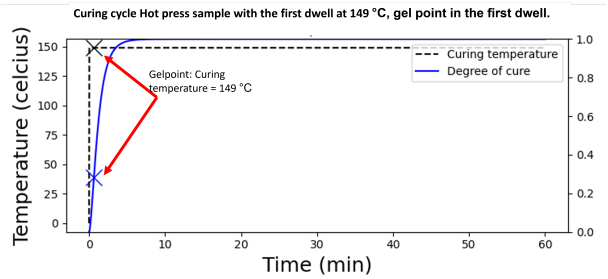
(c) Gel point for the sample with the first dwell at 125 °C.Curing temperature at the moment of reaching the gel point is 118°C, not the temperature of the first dwell.



(d) Gel point for the sample with the first dwell at 135 °C.Curing temperature at the moment of reaching the gel point is 118°C, not the temperature of the first dwell.



(e) Gel point for the sample with isothermal cure at 135 °C without a heating ramp. Curing temperature at the moment of reaching the gel point is 135°C, the temperature of the first dwell.



(f) Gel point for the sample with isothermal cure at 149 °C without a heating ramp. Curing temperature at the moment of reaching the gel point is 149°C, the temperature of the first dwell.

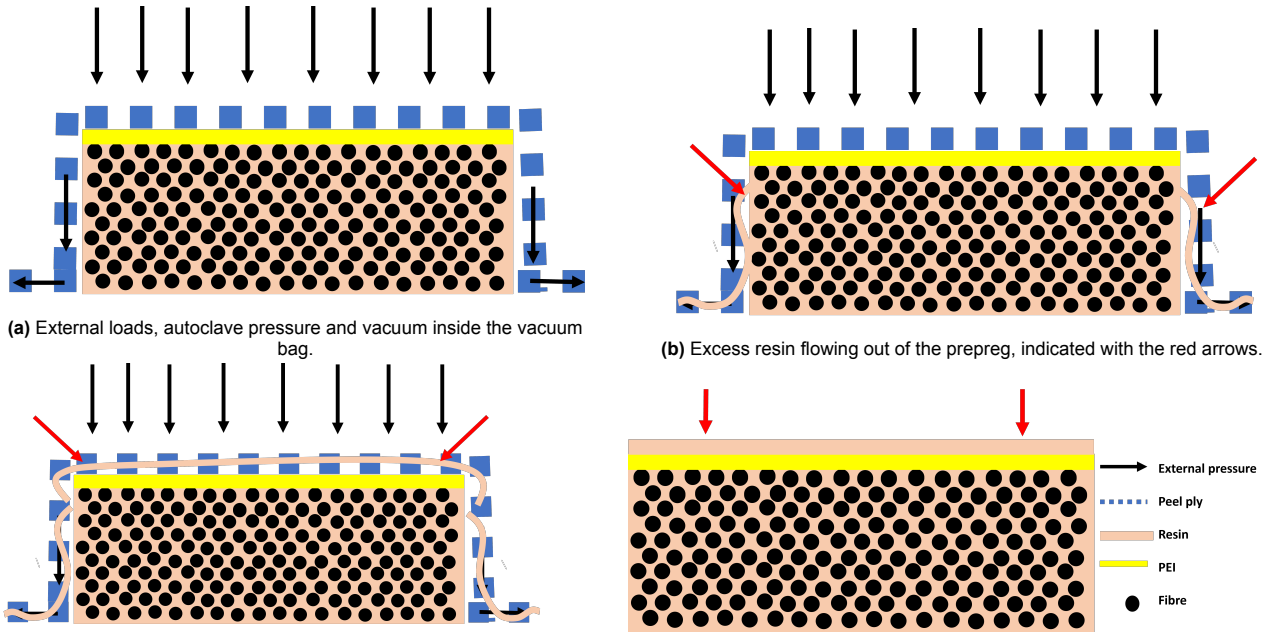
Figure 5.8: The cure kinetic model, in combination with the datasheet, is used to estimate the gel points. Gel points for the samples are indicated with the 'X'. Provides information on the curing temperature at the gelation point for each curing cycle.

Capillary flow

In item 5a, the manufacturing is described to co-cure PEI with epoxy carbon fibre prepreg, see Figure 6.12. The viscosity profile of epoxy is shown in Figure 4.30. At the beginning of the curing process, the thermoset is uncured and far from reaching its gel point. This means the polymer chains are short and mobile, and few crosslinks have formed yet. The lower reactivity of the thermoset at this stage of curing is due to lower temperatures. Once the curing temperature increases, a decrease in viscosity is observed. The thermal energy of the molecules increases, causing the chains to move further away from each other. Therefore, the free volume increases and the chains can move more freely. Simontainously, due to this temperature increase, the reactivity of the molecules increases. Crosslinks start forming, and the molecular weight increases, increasing viscosity. At the gel point, the viscosity increases exponentially. This sudden increase in viscosity is marked in yellow in Figure 4.30.

During curing in the autoclave, external pressure is pressed onto the sample. Additionally, a vacuum is created. Both loads are displayed in Figure 5.9a. Due to the temperature increases, the viscosity decreases. The excess resin flows out of the prepreg, illustrated in Figure 5.9b. This flow is created by the vacuum insides of the vacuum bag in combination with the external pressure onto the sample created by the autoclave. There

is a peel ply placed on top of the PEI. The peel ply has small spaces in between the fibres. The epoxy is drawn into these tight spaces due to capillary flow. Also described as a spontaneous flow of liquids in narrow spaces without the assistance of external forces [72]. This results in the cured epoxy surrounding the PEI film, see Figure 5.9d. The epoxy droplets reached the PEI's top side. This process was undesired. However, it allows comparing PEI/ "bulk" epoxy interface and PEI/ epoxy surrounded by fibres interface. The impact of the capillary flow on the manufacturing process will be discussed in section 7.2.



(a) External loads, autoclave pressure and vacuum inside the vacuum bag.

(b) Excess resin flowing out of the prepreg, indicated with the red arrows.

(c) Excess resin flowing on top of the PEI due to capillary flow, indicated with the red arrows.

(d) Cured epoxy surrounding the PEI film, indicated with the red arrows. Legend is added and applies to all four figures.

Figure 5.9: The curing process with the unintended capillary flow. Process displayed in four steps. Steps 2 and 3 happen simultaneously. However, for clarification, these are split up into two figures.

Tortuosity

In the literature section 2.7, the driver of this interphase formation is explained. A process parameter which is varied in this study is the temperature. However, a second variable is added due to the capillary flow of the epoxy resin during curing, explained in Figure 5.3. The bulk epoxy resin flowed on top of the PEI film. This allowed for comparing bulk and diffusivity with carbon fibres in the epoxy. The carbon fibres block epoxy particles; the epoxy needs to travel around these fibres to diffuse towards the PEI interface. Diffusion is often described as the diffusion of a medium in a clear fluid. However, a reduction factor β is introduced in the literature to modify diffusion in a clear media, D_{AB}, to diffusion in a porous media D^*_{AB} [73]. In Equation 5.1, the scale factor β is defined. S_{g} is the gas saturation factor assumed to be 1 for an all-gas situation. PEI and epoxy are not gasses. However, the gas saturation factor is set at 1. Introducing this equation aims to understand the impact of carbon fibres on diffusion and to gain a feeling for the order of magnitude of this impact. ϕ is the porosity, the inverse of the fibre volume fraction, 35%. τ is the tortuosity. This is the shortest path length through the pores dived by the straight line, $\Delta L_{fibres}/\Delta X_{fibres}$. This is illustrated in Figure 5.10. The tortuosity through bulk resin is 1 since there is nothing to block the straight line $\Delta L_{bulk}/\Delta X_{bulk}$.

$$\beta = \phi S_{\mathrm{g}} \tau \tag{5.1}$$

According to the model described by Millington and Quirck, the tortuosity relation is given by Equation 5.1[74]. Replacing S_{g} by 1 gives Equation 5.3. With a fibre volume fraction of 65%, the porosity is 35%. Resulting in a diffusion reduction factor of 0.247 according to Equation 5.2. In other words, the diffusion on the interface with the bulk resin will be expected to be four times as large as the diffusion on the carbon fibre/ epoxy PEI interface [75] [76].

$$\tau = \phi^{1/3} S_{\mathrm{g}}^{7/3} \tag{5.2}$$

$$\tau\left(S_{\mathrm{g}}=1.0\right)=\tau_{\mathrm{o}}=\phi^{1/3} \tag{5.3}$$

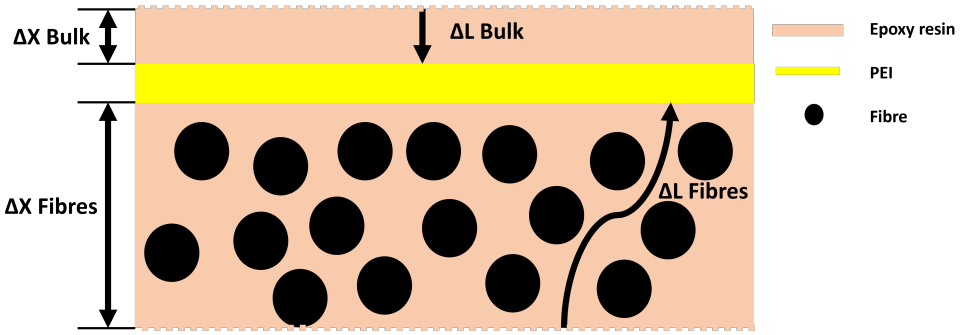
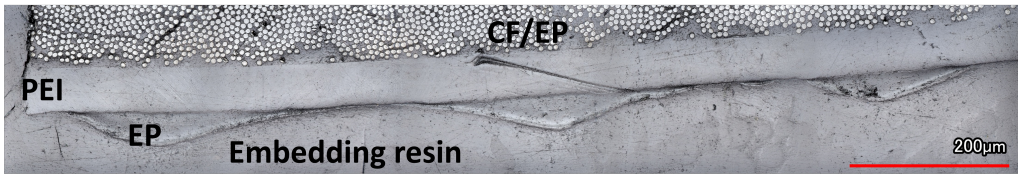


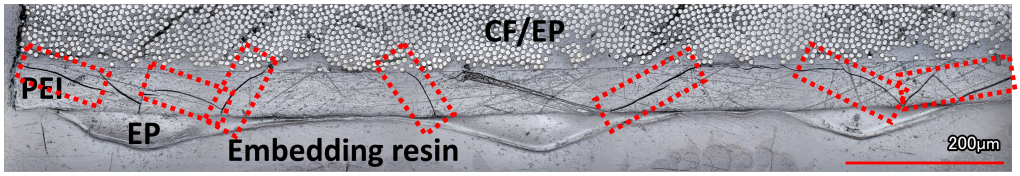
Figure 5.10: Diffusion towards the PEI film. Comparison of the travelled path for epoxy particles around the fibres and epoxy particles through the bulk resin.

Etching

In Figure 5.11a, the cross-section of the carbon fibre epoxy and the PEI film is shown before the NMP treatment. In Figure 5.11a, the cross-section after the NMP treatment is shown. Here the PEI film, epoxy/fibres and bulk epoxy are visible. Additionally, the embedding resin can be observed; this is the resin to embed the sample for polishing. As a result of the solvent, a top layer of the PEI dissolves. This enables visual distinction between the PEI film and the epoxy. Additionally, scratches in the PEI layer appear due to the NMP etching process. According to Abbasi et al. NMP acts as a plasticizer [1]. Adding NMP to PEI decreases the glass transition temperature of the PEI. Molecules of a plasticizer place themselves in between the thermoplastic molecules. Therefore the free volume increases. This results in higher mobility, and the glass transition temperature decreases. When the T_g is lower than room temperature, the polymer transitioned into the rubbery state. Due to the increase in mobility, the PEI penetrates further into the polymer network. The transition from glassy to rubbery domain causes a sudden increase in volume, called swelling. During swelling, the osmotic and viscoelastic forces are out of balance, causing the polymer to swell until an equilibrium is reached. After 10 seconds, the NMP solvent is removed from the surface. The sample is rinsed with ethanol and distilled water, causing the T_g to increase. Sudden deswelling occurs in the polymer matrix. In other words, a sudden shrinkage. This could potentially explain the cracks in the PEI film after the NMP treatment [77].



(a) Before NMP treatment. A smooth PEI surface.



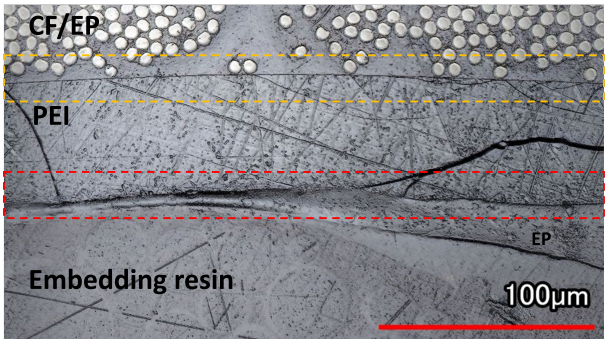
(b) After NMP treatment. A scratchy-like surface appears the in the PEI film, indicated by the red boxes.

Figure 5.11: Cros-section view of the epoxy/PEI interface, laser + optical microscope used with 50x zoom. CF/EP: carbon fibre epoxy, PEI: PEI film, EP: bulk epoxy, Embedding resin embeds the samples. The difference before and after NMP treatment is visible in the PEI film.

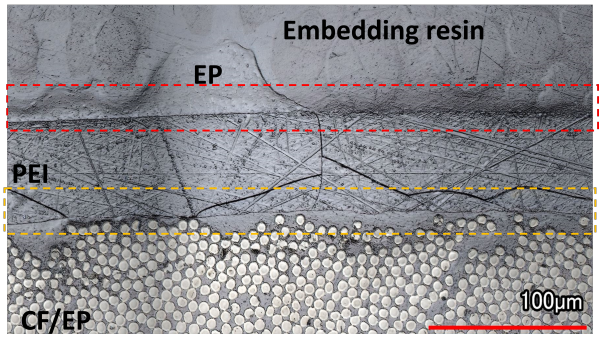
[1] Plasticizer: a substance (typically a solvent) added to a synthetic resin to produce or promote plasticity and flexibility and to reduce brittleness

5.3.1. Laser confocal microscopy of cross sections

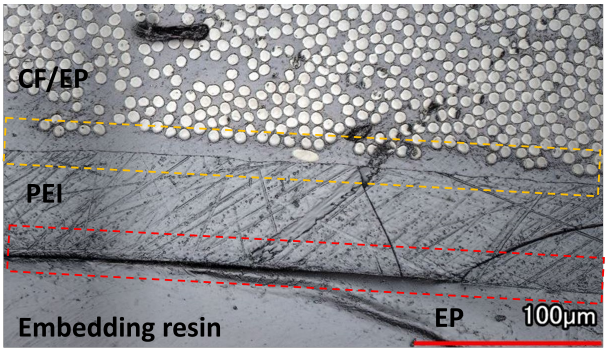
In this section, the microscopy figures of the Keyence confocal laser microscope are shown. These samples are manufactured in the autoclave with the isothermal curing temperatures 105°C, 115 °C, 125 °C and 135 °C. In Figure 5.12, the results of 50x magnification are illustrated. At the interphase between the PEI and the bulk, epoxy is visibly affected by the interdiffusion. A darker wavy shape indicates interdiffusion. No apparent signs of phase separation are visible with the microscope. These phase separations are reported in the literature. However, this was for higher isothermal temperatures, around 160 °C. The interphase between the PEI and the epoxy/carbon fibre is straight, indicating less interdiffusion activity than the bulk epoxy side. The diffusivity difference can explain this visible difference in the interphase shape due to tortuosity. This is explained in Figure 5.3. Scanning electron miscopy is required to examine the interphase closely. The images taken with the Keyence confocal laser microscope provide insight into the indication that interdiffusion has occurred. In Figure 5.12, minimal differences are spotted between the impact of the isothermal curing temperature. In Figure 5.12, the resin used to embed the sample is also visible. This is indicated in the figures and is not relevant to the analysis.



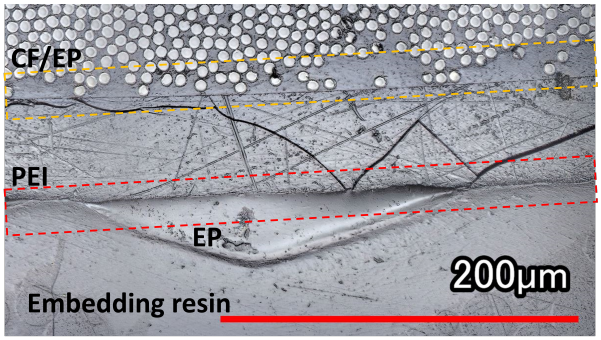
(a) Sample with isothermal curing temperature at 105 °C, 50x magnification.



(b) Sample with isothermal curing temperature at 115 °C, 50x magnification.



(c) Sample with isothermal curing temperature at 125 °C, 50x magnification.



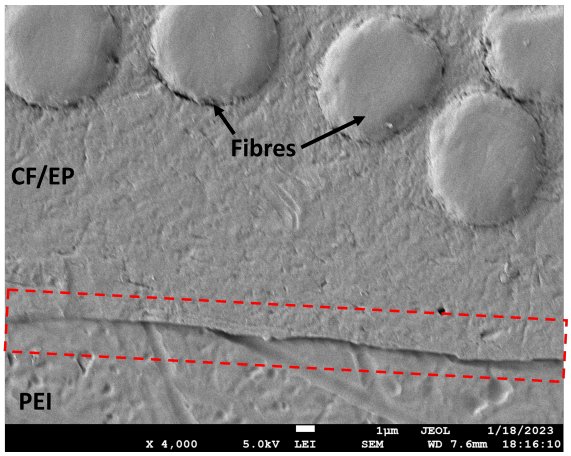
(d) Sample with isothermal curing temperature at 135 °C, 50x magnification.

Figure 5.12: Samples cured in the autoclave, 50x magnification is used to create the images. The red box indicates the interface between the PEI and the bulk epoxy. A dark wavy pattern is visible. The orange boxes indicate the carbon fibre /PEI interface. A straight interface is visible. No difference between the samples is visible in the laser confocal microscope.

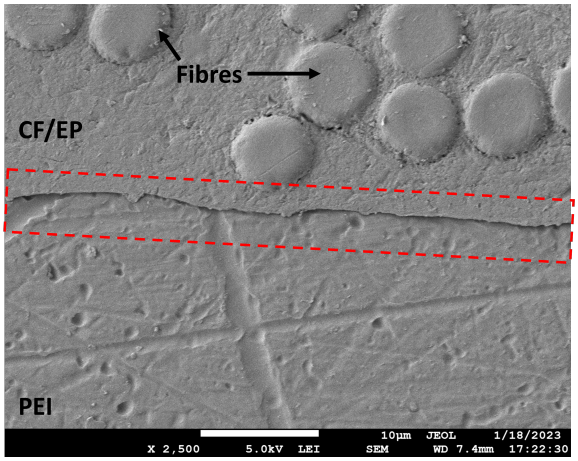
5.3.2. Scanning electron microscopy of cross sections

Scanning electron microscope images are taken to study the interphase between the PEI film and the epoxy. The cracks formed by the NMP treatment are visible in the PEI film. The epoxy droplet, PEI film and carbon fibre epoxy are visible in these images. The interphase at the droplet size is characterized by its wavy shape. The carbon fibre/epoxy PEI interphase is indicated with a straight line. A closer look needs to be taken at the interphases. Zooming in on the interphase between the epoxy/carbon fibre and the PEI shows no signs of phase separation at the micron scale. This is displayed in Figure 5.13. The samples with the isothermal dwell at 105 °C,115 °and 125 °C show no signs of interdiffusion. There is a distinct straight line visible, which separates both materials. This line is visible in the sample with the dwell at 135 °C. However, this line is less distinct than the other samples. In Figure 5.14, a closer SEM image of the epoxy droplet and PEI interphase is

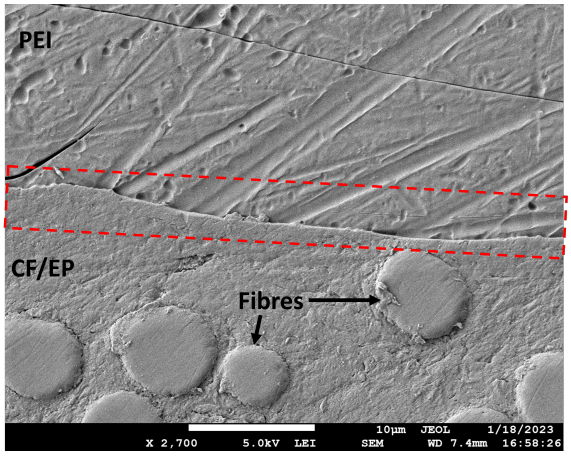
taken. Here a clear interphase formation is visible for the higher curing temperatures. However, no droplets are observed, which indicates phase indication. It can be noted for the 125 and 135 °C samples that the scratch-like surface caused by the etching slowly fades away towards the epoxy region. The boundary between the PEI and the epoxy also becomes more wavy-like the higher the isothermal curing temperature. Indicating a higher activity at a higher curing temperature. The depth and the formation of the interphase can be smaller than 1 micron, which makes it hard to observe with the SEM [78]



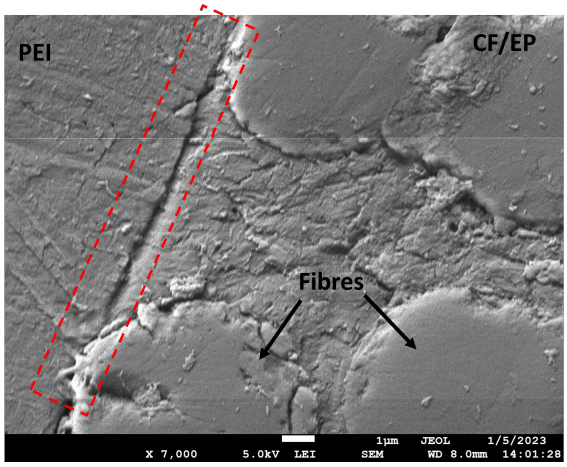
(a) Autoclave sample with the first dwell at 105 °. A straight line separates the PEI/ epoxy carbon fibre.



(b) Autoclave sample with the first dwell at 115 °. A straight line separates the PEI/ epoxy carbon fibre.

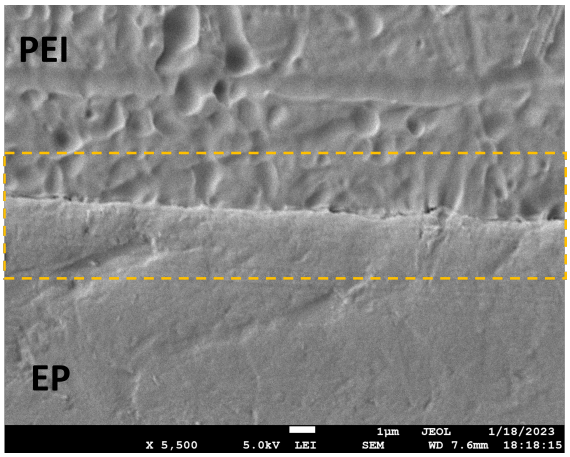


(c) Autoclave sample with the first dwell at 125 °. A straight line separates the PEI/ epoxy carbon fibre.

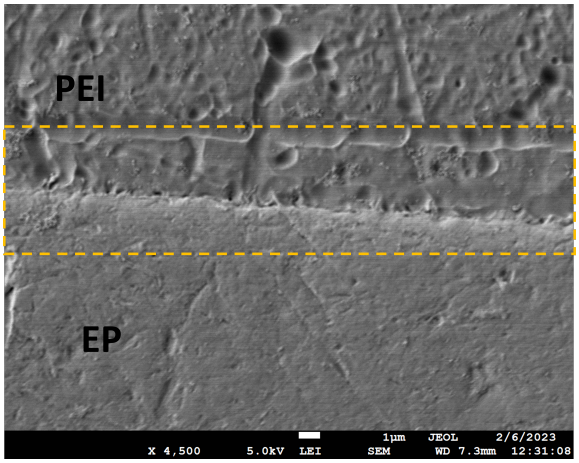


(d) Autoclave sample with the first dwell at 135 °. A straight line separates the PEI/ epoxy carbon fibre. However, this line is less distinct than the other samples, indicating more interdiffusion.

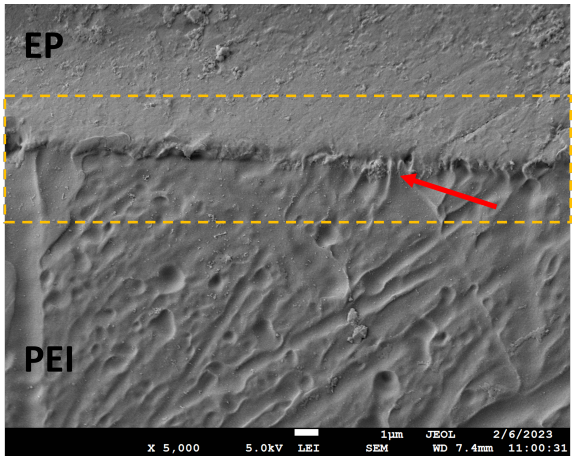
Figure 5.13: Epoxy/carbon fibre - PEI interphase, SEM images. The Interphase between PEI and carbon fibre epoxy is indicated with the red box. No signs of phase separation at the micron scale. For the sample at 135 °C, more interdiffusion occurred at the interphase. For the other samples, the interphase is a straight line.



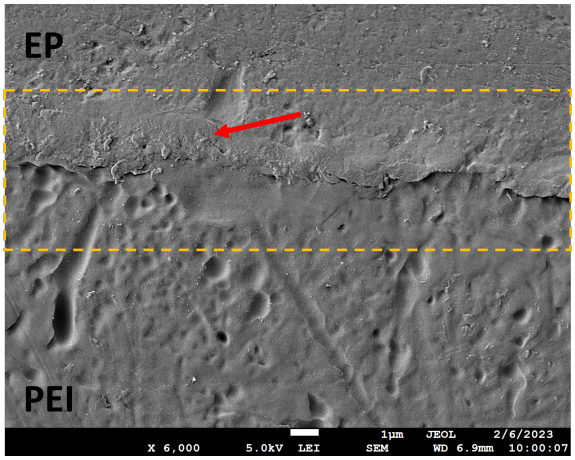
(a) Autoclave sample with the first dwell at 105 °. A wavy interphase separates the PEI/ epoxy carbon fibre.



(b) Autoclave sample with the first dwell at 115 °. A wavy interphase separates the PEI/ epoxy carbon fibre.



(c) Autoclave sample with the first dwell at 125 °. A wavy interphase separates the PEI/ epoxy carbon fibre. The red arrow indicates a scratchy-like surface around the interphase.



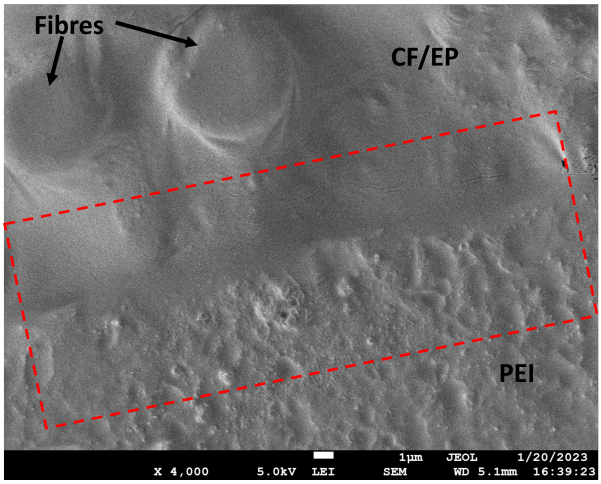
(d) Autoclave sample with the first dwell at 135 °. A wavy interphase separates the PEI/ epoxy carbon fibre. The red arrow indicates a scratchy-like surface around the interphase.

Figure 5.14: Bulk epoxy - PEI interphase, SEM images Interphase between PEI and bulk epoxy is indicated with the orange box. The higher the curing temperature of the first dwell, the less straight (wavier) the interphase is. Indicating higher activity at the interphase during co-curing.

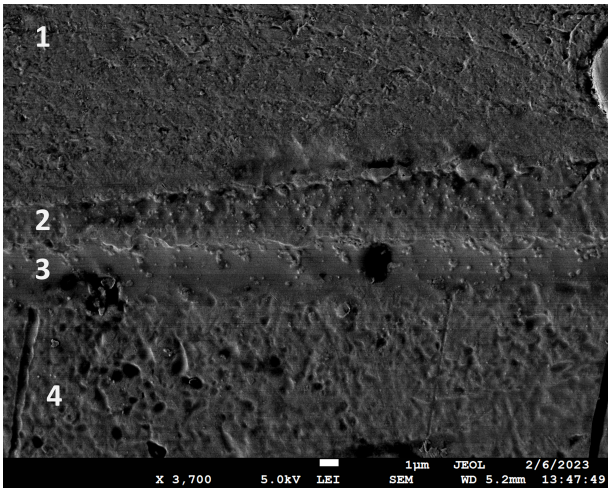
As described in the section 5.2, two samples are manufactured with the hot press. The purpose of manufacturing samples with the hot press is to remove the thermal ramp and make a direct comparison of the impact of this ramp. As a result, gelation occurs at the isothermal curing temperature rather than during the heating ramp, as it did for the samples cured in the autoclave at isothermal 125 and 135 °C, see Figure 5.12. The literature study section 2.7, that due to the loss of mobility of the thermoset, diffusion slowed down after gelation. Causing the majority of the interdiffusion to occur before gelation. Comparing the sample cured at 135 °(Figure 5.13d) with and without the heating ramp (Figure 5.15a shows a smoother transition between the PEI and epoxy/carbon fibre interphase for the sample without the heating ramp. The straight line visible for the sample with the ramp has vanished, which indicates increased diffusion. Only the bulk epoxy side of the 135with heating ramp sample showed this type of interphase.

The hot press sample isothermally cured at 149°C shows even greater interphase. Allowing the different regions described in section 2.7 to be more distinguishable. The different interphase regions are indicated in Figure 5.16b. Region 1 is pure epoxy. Between 1 and 2, the initial interphase line is visible. In region 2, epoxy particles are diffused into the PEI matrix. In 3, moving towards 4, the scratchy-like surface increases. In the literature, this is defined as an interdiffusion between PEI/epoxy. In 4, the pure PEI matrix can be found, which is indicated by this scratchy texture. The void content is high in both samples manufactured with the hot press. This indicates and shows the importance of using a heating ramp. The viscosity profile of curing thermoset resins is explained subsection 4.4.5. One of the main reasons to use a slow heating ramp is to

allow the viscosity of the resin to decrease before curing, making it easier to allow the trapped air to flow out of the sample and resulting in an interphase with a minimal amount of voids. However, the air is trapped when the sample is heated too quickly. The gel point is reached within the first minute, see Figure 5.8e, causing the viscosity to increase. Therefore, trapped air does not get the change to flow out of the sample. Nevertheless, these samples helped demonstrate the effect of the ramp on the diffusion process despite the high void content. Parts without voids were chosen for study in the SEM figures since the voids were not the focus of this specific experiment.



(a) Interphase between the carbon fibre epoxy and PEI. The interphase line has varnished, and a smooth interphase has formed, indicated by the red box.



(b) Interphase 149 hot press: Region 1 is pure epoxy. Between 1 and 2, the initial interphase line is visible. In region 2, epoxy particles are diffused into the PEI matrix. In 3, moving towards 4, the scratchy-like surface increases. In the literature, this is defined as an interdiffusion between PEI/epoxy. In 4, the pure PEI matrix can be found, which is indicated by this scratchy texture.

Figure 5.15: SEM figures from the samples cured with the hot press at (1) 135 °C and (2) 149 °C.

Thickness of the interphase measured with the SEM

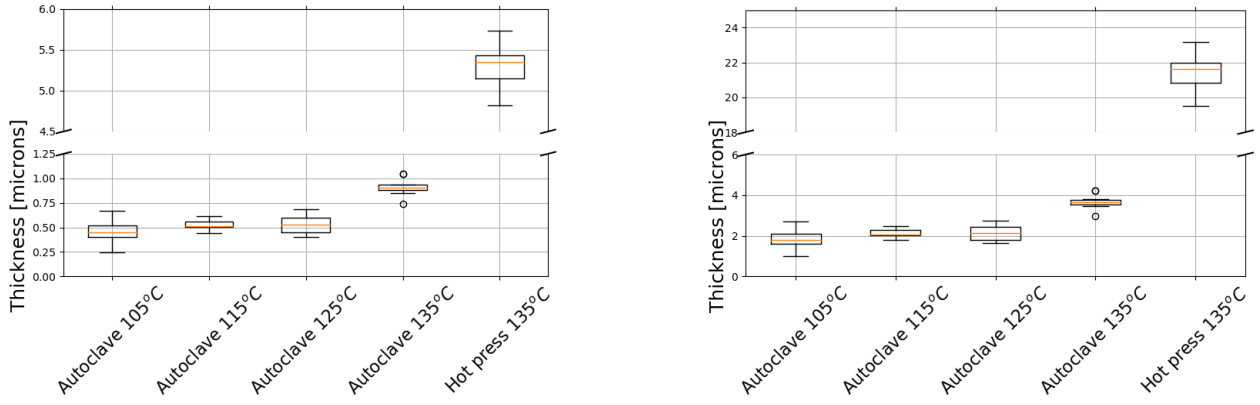
As mentioned in Figure 5.3, the diffusivity at the PEI - epoxy/carbon fibre interface is reduced by 24.7 % in comparison to bulk diffusivity. The SEM is used to measure the thickness of the PEI film after curing. Initially, the film has a thickness of 60 microns. The bottom interface is PEI - epoxy/carbon fibre for the samples cured in the autoclave. The top interface is PEI - bulk epoxy resin. The total diffusion length of the PEI - epoxy/carbon fibre is calculated with Equation 5.4, and the total diffusion length of PEI - bulk epoxy resin is calculated with Equation 5.5. The SEM is used to measure the thickness of the PEI film. It is assumed that the shrinkage in measured PEI film results in epoxy/PEI interphase formation. The parts cured in the hot press have a prepreg above and below the PEI film. Resulting in two PEI - epoxy/carbon fibre interfaces. Therefore, the diffusion length of this interphase is calculated by Equation 5.6. Lastly, the diffusion depth of the PEI-epoxy bulk is calculated for these samples with Equation 5.7. The results are represented in Figure 5.16. It was impossible to determine the PEI thickness in the sample produced through hot pressing at 149°C due to a high concentration of voids. An illustration of an SEM image of the PEI thickness measurements can be found in the appendix section C.8.

$$Diffusiondepth PEI - ep/cf = (Initialthickness - measuredthickness)/124.7\% * 24.7 \tag{5.4}$$

$$Diffusiondepth PEI - ep/bulk = (Initialthickness - measuredthickness)/124.7\% * 100 \tag{5.5}$$

$$Diffusiondepth PEI - ep/cf = (Initialthickness - measuredthickness)/2 \tag{5.6}$$

$$Diffusiondepth PEI - ep/bulk = (Diffusiondepth PEI - ep/cf)/24.7\% * 100 \tag{5.7}$$



(a) Diffusion depth PEI - epoxy /carbon fibre interface

(b) Diffusion depth PEI - bulk epoxy resin interface

Figure 5.16: The diffusion length in microns, measured with the SEM. The higher the curing temperature, the higher the interphase thickness and therefore the diffusion length.

All the observations of the interphase analysis of this chapter are summarized in Table 5.2.

Table 5.2: Comparative tables of the results of the interphase analysis in this section.

	Heating ramp + 105 °C isothermal	**Heating ramp + 115 °C isothermal**	**Heating ramp + 125 °C isothermal**	**Heating ramp + 135 °C isothermal**	**135 °C without ramp**	**149 °C without ramp**
Microscopy: Bulk epoxy- PEI	-Wavy shape -Dark shaded area	-Wavy shape -Dark shaded area	-Wavy shape -Dark shaded area	-Wavy shape -Dark shaded area	N/A	N/A
Microscopy: Epoxy/CF- PEI	-Straight line -No colour changes	-Straight line -No colour changes	-Straight line -No colour changes	-Straight line -No colour changes	N/A	N/A
SEM: Bulk epoxy-PEI	-Wavy shape -Clear boundary line	-Wavy shape -Interphase visible	-Clear interphase visible -Boundary line faded away	-Clear interphase visible -Boundary line faded away	N/A	N/A
SEM: epoxy/CF-PEI	-Clear boundary line -No interphase visible	-Clear boundary line -No interphase visible	-Clear boundary line -No interphase visible	-Boundary line less visible -Interphase starts to get visible	-No boundary line - Different interphase regions visible	-No boundary line - Different interphase regions visible
Length interphase: Bulk epoxy- PEI	1.81 $\pm 0.48 \mu$m	2.12 $\pm 0.21 \mu$m	2.13 $\pm 0.37 \mu$m	3.69 $\pm 0.34 \mu$m	21.42 $\pm 0.97 \mu$m	N/A
Length interphase: Epoxy/CF- PEI	0.45 $\pm 0.12 \mu$m	0.52 $\pm 0.05 \mu$m	0.52 $\pm 0.09 \mu$m	0.91 $\pm 0.09 \mu$m	5.29$\pm 0.24 \mu$m	N/A
Gelation in ramp or isothermal phase	Isothermal	Isothermal	Ramp	Ramp	Isothermal	Isothermal

5.4. Concluding remarks

- The selected thermoplastic film for this study is PEI. This is based on the literature study and the availability of the DASML lab.
- Interphase formation occurs in the relevant temperature range (105 -135 °C).
- The tortuosity causes a difference in diffusion, with carbon fibres obstructing the diffusion of epoxy particles compared to diffusion in a pure resin. This effect is observed in this chapter.
- The interphase formation is hard to observe with the cross-sectional images with the Keyence laser confocal microscopy. No interphase formation is observed at the epoxy/carbon fibre - PEI interphase. A wavy shape and a dark-shaded area are observed at the bulk epoxy- PEI interphase. Indicating interphase formation has taken place.
- The interphase formation is observed with the scanning electron microscope. The higher the isothermal temperature, the stronger the interphase formation. At low temperatures, the interphase is indicated by a straight line. At high temperatures, this starts to fade away in a transition zone.
- Gelation occurs in the heating ramp for the autoclave samples 125 °C and 135°. However, the interphase length of the 135 °C sample is two times larger. Additionally, the epoxy/CF-PEI interphase is not visible for the 125 °C sample but for the 135 °C sample. Indicating interdiffusion does take place after gelation.
- The sample at 135°C without a heating ramp has about a five times larger interphase length than the sample with a heating ramp cured at 135°C. Therefore, it is concluded that most of the interdiffusion does take place before gelation.
- The higher the temperature, the stronger the interphase formation. According to the datasheets, the maximum curing temperature is 149 °C. The potential of this interphase is shown, and different transition zones can be identified. However, curing without a heating ramp causes a high void content.

- The phase separation phenomenon described in the literature study is not observed. This most likely occurred on a smaller scale and was not observable. Additionally, studies describing this phenomenon do have curing temperatures in the range of 160-180 °C.

6

Mechanical strength

In this chapter, the lap shear strength of the joints will be tested. The current at Hall Spars used the joining method, epoxy adhesive, which will be used as the benchmark. Therefore, it will be referred to as adhesive film or benchmark. The methodology will be described in section 6.1. section 6.2 presents the sample preparation. In section 4.3, the measurements are shown, and the results are shown and discussed in section 6.4. Lastly, the concluding remarks of this chapter are given in section 6.5.

6.1. Methodology

The function of a joint is to transfer load. Load transfer occurs via shear stresses in the adhesive. To compare different types of joints, it is useful to compare the shear strength of the joints. The ultimate strength will be tested. The ultimate shear strength is a property of a joint. The maximum stress a joint can withstand before failure is called the ultimate strength. The stress over strain curve is schematically represented in the Figure 6.1. The top of the curve is the ultimate strength. Note that this is the average shear strength. The shear stress is distributed along the length of the joint. This stress distribution will be explained more deeply in section 6.4.

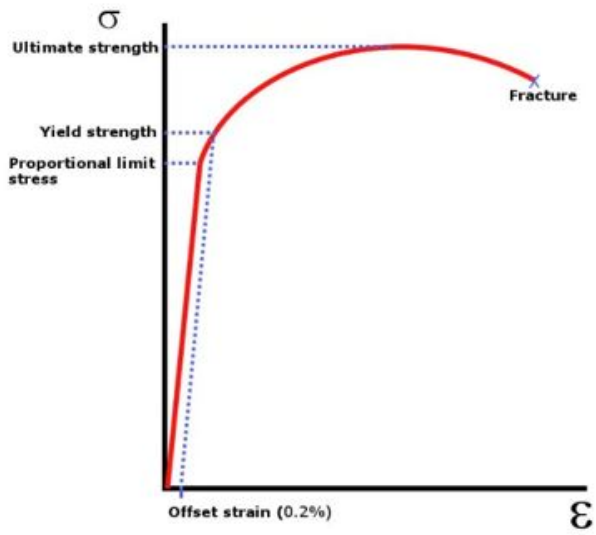
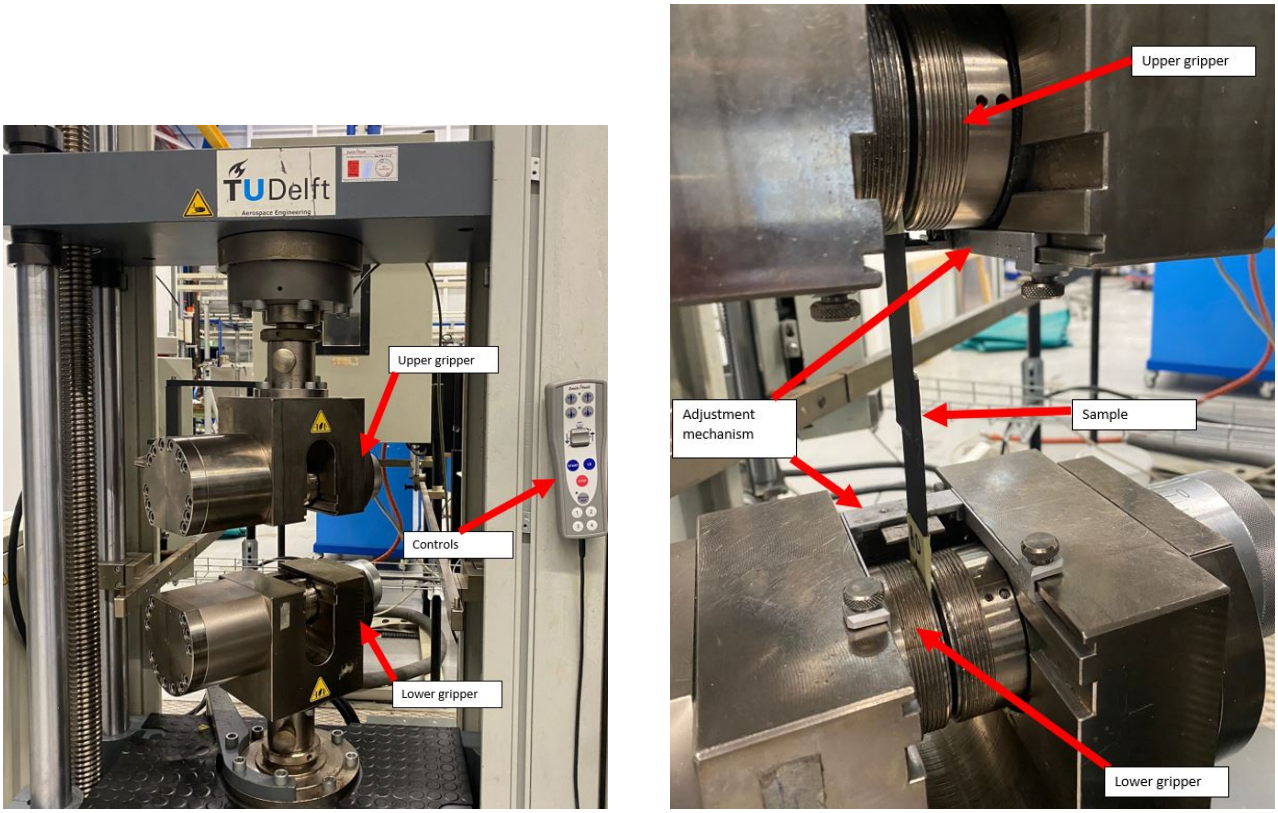


Figure 6.1: Schematic figure, ultimate strength is the top of the curve

Three joint configurations are introduced in this study. Firstly, a joint using the epoxy adhesive. From now on, this will be called ”adhesive film”. This joint configuration represents the benchmark. This configuration is currently used at Hall Spars. The second configuration uses a PEI film as coupling. Lastly, joints will be manufactured using partially cured epoxy. The joint configurations, materials and sample manufacturing will

be discussed in more detail in the next section. One of the components which will be tested is the ultimate shear strength of the joint. In combination with a fracture surface analysis, a judgement of the mechanical performance of the joints can be made. The 250 kN Zwick tensile testing machine in the DASML lab will be used. The maximum measured value will be reported as the ultimate shear strength (USS). The D5868 standard test method for lap shear adhesion for fibre-reinforced plastic bonding will be used for this experiment [21]. The recommended loading rate is changed from 13 to 1 mm/sec to create more data points to get more reliable data. This is decided together with a DASML lab assistant. Five samples in each case are created and tested.



(a) Test setup without sample

(b) Test setup with sample

Figure 6.2: 250 kN Zwick tensile testing machine in the DASML lab

The test setup is represented in Figure 6.2. The adjustment mechanism is shown in the Figure 6.2b. This is carefully aligned for the first sample. After the first sample, this mechanism is fixed. This ensures that all samples are equally aligned and loaded in the same direction. The Load per strain and the type of failure will be reported. The data will be collected and saved in the Zwick software. The deformation of the sample and the deformation of the entire machine will cause the measured strain. However, the expected maximum shear load will be in the order of 10-20 kN. This is 5-10 % of the maximum capacity of the machine, and the machine's deformation is expected to be negligible. Secondly, the measured data of all the samples will be compared. The machine will deform in the same manner for all the samples. Therefore the deformation of the machine will be neglected. Therefore no digital image correlation measurements are needed to measure the strain.

6.2. Sample preparation and material definition

As mentioned above, three types of joints will be tested. Adhesive film, partially cured and with a PEI film. The adhesive used for the benchmark sample will be called the epoxy adhesive from now on due to confidentiality. The carbon fibre epoxy pre-preg is mentioned in section 4.1 and the PEI film is introduced in section 5.1. The dimensions of the lap shear samples were manufactured accordingly to the standard; see figure Figure 6.3 [21].

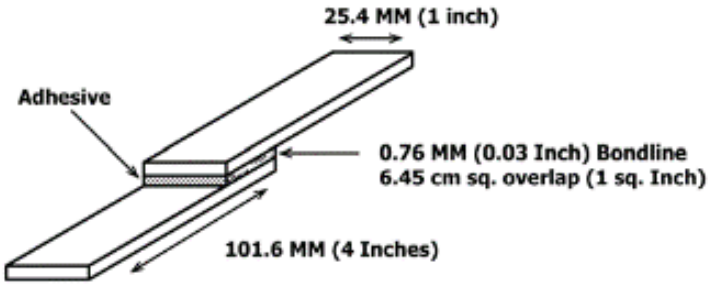


Figure 6.3: Dimensions lap shear joint according to the D5868 standard [21]

To avoid bending loads or imperfections in the adhesive layer, support parts will be manufactured. These parts will be used during the curing phase in the autoclave. They also help to distribute the pressure onto the sample evenly. These support parts will have the same thickness as the adherents. These supports are wrapped in release film to avoid sticking to the sample. In Figure 6.4 this is schematically represented. Note: This representation is not in the correct scale. It is an illustration.

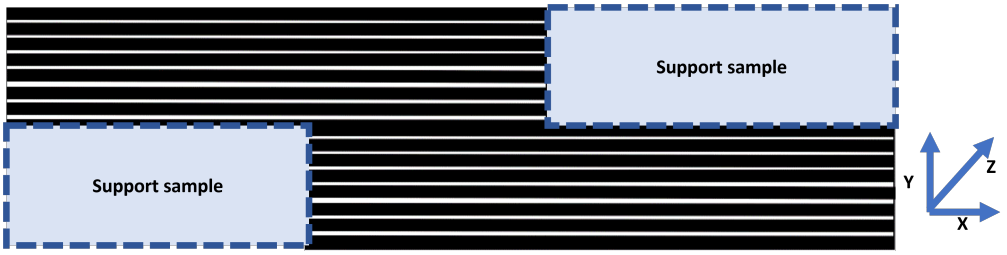


Figure 6.4: Support parts supporting the sample during curing. The black lines are the part, (cured carbon fibre epoxy prepreg) and in the blue, the support samples are indicated.

The density of the carbon fibre prepreg is $300 gram/m^2$, and the thickness of a single layer is 0.3 mm. The quasi-isotropic layup $[0/-45/90/45]_s$ will be used to avoid coupling. The ABD stiffness matrix is given in the appendix section C.9. Due to symmetry, the B matrix is zero, which results in no in-plane out-f-plane coupling. A_{16} and A_{26} are zero, this results in no extension-shear coupling. In the lap shear test, a load along the joint direction, X, see Figure 6.4. For this quasi-isotropic, the response will be an extension along the x-axis,ϵ_X, and compression along the y-axis,ϵ_Y, due to the Poisson effect. The layup is illustrated in Figure 6.5. The plates will be 2.4 mm thick, 177.8 mm wide and 177.8 mm long. The plates will later be cut into smaller samples. This will be explained in the next section.

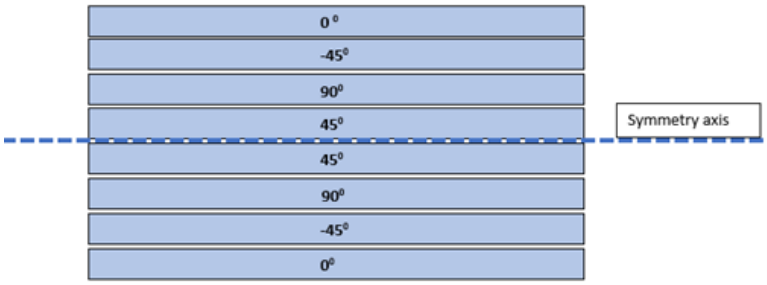


Figure 6.5: Schematic illustration of the layup

Sample manufacturing

The next step is to manufacture the samples. First, the final configuration will be represented and explained.

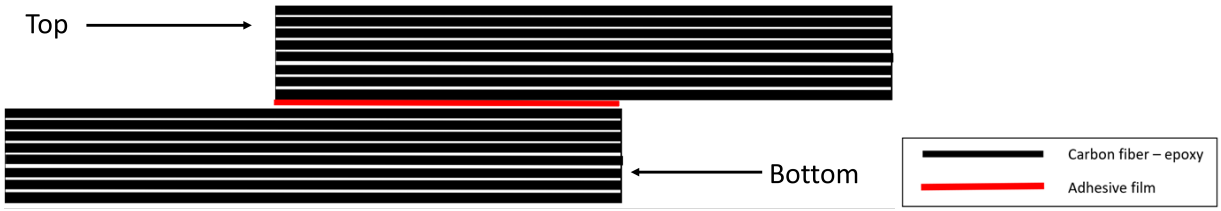


Figure 6.6: Benchmark sample, parts joined with epoxy adhesive film

The benchmark sample is manufactured with the epoxy adhesive. This is represented in Figure 6.6. The bottom part is cured with the adhesive in the first curing cycle. The top part is placed on the adhesive in a second curing cycle and cured.

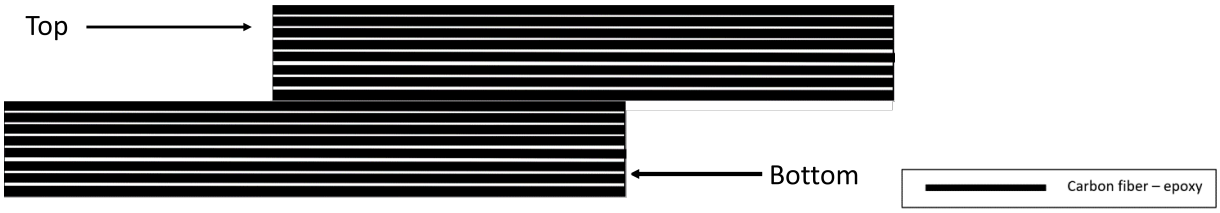


Figure 6.7: Partially cured sample

For the partially cured samples, no adhesive is used. This is represented in Figure 6.7. In the first curing cycle, the bottom part is partially cured. So the cycle is stopped before the curing reaction is finished. The top part is placed on the partly cured bottom in a second curing cycle. In the second cycle, both parts are fully cured. Two types of partially cured samples are made, one series where the degree of cure of the bottom is 0.5 and one with 0.7.

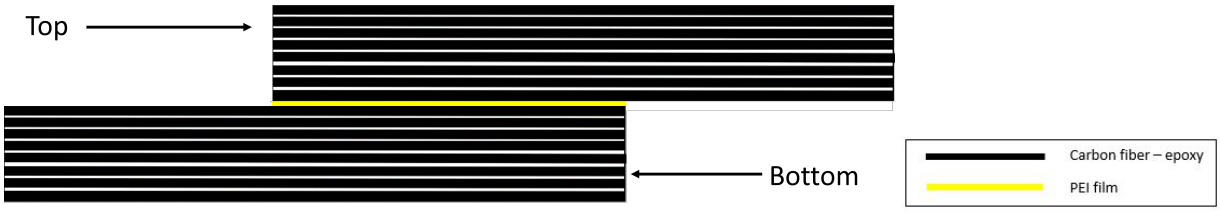


Figure 6.8: PEI film as adhesive coupling layer

In Figure 6.8, the configuration of the samples with the PEI film as a coupling layer is shown. The bottom part is cured with the PEI film in the first curing cycle. The top part is placed on the PEI in a second curing cycle and cured. Co-curing the PEI film together with first the bottom and secondly the top adherend avoids the usage of a heating mechanism.

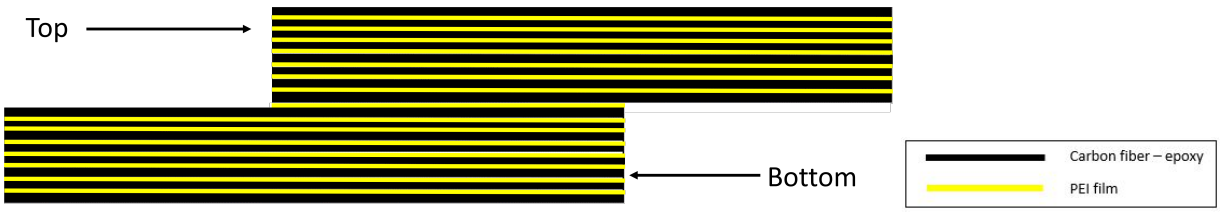


Figure 6.9: Illustration of two types of parts which will be B-staged and co-cured together [4]

In Figure 6.8, the configuration of the samples with the PEI film as coupling and as an interlayer between each prepreg is shown. The bottom part is cured with the PEI film in the first curing cycle. The top part is placed on the PEI in a second curing cycle and cured. A PEI film is placed in the layup between each carbon fibre epoxy

prepreg. Two types of this configuration are made. The first series, the PEI interlayer, has a thickness of 60 microns. In the second series, the interlayer is 120 microns. In both series, the PEI interlayers are 60 microns.

The manufacturing process is listed below. Different steps are required for different configurations. This will be reported. Note scale of the schematic illustrations is not correct.

1. **Defrost:** The carbon fibre epoxy prepreg is taken out of the freezer. Wait till the temperature of the material reaches room temperature.
2. **Mold preparation:** The sides are sanded so the sealant tape will stick. Secondly, the mould is cleaned with isopropanol, and the sides are taped off to keep the surface clean for the sealant tape. Mould is treated with Marbocote. This should be rubbed onto the mould at least four times, separated by at least five minutes.
3. **Cutting:** Once the prepreg is up to room temperature, the prepreg is cut by hand with a rotary cutter. Covers with the required size are 3D printed and placed on top of the prepreg to increase the accuracy of the cutting. The PEI, adhesive, and release film are cut with a Stanley knife. Lastly, the vacuum bag and breather are cut with scissors.
4. **Building up laminate:** The build-up of each configuration is different. They will be explained separately. For all samples, the breather and peel ply should stick out and lead to the vacuum connection. This allows the air to flow out and create a vacuum, see Figure 5.3.

    - **Adhesive film sample:** Peel ply is placed at the mould to create a path for the excess resin and the air to flow. The Adhesive film is placed on top of the peel ply. The prepreg is placed; every three layers, the sample is debulked for three minutes per layer. At the top comes the peel ply, release film, breather and vacuum bag are placed. The vacuum bag is stuck onto the sealant tape.

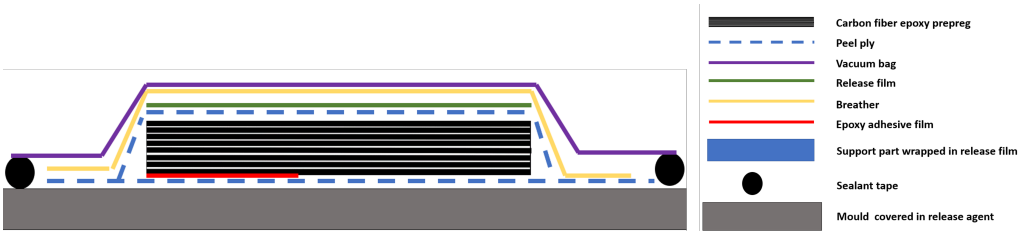


Figure 6.10: Build up bottom part, configuration with adhesive film, including the legend.

- **Partially cured sample:** Peel ply is placed at the mould to create a path for the excess resin and the air to flow. The prepreg is placed; every three layers, the sample is debulked for three minutes per layer. At the top comes the peel ply, release film, breather and vacuum bag are placed. The vacuum bag is stuck onto the sealant tape.

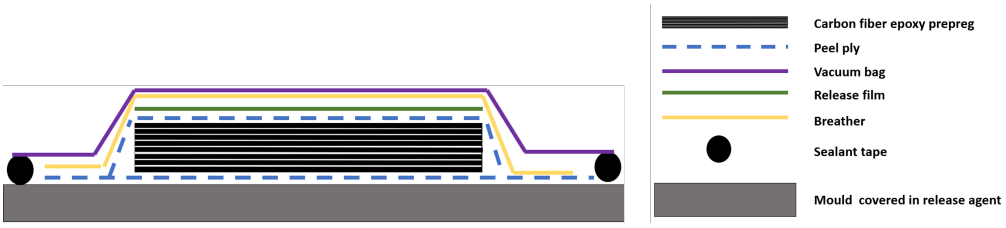


Figure 6.11: Build up bottom part, configuration with partial cure, including the legend.

- **PEI film sample:** The PEI film is cleaned with isopropanol and placed directly onto the mould. Next to the PEI film, the Peel ply is placed at the mould to create a path for the excess resin and the air to flow. The prepreg is placed; every three layers, the sample is debulked for three minutes per layer. At the top comes the peel ply, release film, breather and vacuum bag are placed. The vacuum bag is stuck onto the sealant tape.

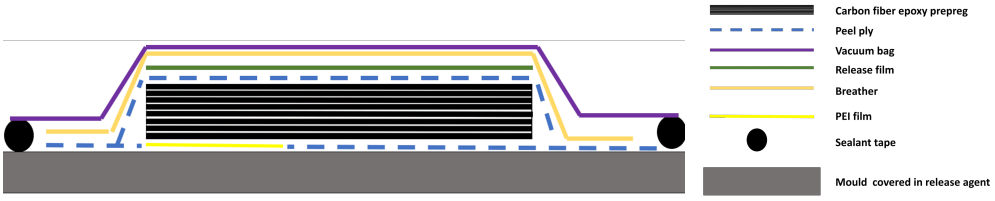


Figure 6.12: Build up bottom part, configuration with PEI film, including the legend.

- **PEI film and PEI interlayer sample:** The PEI film is cleaned with isopropanol and placed directly onto the mould. Next to the PEI film, the Peel ply is placed at the mould to create a path for the excess resin and the air to flow. The prepreg is placed with a PEI film between every layer; for every three layers, the sample is debulked for three minutes per layer. At the top comes the peel ply, release film, breather and vacuum bag are placed. The vacuum bag is stuck onto the sealant tape.

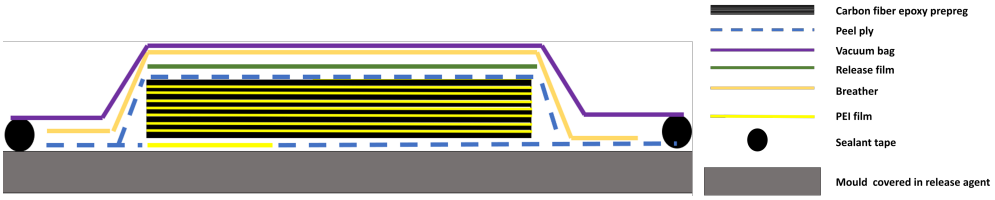


Figure 6.13: Build up bottom part, configuration with PEI film and interlayer, including the legend.

5. **Cure bottom part:** Once the vacuum bag is connected to the sealant tape, a leak test should be performed. The next step is to cure the bottom parts.

   - **Epoxy adhesive film, PEI film and PEI film + PEI interlayer:** For these samples, the curing cycle of Hall Spars is used. This is to create testing conditions as close as possible to the application. During the entire cure cycle, the pressure in the autoclave is 3.45 bar, and the pressure in the vacuum bag is a vacuum (typically around 0.08 bar). The temperature ramp is 1 °C/min. The isothermal phase is 120 minutes at 120 °C. Then the sample is cooled to room temperature with 5 °C/min. The curing cycle is shown in Figure 6.14. The estimated degree of cure and glass transition temperature are also shown. These values are based on the models derived in chapter 4.

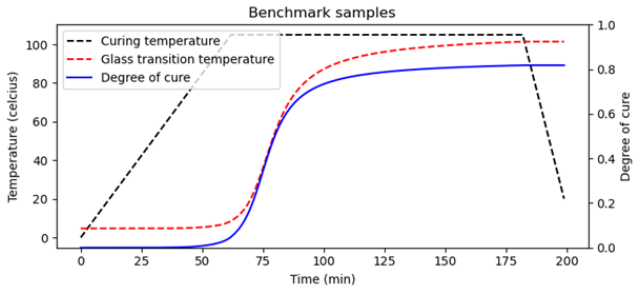


Figure 6.14: Curing temperature, calculated degree of cure and calculated glass transition temperature.

   - **Partially cured sample with a degree of cure of 0.7:** During the entire cure cycle, the pressure in the autoclave is 3.45 bar, and the pressure in the vacuum bag is a vacuum (typically around 0.08 bar). The temperature ramp is 1.7 °C/min. The isothermal phase is 105 minutes at 30 °C. Then the sample is cooled to room temperature with 15 °C/min. The curing cycle is shown in Figure 6.15. The estimated degree of cure and glass transition temperature are also shown. These values are based on the models derived in chapter 4. The degree of cure after this cycle is estimated to be 0.7.

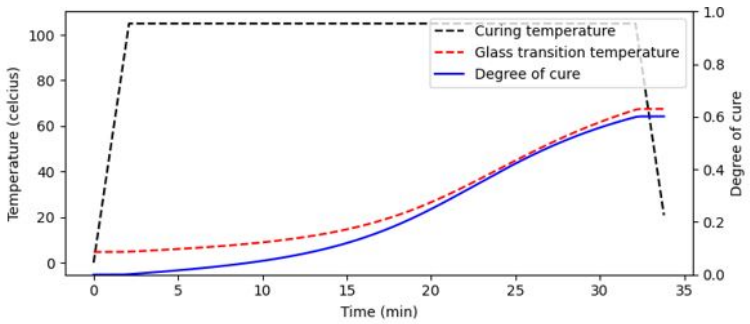


Figure 6.15: Curing temperature, calculated degree of cure and calculated glass transition temperature. Cure cycle for the partially cured sample with DOC of 0.7.

- **Partially cured sample with a degree of cure of 0.5:** During the entire cure cycle, the pressure in the autoclave is 3.45 bar, and the pressure in the vacuum bag is a vacuum (typically around 0.08 bar). The temperature ramp is 1.7 °C/min. The isothermal phase is 105 minutes at 25 °C. Then the sample is cooled to room temperature with 15 °C/min. The curing cycle is shown in Figure 6.16. The estimated degree of cure and glass transition temperature are also shown. These values are based on the models derived in chapter 4. The degree of cure after this cycle is estimated to be 0.5.

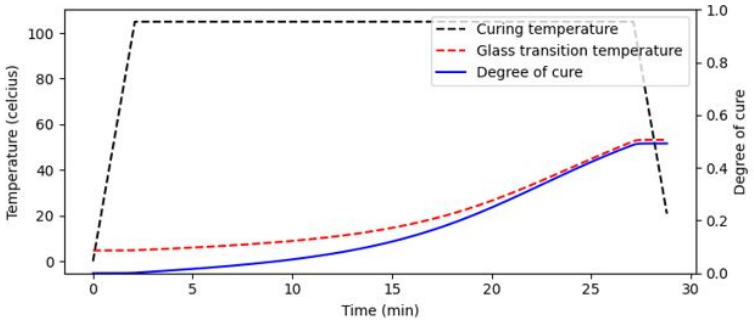


Figure 6.16: Curing temperature, calculated degree of cure and calculated glass transition temperature. Cure cycle for the partially cured sample with DOC of 0.5.

6. **Layup top part:** The mould is prepared as described above. The support samples are wrapped into release film, which prevents the support samples from sticking onto the sample.

   - **Adhesive film sample:** The bottom support part is placed. Peel ply is placed onto the support sample to create a path for the excess resin and the air to flow. The prepreg is placed onto the adhesive film. The prepreg is placed; For every three layers. The sample is debulked for three minutes per layer. The top support sample is placed. At the top comes the peel ply, release film, breather and vacuum bag are placed. The vacuum bag is stuck onto the sealant tape.

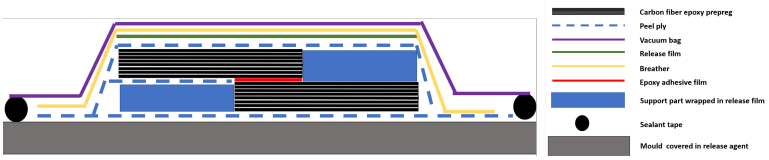


Figure 6.17: Build up the top part, configuration with adhesive film, including the legend.

   - **Partially cured sample:** The bottom support part is placed. Peel ply is placed onto the support sample to create a path for the excess resin and the air to flow. The prepreg is placed; For every three layers, the sample is debulked for three minutes per layer. The top support sample is placed. At the top comes the peel ply, release film, breather and vacuum bag are placed. The vacuum bag is stuck onto the sealant tape.

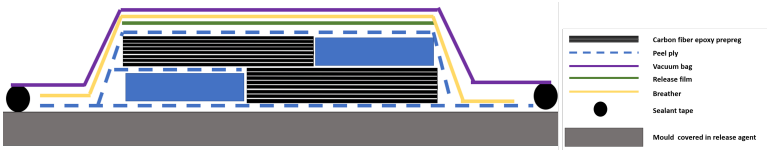


Figure 6.18: Build up the top part, configuration with partial cure, including the legend.

- **PEI film sample:** The bottom support sample is placed. Peel ply is placed onto the support sample to create a path for the excess resin and the air to flow. The prepreg is placed onto the PEI film. The prepreg is placed; For every three layers, the sample is debulked for three minutes per layer. The top support sample is placed. At the top comes the peel ply, release film, breather and vacuum bag are placed. The vacuum bag is stuck onto the sealant tape.

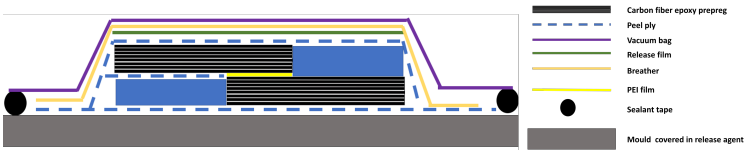


Figure 6.19: Build up the top part, configuration with PEI film, including the legend.

- **PEI film and PEI interlayer sample:** The bottom support sample is placed. Peel ply is placed onto the support sample to create a path for the excess resin and the air to flow. The prepreg is placed onto the adhesive film. The prepreg is placed with a PEI film between every layer; For every three layers, the sample is debulked for three minutes per layer. The top support sample is placed. At the top comes the peel ply, release film, breather and vacuum bag are placed. The vacuum bag is stuck onto the sealant tape.

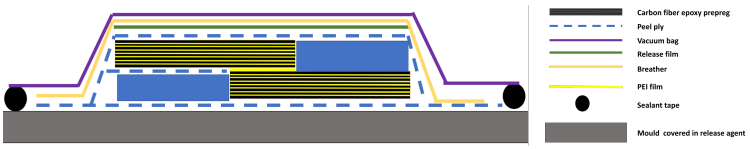


Figure 6.20: Build up the top part, configuration with PEI film and PEI interlayer, including the legend.

7. **Cure samples:** Once the vacuum bag is connected to the sealant tape, a leak test should be performed. The next step is to cure the bottom parts. For all the joint configurations, the second curing cycle is the same. This is the curing cycle used at Hall Spars. During the entire cure cycle, the pressure in the autoclave is 3.45 bar, and the pressure in the vacuum bag is a vacuum (typically around 0.08 bar). The temperature ramp is 1 °C/min. The isothermal phase is 120 minutes at 120 °C. Then the sample is cooled to room temperature with 5 °C/min. The curing cycle is shown in Figure 6.14. The estimated degree of cure and glass transition temperature are also shown. These values are based on the models derived in chapter 4.
8. **Cut samples:** The final step is to cut the samples into the correct size according to the standard [21]. It is recommended to cut this with a diamond-tip water-coiled blade. These cuts are made with the digitally automatable Proth column cutter. This cutter has a diamond-coated circular blade which is 2 mm thick. The sample width is 25.4 mm. The Proth removes 100 microns per horizontal movement.
9. **Setting up the machine:**The sample is loaded in the tensile testing machine. The adjustment mechanism is set to ensure that all samples are loaded in the same orientation. The grip distance is 150 mm, and the speed is 1 mm/min.

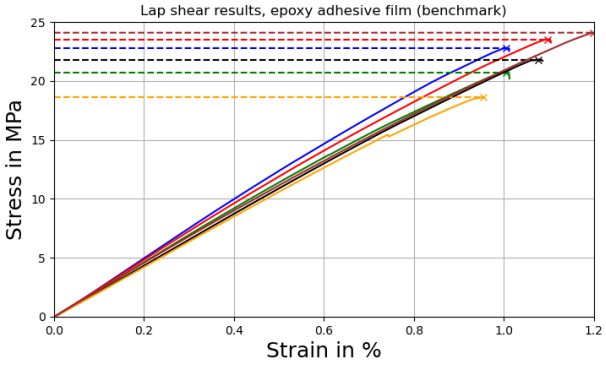
6.3. Measurements

The area of the overlap of the joint is reported and can be found in the appendix Appendix F. The average shear stress in the joint is calculated with Equation 6.1, where P is the measured load, and A is the overlap area of the joint. The ultimate shear load is calculated with Equation 6.2. Note this ultimate shear load is the *average* ultimate shear load.

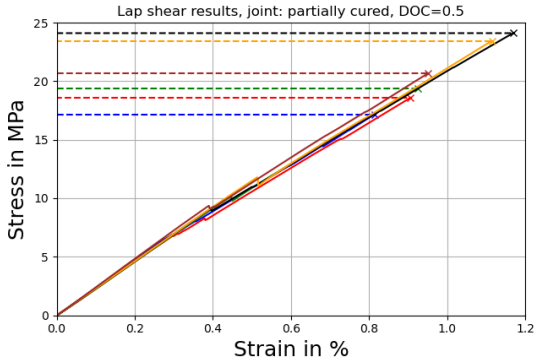
$$\tau_{av} = P/A \tag{6.1}$$

$$\tau_{avmax} = P_{\text{max}}/A_0 \tag{6.2}$$

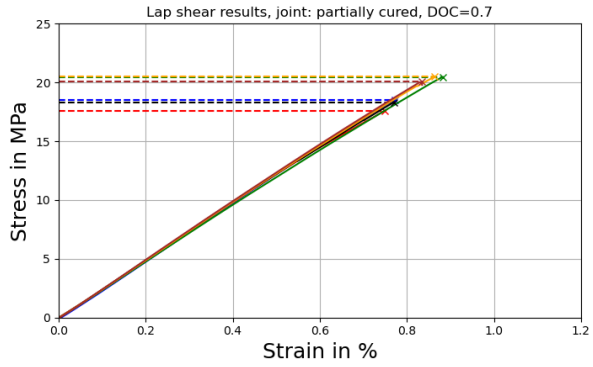
The measured shear stress over strain for each sample is reported. The measurements are shown in Figure 6.21 and in Figure 6.22. The measurement will be discussed in detail in section 6.4. The Partially cured DOC=0.7 configuration and the parts with the PEI as the coupling layer show results comparable to the benchmark samples. However, the PEI coupling samples have a standard deviation half the size of the benchmark samples and the partially cured DOC=0.7. The partially cured DOC=0.5 and the PEI coupling + interlayer samples perform less in terms of ultimate lap shear strength. However, interesting to point out is the positive outlier for the PEI 120 microns coupling and 60 microns PEI interlayer.



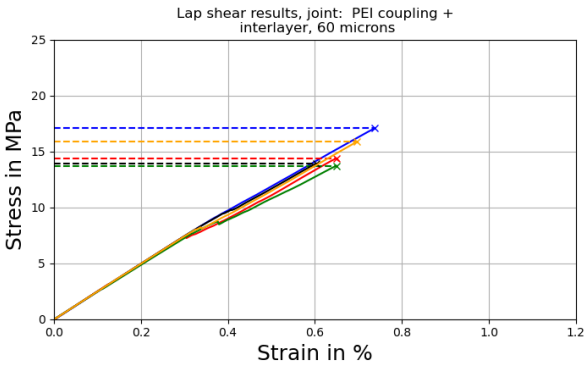
(a) Lap shear results of the benchmark sample, epoxy adhesive film.



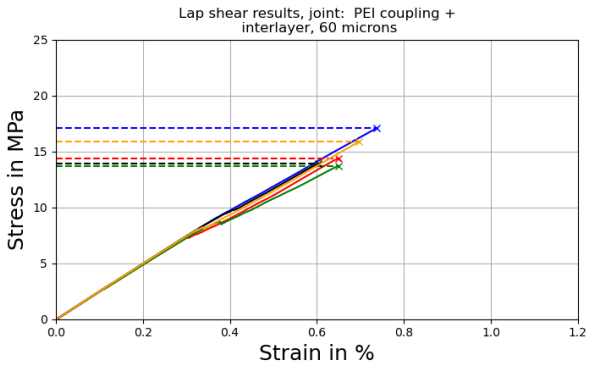
(b) Lap shear results of the partially cured bottom part after the first curing cycle. The degree of cure was 0.5



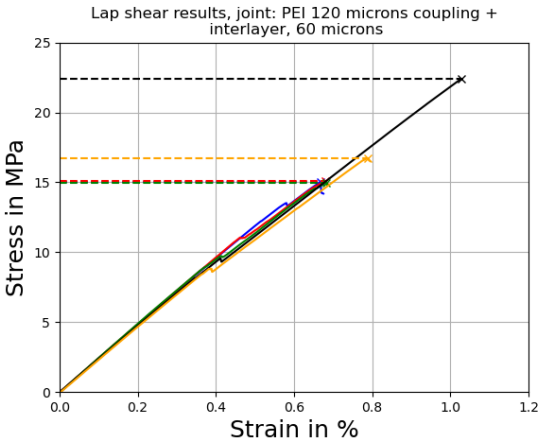
(c) Lap shear results of the partially cured bottom part after the first curing cycle. The degree of cure was 0.7



(d) Lap shear results with a PEI coupling layer of 60 microns.



(e) Lap shear results with a PEI coupling layer of 60 microns and the 60 micron PEI interlayer.



(f) Lap shear results with a PEI coupling layer of 120 microns and the 60 micron PEI interlayer.

Figure 6.21: The results of the lap shear tests. The shear stress is displayed over the strain. Each colour indicates a sample. The ultimate shear stress of each sample is indicated with the cross.

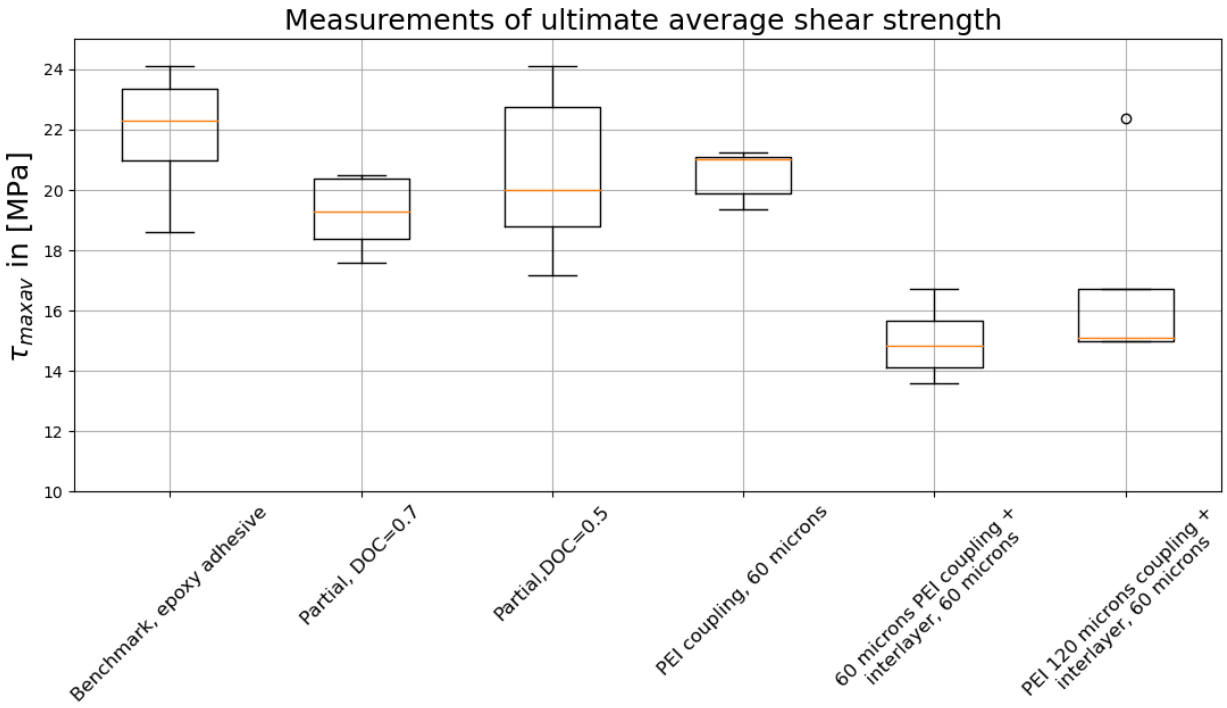


Figure 6.22: Measured ultimate lap shear strength of each configuration. Data is represented in a box chart. This data will be discussed in section 6.4

6.4. Results and discussion

The measured results from the single lap shear experiments in the Zwick will be discussed in this section. Additionally, the fracture surfaces will be used to explain these results.

6.4.1. Fracture surface

The lap shear strength is derived with the failure stress analysis with the Zwick. Additionally, the fracture surface is reported. Acceptable failure modes are cohesive failure of adhesive, surface ply delimitations or adherend failure. Other failure modes are unacceptable and indicate either a test misalignment/manufacturing error or a weak adhesive/adherent interface. This is illustrated in Figure 6.23. The fracture surface of the samples is analysed with the Keyence VK-X1000 3D laser scanning confocal microscope, zoomed 10x. This microscope analyses the height of the surface. Therefore, ply failure becomes visible.

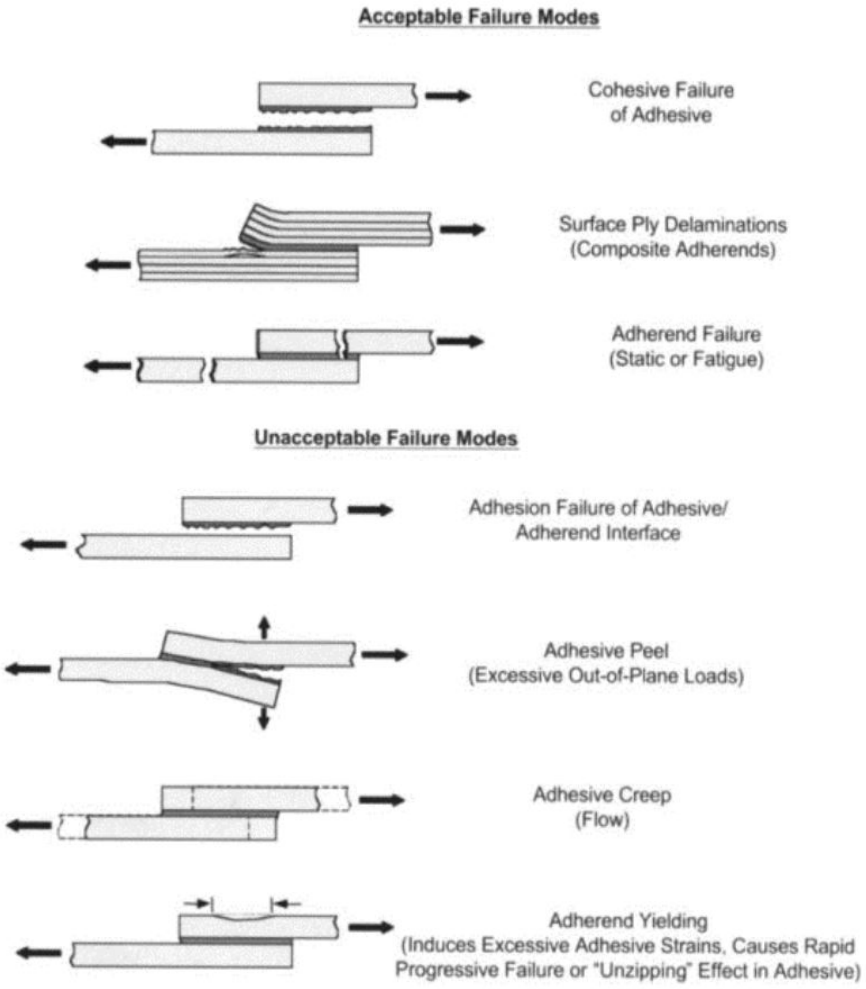


Figure 6.23: Acceptable and unacceptable failure modes [21]

The results of the surface analysis of the top view of the specimens. The top view is illustrated in red inFigure 6.24. The result of each configuration will be discussed.

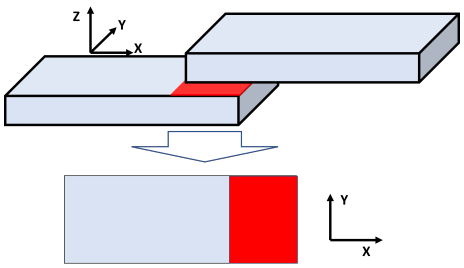
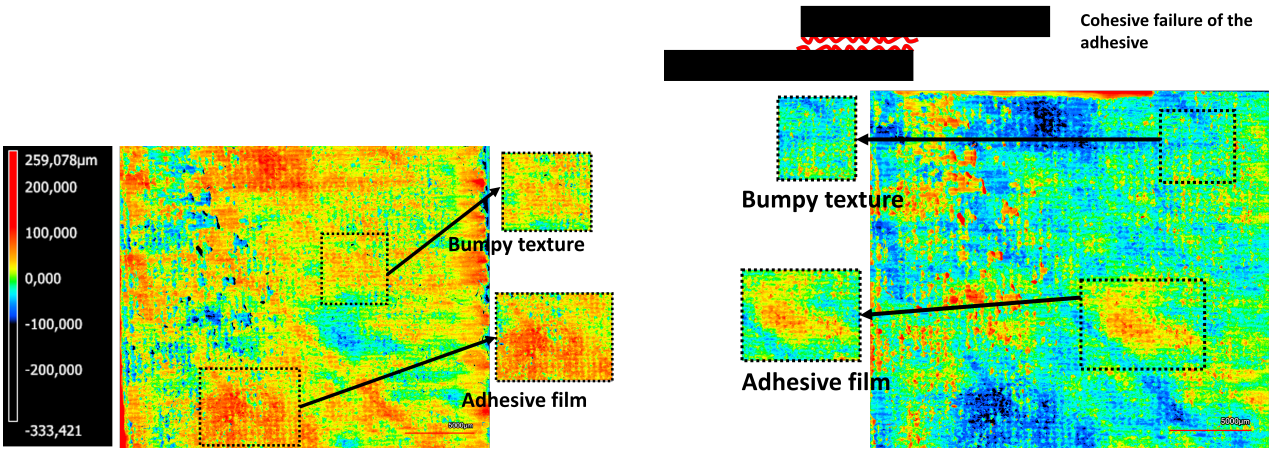


Figure 6.24: Top view fracture surface. Fracture surface in red

Epoxy film adhesive, benchmark sample

The failure mode is the cohesive failure of the adhesive. This is an accepted failure mode and could therefore be expected to occur. The failure occurs in the epoxy-based adhesive film, which is a thermoset. This thermoset is brittle. Local defects could initiate a crack. These cracks cause failure due to the brittle characteristics of a thermoset. Little energy is stored in the joint due to its relatively low fracture toughness (in perspective to a thermoplastic polymer). Therefore, it is likely for this type of joint to have this cohesive failure in the adhesive. This concept will be explained in more detail in subsection 6.4.2. The fracture surface is

displayed in the Figure 6.25. It becomes visible the adhesive remained partially on both sides (marked in red, height). This indicates the cohesive failure of the adhesive. The bumpy texture, visible in Figure 6.25, is a desired result of the peel ply on the surface in the manufacturing process.

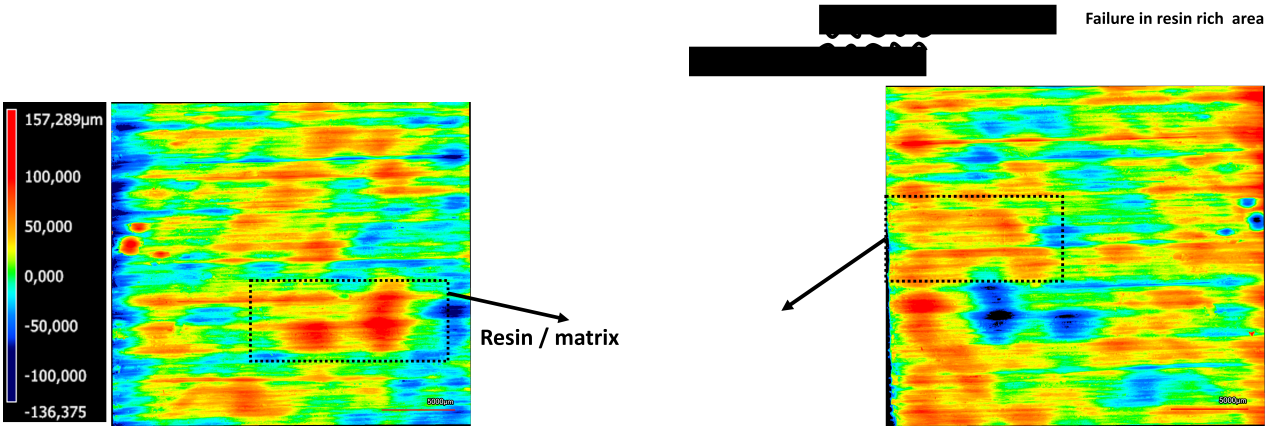


(a) Bottom side of the fracture surface

(b) Top side of the fracture surface

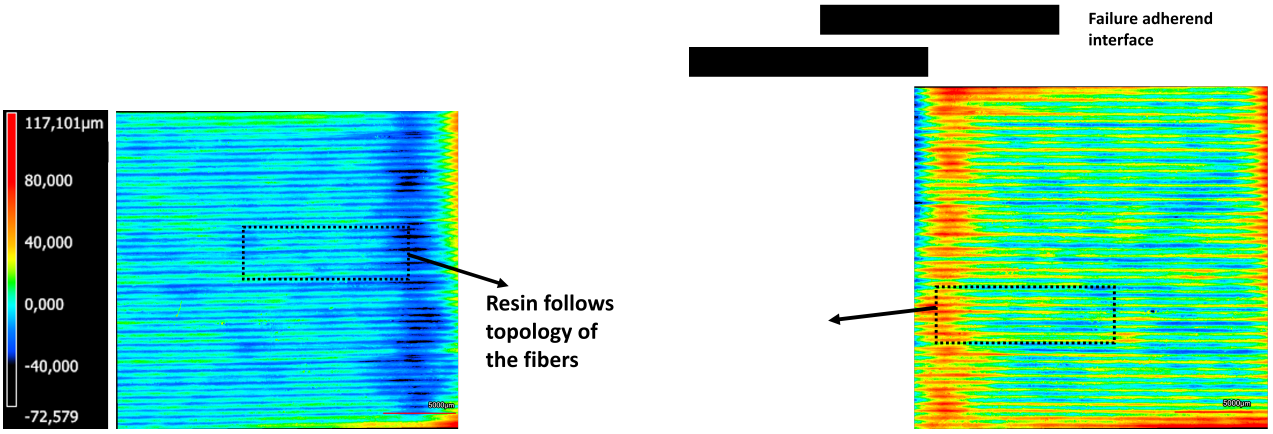
Figure 6.25: Height image of the fracture surface of the adhesive joint with epoxy film adhesive. The failure mode is the *cohesive failure of the adhesive*.

Joints with the partially cured samples.
The crack has formed at the interface between the two adherends. No adhesive is used for this joint configuration. The joint is formed based on cross-linking between the partially cured bottom and the non-cured top part, described in section 2.2. Two different configurations are made. One with the b-staged part cured for 50%, and a part b-staged to 70%. Respectively the interface is formed with 50% and 30% of the potential cross-links if both parts would have been co-cured. Therefore, this interface is weaker than the interlaminar shear strength internally in the adherends and will be the expected interface to fail. In the literature study, section 2.6, it has been mentioned that a resin-rich area forms at the top surface as the effect of the peel ply. During curing, the viscous resin flows into the peel ply. During the peel ply removal, this resin breaks and leaves a rough surface behind. Due to this effect, the bonding surface in a partially cured joint will be a resin-rich area. The fracture surface of the joint with the 50% cured part after the first curing cycle is represented in Figure 6.26. The crack formed in the resin/matrix-rich area. Strong bonding covalent bonds are formed between both parts; this can be concluded by the fact that the resin partly remained (equally) on both parts, which can be recognized in the red/higher areas. This could indicate that the resin of both the top and bottom parts was vicious in the second curing cycle. This free flow allowed the resin to mix. In Figure 6.27, the fracture surface of the joint with the 70% cured part after the first curing cycle is represented. This surface differs from Figure 6.26. The crack formed exactly on the interface between both parts. This could indicate that the resin of the bottom part (partially cured) was not vicious enough during curing. The glass transition temperature could cause this, which is, in reality, not a fixed temperature but a transition zone causing the resin to transition from rubbery to glassy. Additionally, thermal overshoot could have occurred in the curing process. Causing the actual degree of cure to differ, and therefore to be higher, than the calculated degree of cure. In Figure 6.26, the imprint of top plies (0 and 45 orientation) is visible in the resin. For both partially cured samples, no adhesive is used. So there is no adhesive failure mode.



(a) Bottom side of the fracture surface **(b)** Top side of the fracture surface

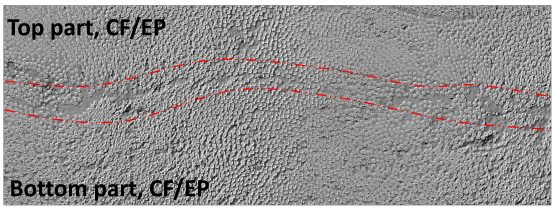
Figure 6.26: Height image of the fracture surface of the joint with the partially cured bottom part after the first curing cycle. DOC=0.5. The failure occurred in the resin-rich layer in between adherends. Strong bonding covalent bonds are formed between both parts; this can be concluded by the fact that the resin partly remained (equally) on both parts, which can be recognized in the red/higher areas.



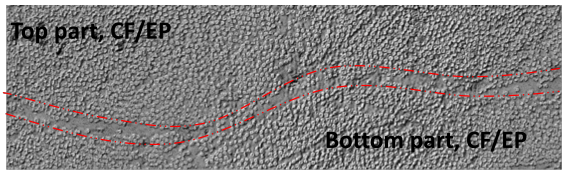
(a) Bottom side of the fracture surface **(b)** Top side of the fracture surface

Figure 6.27: Height image of the fracture surface of the joint with the partially cured bottom part after the first curing cycle. DOC=0.7. e crack formed exactly on the interface between both parts. This could indicate that the resin of the bottom part (partially cured) was not vicious enough during curing

Microscopy images are created of the cross-sectional between the two adherents. The fracture surface of the 50% part shows that the resin of the top and bottom parts have mixed in the resin-rich area. Analysing the cross-sectional C-scan in Figure 6.28a shows this effect. The resin of both parts has mixed, and the resin-rich area is nearly disappeared. Fibres can be found in this area, indicating that the resin is viscous during the second curing cycle. The fracture surface of the 70% part took the shape of the fibres of the top layer. Indicating that the resin has not been vicious enough to lose its shape after the first curing cycle. The top and bottom parts have bonded via cross-linking, but the resin was not mobile enough to mix. Analysing the c-scan in the Figure 6.28b shows this effect. A resin-rich area can be spotted between the parts. In this area, few fibres can be spotted, indicating there was little limited viscous flow between the resins to mix.



(a) C-scan, cross-section partially cured sample. DOC after the first curing cycle was 0.5. The resin of both parts has mixed, and the resin-rich area is nearly disappeared. Fibres can be found in this area, indicating that the resin is viscous during the second curing cycle.



(b) C-scan, cross-section partially cured sample. DOC after the first curing cycle was 0.7. A resin-rich area can be spotted between the parts. In this area, few fibres can be spotted, indicating there was little limited viscous flow between the resins to mix.

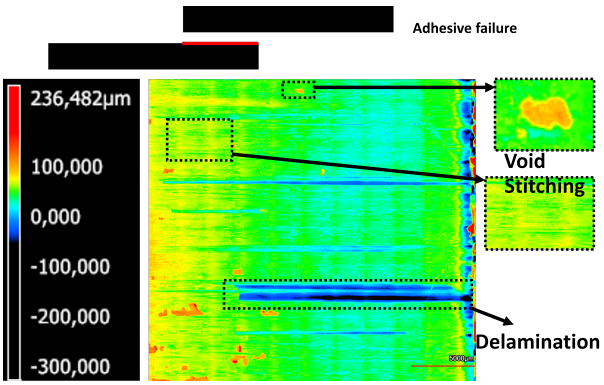
Figure 6.28: C-scan cross-sectional samples which are joined. The bottom part was partially cured.

Joints with PEI as coupling layer

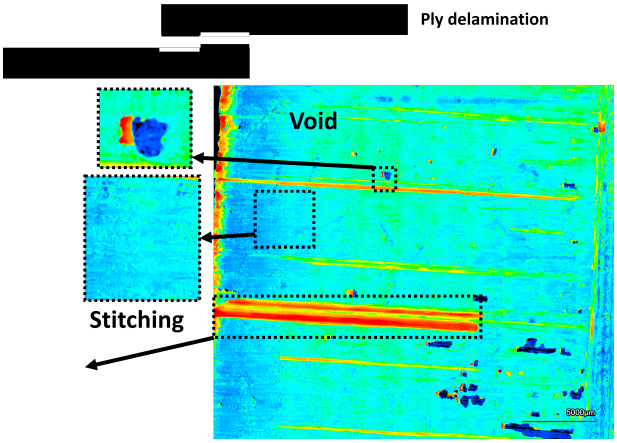
Three configurations are manufactured with a PEI coupling layer. A configuration with just a 60 microns coupling layer. One with a 60 microns coupling layer and a 60 micron interlayer between each epoxy prepreg ply. And lastly, with a 120 microns coupling layer and a 60 microns interlayer between each epoxy prepreg ply.

60 microns PEI coupling layer

This joint configuration has a PEI film as coupling. It joins two CFRP adherends. The thickness of the PEI film is 60 microns. This manufacturing method is described in Figure 6.2. The fracture surface is shown in Figure 6.29. The failure mode is surface ply delamination. This is an acceptable failure mode. The internal stress caused by the Zwick single lap shear locally exceeds the interlaminar shear strength. These delaminations are visible by the colour differences. The colour indicates a ply layer. Note that the zero direction is horizontal in the image. The top layer delaminated along the fibre direction. A porous structure, voids, is visible on the fracture surface. This is indicated in Figure 6.29 and caused by local adhesion failure between the PEI film and the epoxy (adherend), an unacceptable failure mode. These voids could initiate a crack. This detail will be discussed later in more detail. The Keyence confocal microscope with a zoom of 10x is used. These images are stitched together. A wavy pattern is visible at the side of each stitch. This does not influence the end quality of the image. However, it is noted and displayed in Figure 6.25.



(a) Bottom side of the fracture surface

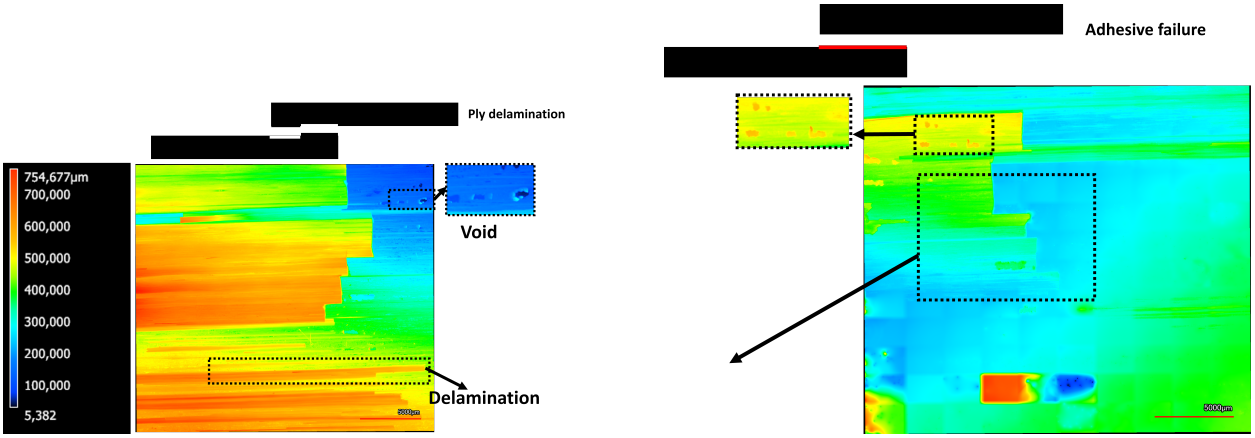


(b) Top side of the fracture surface.

Figure 6.29: Height image of the fracture surface of the joint with 60 microns PEI film as coupling. Failure modes are delamination and adhesive failure.

60 microns PEI coupling layer and 60 microns PEI sheet as an interlayer between each ply

This joint configuration has a 60 microns PEI film as coupling. It joins two CFRP adherends and, therefore toughens the interlayer. A sheet of 60 microns PEI is placed between each carbon fibre epoxy prepreg ply. This manufacturing method is described in section 6.2. The fracture surface is shown in Figure 6.30. The top layer delaminated along the fibre direction. A porous structure, voids, is visible on the fracture surface. Voids are also spotted in this fracture surface, just as in Figure 6.29.



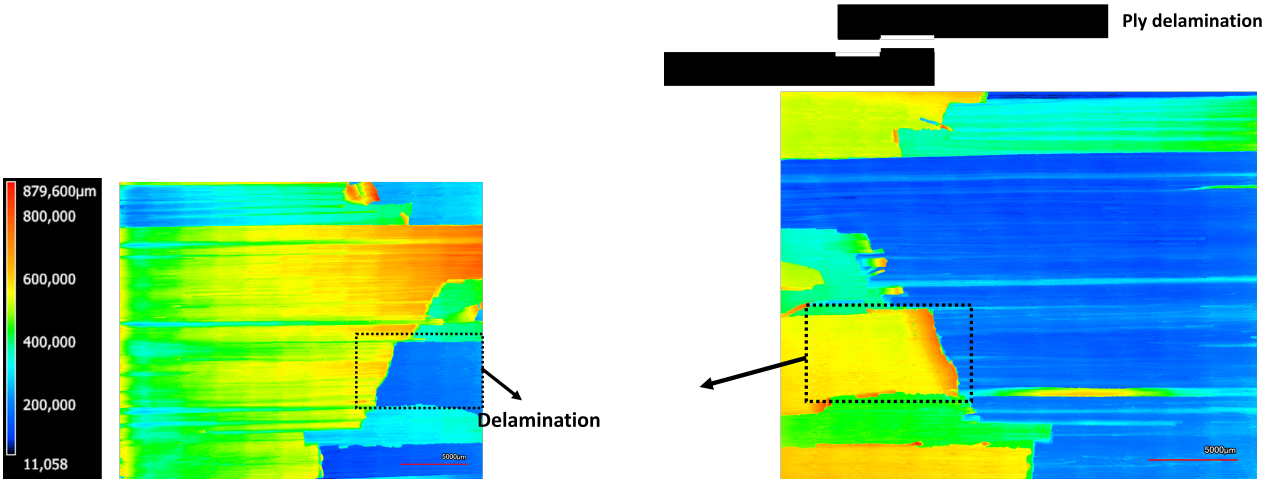
(a) Bottom side of the fracture surface

(b) Top side of the fracture surface

Figure 6.30: Height image of the fracture surface of the joint with 60 microns PEI film as coupling and 60 microns of PEI between each ply. The failure modes are delamination and adhesive failure.

120 microns PEI coupling layer and 60 microns PEI sheet as an interlayer between each ply

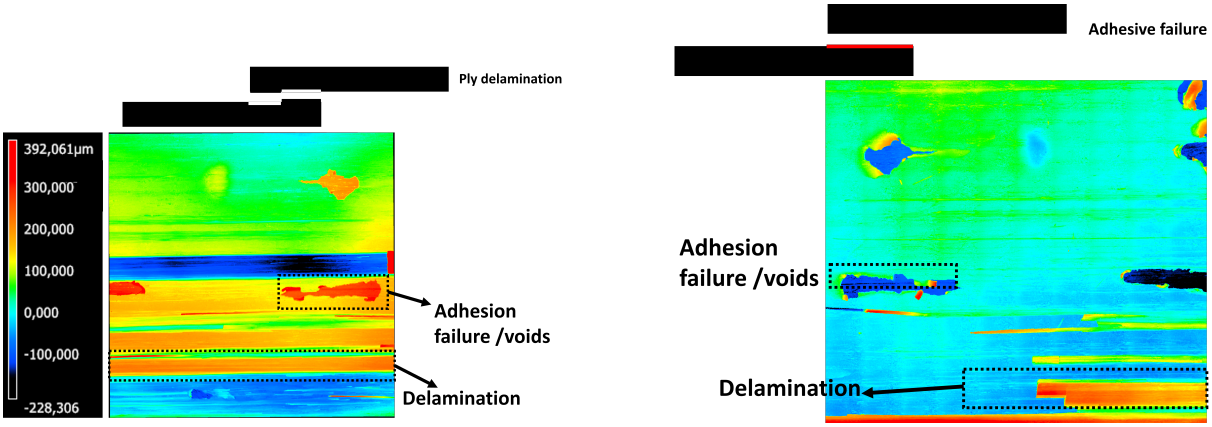
This joint configuration has a 60 microns PEI film as coupling. It joins two CFRP adherends. A sheet of 60 microns PEI is placed between each carbon fibre epoxy prepreg ply. This manufacturing method is described in Figure 6.2. The fracture surface is shown in Figure 6.31b, a sample with no voids. These voids cause adhesive failure between the PEI and epoxy interface. Delamination is the only failure mode in this sample. However, in this batch, there were samples with voids on the PEI/epoxy surface. An example of such a sample is given in Figure 6.32b



(a) Bottom side of the fracture surface

(b) Top side of the fracture surface

Figure 6.31: Height image of the fracture surface of the joint with 120 microns PEI film as coupling and 60 microns of PEI between each ply. This is the image of the positive outlier. No voids are spotted, which indicates adhesive failure of the PEI and epoxy. The failure mode is delamination.

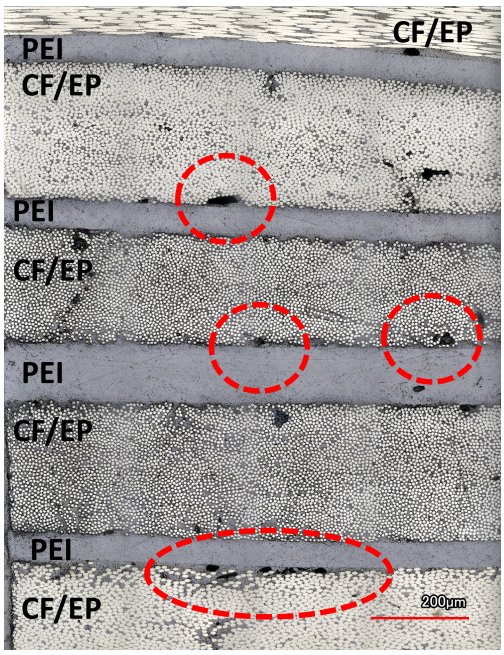


(a) Bottom side of the fracture surface

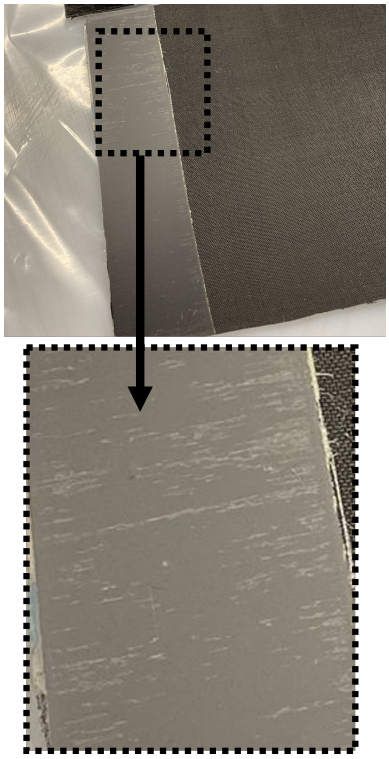
(b) Top side of the fracture surface

Figure 6.32: Height image of the fracture surface of the joint with 120 microns PEI film as coupling and 60 microns of PEI between each ply. This is the image of the sample with voids, which indicates adhesion failure of the PEI and epoxy.

In the analysed samples, delamination is an observed failure mode. This is an acceptable failure mode. Additionally, adhesive failure due to voids is observed, which is unacceptable. This can be caused by the air trapped between the PEI film and the epoxy. The curing temperature does not exceed the melting temperature of PEI during curing, meaning that the PEI remains solid during the curing process. The air could not escape through the PEI, leading to the formation of local defects in the interface, also known as porosity. This porosity is observed even while debulking is performed in the manufacturing process.Figure 6.33a displays a cross-sectional view, showing the voids circled in red in the interface. Figure 6.33b shows a photograph taken after the first curing cycle, displaying a porous structure beneath the PEI films, indicating the formation of voids in the interface.



(a) Laser confocal microscopy image of the cross-sectional of a sample with a 120 PEI microns coupling layer and 60 microns PEI interlayers. Voids are observed at the interface and circled in red.



(b) Picture was taken in the lab of the bottom part of a sample with a PEI coupling layer. The picture was taken before joining. Voids are visible through the PEI film. Voids are orientated along the fibre direction.

Figure 6.33: Two figures which show the voids which are formed between the PEI and CF/EP interface. (1) a laser confocal microscopiy figure. (2) a picture was taken in the lab with an iPhone.

6.4.2. Shear strength

In this section, the shear strength of the joints will be evaluated.

Ultimate shear strength

The ultimate shear strength of the joint configurations are represented in Figure 6.22. The benchmark configuration, the joint with the adhesive film, is set at 20.8 MPa with a standard deviation of 1.34 MPa. The samples where the PEI film is used as coupling have an average of 20.5 MPA with a standard deviation of 0.7 MPa. This lies within the same range as the benchmark samples. However, the standard deviation of the adhesive is twice as high as the standard deviation of the PEI film. The material properties of the epoxy and PEI could explain this. Epoxy is a brittle thermoset polymer. Brittle materials allow little local plastic deformations. Once the material enters the plastic regime, the material will fail. This results in little local energy storage. A local defect initiates a crack. The brittle material cannot redistribute the stress. In other words, the load does not equalize everywhere. The load is now zero at the defect location and increased in the area that is still intact. Therefore, peak loads will occur in the areas which are still intact. These peak loads will lead to direct failure. In contrast, PEI, a thermoplastic polymer, is a more ductile material. This material can locally store more energy and redistribute stress once a crack is initiated. This local energy storage occurs by local strains. The stress equalizes in the joint, and no peak loads will occur. This redistribution leads to a lower standard deviation of ultimate average shear stress than the brittle epoxy. These local defects in both materials are often a result of small manufacturing defects, which can function as crack initiators. The plastic and elastic regime are illustrated in Figure 6.34, where A is the Yield stress, and B is the ultimate stress before failure. After reaching the yield point, a brittle material has little strain before failure. Ductile material has with respect to brittle material, a lot of strain in the plastic regime.

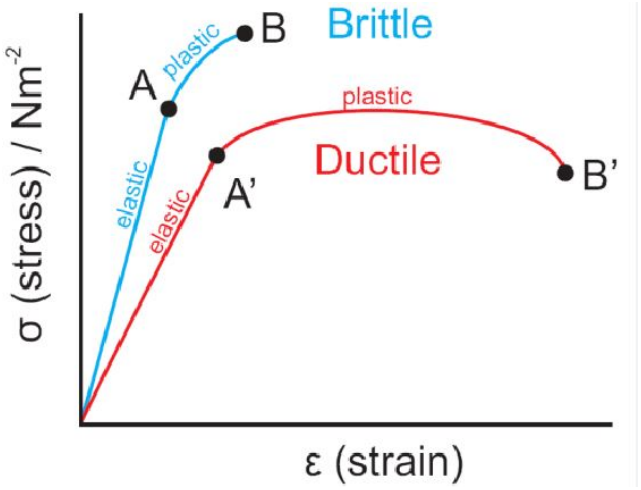


Figure 6.34: Stress strain curves. A brittle material has little to no strain in the plastic regime. A ductile material has a lot of strain in the plastic regime.

By using the PEI in the joint configuration, it is aimed to increase the fracture toughness by utilizing the PEI's plastically deform ability. Therefore, more energy can be stored. The impact on the ultimate shear would be increased due to the ability to deform and store energy after a fracture. However, analysis of the fracture surfaces revealed the presence of interface voids in the epoxy/PEI, as discussed in Figure 6.33a. These voids have a negative impact on the joint's shear strength. A void results in a lack of interdiffusion between the PEI and epoxy, leading to locally poor adhesion and no shear transfer. A void is a defect, and this defect can potentially initiate a crack. However, the joint can transfer load at locations where good adhesion is present. The PEI sample with a 60 microns coupling layer shows performance (ultimate shear strength) which is in line with the benchmark sample. Interlayer toughening was expected to increase the ultimate shear strength by adding a PEI layer between each prepreg layer, reducing the likelihood of delamination. However, the ultimate shear strength was lower when interlayers were used, see Figure 6.22. This can be explained by Figure 6.32a. Adding interlayers also adds voids in between each layer. These voids initiate cracks during the loading of the sample. The formation of these cracks is evident in Figure 6.35by the spontaneous drops in the stress-strain curves, followed by a crack heard in the Lab. These cracks can result in delaminations, failing the joint. However, in a sample with 120 microns coupling layer and 60-micron interlayers, very few voids were spotted in the fracture surface, see Figure 6.31b. In Figure 6.21, this sample shows to be a positive outlier. While this sample had a few voids, the sample showed a representative ultimate shear stress. Showing there is potential in this joint configuration without the presence of voids.

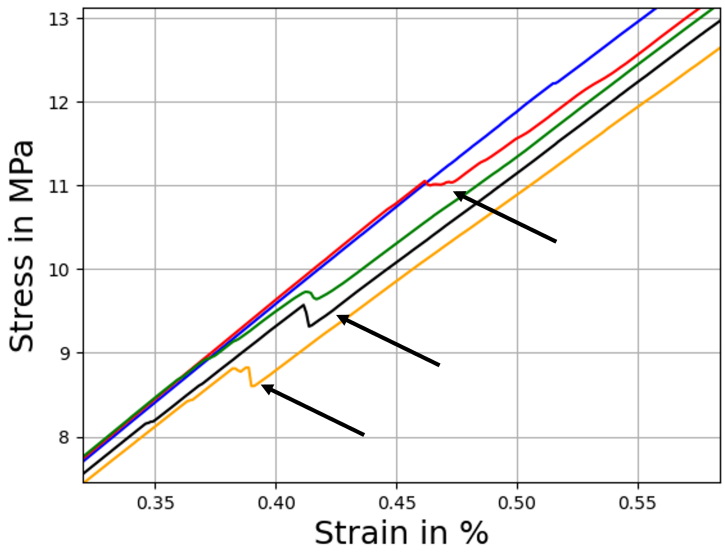
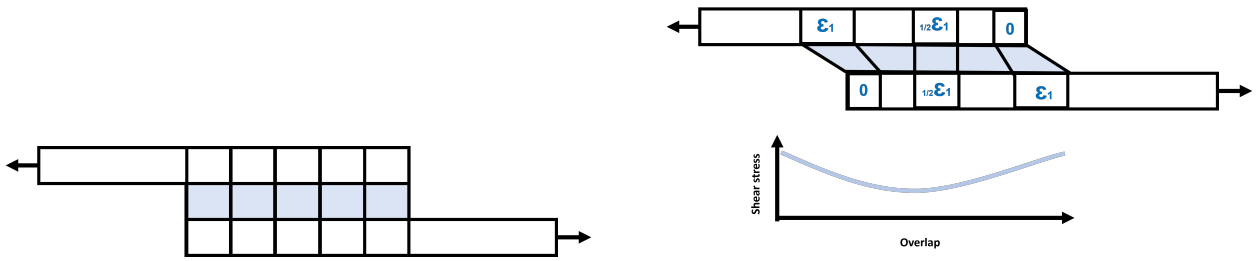


Figure 6.35: Stepwise change in the stress-strain curve, indicated with the black arrows.

In Equation 6.1, the equation for the average shear stress in the joint is given. However, to understand the performance of a lap shear joint, it is necessary to look into the shear stress distribution along the joint length. The load is transferred from the adherents into the adhesive. The load in the adhesive is shear. In Figure 6.36a an unloaded single lap shear joint is illustrated. Here the joint is split up into five equal parts. Now the joint is loaded with a load P. In Figure 6.36b, the deformation of the adherend and adhesive is displayed. The difference in deformation of the adherent causes the adhesive to shear. The shear stress distribution in the adhesive due to the shear is displayed in Figure 6.36b.



(a) Unloaded single lap shear joint.

(b) Loaded single lap shear joint and the shear stress profile.

Figure 6.36: (1) Unloaded single lap shear joint. Loading the single lap shear joint (2) causes the adherends and, therefore, the adhesive to strain. Resulting in the shear stress profile shown in (2)

The shear stress in the elastic regimen is the sum of the shear modulus times the actual shear, $\tau = \mathbf{G} * \gamma$. The peak loads of the shear stress will occur at the edges of the adhesive joint. The stress distribution is displayed in Figure 6.36b. Additionally, the yield stress is illustrated with the blue dotted line. If a brittle material, epoxy, reaches the yield point, little strain will occur before failure. In other words, the shear stress will hardly redistribute. A ductile material, PEI, will strain in the plastic regime. This results in plastic deformation after the yield point before the final failure. This allows for redistribution of the stress along the length of the overlap of the joint. Therefore the middle part, the less stressed part, can be used. This allows for an equal distribution of the joint's shear stress, resulting in lower peaks. The total average stress remains the same. The redistribution of the shear stress of a ductile joint is displayed in Figure 6.37.

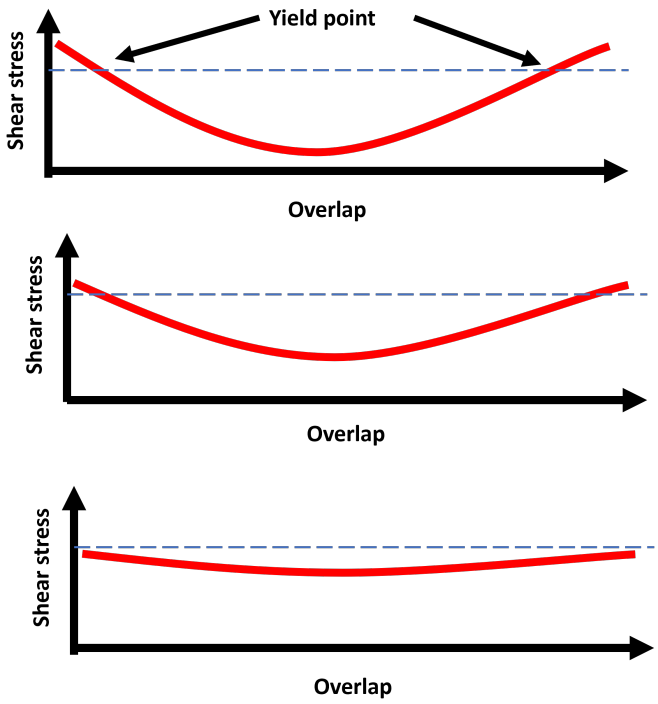


Figure 6.37: The redistribution of the shear stress of a ductile joint. This occurs in the plastic regime, after reaching the Yield point. In blue indicated the ultimate shear stress and in red the shear stress.

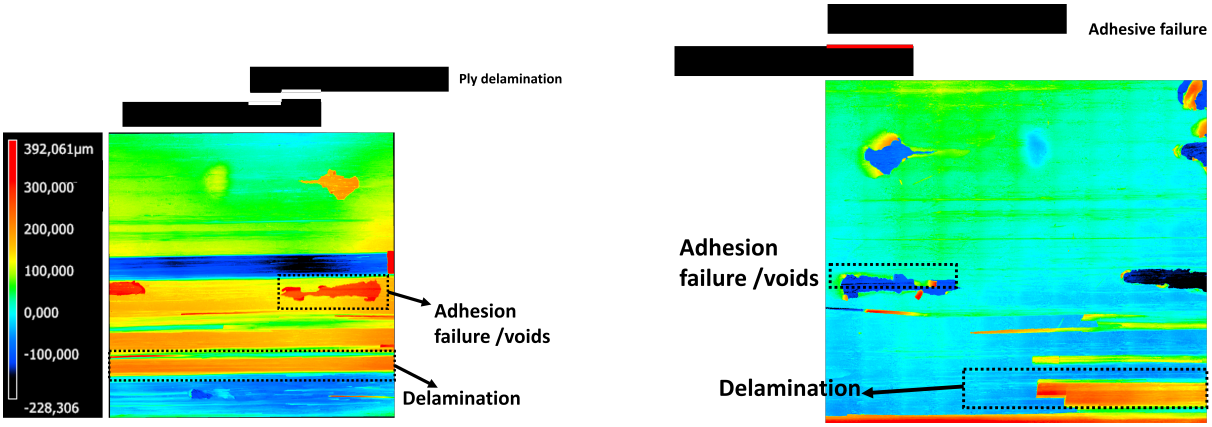
A thicker adhesive film results in a lower peak shear stress. This theory can be supported with Equation 6.3. This equation represents the peak shear stress which applies in the elastic regime. Where b is the adherend width. $\tau_{K\,max}$ is the peak shear stress, P is applied load, E is the adherend Young's modulus, G_K is the adhesive shear modulus, t is the adherend thickness, and t_k is the adhesive thickness. A thicker adhesive film results in a lower peak shear stress. This is in line with the equation for shear: $\delta x/L$. Where δx is the shear caused by the adherend in L is the thickness. The larger the L, the thickness. The smaller the shear, the smaller the shear stress. Two joint configurations can be compared to study the impact of the thickness. The joints with the interlayer and PEI coupling. 60 microns PEI coupling versus the joint with 120 microns PEI coupling. The thicker joint had an average ultimate shear stress of 16.8 MPa, whereas the thinner coupling PEI film had an average ultimate shear stress of 15.0 MPa. A difference of 1.8 MPa. An increase in the thickness of the polymer interlayer (coupling layer) leads to an increase in the energy dissipation during the fracture [79].

$$\tau_{K\,max} = \frac{F_{10}}{b}\sqrt{\frac{1}{2}\cdot\frac{1}{Et}\cdot\frac{G_K}{t_K}} \tag{6.3}$$

The partially cured samples with 70% show a lower ultimate shear strength compared to the sample cured to 50%. This trend is expected due to fewer cross-links formed in the interface in the second curing cycle. The glass transition temperature of this part fell far below the curing temperature, which led to a loss of structural integrity. Due to this loss of dimensional stability in the lower part, the top part developed a minor kink during curing due to a not perfectly aligned buildup. This imperfection could have led to a bending moment during testing, causing some samples to crack earlier than those without this kink. Steps such as Figure 6.35 are observed, with the sudden jumps in the stress-strain curve indicating delamination caused by bending. However, there are samples without this kink, and they exhibit a high ultimate shear strength of up to 24 MPa. This shows the potential of the partially cured samples. Both parts could potentially have higher degrees of cure after the first curing cycle. The cooling ratios of the autoclave can explain this. The mould cooled down than what was programmed in the settings in the autoclave. This difference could cause a difference in applied heat.

Effect of debulking

In the joint optimisation process, two extra samples were made. However, both these samples were not debulked. The impact of debulking was still unknown at this stage of the process. However, these samples are relevant to show the impact of debulking on the PEI/epoxy interface. It is shown in Figure 6.33a that this interface is prone to voids. Despite the thorough debulking process, a few voids have been observed in the interface. However, the un-debulked sample had a high void content, resulting in poor adhesion of the 60 microns of PEI film to the epoxy. The adhesion/adhesive interface failed, which is an unacceptable failure mode. Loose PEI is visible, which has not bonded to the epoxy due to voids. Delamination occurred where adhesion was sufficient, so at places without voids. Indicating that successful bonding results from diffusion at adhesion locations. The fracture surface is visible in Figure 1. This sample is tested in the Zwick tensile test machine in the DASML lab. The results of these measurements are displayed in Figure 6.39. The average lap shear strength is 14 MPa, 1 Mpa less than the debulked samples. The stepwise change in the stress-strain curve in Figure 6.39 indicates crack formation due to voids.



(a) Bottom side of the fracture surface

(b) Bottom side of the fracture surface

Figure 6.38: This sample is not debulked. This results in adhesive failure as the main failure mode. Additionally, some ply delaminations are visible.

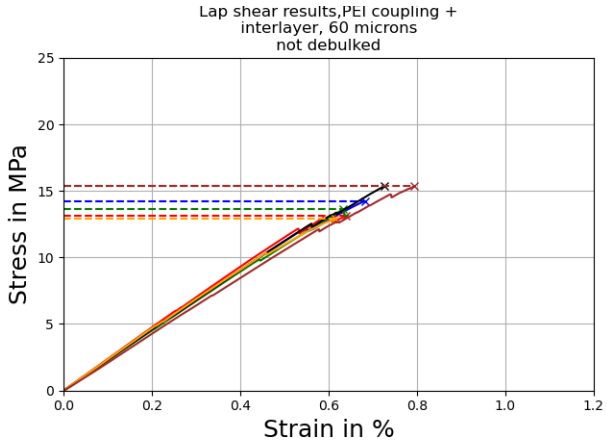


Figure 6.39: Lap shear strength of not debulked samples with a 60 micron PEI film a 60 microns PEI interlayer.

Effect of the test method

Single lap shear specimens are used during this test. This testing is relevant to comparing different joining methods (different adhesives). The test method aims to test the specimen in tensile load. The load transfers via the adhesive between the adherends. The neutral axis will try to align due to the asymmetric joint design. Due to this effect, a bending moment can be created in the sample. Peel stresses could occur at the edges of the adhesive. An adhesive is not designed to withstand peel stresses. This effect is illustrated in Figure 6.40. These peel stresses can cause the unacceptable failure mode: ”adhesive peel (excessive out-of-plane loading)”, to occur.

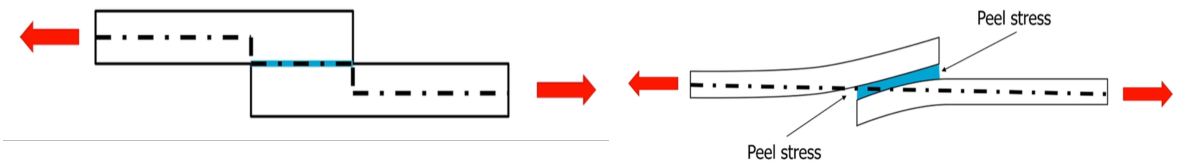


Figure 6.40: Bending moment due to sample asymmetry can cause peel stresses in the joint.

6.5. Concluding remarks

- It is feasible to manufacture fusion welding joints with Hall Spars’ prepreg system. The PEI film is co-cured with both epoxy adherents, so no heating element is required.

- It is feasible to manufacture joints with partially cured adherends with Hall Spars' prepreg system.
- The partially cured sample with DOC=0.5 shows equal performance to the benchmark sample in lap shear strength. DOC=0.7 shows weaker performance than DOC=0.5. This trend is to be expected. Both parts could potentially have higher degrees of cure after the first curing cycle due to the slower cooling of the autoclave. This could lower the number of cross-links formed in the joining step and therefore decrease mechanical performance. Both partially cured samples do show an accepted failure mode.
- It is feasible to manufacture joints with fusion welding using PEI and the adherends with Hall Spars' prepreg system.
- Placing PEI films, as interlayer and/or coupling layer, in between the carbon fibre prepregs does not lead to void-free interface. The PEI film remains solid during the curing, which blocks through-the-thickness travelling of the trapped air. These voids are manufacturing defects, causing cracks to occur and will therefore weaken the sample.
- The sample without interlayer toughening but with the PEI coupling layer has an accepted failure mode (delaminations of the adherend). It has a comparable shear strength with benchmark joints. This highlights the potential of this joint, demonstrating that even in the presence of voids, acceptable mechanical strength can be achieved
- The samples with both PEI inter and coupling layers show a significantly reduced shear strength. This can be caused by the increased void content caused by the air inclusion between the PEI/epoxy interface.
- Among the samples with both PEI inter and coupling layers, a variety of voids is spotted in the fracture surface. Samples with a higher level of voids show a decreased shear strength. They have the unacceptable failure mode ”adhesion failure” or the combination of ”adhesion failure” and delamination of the adherend. Conversely, samples with fewer voids show an acceptable failure mode of delamination of the adherend. The positive outlier, with no visible voids on its fracture surface, shows promising mechanical performance.
- Increasing the PEI coupling layer leads to an increase in the ultimate shear strength of the joint.
- Debulking is extra relevant using PEI films. Without debulking, the void content in the interface is too high, and weak adhesion will occur between the epoxy and PEI. Adhesion failure will be the result of this.

7

Applicability from lab scale to industrial scale

7.1. Free standing patch

In the literature review, section 2.7, successful examples of joining using partially cured epoxies have been documented. These studies involve the joining of two parts. Ideally, the degree of cure of a partially cured epoxy should be as low as possible because the lower the degree of cure, the more unreacted groups are present, which allows for more cross-links between the two parts. In an ideal scenario, one component must have the ability to maintain its structural integrity during the curing process, also called a free-standing patch. To achieve this, the glass transition temperature of this component must remain above the curing temperatures throughout the co-curing phase. This allows one to leave the part unsupported during the second curing cycle. The other component should be manageable at room temperature. Its glass transition temperature must be higher than room temperature to ensure this. Additionally, the degree of cure should be below the gelation point. This facilitates flow during curing, enhancing the adhesion and reducing the likelihood of high void content in the joint. The steps to achieve this joining on a lab scale are illustrated in Figure 2.13

This study focuses on the application of joining a component to a carbon fibre-reinforced polymer hollow tubular structure with limited access, also known as internal bonding. This is currently used at Hall Spars. To introduce the concept of b-stage joining (partially cured joining) into this industrial process, the tubular hollow tubular structure should undergo a partial cure during the first curing cycle instead of a complete cure. The current method involves inserting the component into a carbon fibre-reinforced polymer hollow tubular structure in an uncured state. This is optimal as it allows for the maximum number of possible cross-links. As a result, the component should remain uncured until the second curing cycle, also called the co-curing cycle. During the second cycle, the hollow structure and the component will undergo curing and reach a fully cured state.

In the co-curing cycle, the glass transition temperature (Tg) of epoxy systems used for b-stage joining of free-standing parts remains above the curing temperature, as described in the literature, section 2.6 This is illustrated in Figure 7.1. The partially cured part has a Glass transition temperature 'X'. As the curing temperature increases, the epoxy system begins to cure, leading to a rise in the degree of cure and the Tg. The Tg remains higher than the degree of cure, ensuring that the part maintains its structural integrity during the co-curing cycle. In Figure 7.1, the degree of cure of the part goes from partially cured 'Y' to fully cured, 1.

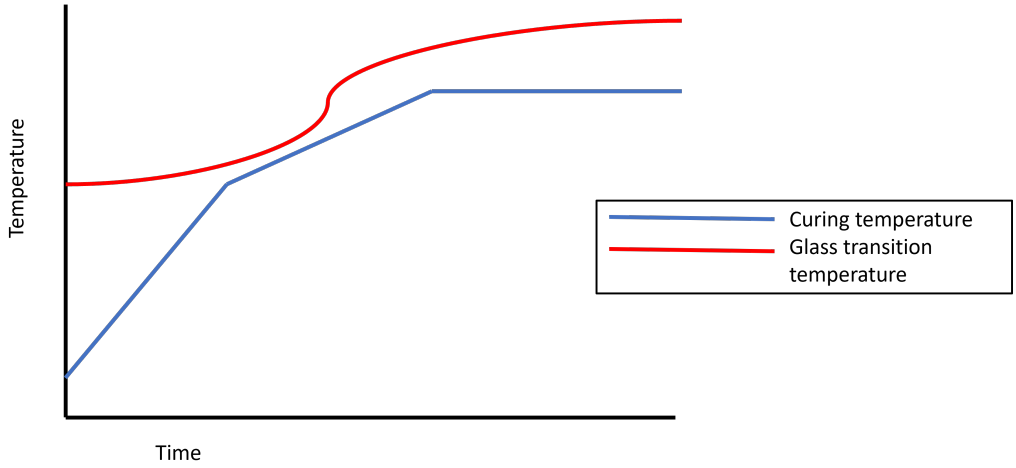
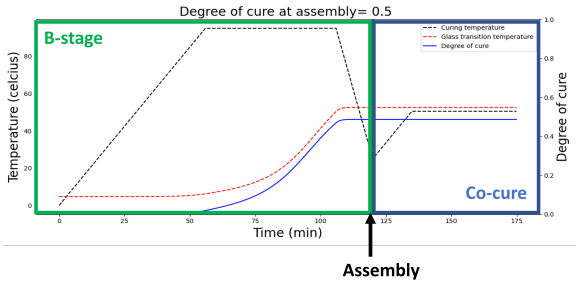
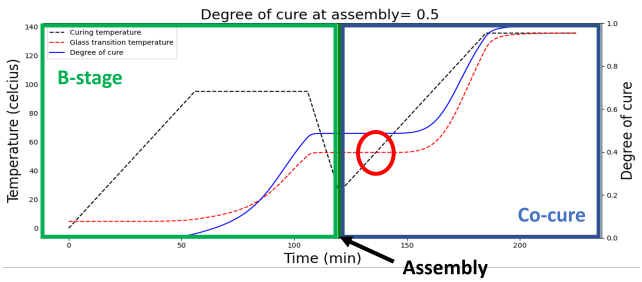


Figure 7.1: Simplified illustration, the Glass transition temperature is ”being pushed up” by the curing temperature. This is in the co-curing cycle. In the first cycle, the part is cured to the degree of cure 'Y'.

In chapter 4, a curing model and the model for the glass transition temperature are derived. These models are needed to determine the degree of cure of the ”free-standing” patch after the first curing cycle. The assembly step. The cure kinetic model is used to find the ideal degree of cure after the b-stage curing (first curing cycle) to achieve a co-curing phase (second curing cycle) with remaining structural integrity. However, after exploring the relationship between the degree of cure and the glass transition temperature, it must be concluded that it is impossible to create a free-standing patch. For this specific epoxy, it is impossible to find a degree of cure to start at the second curing cycle where **the glass transition temperature remains higher than the curing temperature during curing.** .A scenario where the degree of cure after the first cycle (b-stage cycle) is 0.5 is illustrated in Figure 7.2. In Figure 7.2a, the scenario is simulated where the glass transition temperature remains above the curing temperature. However, after the ”assembly step”, at the beginning of the second curing cycle, the reactivity of the resin is too low at these specific curing temperatures. Therefore, the resin will not cure at these curing temperatures. To achieve curing, the reactivity must be increased. This can only be forced by increasing the curing temperature. This is illustrated in Figure 7.2b, where the curing temperature is increased above the glass transition temperature. The reactivity increases, causing the resin to cure. However, the red circle indicates that the curing temperature exceeds the glass transition temperature. This caused the resin to go from a glassy to a rubbery state. It loses its structural integrity and is no longer a free-standing part. Therefore, applying this joining in the mast building industry is theoretically impossible without creating new tooling. This is tried for all the degrees of cure between 0.3 and 0.9. This can be found in the appendix Appendix E. In neither of these cases, it could create a free-standing patch.



(a) Curing temperature remains below the glass transition temperature in the co-cure cycle. However, the reactivity of the resin is too low. The resin is not curing.



(b) Curing temperature remains above the glass transition temperature in the co-cure cycle. However, the part will lose its structural integrity in the co-curing phase.

Figure 7.2: Cure kinetic model simulates the two curing cycles. The first is the b-stage cycle (in green); the degree of cure after this cycle is 0.5. And the second cycle after assembly is the co-cure cycle (in blue). (1) shows the scenario where the curing temperature remains below the glass transition temperature, (2) shows the opposite scenario.

7.2. Capillary flow

In Figure 5.3, the effect of the capillary flow is introduced. Due to capillary flow, the epoxy could flow to the top side of the PEI. This is illustrated in Figure 5.9. Epoxy will flow onto the top side of the PEI. The top side is supposed to form the bonding interface. However, if the epoxy cures on top of the PEI film, the film is surrounded by epoxy. Therefore, this setup will not create a thermoset/thermoplastic joint. The peel ply is placed on top to create a path for the resin and air to flow; secondly, the peel ply creates a texture. This texture allows the gripper of the Zwick testing machine to have a better grip. A new manufacturing method must be devised to prevent this from occurring.

In this version of the thesis the location of the joint will not be discussed. Therefore this part will be skipped and the result will be shown directly. For more information ask for the confidential version. The schematic simplification is shown in Figure 7.3.

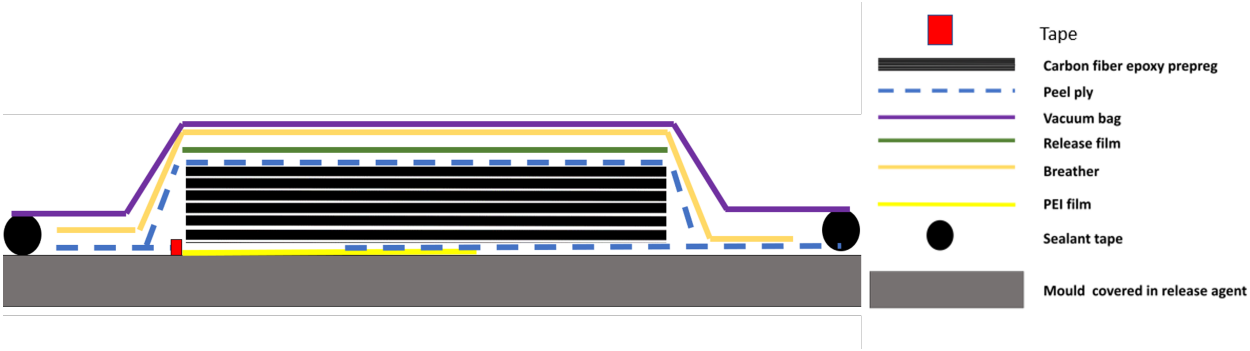


Figure 7.3: The PEI film is directly positioned onto the mould in this method. It is presupposed that no resin flow will occur between the PEI film and the mould

7.2.1. Results from new designs to avoid capillary flow.

The assumption that no resin will flow in between the PEI film and the mould is a correct assumption. In Figure 7.4, it is shown that the PEI film is not covered with prepreg. This can be seen because this film is still shiny. There is no resin flow between the PEI film and mould, making this method applicable and useful.

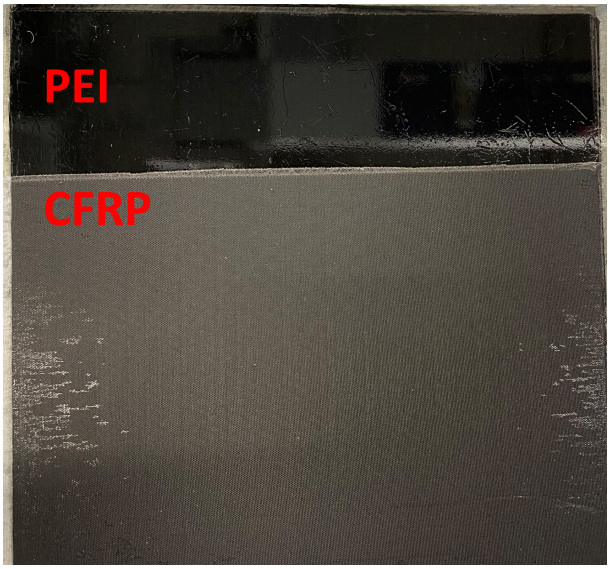


Figure 7.4: No epoxy resin flowed on top of the PEI film. The PEI film is free of epoxy resin. No capillary flow occurred during curing, causing the PEI interface to be free and ready to be used for a joint.

8

Conclusions and recommendations

8.1. Conclusions

- Isothermal, dynamical, and temperature-modulated DSC measurements on an epoxy resin used in Hall Spars. The ASTM standards are followed to ensure reliable data analysis, and a python script is used to analyse the data. The literature review suggested using the Bailleul model. However, a second cure kinetic model is introduced to improve the cure kinetic modelling. This is the Kamal model. This is the most suitable for the epoxy resin of Hall Spars. The modified curve-fitting method is used to derive the cure kinetic parameters accurately. Additionally, the DiBenedetto and the model to derive the maximum degree of cure are successfully derived. This provides an understanding and the ability to predict the curing characteristics and the glass transition temperature in the relevant range (105-135 °C and heating rates up to 2.5 °C). However, the R-squared value of the Kamal model for 2.5 °C/ min was 0.88, which was lower than the target of 0.9 set in the research objective. Nevertheless, after conducting an interphase analysis, it was determined that this model is still suitable for this study.
- PEI is selected as the thermoplastic film material for the fusion welding joining. For this joining method, interphase formation is required during co-curing between this PEI and the epoxy resin of Hall Spars. Samples are manufactured to create an Epoxy / PEI interphase. The interphase formation has taken place and could be observed with the scanning electron microscope. The higher the temperature, the bigger the interphase formation. The gel point is studied, and it is concluded that this takes place in the heating ramp for the samples cured at 125 and 135 °C. To avoid this, samples are manufactured in the hot press. The hot press can be preheated. No ramp is required. Most of the interdiffusion takes place before gelation. However, there is interdiffusion after the gel point is observed. The carbon fibres hinder the epoxy particles from diffusing towards the PEI matrix. However, even with the presence of the fibres, interdiffusion takes place.
- It is feasible to manufacture lab-scale samples with alternative joining methods using Hall Spars's prepreg system and their curing conditions. However, manufacturing challenges arose regarding the air inclusion between the PEI film and the epoxy, causing a high void content at the interface after curing. These voids do decrease the lap shear strength of the joints. Nevertheless, the joints formed with PEI coupling exhibit a comparable shear strength to the benchmark. This is due to the high fracture toughness of the thermoplastic PEI. More energy can be stored in the tougher interlayer than in a brittle epoxy joint. However, toughening each interlayer with PEI did not lead to an increase in shear strength. Placing a PEI interlayer in between each prepreg layer increases the void content. This increase in void content increases defects, weakening the joint and causing adhesion failure. Joining with partially cured thermosets shows comparable shear strength to the benchmark. Overshoots in the degree of cure can potentially cause a lower shear strength than expected. However, on a lab scale, it was able to create these joints and test them successfully.
- Modelling the glass transition temperature profile due to the degree of cure shows that it is impossible to create a part that maintains structural integrity while curing with Hall Spars' epoxy resin. Therefore, applying the joining method "partially cured thermosets" in the mast building industry is impossible without creating new tooling. To implement the joining method "fusion welding of thermoset composites" in the mast building industry, a solution must be found for the high void content in the interface between

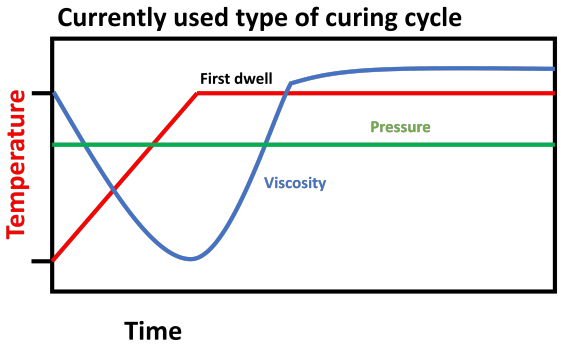
the PEI and epoxy. The epoxy resin's capillary flow into the peel ply during the curing cycle must be considered. Due to this flow, the resin can flow to the top side of the joint, which is undesired. A modified layup is suggested and successfully tested.

8.2. Recommendations

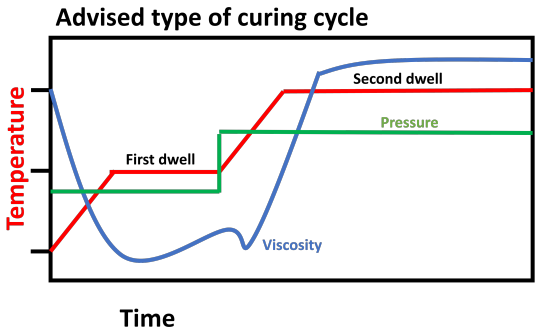
- Firstly, a co-cure process where the thermoplastic film is co-cured on top of a thermoset prepreg. Based on the literature review PEI and epoxy show significant interdiffusion, even with carbon fibre. This co-curing can be achieved in the autoclave during the regular curing of the thermoset composite. The bottom adherend will be co-cured in the curing cycle step. The PEI part will be co-cured with the second adherend in a second step. And therefore, it will couple the two adherents. By using this co-curing as a coupling mechanism, welding can be avoided. By taking this approach, potential challenges (described in the literature study) of welding can be avoided. However, in Figure 6.4.1, the formation of voids at the epoxy / PEI interface in the co-curing phase is described. This void content has a negative impact on joint strength and reliability.

  The currently used type of curing cycle for the co-curing step is illustrated in Figure 8.1a. A temperature ramp until the first dwell. The pressure remains constant throughout the cycle. The viscosity profile is displayed. The viscosity decreases and increases drastically at the gel point. Explained in detail in chapter 4.

  A recommended curing cycle for PEI/epoxy joining is a curing cycle with a first and second dwell. This profile is illustrated in Figure 8.1b. A first dwell at a lower temperature allows the resin to get vicious. The autoclave pressure is not completely applied to the sample yet. During this first dwell, the air can flow out of the system due to the low viscosity of the resin. This dwell is held for a time period. During this first dwell, the resin will not (significantly) cure. Therefore, the viscosity will not increase as a function of the degree of cure. A second ramp brings the temperature up to the second dwell temperature. The viscosity first decreases due to a temperature increase but will quickly increase at the gel point. The autoclave pressure is brought up to the prescribed pressure of the manufacturer.



(a) Currently used type of curing cycle for co-curing epoxy and PEI. One dwell phase.



(b) The advised type of curing cycle for co-curing epoxy and PEI. Two dwell phases.

Figure 8.1: A comparison of the currently used and advised type of curing cycle for PEI/epoxy joining. The difference is the added dwell phase for the advised curing cycle. Resulting in a different viscosity profile.

- The temperature ramp used in the heating cycle in this study is based on the manufacturing sheets. It could be advised the investigate the impact of different ramps on the interdiffusion depth. In chapter 5, the impact of gelation is shown. In other words, after gelation, the interdiffusion slows down. Therefore, varying the heating rate could result in higher interdiffusion and therefore a higher lap shear strength in the join.
- In this study PEI film is used based on the literature study and the availability. However, no studies are available about thermoplastic interdiffusion with this specific epoxy resin. For the fusion welding joints, different thermoplastic materials can be investigated to see if a thicker interphase can be formed.

The same applies to the thickness of the PEI film. In the current study, two thicknesses are studied; however, to create more insight into the relationship between the thickness and the lap shear strength, more experiments should be performed. Additionally, for the partially cured joints, it could be advised to study different prepreg systems. To see if there is a prepreg system where it is possible to create a free-standing patch.

- In subsection 6.4.2, it described that single lap shear joints turned out not to be perfect. Limitations occurred during manufacturing and loading. In future work, different types of joints should be tested. Such as double lap shear to avoid these imperfections in testing.

Bibliography

[1] C. M. Rizzo and D. Boote, “Scantling of Mast and Rigging of Sail Boats: a Few Hints from a Test Case to Develop Improved Design Procedures,” tech. rep., 2010.

[2] C. Jareteg, K. Wärmefjord, C. Cromvik, R. Söderberg, L. Lindkvist, J. Carlson, S. Larsson, and F. Edelvik, “Geometry Assurance Integrating Process Variation with Simulation of Spring-In for Composite Parts and Assemblies,” *Journal of Computing and Information Science in Engineering*, vol. 16, 9 2016.

[3] J. Holtmannspötter, J. V. Czarnecki, M. Wetzel, D. Dolderer, and C. Eisenschink, “The use of peel ply as a method to create reproduceable but contaminated surfaces for structural adhesive bonding of carbon fiber reinforced plastics,” *Journal of Adhesion*, vol. 89, pp. 96–110, 2 2013.

[4] J. Studer, C. Dransfeld, and K. Masania, “An analytical model for B-stage joining and co-curing of carbon fibre epoxy composites,” *Composites Part A: Applied Science and Manufacturing*, vol. 87, pp. 282–289, 8 2016.

[5] J. Studer, K. Masania, C. Dransfeld, J. Studer, K. Masania, and C. Dransfeld, “Reinforcement of partially cured aerospace structures with B-staged patches,” tech. rep., 2014.

[6] M. Müller, A. Winkler, M. Gude, and H. Jäger, “Aspects of reproducibility and stability for partial cure of epoxy matrix resin,” *Journal of Applied Polymer Science*, vol. 137, 2 2020.

[7] F. Rieger, T. Rief, N. Motsch, and J. Hausmann, “INTEGRAL DESIGN OF COMPOSITE STRUCTURES USING A MODIFIED CO-CURING PROCESS,” tech. rep., 2017.

[8] J. Moosburger-Will, M. Günter, R. Sause, M. Greisel, R. Horny, M. G. R. Sause, R. Horny, J. Scholler, L. L. Prieto, and S. Horn, “INTERFACIAL PROPERTIES OF CARBON FIBER REINFORCED POLYMER LAMINATES JOINED BY A NOVEL PARTIAL CROSS-LINKING PROCESS,” tech. rep., 2015.

[9] N. Motsch-Eichmann, F. Rieger, T. Rief, J. Hausmann, N. Motsch, and . T. Rief, “INVESTIGATION OF PRE-CURED CARBON FIBER/EPOXY-LAMINATES FOR MODIFIED CO-CURING PROCESS,” tech. rep., 2019.

[10] J. Moosburger-Will, M. Greisel, M. G. Sause, R. Horny, and S. Horn, “Influence of partial cross-linking degree on basic physical properties of RTM6 epoxy resin,” *Journal of Applied Polymer Science*, vol. 130, pp. 4338–4346, 12 2013.

[11] R. Paton, “670,” *International congress of the aeronautical sciences*, 2006.

[12] U. Farooq, J. Teuwen, and C. Dransfeld, “polymers Toughening of Epoxy Systems with Interpenetrating Polymer Network (IPN): A Review,” *Polymers*, 2020.

[13] J. Niskanen and H. Tenhu, “How to manipulate the upper critical solution temperature (UCST)?,” *Polymer Chemistry*, vol. 8, no. 1, pp. 220–232, 2017.

[14] K. Mimura, H. Ito, and H. Fujioka, “Improvement of thermal and mechanical properties by control of morphologies in PES-modified epoxy resins,” *Polymer*, vol. 41, pp. 4451–4459, 6 2000.

[15] C. Ageorges, L. Ye, and M. Hou, “Advances in fusion bonding techniques for joining thermoplastic matrix composites: a review,” *Composites Part A: Applied Science and Manufacturing*, vol. 32, pp. 839–857, 6 2001.

[16] S. H. McKnight, B. K. Fink, V. Monnard, P.-e. Bourban, J.-A. E. Manson, D. A. Eckel, and J. W. Gillespie, “Army Research Laboratory Processing and Characterization of Welded Bonds Between Thermoset and Thermoplastic Composites,” tech. rep., 2001.

[17] P. Chandran, M. Rantatalo, J. Odelius, X. Cui, L. Tian, D. S. Wang, and J. P. Dong, “You may also like Train-based differential eddy current sensor system for rail fastener detection Summary of thermosetting composite material welding,” 2021.

[18] X. Xiong, D. Wang, J. Wei, P. Zhao, R. Ren, J. Dong, and X. Cui, “Resistance welding technology of fiber reinforced polymer composites: a review,” 2021.

[19] O. Schieler and U. Beier, “Induction Welding of Hybrid Thermoplastic-thermoset Composite Parts,” *KMUTNB International Journal of Applied Science and Technology*, pp. 27–36, 12 2015.

[20] J. J. E. Teuwen, J. Asquier, P. Inderkum, K. Masania, C. Brauner, I. Fernandez Villegas, and C. A. Dransfeld, “GRADIENT INTERPHASES BETWEEN HIGH-TG EPOXY AND POLYETHERIMIDE FOR ADVANCED JOINING PROCESSES,” tech. rep., 2018.

[21] “Standard Test Method for Lap Shear Adhesion for Fiber Reinforced Plastic (FRP) Bonding,”

[22] N. Motsch-Eichmann, F. Rieger, T. Rief, and J. Hausmann, “Experimental investigation of modified co-curing process for carbon fiber/epoxy-laminates,” *Journal of Micromechanics and Molecular Physics*, vol. 6, pp. 1–12, 9 2021.

[23] Shenio A., “ISSC 2009 committee Sailing Yacht Design,” *17th international ship and offshore structures congress*, pp. 433–493, 2009.

[24] H. Hoffmeister, “Modern yacht rig design,” in *Marine Composites*, pp. 417–450, Elsevier, 2019.

[25] D. G. As, “DNVGL-ST-0412 Design and construction of large modern yacht rigs,” tech. rep., 2016.

[26] L. Xie, H. Liu, W. Wu, D. Abliz, Y. Duan, and D. Li, “Fusion bonding of thermosets composite structures with thermoplastic binder co-cure and prepreg interlayer in electrical resistance welding,” *Materials and Design*, vol. 98, pp. 143–149, 5 2016.

[27] A. WINDLE, “A METALLURGIST’S GUIDE TO POLYMERS,” *Physical Metallurgy*, pp. 2663–2740, 1 1996.

[28] J. Mohan, A. Ivanković, and N. Murphy, “Mixed-mode fracture toughness of co-cured and secondary bonded composite joints,” *Engineering Fracture Mechanics*, vol. 134, pp. 148–167, 1 2015.

[29] J. Mohan, A. Ivanković, and N. Murphy, “Mode i fracture toughness of co-cured and secondary bonded composite joints,” *International Journal of Adhesion and Adhesives*, vol. 51, pp. 13–22, 6 2014.

[30] K. S. Kim, J. S. Yoo, Y. M. Yi, and C. G. Kim, “Failure mode and strength of uni-directional composite single lap bonded joints with different bonding methods,” *Composite Structures*, vol. 72, pp. 477–485, 4 2006.

[31] A. Yudhanto, M. Alfano, and G. Lubineau, “Surface preparation strategies in secondary bonded thermoset-based composite materials: A review,” 8 2021.

[32] T. A. Schmid Fuertes, T. Kruse, T. Körwien, and M. Geistbeck, “Bonding of CFRP primary aerospace structures - Discussion of the certification boundary conditions and related technology fields addressing the needs for development,” *Composite Interfaces*, vol. 22, pp. 795–808, 10 2015.

[33] F. Rieger, T. Rief, N. Motsch, and J. Hausmann, “Manufacturing CFRP-parts using a modified co-curing method – Fundamental experimental analysis,” in *Key Engineering Materials*, vol. 809 KEM, pp. 372–377, Trans Tech Publications Ltd, 2019.

[34] P. Mallick, “Fiber Reinforced Composites Materials, Manufacturing, and Design,” tech. rep., Taylor & Francis Group, L.L.C., Michigan, 2007.

[35] V. D. Serban C. Moldoveanu, *Chapter 7 RP HPLC analytical columns*. 2017.

[36] Q. Bénard, M. Fois, and M. Grisel, “Peel ply surface treatment for composite assemblies: Chemistry and morphology effects,” *Composites Part A: Applied Science and Manufacturing*, vol. 36, pp. 1562–1568, 11 2005.

[37] A. Baldan, “Adhesively-bonded joints and repairs in metallic alloys, polymers and composite materials: Adhesives, adhesion theories and surface pretreatment,” *Journal of Materials Science*, vol. 39, pp. 1–49, 1 2004.

[38] M. Kanerva and O. Saarela, “The peel ply surface treatment for adhesive bonding of composites: A review,” 2013.

[39] D. N. Markatos, K. I. Tserpes, E. Rau, S. Markus, B. Ehrhart, and S. Pantelakis, “The effects of manufacturing-induced and in-service related bonding quality reduction on the mode-I fracture toughness of composite bonded joints for aeronautical use,” *Composites Part B: Engineering*, vol. 45, pp. 556–564, 2 2013.

[40] L. X. A. P. v. d. V. M. H. Erkens S., Schlangen E., “Experimental characterization of chemical and physical performance of epoxy modified bitumen,” 2018.

[41] D. D. J. Y. Bailleul J.L., “Determination of temperature variable properties of composite mateirals: methodology and experimental results,” 1996.

[42] J. K. Fink, “Epoxy Resins,” *Reactive Polymers Fundamentals and Applications*, pp. 95–153, 1 2013.

[43] E. Ruiz and F. Trochu, “Thermomechanical properties during cure of glass-polyester RTM composites: Elastic and viscoelastic modeling,” *Journal of Composite Materials*, vol. 39, no. 10, pp. 881–916, 2005.

[44] U. Farooq, S. Heuer, J. Teuwen, and C. Dransfeld, “Effect of a Dwell Stage in the Cure Cycle on the Interphase Formation in a Poly(ether imide)/High TgEpoxy System,” *ACS Applied Polymer Materials*, vol. 3, pp. 6111–6119, 12 2021.

[45] R. Geissberger, J. Maldonado, N. Bahamonde, A. Keller, C. Dransfeld, and K. Masania, “Rheological modelling of thermoset composite processing,” 2017.

[46] J. Moosburger-Will, M. G. Sause, R. Horny, S. Horn, J. Scholler, and L. Llopard Prieto, “Joining of carbon fiber reinforced polymer laminates by a novel partial cross-linking process,” *Journal of Applied Polymer Science*, vol. 132, 7 2015.

[47] Y. H. Roos, “Introduction to Phase Transitions,” *Phase Transitions in Foods*, pp. 1–18, 1 1995.

[48] G. Fourche, “An Overview of the Basic Aspects of Polymer Adhesion. Part I: Fundamentals,” tech. rep., 1995.

[49] F. Lionetto, M. N. Morillas, S. Pappadà, G. Buccoliero, I. Fernandez Villegas, and A. Maffezzoli, “Hybrid welding of carbon-fiber reinforced epoxy based composites,” *Composites Part A: Applied Science and Manufacturing*, vol. 104, pp. 32–40, 1 2018.

[50] Hou M., “Fusion bonding of carbon fibre reinforced epoxy laminates,” *Trans Tech Publications*, 2013.

[51] Wedgewood AR. and Hardy PE., “Induction welding of thermoset composite adherends using thermoplsatic interlayers and susceptors,” *Proceedings of the 28th international SAMPE technical conference*, 1996.

[52] M. T. Heitzmann, M. Hou, M. Veidt, L. J. Vandi, and R. Paton, “Morphology of an interface between Polyetherimide and epoxy prepreg,” in *Advanced Materials Research*, vol. 393-395, pp. 184–188, 2012.

[53] uqlvandi, “ICAS Paper - LJ Vandi 120713 final,” tech. rep., 2012.

[54] C. Dransfeld, “DEVELOPMENT OF A RESISTANCE WELDING PROCESS FOR THERMOSET FIBER COMPOSITE COMPONENTS WITH CO-CURED THERMOPLASTIC BOUNDARY LAYER Fast manufacturing of tough composites View project Damping supression using natural fibre composites View project,” tech. rep., 2019.

[55] Z. Zhong and Q. Guo, “Miscibility and cure kinetics of nylon/epoxy resin reactive blends,” *Polymer*, vol. 39, pp. 3451–3458, 7 1998.

[56] M. Hou, “Thermoplastic adhesive for thermosetting composites,” in *Materials Science Forum*, vol. 706-709, pp. 2968–2973, Trans Tech Publications Ltd, 2012.

[57] C. Brauner, S. Nakouzi, L. Zweifel, and J. Tresch, “Co-curing behaviour of thermoset composites with a thermoplastic boundary layer for welding purposes,” *Advanced Composites Letters*, vol. 29, 2020.

[58] S. ShuJun, G. MiaoCai, Y. XiaoSu, and Z. ZuoGuang, “SCIENCE CHINA Phase separation morphology and mode II interlaminar fracture toughness of bismaleimide laminates toughened by thermoplastics with triphenylphosphine oxide group,” *Sci China Tech Sci*, vol. 60, no. 3, pp. 444–451, 2017.

[59] A. K. van der vegt, *From polymers to plsatic*. Delft University press, 2002.

[60] I. Harismendy, M. Del Río, C. Marieta, J. Gavalda, and I. Mondragon, “Dicyanate ester-polyetherimide semi-interpenetrating polymer networks. II. Effects of morphology on the fracture toughness and mechanical properties,” *Journal of Applied Polymer Science*, vol. 80, pp. 2759–2767, 6 2001.

[61] H. T. Oyama, T. Solberg, and J. Wightman, “Electron microprobe analysis as a novel technique to study the interface between thermoset and thermoplastic polymers,” *Polymer*, vol. 40, pp. 3001–3011, 5 1999.

[62] A. J. Smiley, F. N. Cogswell, and P. J. Meakin, “Dual Polymer Bonding of Thermoplastic Composite Structures,” tech. rep.

[63] M. Abouhamzeh and J. Sinke, “Effects of fusion bonding on the thermoset composite,” 2019.

[64] I. Fernandez Villegas and P. Vizcaino Rubio, “On avoiding thermal degradation during welding of high-performance thermoplastic composites to thermoset composites,” *Composites Part A: Applied Science and Manufacturing*, vol. 77, pp. 172–180, 10 2015.

[65] “ASTM E2070 ,Standard Test Methods for Kinetic Parameters by Differential Scanning Calorimetry Using Isothermal Methods,”

[66] “ASTM, E2606-22. Standard Test Methods for Assignment of the Glass Transition Temperature by Modulated Temperature Differential Scanning Calorimetry 1,”

[67] “ASTM E2160, Standard Test Method for Heat of Reaction of Thermally Reactive Materials by Differential Scanning Calorimetry 1,”

[68] Q. Li, X. Li, and Y. Meng, “Curing of DGEBA epoxy using a phenol-terminated hyperbranched curing agent: Cure kinetics, gelation, and the TTT cure diagram,” *Thermochimica Acta*, vol. 549, pp. 69–80, 12 2012.

[69] Jose M. Kenney, “Determination of Autocatalytic Kinetic Model Parameters Describing Thermoset Cure,” tech. rep., Naples, Italy, 1993.

[70] J. L. Bailleul, “Determination of temperature variable properties of composite materials: Methodology and experimental results,” *Laboratoire de thermocinetique*, 1996.

[71] A. Keller, K. Masania, A. C. Taylor, and C. Dransfeld, “Fast-curing epoxy polymers with silica nanoparticles: properties and rheo-kinetic modelling,” *Journal of Materials Science*, vol. 51, pp. 236–251, 7 2015.

[72] P. Kolliopoulos and S. Kumar, “Capillary flow of liquids in open microchannels: overview and recent advances,” *npj Microgravity*, vol. 7, p. 51, 12 2021.

[73] Clifford K. Ho and Stephen W. Webb, *Gas transport in a porous media*, vol. 20. Springer, 2006.

[74] Millington and Quirk, “Permeability of porous solids.” 1960.

[75] M. T. Q. S. da Silva, M. do Rocio Cardoso, C. M. P. Veronese, and W. Mazer, “Tortuosity: A brief review,” *Materials Today: Proceedings*, vol. 58, pp. 1344–1349, 2022.

[76] A. Idris, A. Muntean, and B. Mesic, “A review on predictive tortuosity models for composite films in gas barrier applications,” *Journal of Coatings Technology and Research*, vol. 19, pp. 699–716, 5 2022.

[77] A. Gugliuzza, “Solvent Swollen Polymer,” in *Encyclopedia of Membranes*, pp. 1801–1802, Berlin, Heidelberg: Springer Berlin Heidelberg, 2016.

[78] A. Levy, S. Le Corre, and I. Fernandez Villegas, “Modeling of the heating phenomena in ultrasonic welding of thermoplastic composites with flat energy directors,” *Journal of Materials Processing Technology*, vol. 214, pp. 1361–1371, 7 2014.

[79] M. Grossman, D. Pivovarov, F. Bouville, C. Dransfeld, K. Masania, and A. R. Studart, “Hierarchical Toughening of Nacre□Like Composites,” *Advanced Functional Materials*, vol. 29, p. 1806800, 2 2019.

[80] J. Moosburger-Will, M. Greisel, S. Horn, J. Moosburger-Will, M. Greisel, M. G. R. Sause, R. Horny, and S. Horn, “Physical Properties of Partially Cross-Linked RTM6 Epoxy Resin V2O3 thin films View project Low Dimensional Quantum Magnets View project PHYSICAL PROPERTIES OF PARTIALLY CROSS-LINKED RTM6 EPOXY RESIN,” tech. rep., 2014.

[81] J. Moosburger-Will, M. Greisel, and S. Horn, “Physical aging of partially crosslinked RTM6 epoxy resin,” *Journal of Applied Polymer Science*, vol. 131, 12 2014.

[82] G. Brunner, “Properties of Pure Water,” *Supercritical Fluid Science and Technology*, vol. 5, pp. 9–93, 1 2014.

[83] V. A. Kagan and W. P. Kuhn, “Laser Transmission Welding of Semi-Crystalline Thermoplastics-Part I: Optical Characterization of Nylon Based Plastics,” *Journal of REINFORCED PLASTICS AND COMPOSITES*, vol. 21, no. 12, 2002.

[84] S. Deng, L. Djukic, R. Paton, and L. Ye, “Thermoplastic-epoxy interactions and their potential applications in joining composite structures-A review,” 2014.

Appendix: Literature study, curing history impact on material parameters, partially cured resin

Density and modulus The modulus and the density of a polymer are correlated with the molecular structure and weight and the cross-link density. Therefore the density and modulus show the same interdependence with the degree of cure and cure history. Moosburger et al. show the influence of the cooling phase. The mobility in the rubbery state is high. In the glassy state, the polymers have low mobility. Therefore it is cooling down in the rubbery state results in efficient dense chain packing, so a higher density. Conversely, cooling down in the glassy state means low mobility for the polymer chains. Resulting in inefficient packing and a lower density and, therefore, modulus. This briefly explains the relationship with the density and modulus on the cure history [10].

The relationship of the density and the modulus with the degree of cure is investigated by Moosburge et al. If the polymer is in a state where $T_c > T_g$, so below the transition region, an increase in the degree of cure causes the density and the modulus to decrease linearly. This is due to the crosslinking reactions and the forming of a three-dimensional network. The number of molecular arrangements in the rubbery state decreases, which leads to an increase in the specific volume. A step-wise increase is visible in the transition region (rubbery to glassy state) due to molecular rearrangement and structural relaxation. After this step-wise increase, a linear decrease with an increasing degree of cure is observed. In this region, the three-dimensional cross-linking has a dominant effect on the decrease in the modulus and density [10]. These relationships are shown in Figure A.1

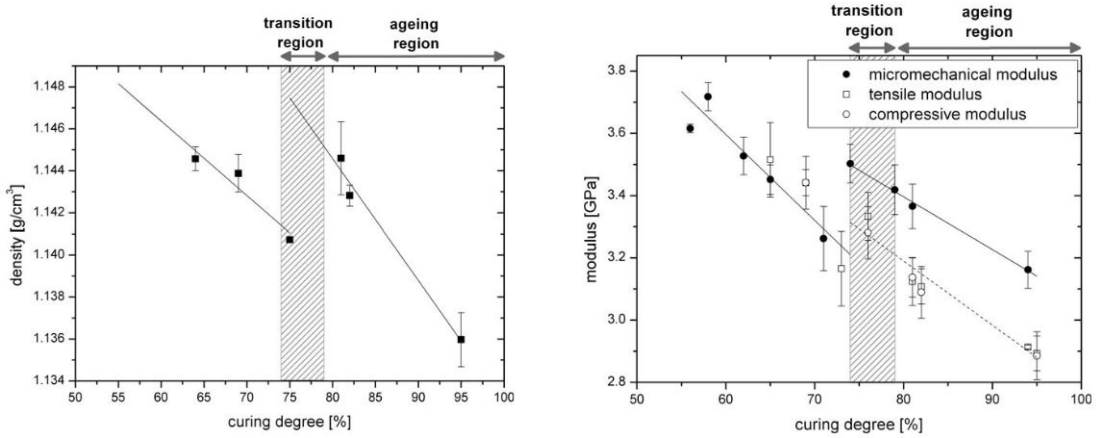


Figure A.1: Left: Relationship between curing degree and density, right: the relationship between curing degree and modulus [10]

Moosburger et al. also investigated the properties of partially cured parts after the final curing cycle, so once they are fully cured. It has been found that the degree of cure, glass transition temperature and modulus are similar to a part which is cured according to the conventional method, so without a partial cure step. This is relevant since one does not want a mismatch between properties, for example, to avoid stress concentrations. A non-negligible increase of modulus has been found for a part which is fully cured and run for another curing cycle (conventional method). A slight increase in modulus is observed. The hypothesis is that structural relaxations in the annealing process cause this increase since, for this part, $T_c < T_g$. This can lead to an increase of modulus and can locally embrittle a component [10]. Density values of fully cured parts which are cured again tend to be smaller than completely cured parts which are just cured once due to the more restricted packing caused by further cross-linking [80].

Hardness

In contrast to the density and the modulus, the hardness does not show a minimal dependency on the degree of cure. The hardness tends to increase slightly after the final cure step. No step-wise change is also visible in the transition region[81].

Physical aging

Once the polymer reaches, the glassy state is highly cross-linked and amorphous. This state is not a thermodynamic equilibrium which makes it an unstable state. In other words, once the temperature stays below the T_g, the polymer will slowly approach an equilibrium by lowering its specific enthalpy [1]. Two factors achieve this. Firstly by contraction, so densifies to reach a lower energy molecular state (volumetric relaxation). Secondly, lowering the energy structure by rearrangements of molecular segments (enthalpy relaxation). These reversible processes are called physical ageing [81]. In Figure 2.20 andFigure A.1, the ageing regions are shown. Ageing is a time-dependent process and can cause material changes.

Moosburger et al. performed experiments to investigate the ageing effects on partially and fully cured tetrafunctional epoxies in ambient conditions [81]. It is shown that the density and modulus increase over time due to ageing. This effect is higher at the surface than in the bulk of the polymer. This can be explained by the fact that the surface is in direct contact with the environment. It causes the modulus at the surface to be higher than in bulk. This is relevant for surface-sensitive applications such as the joining of measurements. Minor physical ageing is observed for low curing degrees [81].

[1]"Enthalpy is the sum of the internal energy of the system plus the product of the pressure of the gas in the system and its volume: H = U + PV" [82]

B

Appendix: Literature study, fusion welding methods

Table B.1: Bulk heating

Method	Description	Applicability
Co-consolidation (autoclaving)	In both these methods, the bulk is heated. In other words, the entire structure is brought up to the required temperature to weld the thermoplastic film. Bond strength is equal to the parent strength of the thermoplastic.	No extra weight is added to the structure and the autoclave is the only required tool. The autoclave is available for this project. Potential thermal degradation to the thermoset due to bulk heating.
Hot press		A hot press is needed with the size of the mast, which is not realistic.

Table B.2: Two-stage techniques

Method	Description	Applicability
Hot plate welding	Hot plate welding, hot gas welding, infrared heating and laser heating all follow the same working principle. Both joining interfaces are heated separately. Shortly after heating, the heating element will get removed. As soon as this heating element is removed, pressure will be applied.	Due to geometrical limitations, these methods are not applicable in the manufacturing process of a mast. It is not possible to heat both surfaces separately and then quickly insert the component and apply pressure all at the same time. For laser heating, the laser needs to get through a transparent layer which is not possible when long carbon fibres are used [83].
Hot gas welding		
Infrared heating		
Laser heating		

Table B.3: Frictional heating

Method	Description	Applicability
Friction spin welding	These four methods are making use of friction, friction is generating heat which fuses the thermoplastic polymers together. Heat is generated either by spinning, stirring, the vibration of ultrasonic vibration. Here are ultrasonic high-frequency vibrations. During all these four methods pressure must be applied. [64].	Due to geometrical limitations, these methods are challenging to implement. Secondly, in mast long carbon fibres are used. These techniques can cause fibre displacement, they are more suitable for short fibre composites.
Friction stir welding		
Vibration welding		This method is capable of welding larger structures. However, the mast is slightly curved which can cause alignment challenges and therefore limited linear movement. [84].
Ultrasonic welding		Short heating times cause thermal degradation to be less of a problem in comparison to alternative methods. However, a complex setup is required which is out of scope for the manufacturing process of a mast. \[64] Secondly, welding length is limited to several centimetres due to the upper power limits of welding machines [84].

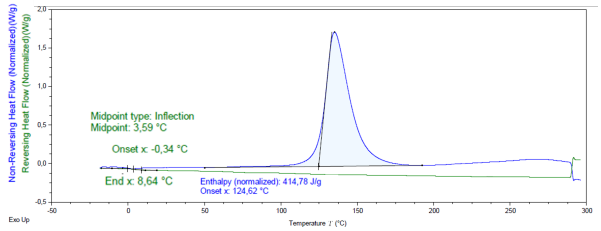
Table B.4: Electromagnetic heating

Method	Description	Applicability
Resistance welding	An electrical current flows through an inserted resistive heating element. This is a material which generates heat by conducting a current.	This application shows potential for mast manufacturing. A potential downside is the low welding speed, 1 mm/s [84].
Induction welding	The changing magnetic field generates heat. An alternating current generates this heat. This can be achieved without adding heating elements since the carbon fibre [19].	This method can be applied to mast manufacturing, however, the welding speed around 0.1 m/min which causes the entire process to be time-consuming. The high welding temperatures can lead to thermal degradation [19].
Dielectric welding	Dielectric welding, a high-frequency electric field which is being applied a pair of electrodes.	Both dielectric welding and microwave welding is limited to specific dipolar materials. Adding the fact that carbon fibre will work as a shield making this technique not possible for mast manufacturing.
Microwave welding	A microwave field causes molecular motions with the material. This effect generates heat.	

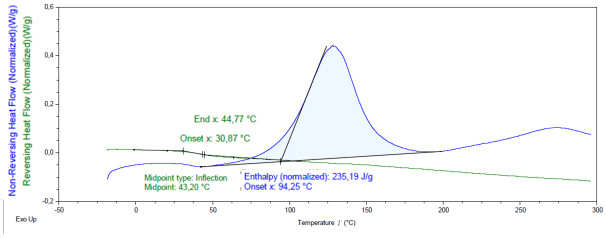
C

Appendix: Literature study, results measurements

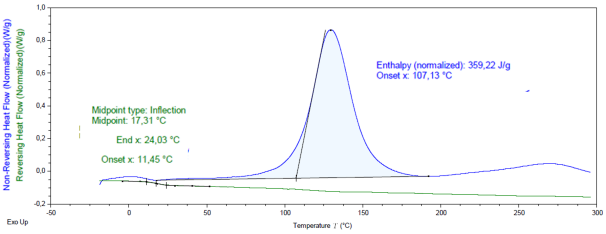
C.1. Results TMDSC



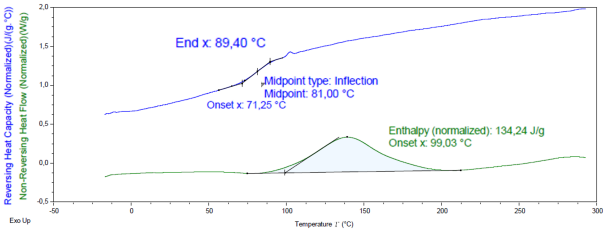
(a) Initial degree of cure 0 = , Glass transition temperature [°C]= 3.6



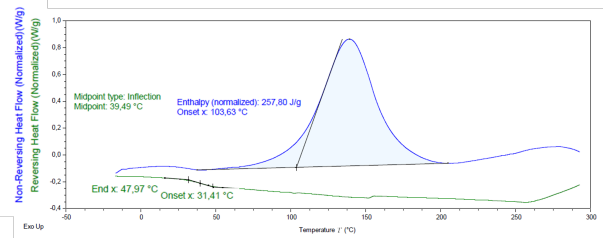
(b) Initial degree of cure 0.45 = , Glass transition temperature [°C]= 43.2



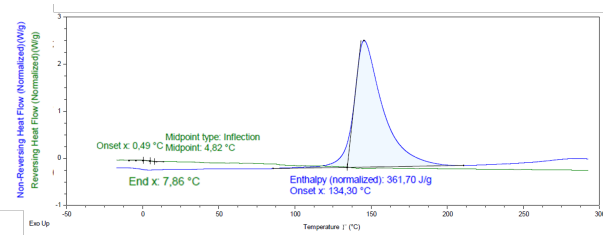
(c) Initial degree of cure =0.16 , Glass transition temperature [°C]=17



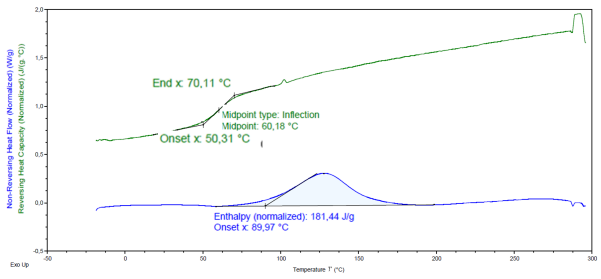
(d) Initial degree of cure =0.68 , Glass transition temperature [°C]= 81



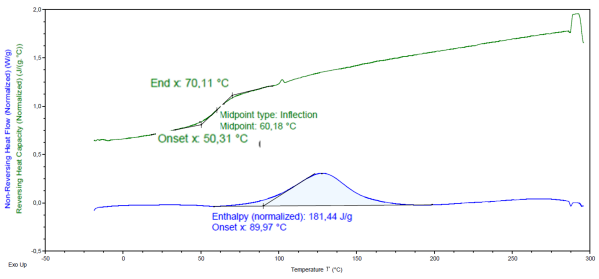
(e) Initial degree of cure = 0.40, Glass transition temperature [°C]= 39



(f) Initial degree of cure =0 , Glass transition temperature [°C]= 4.8



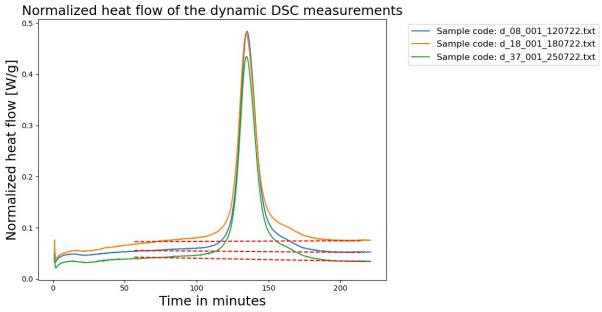
(g) Initial degree of cure =0.57 , Glass transition temperature [°C]= 60



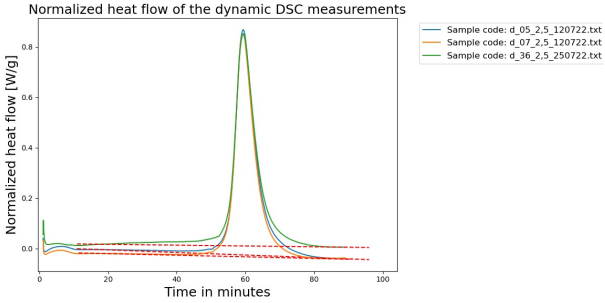
(h) Initial degree of cure = , Glass transition temperature [°C]=

Figure C.1: Results temperature modulated DSC measurements.

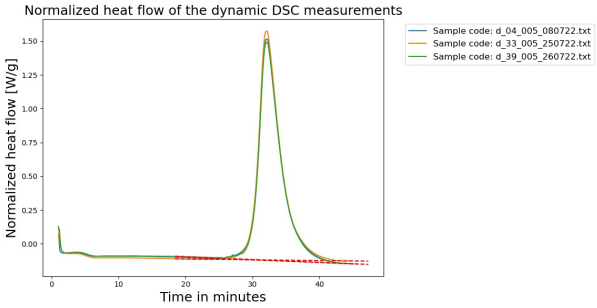
C.2. Results dynamic DSC



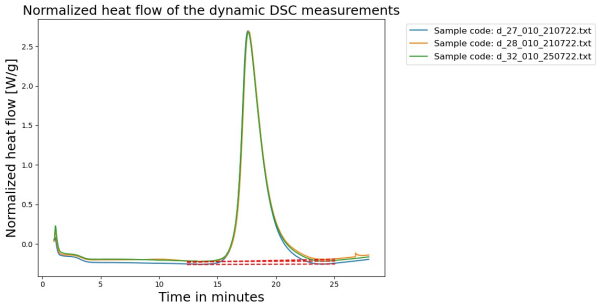
(a) Heating rate = 1°C/minute



(b) Heating rate = 2.5°C/minute



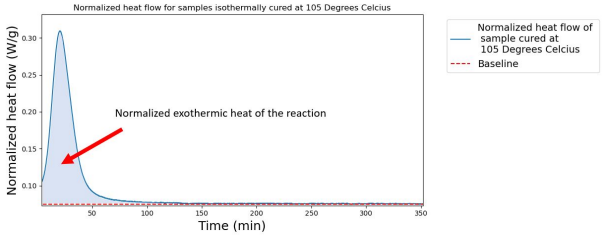
(c) Heating rate = 5°C/minute



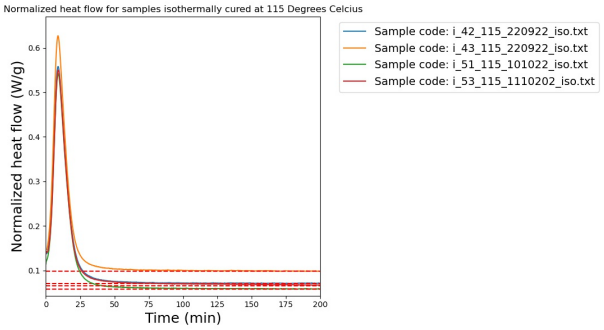
(d) Heating rate = 10°C/minute

Figure C.2: Results the heating rates 1,2.5,5 and 10 °C / minute. Note the lower the heating rate, the smaller the peak.

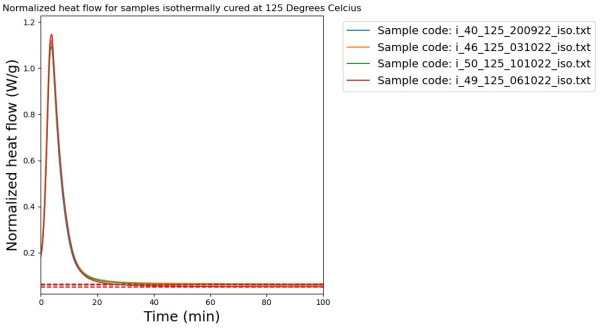
C.3. Isothermal DSC



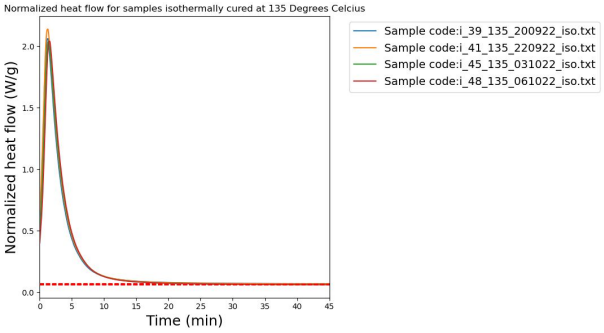
(a) Isothermal curing at 105°C/minute



(b) Isothermal curing at 115°C/minute



(c) Isothermal curing at 125°C/minute



(d) Isothermal curing at 135°C/minute

Figure C.3: Isothermal measurements at 105,115,125 and 135 °C. Heat flow is determined by the area under the curve and the baseline.

C.4. Second measurement, dynamic DSC

Table C.1: Residual heat flow, maximum degree of cure and reaction enthalpy of the samples

Isothermal curing temperature [Celcius] T_c	**sample #**	**Maximum degree of cure at isothermal temperature** $_{max}$	**Reaction enthalpy** ΔH_{iso} **[J/g]**	**Residual reaction enthalpy** ΔH_{tot}**[J/g]**	**Tptal reaction enthalpy** ΔH_{tot} **[J/g]**
105	44	0.82	350.6	37.9	388.5
115	42	0.88	372.0	7.1	379.1
115	43	0.90	381.6	21.9	403.5
115	51	0.86	364.8	15.3	380.1
115	53	0.90	381.1	15.0	396.1
125	40	0.91	387.2	6.5	393.7
125	46	0.96	409.5	3.1	412.6
125	50	0.93	396.6	4.1	400.7
135	39	0.93	396.0	0.4	396.4
135	41	0.99	419.2	0.2	419.4
135	45	0.97	411.8	0.0	411.8
135	48	0.95	405.6	0.3	405.9

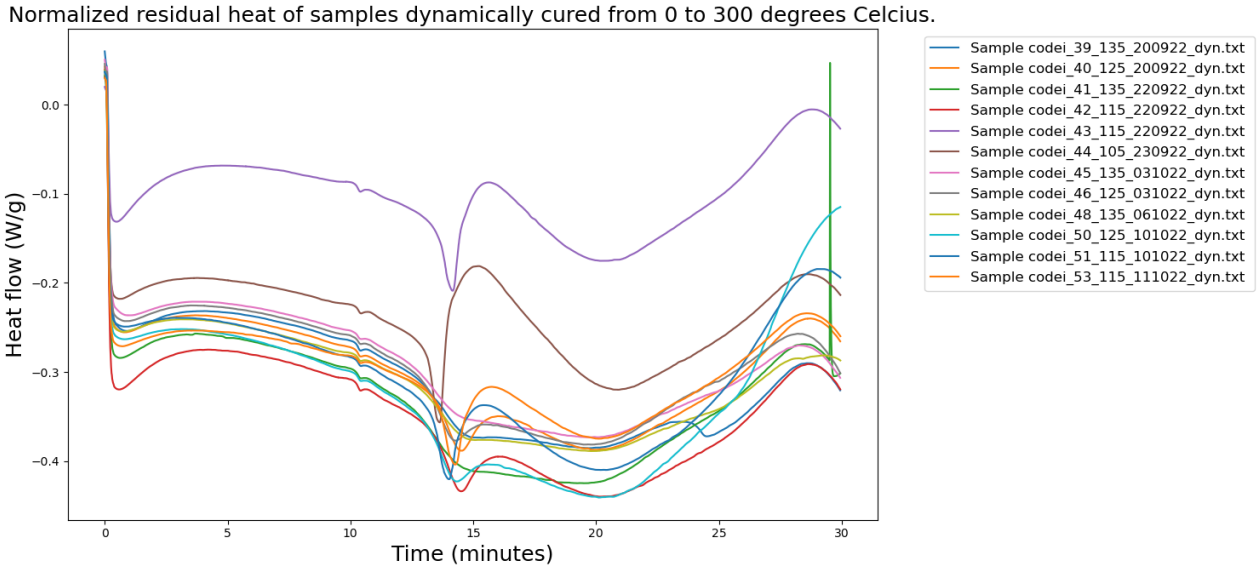
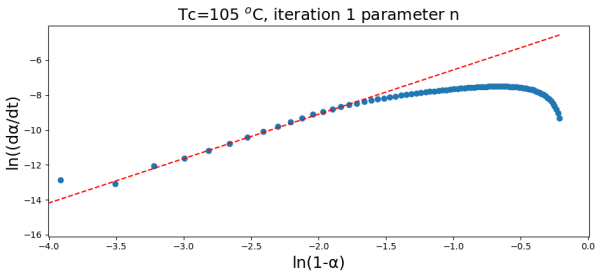
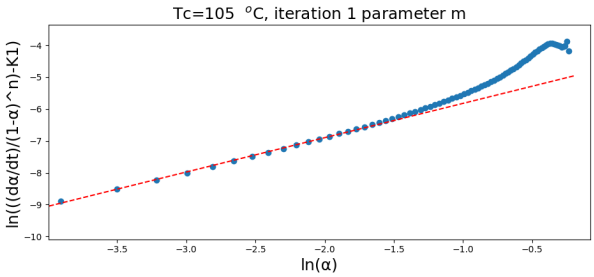


Figure C.4: Normalized residual heat of all the samples sample initially isothermally. The area determines the heat in between the curve and the baseline with the python code.

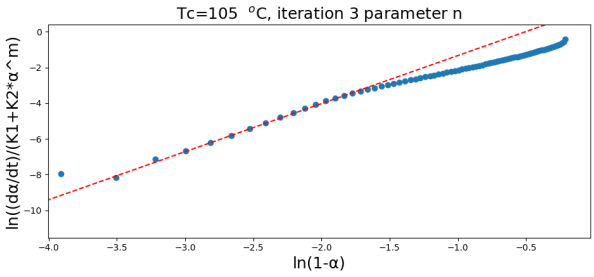
C.5. Results derivation Kamal model parameters, graphical analytical method



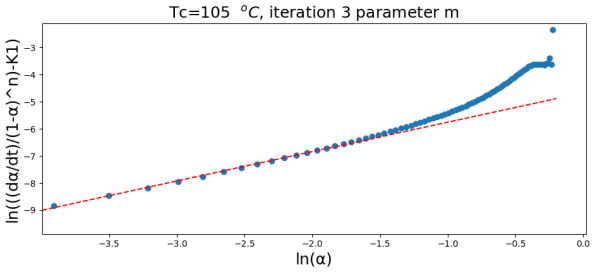
(a) Graphic representation of Equation 4.19 with the measured data, slope results in n.



(b) Graphic representation of Equation 4.23 with the measured data, slope m and constant K_2.

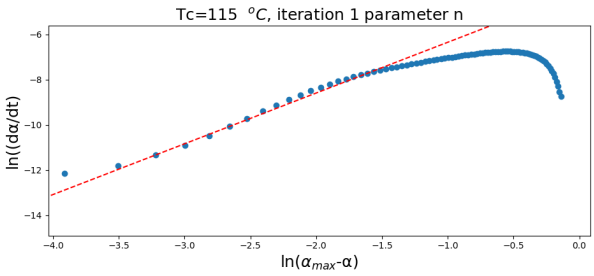


(c) Final iteration to find the slope n with Equation 4.24

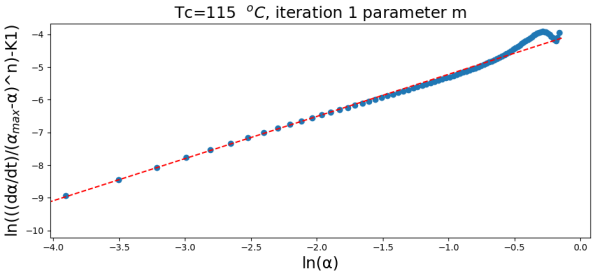


(d) Graphic representation of final iteration Equation 4.23 with the measured data, slope m and constant K_2.

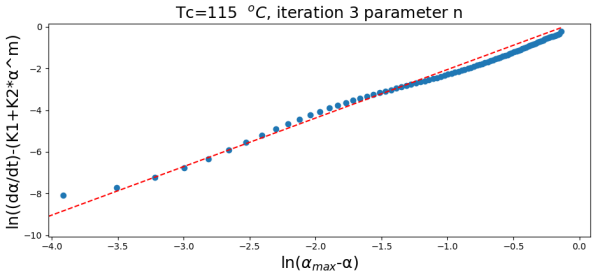
Figure C.5: Graphic representations of Equation 4.19,Equation 4.23 and Equation 4.24 for the isothermal DSC results obtained at 105°C. Slope is represented by the red dotted line.



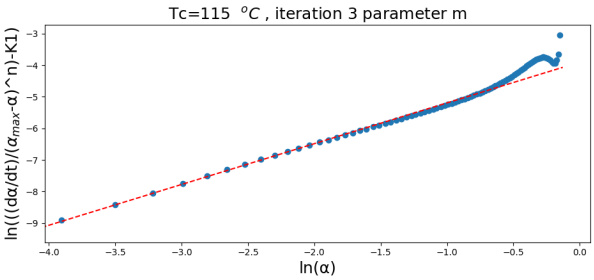
(a) Graphic representation of Equation 4.19 with the measured data, slope results in n.



(b) Graphic representation of Equation 4.23 with the measured data, slope m and constant K_2.

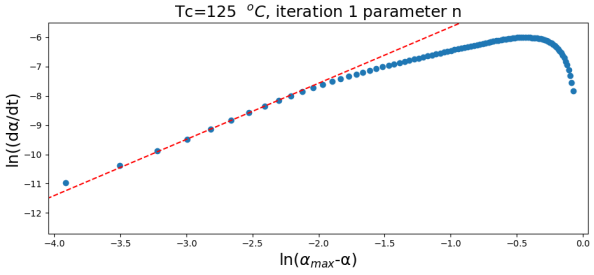


(c) Final iteration to find the slope n with Equation 4.24

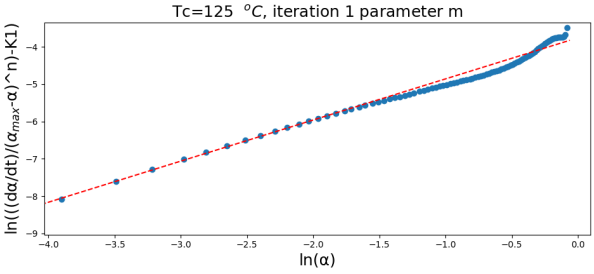


(d) Graphic representation of final iteration Equation 4.23 with the measured data, slope m and constant K_2.

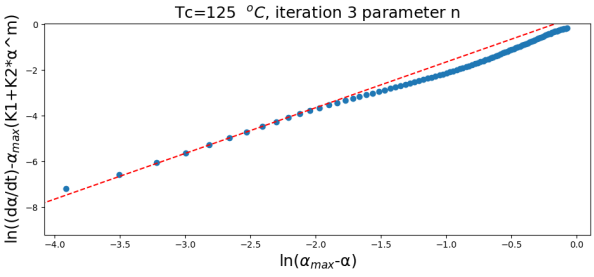
Figure C.6: Graphic representations of Equation 4.19,Equation 4.23 and Equation 4.24 for the isothermal DSC results obtained at 115°C. Slope is represented by the red dotted line.



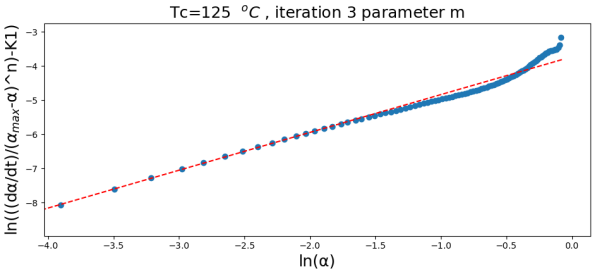
(a) Graphic representation of Equation 4.19 with the measured data, slope results in n.



(b) Graphic representation of Equation 4.23 with the measured data, slope m and constant K_2.

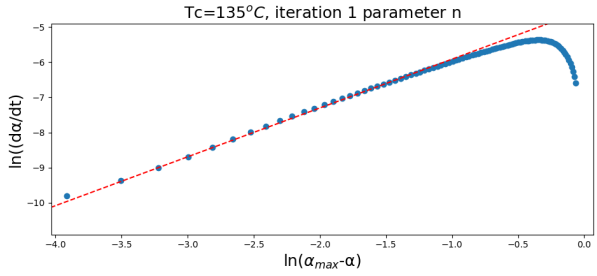


(c) Final iteration to find the slope n with Equation 4.24

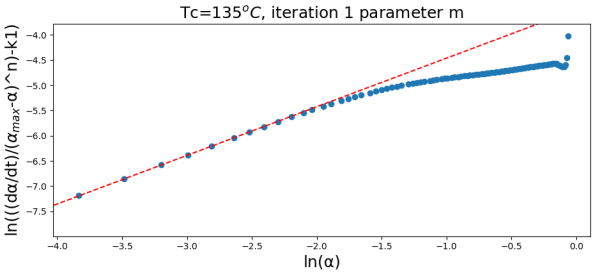


(d) Graphic representation of final iteration Equation 4.23 with the measured data, slope m and constant K_2.

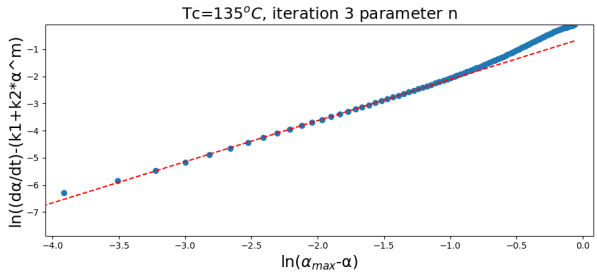
Figure C.7: Graphic representations of Equation 4.19,Equation 4.23 and Equation 4.24 for the isothermal DSC results obtained at 125°C. Slope is represented by the red dotted line.



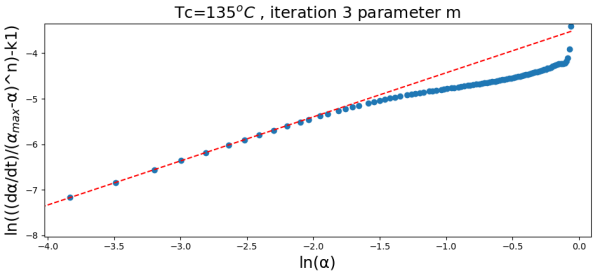
(a) Graphic representation of Equation 4.19 with the measured data, slope results in n.



(b) Graphic representation of Equation 4.23 with the measured data, slope m and constant K_2.

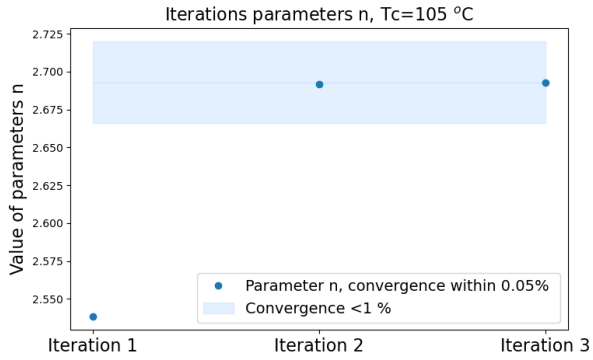


(c) Final iteration to find the slope n with Equation 4.24

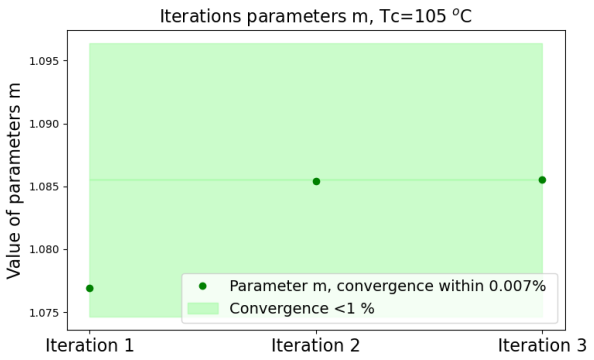


(d) Graphic representation of final iteration Equation 4.23 with the measured data, slope m and constant K_2.

Figure C.8: Graphic representations of Equation 4.19,Equation 4.23 and Equation 4.24 for the isothermal DSC results obtained at 135°C. Slope is represented by the red dotted line.

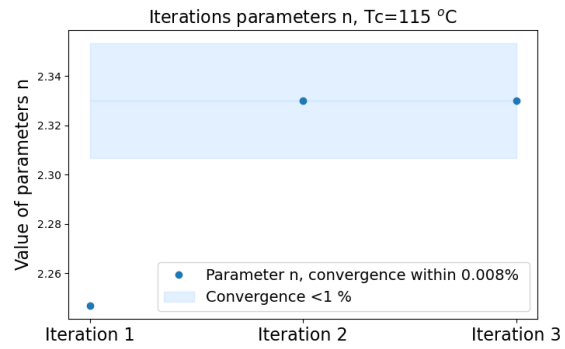


(a) Calculated value n after each iteration. The shaded area is the region where the difference between two iterations is $< 1\%$

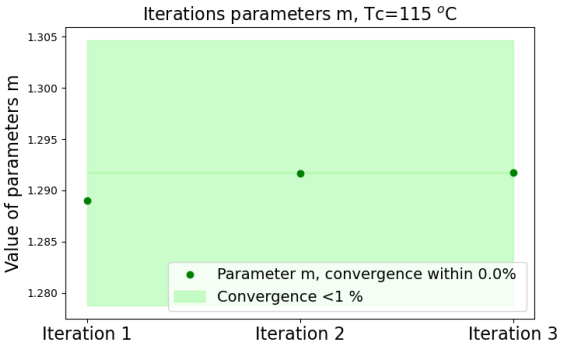


(b) Calculated value m after each iteration. The shaded area is the region where the difference between two iterations is $< 1\%$

Figure C.9: Result of the parameters n and m after each iteration for curing temperature = 105 °C. If the parameter point is within the convergence zone, convergence is achieved.

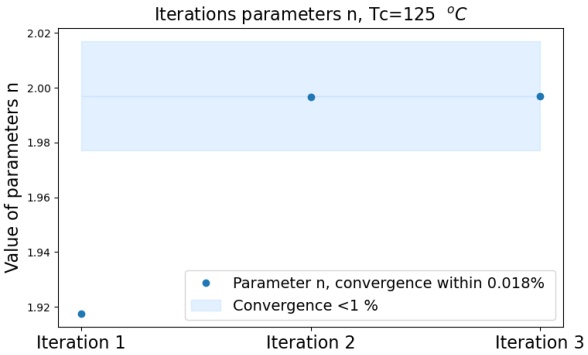


(a) Calculated value n after each iteration. The shaded area is the region where the difference between two iterations is $< 1\%$

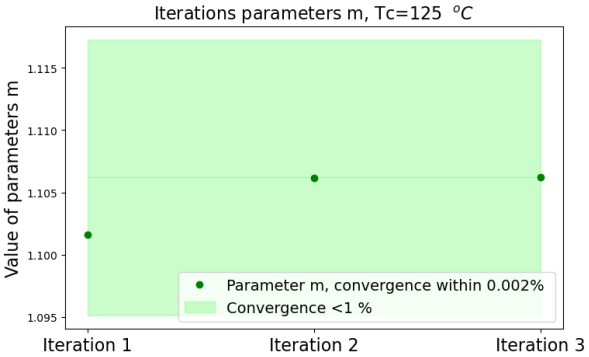


(b) Calculated value m after each iteration. The shaded area is the region where the difference between two iterations is $< 1\%$

Figure C.10: Result of the parameters n and m after each iteration for curing temperature = 115 °C. If the parameter point is within the convergence zone, convergence is achieved.

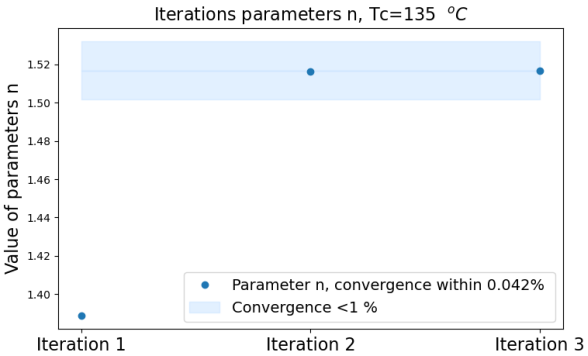


(a) Calculated value n after each iteration. The shaded area is the region where the difference between two iterations is $< 1\%$

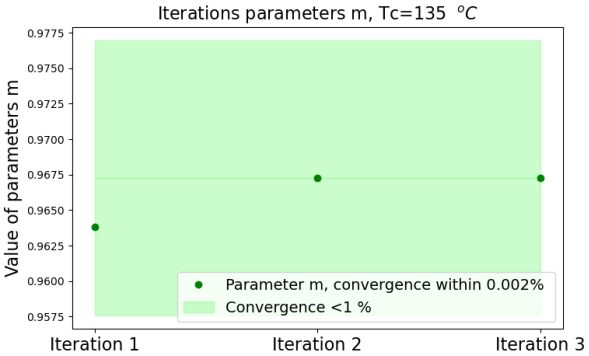


(b) Calculated value m after each iteration. The shaded area is the region where the difference between two iterations is $< 1\%$

Figure C.11: Result of the parameters n and m after each iteration for curing temperature = 125 °C. If the parameter point is within the convergence zone, convergence is achieved.



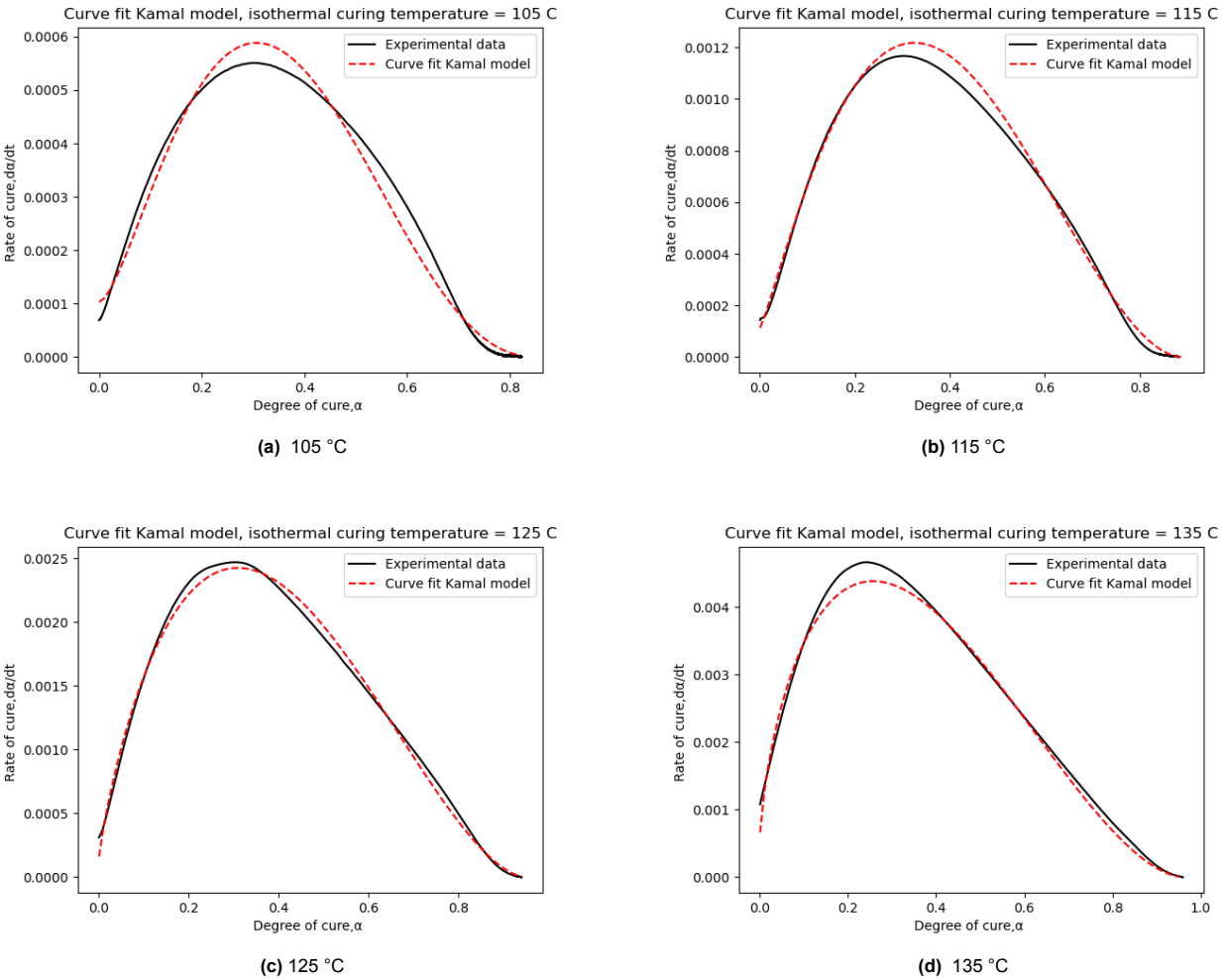
(a) Calculated value n after each iteration. The shaded area is the region where the difference between two iterations is $< 1\%$



(b) Calculated value m after each iteration. The shaded area is the region where the difference between two iterations is $< 1\%$

Figure C.12: Result of the parameters n and m after each iteration for curing temperature = 135 °C. If the parameter point is within the convergence zone, convergence is achieved.

C.6. Results derivation Kamal model parameters, curve fit method



(a) 105 °C

(b) 115 °C

(c) 125 °C

(d) 135 °C

Figure C.13: Isothermal measurements at 105,115,125 and 135 °C, with the curve, fits for the Kamal model

C.7. Gelpoint for dynamic heating rates

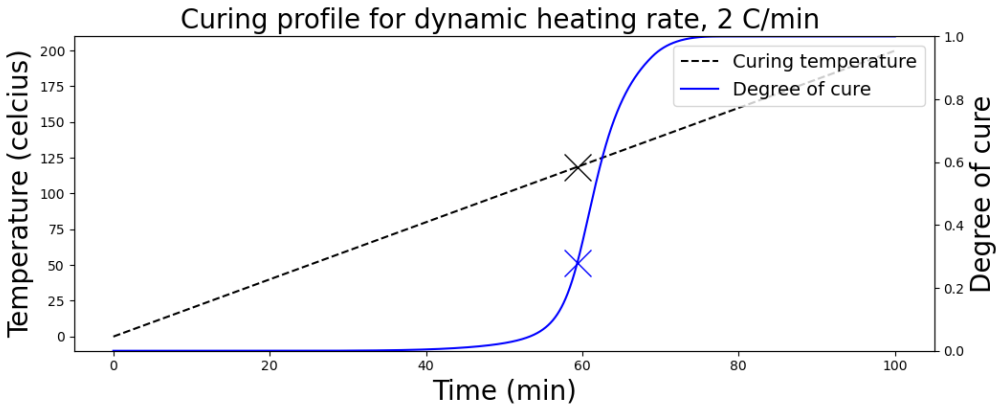


Figure C.14: Viscosity profile for dynamic heating rate 2 °C, according to python script. The curing temperature at the gel point is: 118 °C.

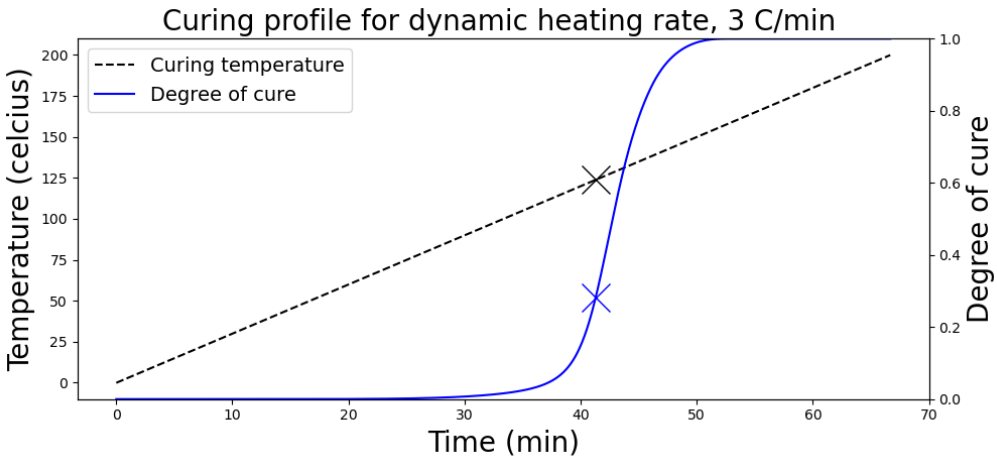


Figure C.15: Viscosity profile for dynamic heating rate 3 °C, according to python script. The curing temperature at the gel point is:123 °C.

C.8. Thickness of PEI film measured with the SEM

For each sample 10 measurements are performed. An indication of how such a measurement looks is given in Figure C.16.

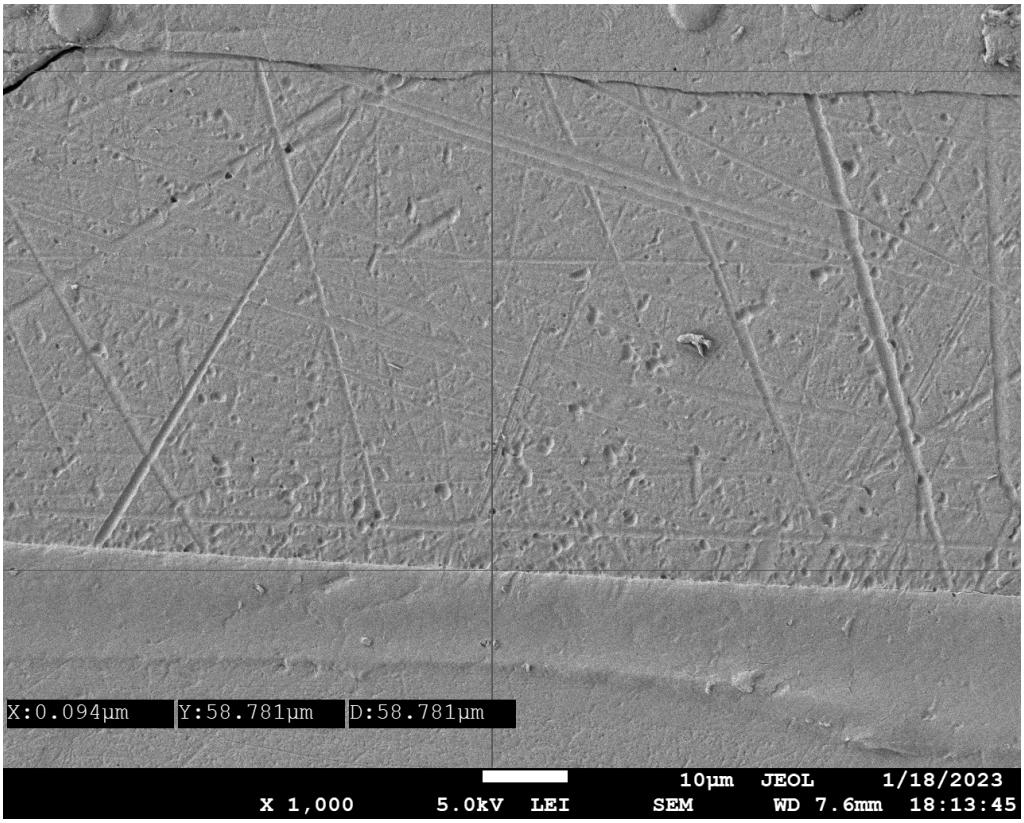


Figure C.16: Thickness of PEI film measured with the SEM for a sample cured at 105 °C.

C.9. ABD matrix

$$\begin{bmatrix} N_x \\ N_y \\ N_{xy} \\ M_x \\ M_y \\ M_{xy} \end{bmatrix} = \begin{bmatrix} A_{11} & A_{12} & A_{16} & B_{11} & B_{12} & B_{16} \\ A_{12} & A_{22} & A_{26} & B_{12} & B_{22} & B_{26} \\ A_{16} & A_{26} & A_{66} & B_{16} & B_{26} & B_{66} \\ B_{11} & B_{12} & B_{16} & D_{11} & D_{12} & D_{16} \\ B_{12} & B_{22} & B_{26} & D_{12} & D_{22} & D_{26} \\ B_{16} & B_{26} & B_{66} & D_{16} & D_{26} & D_{66} \end{bmatrix} \begin{bmatrix} \varepsilon_x^0 \\ \varepsilon_y^0 \\ \gamma_{xy}^0 \\ \kappa_x \\ \kappa_y \\ K_{xy} \end{bmatrix} \tag{C.1}$$

D

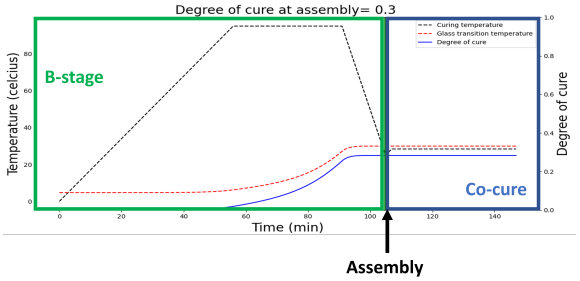
Appendix: Literature study, grinding and polishing

Table D.1: Grinding and polishing procedure.

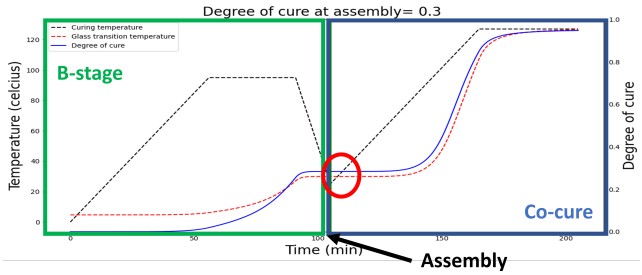
#	Type	Grainsize [μm]	Type of lubricant	Rotation speed [rpm]	Time [sec]
1	Grinding	75	water	250	60
2	Grinding	35	water	250	60
3	Grinding	20	water	250	60
4	Grinding	10	water	250	60
5	Grinding	5	water	250	60
6	Polishing	6	Ethanol +	250	180
7	Polishing	3	Ethanol +	250	180
8	Polishing	1	Ethanol +	250	180

E

Appendix: Literature study, glass transition temperature co-curing, partially cured samples

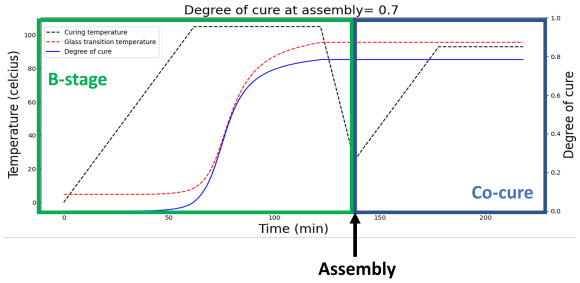


(a) Curing temperature remains below the glass transition temperature in the co-cure cycle. However, the reactivity of the resin is too low. The resin is not curing.

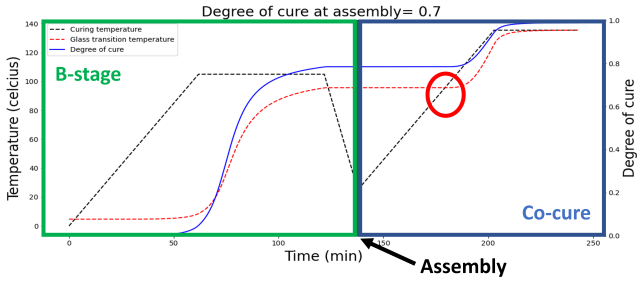


(b) Curing temperature remains above the glass transition temperature in the co-cure cycle. However, the part will lose its structural integrity in the co-curing phase.

Figure E.1: Cure kinetic model simulates the two curing cycles. The first is the b-stage cycle (in green); the degree of cure after this cycle is 0.3. And the second cycle after assembly is the co-cure cycle (in blue). (1) shows the scenario where the curing temperature remains below the glass transition temperature, (2) shows the opposite scenario.

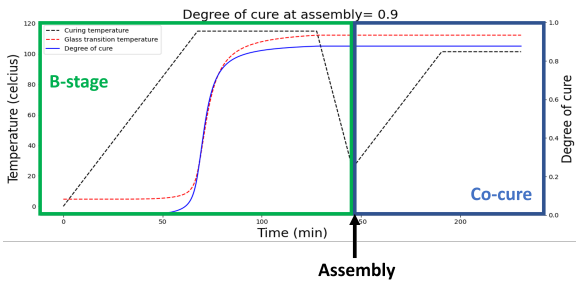


(a) Curing temperature remains below the glass transition temperature in the co-cure cycle. However, the reactivity of the resin is too low. The resin is not curing.

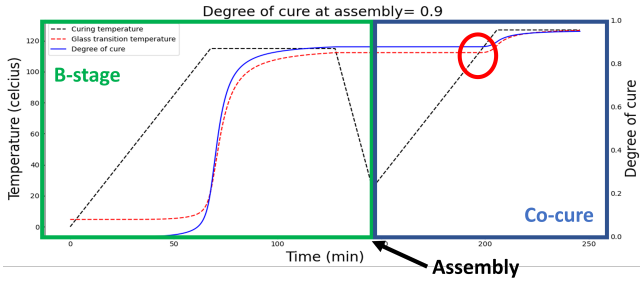


(b) Curing temperature remains above the glass transition temperature in the co-cure cycle. However, the part will lose its structural integrity in the co-curing phase.

Figure E.2: Cure kinetic model simulates the two curing cycles. The first is the b-stage cycle (in green); the degree of cure after this cycle is 0.7. And the second cycle after assembly is the co-cure cycle (in blue). (1) shows the scenario where the curing temperature remains below the glass transition temperature, (2) shows the opposite scenario.



(a) Curing temperature remains below the glass transition temperature in the co-cure cycle. However, the reactivity of the resin is too low. The resin is not curing.



(b) Curing temperature remains above the glass transition temperature in the co-cure cycle. However, the part will lose its structural integrity in the co-curing phase.

Figure E.3: Cure kinetic model simulates the two curing cycles. The first is the b-stage cycle (in green); the degree of cure after this cycle is 0.9. And the second cycle after assembly is the co-cure cycle (in blue). (1) shows the scenario where the curing temperature remains below the glass transition temperature, (2) shows the opposite scenario.

F

Appendix: Literature study, dimensions lap shear joints

Type sample	Sample #	Width [mm]	length [mm]	Surface [mm
Adhesive epoxy film	1	26.19	25.72	673.6068
	2	25.56	26.3	672.228
	3	27.55	25.46	701.423
	4	26.52	25.5	676.26
	5	26.52	28.22	748.3944
	6	27.4	25.53	699.522
Partiall cured 1, DOC =0.7	1	25.41	25.52	648.4632
	2	25.5	25.94	661.47
	3	25.73	25.73	662.0329
	4	25.52	25.63	654.0776
	5	25.46	25.62	652.2852
	6	25.48	25.47	648.9756
Partiall cured 2, DOC=0.5	1	25.56	26.24	670.6944
	2	25.44	26.91	684.5904
	3	25.58	26.95	689.381
	4	25.44	25.81	656.6064
	5	25.6	25.46	651.776
	6	25.58	25.58	654.3364
PEI 60 microns coupling	1	25.41	27.02	686.5782
	2	25.43	26.23	667.0289
	3	28.6	25.45	727.87
	4	25.48	26.87	684.6476
	5	25.59	28.46	728.2914
PEI 60 microns coupling + 60 micron interlayer, debulked	1	25.43	28.2	717.126
	2	25.46	28	712.88
	3	25.4	28.04	712.216
	4	25.46	28.04	713.8984
	5	25.58	28.46	728.0068
PEI 120 microns coupling + 60 micron interlayer, debulked	1	25.41	26.11	663.4551
	2	25.46	26.88	684.3648
	3	25.48	26.61	678.0228
	4	25.45	27.02	687.659
	5	25.51	26.56	677.5456
PEI 60 microns coupling + 60 micron interlayer, not debulked	1	25.48	28.02	713.9496

	2	25.41	27.96	710.4636
	3	25.4	28.01	711.454
	4	25.51	27.52	702.0352
	5	25.56	27.51	703.1556
	6	24.4	29.17	711.748

G

Appendix: Literature study, python codes

G.1. Dynamic DSC measurements

```
# -*- coding: utf-8 -*-
"""
Created on Tue Aug 30 15:13:12 2022

@author: thomv
"""

#import packages here
import numpy as np
from matplotlib import pyplot as plt
import pandas as pd
import matplotlib
import math
from IPython import get_ipython
get_ipython().magic('reset -sf')
plt.close('all')
from sklearn.metrics import r2_score


#settings plot
plot_time_or_temp='time'                #time or temp
show='005'                              #options: dynamic speed/ temp

#input
H_ult=426      #j/g

#definitions
def onsetindex_temp(x,onsettable,temp):
    #get data table
    lower=onsettable[x][3]
    upper=onsettable[x][4]
    index_lower = next(x for x, val in enumerate(temp)    # get the index of the first value which is bigger than lower limit temp
                                    if val > lower)
    index_upper = next(x for x, val in enumerate(temp)     # get the index of the first value which is bigger than upper limit temp
                                    if val > upper)

    return index_lower,index_upper

#linking the onset time  matchin index
def onsetindex_time(x,onsettable,time):
    #get data table
    lower=onsettable[x][3]
    upper=onsettable[x][4]
    index_lower = next(x for x, val in enumerate(time)    # get the index of the first value which is bigger than lower limit temp
                                    if val > lower)
```

```
46      index_upper = next(x for x, val in enumerate(time)      # get the index of the first value which
            is bigger than upper limit temp
47                                      if val > upper)
48
49      return index_lower,index_upper
50
51  def linear(dH_t,time,index_lower,index_upper):#making linear line
52      a=(dH_t[index_upper]-dH_t[index_lower])/(time[index_upper]-time[index_lower])
53      b=dH_t[index_lower]-(a*time[index_lower])
54      return a,b
55
56  def enthalpy(dH_t,time,index_lower,index_upper):
57      time=time*60   # from seconds to minutes
58      integral_value = 0
59      a,b=linear(dH_t,time,index_lower,index_upper) # get linear line
60      for i in range(index_lower,index_upper):
61          width = time[i + 1] - time[i]
62          height = dH_t[i]- ( a * time[i] + b )
63          integral_value += width * height
64
65      return integral_value
66
67  def filterdata(namessamples)  :
68      iso_or_dyn=[]
69      samplenumbers=[]
70      temp_rate=[]
71      date=[]
72
73      for x in range(len(namessamples)):
74          i=namessamples[x]
75          j=i[0]
76          samplenumbers.append(i[2]+i[3])
77          temp_rate.append(i[5]+i[6]+i[7])
78          date.append(i[9]+i[10]+i[11]+i[12]+i[13]+i[14])
79
80          if j == "d":
81              iso_or_dyn.append( "dynamic")
82          elif j =="i":
83              second=i[16]
84              if second == "i":
85                      iso_or_dyn.append( "isothermic first run")
86              elif second == "d":
87                      iso_or_dyn.append( "isothermic second dynamic run")
88
89
90      return iso_or_dyn, samplenumbers, temp_rate, date
91
92
93  def alpha(dH_t,time,index_lower,index_upper,dH_ult):
94      time=time*60   # from seconds to minutes
95      integral_value = 0
96      a,b=linear(dH_t,time,index_lower,index_upper) # get linear line
97      #DOC=np.zeros(len(dH_t))
98      DOC=[]
99      curetime=[]
100     tijd=0
101     for x in range(len(dH_t)):
102         if x >= index_lower and x <= index_upper:
103             width = time[x + 1] - time[x]
104             height = dH_t[x]- ( a * time[x] + b )
105             integral_value += width * height
106             #DOC[x]=(integral_value/dH_ult)
107             DOC.append(integral_value/dH_ult)
108             tijd=tijd+width/60
109             curetime.append(tijd)
110         #elif x < index_lower:
111             #DOC[x]=0
112         #elif x> index_upper:
113             #DOC[x]=(integral_value/dH_ult)
114
115     alpha=DOC
```

```
    curetime=curetime
    return alpha,curetime

#input data
namessamples=['d_04_005_080722.txt',
              'd_05_2,5_120722.txt','d_07_2,5_120722.txt','d_08_001_120722.txt',
                'd_18_001_180722.txt', 'd_27_010_210722.txt','d_28_010_210722.txt',
              'd_32_010_250722.txt','d_33_005_250722.txt','d_36_2,5_250722.txt','d_37_001_250722.
                  txt',
             'd_39_005_260722.txt']
#get the data based on the names
iso_or_dyn, samplenumbers, temp_rate, date=filterdata(namessamples)

#set which values to plot
listshow=[]
if show!='all':
    namessamples=namessamples
    for x in range(len(namessamples)):
        if temp_rate[x]==show:
            listshow.append(x)

#forming list with all the onset temperatures
# sample number, type of test (0=iso, 1=dyn), typ eof data, 0 = temperature, 1= time, then upper
    and lower value
samplesslimit,typetest,typedata,lowerr,upperr=np.loadtxt("limits_dynamisch.txt",skiprows=1,unpack=
    True)
onsettable=[]
for x in range(len(namessamples)):
    row=[[samplesslimit[x]],[typetest[x]],[typedata[x]],[lowerr[x]],[upperr[x]]]
    onsettable.append(row)

markerslist=[]   # for the onset and ofset poitns
#importing the data
for x in range(len(namessamples)):
    name=namessamples[x]
    time, temp,dH_t = np.loadtxt(name, skiprows = 3 ,unpack=True)
    #set the lists to the variables
    sample=samplesslimit[x]
    testtype=typetest[x]
    globals()[f"time_{sample}_{testtype}"] = time
    globals()[f"temp_{sample}_{testtype}"] = temp
    globals()[f"dH/dt_{sample}_{testtype}"] = dH_t    #W/g

    # run definitions to get onset and offset points # this looks to the type of input, either
        temperature or time is marked as ofset
    if typedata[x]==0:
        index_lower,index_upper= onsetindex_temp(x,onsettable,temp)    # time in minutes
    elif typedata[x]==1:
        index_lower,index_upper= onsetindex_time(x,onsettable,time)    # time in minutes

    #print( time_lower,time_upper,index_lower,index_upper)
    markers=[index_lower,index_upper]      # index for markers
    #set the lists to the variables
    globals()[f"index_lower_{sample}_{testtype}"] = index_lower
    globals()[f"index_upper_{sample}_{testtype}"] = index_upper

    markerslist.append(markers)

#making the first plots
# dynamic plots      dynamic
plot1 = plt.figure(1)
for x in range(len(namessamples)):
    sample=samplesslimit[x]
    testtype=typetest[x]
    plt.plot( globals()[f"time_{sample}_{testtype}"], globals()[f"dH/dt_{sample}_{testtype}"],label
        =namessamples[x])
plt.xlabel('Time (min)')
plt.ylabel('Heat flow (W/g)')
plt.title('Dynamic measurements')
plt.legend(bbox_to_anchor=(1.05, 1.0), loc='upper left')
plt.tight_layout()
```

```
plt.show()

plot2 = plt.figure(2)
for x in listshow:
    sample=sampleslimit[x]
    testtype=typetest[x]
           #plt.plot( globals()[f"{plot_time_or_temp}_{x+1}"], globals()[f"dH_t_{x+1}"], '-D',
               markevery=globals()[f"markers_{x+1}"],label=namessamples[x])
    plt.plot( globals()[f"{plot_time_or_temp}_{sample}_{testtype}"], globals()[f"dH/dt_{sample}_{
        testtype}"],label='Sample code: ' + namessamples[x])#,marker='o', markevery=markerslist[x],
        label=namessamples[x])
    a,b=linear(globals()[f"dH/dt_{sample}_{testtype}"],globals()[f"{plot_time_or_temp}_{sample}_{
        testtype}"],globals()[f"index_lower_{sample}_{testtype}"], globals()[f"index_upper_{sample}
        _{testtype}"])
    low=onsettable[x][3]
    up=onsettable[x][4]
    distance=abs(low[0]-up[0])   # to get a margin for the y=ax+b

    xaxis=np.linspace(onsettable[x][3]-0.1*distance,onsettable[x][4]+0.1*distance,100)
    y=a*xaxis+b
    plt.plot(xaxis, y,'r--')
plt.xlabel('Time in minutes',fontsize=18)
plt.ylabel('Normalized heat flow [W/g]',fontsize=18)
plt.title('Normalized heat flow of the dynamic DSC measurements',fontsize=18)
plt.legend(bbox_to_anchor=(1.05, 1.0), loc='upper left',fontsize=12)
plt.tight_layout()
plt.show()
#at this point all plots are made, now the next step is to calculate the enthalpy

#plot all degrees of cure #dynamical
fig4 = plt.figure(4)
for x in range(len(namessamples)):
    sample=sampleslimit[x]
    testtype=typetest[x]

    DOC_plot,curetime=alpha(globals()[f"dH/dt_{sample}_{testtype}"], globals()[f"time_{sample}_{
        testtype}"],globals()[f"index_lower_{sample}_{testtype}"], globals()[f"index_upper_{sample}
        _{testtype}"],H_ult)

    globals()[f"curetime_{sample}_{testtype}"] = curetime
    globals()[f"DOC_{sample}_{testtype}"] = DOC_plot
    plt.plot( globals()[f"curetime_{sample}_{testtype}"], DOC_plot,label=namessamples[x])

plt.xlabel('Time (min)')
plt.ylabel('degree of cure')
plt.title('degree of cure versus time, dynamic ')
plt.legend(bbox_to_anchor=(1.05, 1.0), loc='upper left')
plt.tight_layout()
plt.show()

#this is calculated within the boudnaries of the limits
reaction_enthalpy=[]
for x in range(len(namessamples)):
    sample=sampleslimit[x]
    testtype=typetest[x]
    reaction_enthalpy.append(enthalpy(globals()[f"dH/dt_{sample}_{testtype}"], globals()[f"time_{
        sample}_{testtype}"],globals()[f"index_lower_{sample}_{testtype}"], globals()[f"
        index_upper_{sample}_{testtype}"]))
# save enthalpy between the boundaries. this is in J/g
savedata=[]
for x in range(len(namessamples)):
    savedata.append([[iso_or_dyn[x]], [samplenumbers[x]], [temp_rate[x]], [reaction_enthalpy[x]]])

df = pd.DataFrame(savedata)
# saving the dataframe
df.to_csv('enthalpy_dynamisch.csv')

################################################## this is the point to get the mean of each run
sample_rate_1=[]
sample_rate_25=[]
sample_rate_5=[]
```

```
sample_rate_10=[]
for x in range(len(namessamples)):
        if temp_rate[x]=='001':
            sample_rate_1.append(x)
        elif temp_rate[x]=='2,5':
            sample_rate_25.append(x)
        elif temp_rate[x]=='005':
            sample_rate_5.append(x)
        elif temp_rate[x]=='010':
            sample_rate_10.append(x)

mean1=np.mean(np.array([globals()[f"dH/dt_{sampleslimit[sample_rate_1[0]]}_{typetest[sample_rate_1
    [0]]}"],globals()[f"dH/dt_{sampleslimit[sample_rate_1[1]]}_{typetest[sample_rate_1[1]]}"]]),
    axis=0)
std1=np.std(np.array([globals()[f"dH/dt_{sampleslimit[sample_rate_1[0]]}_{typetest[sample_rate_1
    [0]]}"],globals()[f"dH/dt_{sampleslimit[sample_rate_1[1]]}_{typetest[sample_rate_1[1]]}"]]),
    axis=0)
tijd1=globals()[f"time_{sampleslimit[sample_rate_1[0]]}_{typetest[sample_rate_1[0]]}"]

mean25=np.mean(np.array([globals()[f"dH/dt_{sampleslimit[sample_rate_25[0]]}_{typetest[
    sample_rate_25[0]]}"][0:52760],globals()[f"dH/dt_{sampleslimit[sample_rate_25[1]]}_{typetest[
    sample_rate_25[1]]}"][0:52760],globals()[f"dH/dt_{sampleslimit[sample_rate_25[2]]}_{typetest[
    sample_rate_25[2]]}"][0:52760]]),axis=0)
std25=np.std(np.array([globals()[f"dH/dt_{sampleslimit[sample_rate_25[0]]}_{typetest[sample_rate_25
    [0]]}"][0:52760],globals()[f"dH/dt_{sampleslimit[sample_rate_25[1]]}_{typetest[sample_rate_25
    [1]]}"][0:52760],globals()[f"dH/dt_{sampleslimit[sample_rate_25[2]]}_{typetest[sample_rate_25
    [2]]}"][0:52760]]),axis=0)
tijd25=globals()[f"time_{sampleslimit[sample_rate_25[0]]}_{typetest[sample_rate_25[0]]}"][0:52760]

mean5=np.mean(np.array([globals()[f"dH/dt_{sampleslimit[sample_rate_5[0]]}_{typetest[sample_rate_5
    [0]]}"][0:25768],globals()[f"dH/dt_{sampleslimit[sample_rate_5[1]]}_{typetest[sample_rate_5
    [1]]}"][0:25768],globals()[f"dH/dt_{sampleslimit[sample_rate_5[2]]}_{typetest[sample_rate_5
    [2]]}"][0:25768]]),axis=0)
std5=np.std(np.array([globals()[f"dH/dt_{sampleslimit[sample_rate_5[0]]}_{typetest[sample_rate_5
    [0]]}"][0:25768],globals()[f"dH/dt_{sampleslimit[sample_rate_5[1]]}_{typetest[sample_rate_5
    [1]]}"][0:25768],globals()[f"dH/dt_{sampleslimit[sample_rate_5[2]]}_{typetest[sample_rate_5
    [2]]}"][0:25768]]),axis=0)
tijd5=globals()[f"time_{sampleslimit[sample_rate_5[0]]}_{typetest[sample_rate_5[0]]}"][0:25768]

mean10=np.mean(np.array([globals()[f"dH/dt_{sampleslimit[sample_rate_10[0]]}_{typetest[
    sample_rate_10[0]]}"][0:16165],globals()[f"dH/dt_{sampleslimit[sample_rate_10[1]]}_{typetest[
    sample_rate_10[1]]}"][0:16165],globals()[f"dH/dt_{sampleslimit[sample_rate_10[2]]}_{typetest[
    sample_rate_10[2]]}"][0:16165]]),axis=0)
std10=np.std(np.array([globals()[f"dH/dt_{sampleslimit[sample_rate_10[0]]}_{typetest[sample_rate_10
    [0]]}"][0:16165],globals()[f"dH/dt_{sampleslimit[sample_rate_10[1]]}_{typetest[sample_rate_10
    [1]]}"][0:16165],globals()[f"dH/dt_{sampleslimit[sample_rate_10[2]]}_{typetest[sample_rate_10
    [2]]}"][0:16165]]),axis=0)
tijd10=globals()[f"time_{sampleslimit[sample_rate_10[0]]}_{typetest[sample_rate_10[0]]}"][0:16165]

fig50=plt.figure(50)
plt.plot(tijd1,mean1,color='red', label='Average of samples with \n heating rate 1 $^oC$/min')
plt.fill_between(tijd1,mean1+std1, mean1-std1,alpha=0.5, edgecolor='#C6E2FF', facecolor='#C6E2FF')
plt.plot(tijd25,mean25,color='blue',label='Average of samples with \n heating rate 2.5$^oC$/min')
plt.fill_between(tijd25,mean25+std25, mean25-std25,alpha=0.5, edgecolor='#C6E2FF', facecolor='#
    C6E2FF')
plt.plot(tijd5,mean5,color='green',label='Average of samples with \n heating rate 5 $^oC$/min')
plt.fill_between(tijd5,mean5+std5, mean5-std5,alpha=0.5, edgecolor='#C6E2FF', facecolor='#C6E2FF')
plt.plot(tijd10,mean10,color='orange' ,label='Average of samples with \n heating rate 10 $^oC$/min'
    )
plt.fill_between(tijd10,mean10+std10, mean10-std10,alpha=0.5, edgecolor='#C6E2FF', facecolor='#
    C6E2FF')

plt.xlabel('Time (min)',fontsize=18)
plt.ylabel('Normalized heat flow [W/g]',fontsize=18)
plt.title('Average normlized heat flow , with standard deviation',fontsize=18)
plt.legend(bbox_to_anchor=(1.05, 1.0), loc='upper left',fontsize=16)
plt.tight_layout()
plt.show()

fig51=plt.figure(51)
```

```
DOC_plot_mean1,curetime_mean1=alpha(mean1, tijd1,globals()[f"index_lower_{sampleslimit[sample_rate_1[0]]}_{typetest[sample_rate_1[0]]}"], globals()[f"index_upper_{sampleslimit[sample_rate_1[0]]}_{typetest[sample_rate_1[0]]}"],H_ult)
DOC_plot_std1,curetime_std1=alpha(std1, tijd1,globals()[f"index_lower_{sampleslimit[sample_rate_1[0]]}_{typetest[sample_rate_1[0]]}"], globals()[f"index_upper_{sampleslimit[sample_rate_1[0]]}_{typetest[sample_rate_1[0]]}"],H_ult)
DOC_plot_mean1=np.array(DOC_plot_mean1)
DOC_plot_std1=np.array(DOC_plot_std1)
plt.fill_between(curetime_mean1,DOC_plot_mean1+DOC_plot_std1, DOC_plot_mean1-DOC_plot_std1,alpha=0.5, edgecolor='#C6E2FF', facecolor='#C6E2FF')
plt.plot(curetime_mean1,DOC_plot_mean1, label='Average of samples with \n heating rate 1$^oC$/min', color ='red')
DOC_plot_mean25,curetime_mean25=alpha(mean25, tijd25,globals()[f"index_lower_{sampleslimit[sample_rate_25[0]]}_{typetest[sample_rate_25[0]]}"], globals()[f"index_upper_{sampleslimit[sample_rate_25[0]]}_{typetest[sample_rate_25[0]]}"],H_ult)
DOC_plot_std25,curetime_std25=alpha(std25, tijd25,globals()[f"index_lower_{sampleslimit[sample_rate_25[0]]}_{typetest[sample_rate_25[0]]}"], globals()[f"index_upper_{sampleslimit[sample_rate_25[0]]}_{typetest[sample_rate_25[0]]}"],H_ult)
DOC_plot_mean25=np.array(DOC_plot_mean25)
DOC_plot_std25=np.array(DOC_plot_std25)
plt.fill_between(curetime_mean25,DOC_plot_mean25+DOC_plot_std25, DOC_plot_mean25-DOC_plot_std25, alpha=0.5, edgecolor='#C6E2FF', facecolor='#C6E2FF')
plt.plot(curetime_mean25,DOC_plot_mean25, label='Average of samples with \n heating rate 2,5$^oC$/min', color ='blue')
DOC_plot_mean5,curetime_mean5=alpha(mean5, tijd5,globals()[f"index_lower_{sampleslimit[sample_rate_5[2]]}_{typetest[sample_rate_5[2]]}"], globals()[f"index_upper_{sampleslimit[sample_rate_5[2]]}_{typetest[sample_rate_5[2]]}"],H_ult)
DOC_plot_std5,curetime_std5=alpha(std5, tijd5,globals()[f"index_lower_{sampleslimit[sample_rate_5[2]]}_{typetest[sample_rate_5[2]]}"], globals()[f"index_upper_{sampleslimit[sample_rate_5[2]]}_{typetest[sample_rate_5[2]]}"],H_ult)
DOC_plot_mean5=np.array(DOC_plot_mean5)
DOC_plot_std5=np.array(DOC_plot_std5)
plt.fill_between(curetime_mean5,DOC_plot_mean5+DOC_plot_std5, DOC_plot_mean5-DOC_plot_std5,alpha=0.5, edgecolor='#C6E2FF', facecolor='#C6E2FF')
plt.plot(curetime_mean5,DOC_plot_mean5, label='Average of samples with \n heating rate 5$^oC$/min', color ='green')
DOC_plot_mean10,curetime_mean10=alpha(mean10, tijd10,globals()[f"index_lower_{sampleslimit[sample_rate_10[0]]}_{typetest[sample_rate_10[0]]}"], globals()[f"index_upper_{sampleslimit[sample_rate_10[0]]}_{typetest[sample_rate_10[0]]}"],H_ult)
DOC_plot_std10,curetime_std10=alpha(std10, tijd10,globals()[f"index_lower_{sampleslimit[sample_rate_10[0]]}_{typetest[sample_rate_10[0]]}"], globals()[f"index_upper_{sampleslimit[sample_rate_10[0]]}_{typetest[sample_rate_10[0]]}"],H_ult)
DOC_plot_mean10=np.array(DOC_plot_mean10)
DOC_plot_std10=np.array(DOC_plot_std10)
plt.fill_between(curetime_mean10,DOC_plot_mean10+DOC_plot_std10, DOC_plot_mean10-DOC_plot_std10, alpha=0.5, edgecolor='#C6E2FF', facecolor='#C6E2FF')
plt.plot(curetime_mean10,DOC_plot_mean10, label='Average of samples with \n heating rate 10$^oC$/min', color ='orange')

plt.xlabel('Time (min)',fontsize=18)
plt.ylabel('Degree of cure',fontsize=18)
plt.title('Evolution degree of cure over time, \n average and standard deviation for each \n dynamic heating rate',fontsize=14)
plt.legend(bbox_to_anchor=(1.05, 1.0), loc='upper left',fontsize=16)
plt.tight_layout()
plt.show()
```

G.2. Isothermal measurements

```
# -*- coding: utf-8 -*-
"""
Created on Tue Sep 20 15:05:01 2022

@author: thomv
"""

# -*- coding: utf-8 -*-
"""
Created on Tue Sep  6 11:02:24 2022

```

```
@author: thomv
"""
import numpy as np
from definitions import *
from matplotlib import pyplot as plt
from numpy import log as ln
plt.close('all')
#import data from text file, they will be a list
#time in minutes, temperature in celcius and dH/dT is
#at this point all the data is imported
#the total enthalpy which will be used, normalized
H_ult=426 #j/g
T_135=135         #in Celcius


namessamples=['i_39_135_200922_iso.txt','i_41_135_220922_iso.txt','i_45_135_031022_iso.txt','
    i_48_135_061022_iso.txt']


def data(filenamedsc):

    time_min, T_C,dH_dt =  importfiles(filenamedsc)

    """
    ################################3
    #adjust data to get lost data back
    a_lost,b_lost=np.polyfit([time_min[0],time_min[1]],[dH_dt[0],dH_dt[1]],1)
    a_lost=a_lost
    time_lost_min=(0-b_lost)/a_lost

    #make arrays to get lost data back
    delta=time_min[1]-time_min[0]
    steps_lost=int(np.ceil(abs(time_lost_min)/delta))
    insert_time=np.zeros(steps_lost)
    insert_dH_dt=np.zeros(steps_lost)
    for i in range(steps_lost):
        insert_time[i]=(0+delta*i)
        insert_dH_dt[i]=a_lost*delta*i


        #now we are gonna isnert it to get lost data back
    time_min=time_min+abs(time_lost_min)
    time_min=np.concatenate((insert_time,time_min))
    dH_dt=np.concatenate((insert_dH_dt,dH_dt))
    new=dH_dt
    newtime=time_min
    #"""



    #the time boundaries will be defined to get the exothermic peak, both in minutes
    tmin=0   #minutes
    tmax=59.9    #minutes
    tminsec=int(np.ceil(tmin*60))
    tmaxsec=int(np.ceil(tmax*60))
    hmin=dH_dt[tmaxsec]
    hmax=max(dH_dt)

    #making x and y
    x_135= np.zeros(len(time_min))+time_min
    y_135=np.zeros(len(dH_dt))+dH_dt



    #####
    #here I can insert a way to filter out outliers, not needed yet
    X_135=[]
    Y_135=[]

```

```
82
83      for i in range(len(x_135)):
84          if x_135[i] >= tmin and x_135[i] <= tmax:
85              if y_135[i] < hmin*0.9999:  # this is to filter out the outliers
86                  y_135[i]=hmin
87
88
89              X_135.append(x_135[i])
90              Y_135.append(y_135[i])
91
92
93
94      X_135=np.array(X_135)
95      Y_135=np.array(Y_135)
96
97
98
99
100
101
102     #####
103     t0=tmin*60                              #this is the time back from the origin converted to
            seconds
104     #rint is to round to nearest second
105     time_135=np.rint(X_135*60)-t0                   #gets matched so that only that 0 is the start of
             the reaction [s]
106     dh_dt_reaction135=Y_135-hmin                    #gets matched so that only that 0 is the start of
             the reaction  [w/g]
107     H_135=np.cumsum(dh_dt_reaction135)              #gives us the total cummaltive heat flow , still
            an array
108     alfa_135=H_135/H_ult                            #gives the degree of cure per time step, so in
            the form of an array
109     max_alfa_135=max(alfa_135)                      #gives maximum degree of cure for this isothermal
             temperature
110     alfacum_135=alfa_135/max_alfa_135                #degree of cure per time step (cum)
111     dalfa_dt_135=dh_dt_reaction135/H_ult            #degree of cure per time step
112
113
114
115
116     #next step is to know where&what the maximum dalpha/dt is reached and at which time step
117     max_dalpha_135=max(dalfa_dt_135)      #           point
118     index_max_dalpha_135=np.argmax(dalfa_dt_135)      #point
119
120     #what is the degree of cure at this point
121     DOC_dalpha_max_135= alfa_135[index_max_dalpha_135]
122
123     #normalize d alpha
124     norm_dalfa_135=dalfa_dt_135/max_dalpha_135
125
126     #get the total released energy
127     H_total_135=np.trapz(dh_dt_reaction135,time_135)
128
129
130
131     ############################ plotting
132
133
134
135     #plots
136     plot1 = plt.figure(1)
137     plt.plot(time_135,dh_dt_reaction135,label='Isothermal 135')
138     plt.xlabel('Time (s)')
139     plt.ylabel('Heat flow (W/g)')
140     plt.title('Dynamic measurements')
141     plt.legend(bbox_to_anchor=(1.05, 1.0), loc='upper left')
142     plt.tight_layout()
143     plt.show()
144
145
146     plot2 = plt.figure(2)
```

```
147     plt.plot(time_135,alfa_135,label='Isothermal 135')
148     plt.xlabel('Time (s)')
149     plt.ylabel('Degree of cure')
150     plt.title('Degree of cure versus time, isothermal first run  ')
151     plt.legend(bbox_to_anchor=(1.05, 1.0), loc='upper left')
152     plt.tight_layout()
153     plt.show()
154 
155     plot3=plt.figure(3)
156     plt.plot(alfa_135,dalfa_dt_135,label='Isothermal 135')
157     plt.xlabel('Degree of cure ')
158     plt.ylabel('Reaction rate')
159     plt.title('Reaction rate versus degree of cure ')
160     plt.legend(bbox_to_anchor=(1.05, 1.0), loc='upper left')
161     plt.tight_layout()
162     plt.show()
163 
164 
165     markerslist=[]   # for the onset and ofset poitns
166     index_lower,index_upper= onsetindex_time(tmin,tmax,x_135)
167 
168     index_lower = next(x for x, val in enumerate(dH_dt)    # get the index of the first value which
            is bigger than lower limit temp
169                                     if val >= hmin)
170     markers=[index_lower,index_upper]
171 
172     plot4 = plt.figure(4)
173     plt.plot(x_135 , dH_dt,label='Sample code:'+ namessamples[x])#,marker='o', markevery=markers,
            label='Isothermal 135')
174     fit=np.polyfit(markers,[hmin,hmin],1)
175     #a,b=linear(dH_dt,x_135,tmin, tmax)
176     a,b=fit
177     distance=abs(tmax-tmin)   # to get a margin for the y=ax+b
178     xaxis=np.linspace(tmin-0.4*distance,tmax+0.4*distance,100)
179     y=a*xaxis+b
180     plt.plot(xaxis, y,'r--')
181     plt.xlabel('Time (min)',fontsize='18')
182     plt.ylabel('Normalized heat flow (W/g)',fontsize='18')
183     plt.title('Normalized heat flow for samples isothermally cured at 135 Degrees Celcius',fontsize
            ='18')
184     plt.legend(bbox_to_anchor=(1.05, 1.0), loc='upper left',fontsize='14')
185     plt.tight_layout()
186     plt.show()
187 
188 
189     return alfa_135,dalfa_dt_135,H_total_135,max_alfa_135,alfacum_135,dh_dt_reaction135,
            DOC_dalpha_max_135,norm_dalfa_135,time_135
190 
191 
192 #gather the data for all measurements
193 
194 
195 for x in range(len(namessamples)):
196     globals()[f"alfa_135_{x}"],globals()[f"dalfa_dt_135_{x}"],globals()[f"H_total_135_{x}"]   ,
            globals()[f"max_alfa_135_{x}"],globals()[f"alfacum_135_{x}"],globals()[f"dh_dt_reaction135_
            {x}"],globals()[f"DOC_dalpha_max_135_{x}"],norm_dalfa_135,time_135=data(namessamples[x])
197 
198 
199 size=round(len(alfa_135_0)*0.99)
200 #now get the average
201 mean_alfa = np.mean((alfa_135_0[0:size],alfa_135_1[0:size],alfa_135_2[0:size],alfa_135_3[0:size]),
        axis=0)
202 std_alfa_135=np.std((alfa_135_0[0:size],alfa_135_1[0:size],alfa_135_2[0:size],alfa_135_3[0:size]),
        axis=0)
203 alfa_135=mean_alfa
204 
205 mean_dh = np.mean((dalfa_dt_135_0[0:size],dalfa_dt_135_1[0:size],dalfa_dt_135_2[0:size],
        dalfa_dt_135_3[0:size]), axis=0)
206 std_dh_135=np.std((dalfa_dt_135_0[0:size],dalfa_dt_135_1[0:size],dalfa_dt_135_2[0:size],
        dalfa_dt_135_3[0:size]), axis=0)
207 dalfa_dt_135=mean_dh
```

```
208
209 mean_Htot=np.mean((H_total_135_0,H_total_135_1,H_total_135_2,H_total_135_3), axis=0)
210 std_Htot=np.std((H_total_135_0,H_total_135_1,H_total_135_2,H_total_135_3), axis=0)
211 H_total_135=mean_Htot
212
213 mean_max_alfa=np.mean((max_alfa_135_0,max_alfa_135_1,max_alfa_135_2,max_alfa_135_3), axis=0)
214 std_max_alfa_135=np.std((max_alfa_135_0,max_alfa_135_1,max_alfa_135_2,max_alfa_135_3), axis=0)
215 print(mean_max_alfa,std_max_alfa_135)
216 max_alfa_135=mean_max_alfa
217
218 mean_alfacum_135=np.mean((alfacum_135_0[0:size],alfacum_135_1[0:size],alfacum_135_2[0:size],
        alfacum_135_3[0:size]), axis=0)
219 std_max_alfa=np.std((alfacum_135_0[0:size],alfacum_135_1[0:size],alfacum_135_2[0:size],
        alfacum_135_3[0:size]), axis=0)
220 alfacum_135=mean_alfacum_135
221
222 mean_dh_dt_reaction135=np.mean((dh_dt_reaction135_0[0:size],dh_dt_reaction135_1[0:size],
        dh_dt_reaction135_2[0:size],dh_dt_reaction135_3[0:size]), axis=0)
223 std_max_alfa=np.std((dh_dt_reaction135_0[0:size],dh_dt_reaction135_1[0:size],dh_dt_reaction135_2[0:
        size],dh_dt_reaction135_3[0:size]), axis=0)
224 dh_dt_reaction135=mean_dh_dt_reaction135
225
226 mean_DOC_dalpha_max_135=np.mean((DOC_dalpha_max_135_0,DOC_dalpha_max_135_1,DOC_dalpha_max_135_2,
        DOC_dalpha_max_135_3), axis=0)
227 std_max_alfa=np.std((DOC_dalpha_max_135_0,DOC_dalpha_max_135_1,DOC_dalpha_max_135_2,
        DOC_dalpha_max_135_3), axis=0)
228 DOC_dalpha_max_135=mean_DOC_dalpha_max_135
229
230
231 time_135=time_135[0:size]
232
233
234
235
236
237 """
238 ### method 1, graphical
239
240
241 #first getting the factors n and k1, via formula 7
242 ############## iteration 1
243
244 bottom=500
245 top=bottom+100
246
247 K1_135=dalfa_dt_135[0]
248 y=ln(dalfa_dt_135)
249 x=ln(np.zeros(len(alfa_135))+1-alfa_135)
250
251
252 plot5=plt.figure(5)
253 plt.plot(x,y  )
254
255 plt.title('Tc=135, iteration 1 parameter n',fontsize=18)
256 plt.xlabel('ln(1-\u03B1)',fontsize=18)
257 plt.ylabel('ln((d\u03B1/dt)',fontsize=18)
258 coef = np.polyfit(x[bottom:top],y[bottom:top],1)
259 poly1d_fn = np.poly1d(coef)
260
261 plt.plot( x, poly1d_fn(x), '--k')
262 plt.show()
263
264 print(coef)
265
266 n_135_1=coef[0]
267 print('n',n_135_1)
268
269
270 ####################################now we are going to get the factors k2 using formula 8
271 bottom=20
272 top=bottom+10
```

```
y=ln(  (dalfa_dt_135/  ( 1-alfa_135) ** n_135_1)   - K1_135  )
x= ln(alfa_135)


coef = np.polyfit(x[bottom:top],y[bottom:top],1)
poly1d_fn = np.poly1d(coef)
plot6=plt.figure(6)
plt.title('Tc=135, iteration 1 parameter m',fontsize=18)
plt.ylabel('ln(((d\u03B1/dt)/(1-\u03B1)^n)-k1)',fontsize=18)
plt.xlabel('ln(\u03B1)',fontsize=18)
plt.plot(x,y)
plt.plot( x, poly1d_fn(x), '--k')
plt.show()

m_135_1=coef[0]
K2_135_1=np.exp(coef[1])

print('m_1',m_135_1)
#################################################################now the iteration part with equation 9
########### iteration 2
bottom=600
top=bottom+10
y=ln (dalfa_dt_135) - ln ( K2_135_1 * (alfa_135 ** m_135_1) + K1_135)
x=ln(np.zeros(len(alfa_135))+1-alfa_135)

coef = np.polyfit(x[bottom:top],y[bottom:top],1)
n_135_2=coef[0]
poly1d_fn = np.poly1d(coef)


print('n_2',n_135_2)

#################################################################
bottom=20
top=bottom+10
y=ln(  (dalfa_dt_135/  ( 1-alfa_135) ** n_135_2)   - K1_135  )
x= ln(alfa_135)

coef = np.polyfit(x[bottom:top],y[bottom:top],1)
poly1d_fn = np.poly1d(coef)


m_135_2=coef[0]
K2_135=np.exp(coef[1])

print('m_2',m_135_2)
#####################################################################
######## iteration 3
bottom=600
top=bottom+10
y=ln (dalfa_dt_135) - ln ( K2_135 * (alfa_135 ** m_135_2) + K1_135)
x=ln(np.zeros(len(alfa_135))+1-alfa_135)

coef = np.polyfit(x[bottom:top],y[bottom:top],1)
n_135_3=coef[0]
poly1d_fn = np.poly1d(coef)
plot7=plt.figure(7)
plt.plot(x,y)
plt.title('Tc=135, iteration 3 parameter n',fontsize=18)
plt.xlabel('ln(1-\u03B1)',fontsize=18)
plt.ylabel('ln((d\u03B1/dt)/(k1+k2*\u03B1^m)',fontsize=18)
plt.plot( x, poly1d_fn(x), '--k')
plt.show()


print('n_3',n_135_3)

#################################################################
bottom=20
top=bottom+10
y=ln(  (dalfa_dt_135/  ( 1-alfa_135) ** n_135_3)   - K1_135  )
```

```
x= ln(alfa_135)


coef = np.polyfit(x[bottom:top],y[bottom:top],1)
poly1d_fn = np.poly1d(coef)
plot8=plt.figure(8)
plt.title('Tc=135 , iteration 3 parameter m',fontsize=18)
plt.ylabel('ln(((d\u03B1/dt)/(1-\u03B1)^n)-k1)',fontsize=18)
plt.xlabel('ln(\u03B1)',fontsize=18)
plt.plot(x,y)
plt.plot( x, poly1d_fn(x), '--k')
plt.show()

m_135_3=coef[0]
K2_135=np.exp(coef[1])

print('m_3',m_135_3)




x=[1,2,3]

y_n=[n_135_1,n_135_2,n_135_3]
y_end_n=[n_135_3,n_135_3,n_135_3]
convergence_n=round((n_135_3-n_135_2)/n_135_2*100,3)

y_m=[m_135_1,m_135_2,m_135_3]
y_end_m=[m_135_3,m_135_3,m_135_3]
convergence_m=round((m_135_3-m_135_2)/m_135_2*100,3)



plot20=plt.figure(20)
labels=['Iteration 1', 'Iteration 2', 'Iteration 3']
plt.xticks(x, labels,fontsize='16')
plt.plot(x,y_n,'o',label='Parameter n, convergence within '+str(convergence_n)+'% ')

plt.fill_between(x,y_end_n,y_end_n-0.01*n_135_3,alpha=0.5, edgecolor='#C6E2FF', facecolor='#C6E2FF
    ',label='Convergence <1 %')
plt.fill_between(x,y_end_n,y_end_n+0.01*n_135_3,alpha=0.5, edgecolor='#C6E2FF', facecolor='#C6E2FF
    ')
plt.title('Iterations parameters n, Tc=135',fontsize=16)
plt.ylabel('Value of parameters n',fontsize=16)
plt.legend(loc=4, prop={'size': 14})
plt.show()


plot21=plt.figure(21)
labels=['Iteration 1', 'Iteration 2', 'Iteration 3']
plt.xticks(x, labels,fontsize='16')
plt.plot(x,y_m,'go',label='Parameter m, convergence within '+str(convergence_m)+'% ')

plt.fill_between(x,y_end_m,y_end_m-0.01*m_135_3,alpha=0.5, edgecolor='#98FB98', facecolor='#98FB98
    ',label='Convergence <1 %')
plt.fill_between(x,y_end_m,y_end_m+0.01*m_135_3,alpha=0.5, edgecolor='#98FB98', facecolor='#98FB98
    ')
plt.title('Iterations parameters m, Tc=135',fontsize='16')
plt.ylabel('Value of parameters m',fontsize='16')
plt.legend(loc=4, prop={'size': 14})
plt.show()


#answers of method 1 are being used
n_135=n_135_3
m_135=m_135_3


"""

```

```
411
412
413
414 """
415 # method 2
416 from numpy import sin
417 from numpy import sqrt
418 from numpy import arange
419 from pandas import read_csv
420 from scipy.optimize import curve_fit
421 from matplotlib import pyplot
422
423 # define the true objective function
424 def objective(x, K1,K2,n,m):
425
426         return  ( K1 +K2 * x **m ) * (max(x)*1.01-x)**n
427
428 # load the dataset
429
430 # choose the input and output variables
431 plot8=plt.figure(8)
432 x, y = alfa_135,dalfa_dt_135
433 # curve fit
434 popt,pcov = curve_fit(objective, x, y,method='lm')
435 # summarize the parameter values
436 K1,K2,n,m = popt
437 print(popt)
438 # plot input vs output
439
440 # define a sequence of inputs between the smallest and largest known inputs
441 x_line_plot = arange(min(x), max(x), 0.01)
442 # calculate the output for the range
443 y_line_plot = objective(x_line_plot,  K1,K2,n,m)
444 # create a line plot for the mapping function
445 plt.title('Curve fit Kamal model, isothermal curing temperature = 135 C')
446 plt.xlabel('Degree of cure,\u03B1 ')
447 plt.ylabel('Rate of cure,d\u03B1/dt ')
448
449
450 plt.plot(x,y,label='Experimental data',color='black' )
451 plt.plot(x_line_plot, y_line_plot, '--', color='red',label='Curve fit Kamal model')
452 plt.legend()
453 plt.show()
454
455 #answers of method 2 are being used
456 K1_135=K1
457 K2_135=K2
458 n_135=n
459 m_135=m
460 standarddev_135=np.sqrt(np.diag(pcov))
461 #"""
462
463
464
465
466 #"""
467 ### method 3, graphical  but with dots
468 #now we need equal data points to do the least square fit so with every degree of cure
469
470 index_135=[]
471 #G_105_equal=[]
472 #alfa_105_equal=[]
473 punt=0.01
474 for i in range(len(alfa_135)):
475    if alfa_135[i] >punt:
476         index_135.append(i)
477         punt=punt+0.01
478         #G_105_equal.append(G_105[i])
479         #alfa_105_equal.append(alfa_big[0][i])
480
481 K1_135=dalfa_dt_135[0]
```

```
482
483
484 #name parametrs to use for this optimization
485 alfa_135_use=alfa_135[index_135]
486 dalfa_dt_135_use=dalfa_dt_135[index_135]
487
488 #first getting the factors n and k1, via formula 7
489 ############## iteration 1
490 K1_135=dalfa_dt_135[0]
491
492
493 bottom=70
494 top=bottom+20
495
496
497 y=ln(dalfa_dt_135_use)
498 x=ln(np.zeros(len(alfa_135_use))+max(alfa_135_use)-alfa_135_use)
499
500
501 plot5=plt.figure(5)
502 plt.plot(x,y ,'o' )
503
504 plt.title('Tc=135$^oC$, iteration 1 parameter n',fontsize=18)
505 plt.xlabel('ln($\u03B1_{max}$-\u03B1)',fontsize=18)
506 plt.ylabel('ln((d\u03B1/dt)',fontsize=18)
507
508 a=(y[bottom]-y[top])/(x[bottom]-x[top])
509 b=y[bottom]-a*x[bottom]
510 #plt.plot(x[bottom],y[bottom],'ro')
511 #plt.plot(x[top],y[top],'bo')
512 plt.plot(x,a*x+b,'--r')
513 plt.show()
514
515
516 n_135_1=a
517 print('n',n_135_1)
518
519
520 ####################################now we are going to get the factors k2 using formula 8
521 bottom=2
522 top=bottom+5
523 y=ln(  (dalfa_dt_135_use/  ( max(alfa_135_use)-alfa_135_use) ** n_135_1)   - K1_135  )
524 x= ln(alfa_135_use)
525
526
527 a=(y[bottom]-y[top])/(x[bottom]-x[top])
528 b=y[bottom]-a*x[bottom]
529 plot6=plt.figure(6)
530 plt.title('Tc=135$^oC$, iteration 1 parameter m',fontsize=18)
531 plt.ylabel('ln(((d\u03B1/dt)/($\u03B1_{max}$-\u03B1)^n)-k1)',fontsize=18)
532 plt.xlabel('ln(\u03B1)',fontsize=18)
533 plt.plot(x,y ,'o' )
534 #plt.plot(x[bottom],y[bottom],'ro')
535 #plt.plot(x[top],y[top],'bo')
536 plt.plot(x,a*x+b,'--r')
537 plt.show()
538
539 m_135_1=a
540 K2_135=np.exp(b)
541
542 print('m_1',m_135_1)
543 ##################################################################now the iteration part with equation 9
544 ############ iteration 2
545 bottom=70
546 top=bottom+20
547 y=ln(dalfa_dt_135_use) - ln( K2_135 * (alfa_135_use ** m_135_1) + K1_135)
548 x=ln(np.zeros(len(alfa_135_use))+max(alfa_135_use)-alfa_135_use)
549
550 a=(y[bottom]-y[top])/(x[bottom]-x[top])
551 b=y[bottom]-a*x[bottom]
552
```

```
n_135_2=a



print('n_2',n_135_2)

#################################################################
bottom=2
top=bottom+5
y=ln(  (dalfa_dt_135_use/  ( max(alfa_135_use)-alfa_135_use) ** n_135_2)   - K1_135  )
x= ln(alfa_135_use)

a=(y[bottom]-y[top])/(x[bottom]-x[top])
b=y[bottom]-a*x[bottom]


m_135_2=a
K2_135=np.exp(b)

print('m_2',m_135_2)
#########################################################################
######## iteration 3
bottom=70
top=bottom+20
y=ln (dalfa_dt_135_use) - ln ( K2_135 * (alfa_135_use ** m_135_2) + K1_135)
x=ln(np.zeros(len(alfa_135_use))+max(alfa_135_use)-alfa_135_use)

a=(y[bottom]-y[top])/(x[bottom]-x[top])
b=y[bottom]-a*x[bottom]

plot7=plt.figure(7)
plt.plot(x,y, 'o ')
plt.title('Tc=135$^oC$, iteration 3 parameter n',fontsize=18)
plt.xlabel('ln($\u03B1_{max}$-\u03B1)',fontsize=18)
plt.ylabel('ln((d\u03B1/dt)-(k1+k2*\u03B1^m)',fontsize=18)
#plt.plot(x[bottom],y[bottom],'ro')
#plt.plot(x[top],y[top],'bo')
plt.plot(x,a*x+b,'--r')
plt.show()

n_135_3=a
print('n_3',n_135_3)

#################################################################
bottom=2
top=bottom+5
y=ln(  (dalfa_dt_135_use/  ( max(alfa_135_use)-alfa_135_use) ** n_135_3)   - K1_135  )
x= ln(alfa_135_use)

a=(y[bottom]-y[top])/(x[bottom]-x[top])
b=y[bottom]-a*x[bottom]

plot8=plt.figure(8)
plt.title('Tc=135$^oC$ , iteration 3 parameter m',fontsize=18)
plt.ylabel('ln(((d\u03B1/dt)/($\u03B1_{max}$-\u03B1)^n)-k1)',fontsize=18)
plt.xlabel('ln(\u03B1)',fontsize=18)
plt.plot(x,y,'o')
#plt.plot(x[bottom],y[bottom],'ro')
#plt.plot(x[top],y[top],'bo')
plt.plot(x,a*x+b,'--r')
plt.show()

m_135_3=a
K2_135=np.exp(b)

print('m_3',m_135_3)



x=[1,2,3]
```

```

y_n=[n_135_1,n_135_2,n_135_3]
y_end_n=[n_135_3,n_135_3,n_135_3]
convergence_n=round((n_135_3-n_135_2)/n_135_2*100,3)

y_m=[m_135_1,m_135_2,m_135_3]
y_end_m=[m_135_3,m_135_3,m_135_3]
convergence_m=round((m_135_3-m_135_2)/m_135_2*100,3)



plot20=plt.figure(20)
labels=['Iteration 1', 'Iteration 2', 'Iteration 3']
plt.xticks(x, labels,fontsize='16')
plt.plot(x,y_n,'o',label='Parameter n, convergence within '+str(convergence_n)+'% ')

plt.fill_between(x,y_end_n,y_end_n-0.01*n_135_3,alpha=0.5, edgecolor='#C6E2FF', facecolor='#C6E2FF'
    ,label='Convergence <1 %')
plt.fill_between(x,y_end_n,y_end_n+0.01*n_135_3,alpha=0.5, edgecolor='#C6E2FF', facecolor='#C6E2FF'
    )
plt.title('Iterations parameters n, Tc=135  $^oC$',fontsize=16)
plt.ylabel('Value of parameters n',fontsize=16)
plt.legend(loc=4, prop={'size': 14})
plt.show()


plot21=plt.figure(21)
labels=['Iteration 1', 'Iteration 2', 'Iteration 3']
plt.xticks(x, labels,fontsize='16')
plt.plot(x,y_m,'go',label='Parameter m, convergence within '+str(convergence_m)+'% ')

plt.fill_between(x,y_end_m,y_end_m-0.01*m_135_3,alpha=0.5, edgecolor='#98FB98', facecolor='#98FB98'
    ,label='Convergence <1 %')
plt.fill_between(x,y_end_m,y_end_m+0.01*m_135_3,alpha=0.5, edgecolor='#98FB98', facecolor='#98FB98'
    )
plt.title('Iterations parameters m, Tc=135  $^oC$',fontsize='16')
plt.ylabel('Value of parameters m',fontsize='16')
plt.legend(loc=4, prop={'size': 14})
plt.show()


#answers of method 1 are being used
n_135=n_135_3
m_135=m_135_3
```

G.3. DiBenedetto python code

G.4. Second DSC measurement, dynamic

```
# -*- coding: utf-8 -*-
"""
Created on Wed Oct  5 16:40:26 2022

@author: thomv
"""



#import packages here
import numpy as np
from matplotlib import pyplot as plt
import pandas as pd
import matplotlib

from IPython import get_ipython
get_ipython().magic('reset -sf')
plt.close('all')



#definitions
```

```
23 def onsetindex_temp(x,onsettable,temp):
24     #get data table
25     lower=onsettable[x][3]
26     upper=onsettable[x][4]
27     index_lower = next(x for x, val in enumerate(temp)    # get the index of the first value which
           is bigger than lower limit temp
28                                       if val > lower)
29     index_upper = next(x for x, val in enumerate(temp)     # get the index of the first value which
            is bigger than upper limit temp
30                                       if val > upper)
31
32     return index_lower,index_upper
33
34 #linking the onset time  matchin index
35 def onsetindex_time(x,onsettable,time):
36     #get data table
37     lower=onsettable[x][3]
38     upper=onsettable[x][4]
39     index_lower = next(x for x, val in enumerate(time)    # get the index of the first value which
           is bigger than lower limit temp
40                                       if val > lower)
41     index_upper = next(x for x, val in enumerate(time)     # get the index of the first value which
            is bigger than upper limit temp
42                                       if val > upper)
43
44     return index_lower,index_upper
45
46 def linear(dH_t,time,index_lower,index_upper):#making linear line
47     a=(dH_t[index_upper]-dH_t[index_lower])/(time[index_upper]-time[index_lower])
48     b=dH_t[index_lower]-(a*time[index_lower])
49     return a,b
50
51 def enthalpy(dH_t,time,index_lower,index_upper):
52     time=time*60   # from seconds to minutes
53     integral_value = 0
54     a,b=linear(dH_t,time,index_lower,index_upper) # get linear line
55     for i in range(index_lower,index_upper):
56         width = time[i + 1] - time[i]
57         height = dH_t[i]- ( a * time[i] + b )
58         integral_value += width * height
59
60     return integral_value
61
62 def filterdata(namessamples)  :
63     iso_or_dyn=[]
64     samplenumbers=[]
65     temp_rate=[]
66     date=[]
67
68     for x in range(len(namessamples)):
69         i=namessamples[x]
70         j=i[0]
71         samplenumbers.append(i[2]+i[3])
72         temp_rate.append(i[5]+i[6]+i[7])
73         date.append(i[9]+i[10]+i[11]+i[12]+i[13]+i[14])
74
75         if j == "d":
76             iso_or_dyn.append( "dynamic")
77         elif j =="i":
78             second=i[16]
79             if second == "i":
80                     iso_or_dyn.append( "isothermic first run")
81             elif second == "d":
82                     iso_or_dyn.append( "isothermic second dynamic run")
83
84
85     return iso_or_dyn, samplenumbers, temp_rate, date
86 #settings plot
87 plot_time_or_temp='time'                #time or temp
88 show='105'                              #options: dynamic speed/ temp
89
```

```
#input
H_ult=426      #j/g



#input data
namessamples=['i_39_135_200922_dyn.txt', 'i_40_125_200922_dyn.txt','i_41_135_220922_dyn.txt','i_42_115_220922_dyn.txt ',
              'i_43_115_220922_dyn.txt','i_44_105_230922_dyn.txt','i_45_135_031022_dyn.txt','i_46_125_031022_dyn.txt' ,
              'i_48_135_061022_dyn.txt','i_50_125_101022_dyn.txt','i_51_115_101022_dyn.txt','i_53_115_111022_dyn.txt']

iso_or_dyn, samplenumbers, temp_rate, date=filterdata(namessamples)


#set which values to plot
listshow=[]
if show!='all':
    namessamples=namessamples
    for x in range(len(namessamples)):
        if temp_rate[x]==show:
            listshow.append(x)


#forming list with all the onset temperatures
# sample number, type of test (0=iso, 1=dyn), typ eof data, 0 = temperature, 1= time, then upper and lower value
sampleslimit,typetest,typedata,lowerr,upperr=np.loadtxt("limits_dyn_tweederun.txt",skiprows=1, unpack=True)
onsettable=[]
for x in range(len(namessamples)):
    row=[[sampleslimit[x]],[typetest[x]],[typedata[x]],[lowerr[x]],[upperr[x]]]
    onsettable.append(row)



markerslist=[]   # for the onset and ofset poitns
#importing the data
for x in range(len(namessamples)):
    name=namessamples[x]
    time, temp,dH_t = np.loadtxt(name, skiprows = 3 ,unpack=True)
    #set the lists to the variables
    sample=sampleslimit[x]
    testtype=typetest[x]
    globals()[f"time_{sample}_{testtype}"] = time
    globals()[f"temp_{sample}_{testtype}"] = temp
    globals()[f"dH/dt_{sample}_{testtype}"] = dH_t    #W/g

    # run definitions to get onset and offset points # this looks to the type of input, either temperature or time is marked as ofset
    if typedata[x]==0:
        index_lower,index_upper= onsetindex_temp(x,onsettable,temp)    # time in minutes
    elif typedata[x]==1:
        index_lower,index_upper= onsetindex_time(x,onsettable,time)    # time in minutes

    #print( time_lower,time_upper,index_lower,index_upper)
    markers=[index_lower,index_upper]      # index for markers
    #set the lists to the variables
    globals()[f"index_lower_{sample}_{testtype}"] = index_lower
    globals()[f"index_upper_{sample}_{testtype}"] = index_upper

    markerslist.append(markers)


# dynamic plots
plot1 = plt.figure(1)
for x in range(len(namessamples)):
    sample=sampleslimit[x]
    testtype=typetest[x]
```

```
    if iso_or_dyn[x] == 'isothermic second dynamic run':
            plt.plot( globals()[f"time_{sample}_{testtype}"], globals()[f"dH/dt_{sample}_{testtype}
                "],label='Sample code'+ namessamples[x])

plt.xlabel('Time (minutes)',fontsize='18')
plt.ylabel('Heat flow (W/g)',fontsize='18')
plt.title('Normalized residual heat of samples dynamically cured from 0 to 300 degrees Celcius.',
    fontsize='18')
plt.legend(bbox_to_anchor=(1.05, 1.0), loc='upper left',fontsize='12')
plt.tight_layout()
plt.show()




plot2 = plt.figure(2)
for x in listshow:
    sample=sampleslimit[x]
    testtype=typetest[x]

            #plt.plot( globals()[f"{plot_time_or_temp}_{x+1}"], globals()[f"dH_t_{x+1}"], '-D',
                markevery=globals()[f"markers_{x+1}"],label=namessamples[x])
    plt.plot( globals()[f"{plot_time_or_temp}_{sample}_{testtype}"], globals()[f"dH/dt_{sample}_{
        testtype}"],marker='o', markevery=markerslist[x],label='Sample code'+namessamples[x])

    a,b=linear(globals()[f"dH/dt_{sample}_{testtype}"],globals()[f"{plot_time_or_temp}_{sample}_{
        testtype}"],globals()[f"index_lower_{sample}_{testtype}"], globals()[f"index_upper_{sample}
        _{testtype}"])
    low=onsettable[x][3]
    up=onsettable[x][4]
    distance=abs(low[0]-up[0])   # to get a margin for the y=ax+b

    xaxis=np.linspace(onsettable[x][3]-0.4*distance,onsettable[x][4]+0.4*distance,100)
    y=a*xaxis+b
    plt.plot(xaxis, y,'r--',label='Baseline')


plt.xlabel('Time (minutes)',fontsize='18')
plt.ylabel('Heat flow (W/g)',fontsize='18')
plt.title('Dynamic heat flow to measure residual heat 135 Degree samples',fontsize='18')
plt.legend(bbox_to_anchor=(1.05, 1.0), loc='upper left',fontsize='12')
plt.tight_layout()
plt.show()
#at this point all plots are made, now the next step is to calculate the enthalpy
#this is calculated within the boudnaries of the limits
reaction_enthalpy=[]
for x in range(len(namessamples)):
    sample=sampleslimit[x]
    testtype=typetest[x]
    reaction_enthalpy.append(enthalpy(globals()[f"dH/dt_{sample}_{testtype}"], globals()[f"time_{
        sample}_{testtype}"],globals()[f"index_lower_{sample}_{testtype}"], globals()[f"
        index_upper_{sample}_{testtype}"]))
# save enthalpy between the boundaries. this is in J/g
savedata=[]
for x in range(len(namessamples)):
    savedata.append([[iso_or_dyn[x]], [samplenumbers[x]], [temp_rate[x]], [reaction_enthalpy[x]]])

df = pd.DataFrame(savedata)
# saving the dataframe
df.to_csv('enthalpy_dynamisch_tweederun.csv')
```

G.5. Bailleul model

```
# -*- coding: utf-8 -*-
"""
Created on Mon Sep 19 14:18:39 2022

@author: thomv
"""

```

```
import numpy as np
from scipy.optimize import least_squares
from definitions import *
from matplotlib import pyplot as plt
import matplotlib
from numpy import log as ln
from scipy.integrate import odeint
from runfile import T_ref,T_big,names ,max_alfa_big,alfa_big,dalfa_dt_big,time_big,K1_all,K2_all,
    n_all,m_all,H_ult
from alpha_max import calc_DOC_max,mu,Tg_0,Tg_inf
from scipy.integrate import odeint
from sklearn.metrics import r2_score
import math

# make sure the reference temperature is within the range of the used curing temperatures
T_ref=400

number_poly=4

#make option for colour
colour=[]
for name, hex in matplotlib.colors.cnames.items():
    colour.append(name)


#use this when want to remove items to determine the numbers. Use this for testing, always at 0 for
     final answer
numberskip=0
T_big_use=T_big[numberskip:]

# we are trying to get the function of K, herefore we pick the maximum of the transformation ratio
    to make G=1
x_list=np.zeros(len(T_big_use))
y_list=np.zeros(len(T_big_use))
### now on to the factor k1 an E1
#first making the x and y list for the variables k1 and



#making the lists for the parameters k1 and e1, according to bailleiru
for i in range(len(T_big_use)):
    i=int(i)
    T=T_big
    x_list[i] = (T_ref/T_big_use[i]-1)
    y_list[i]= ln(max(dalfa_dt_big[i+numberskip]))




#getting the paramters by a fit
plot9=plt.figure(9)
coef = np.polyfit(x_list,y_list,1)
poly1d_fn = np.poly1d(coef)
# poly1d_fn is now a function which takes in x and returns an estimate for y
plt.plot(x_list,y_list, 'yo',label='Measurement point')
plt.plot(x_list, poly1d_fn(x_list), '--k',label='Fitted linear function') #'--k'=black dashed line,
     'yo' = yellow circle marker
plt.xlabel('T_ref/T-1', fontsize=18)
plt.ylabel('Ln(K(T))',fontsize=18)
plt.title('Straight line characterizing K(T)',fontsize=18)
plt.legend(loc=3, prop={'size': 14},fontsize=12)
plt.show()

k_1=np.exp(coef[1]) #frequency factor
print('k_1',k_1)
E_1=-coef[0]  #activation energy no unit
print('E_1', E_1)


#can use both in this istuation, both are being found in literature
#"""
```

```
K_105=k_1*np.exp( - E_1 * (T_ref/T_big[0]-1))
K_115=k_1*np.exp( - E_1 * (T_ref/T_big[1]-1))
K_125=k_1*np.exp( - E_1 * (T_ref/T_big[2]-1))
K_135=k_1*np.exp( - E_1 * (T_ref/T_big[3]-1))
"""
K_105=max(dalfa_dt_big[0])
K_115=max(dalfa_dt_big[1])
K_125=max(dalfa_dt_big[2])
K_135=max(dalfa_dt_big[3])

"""
######################### dont use this
index_nummer_105 = next(x for x, val in enumerate(alfa_big[0])    # get the index of the first value which is bigger than lower limit temp
                                    if val > 0.3)
index_nummer_115 = next(x for x, val in enumerate(alfa_big[1])    # get the index of the first value which is bigger than lower limit temp
                                    if val > 0.3)
index_nummer_125 = next(x for x, val in enumerate(alfa_big[2])    # get the index of the first value which is bigger than lower limit temp
                                    if val > 0.3)
index_nummer_135 = next(x for x, val in enumerate(alfa_big[3])    # get the index of the first value which is bigger than lower limit temp
                                    if val > 0.3)

# here you can either use the max, or the formula K. To minimize error i use the max


G_105=dalfa_dt_big[0]/max(dalfa_dt_big[0]) #     #dalfa_dt_big[0][index_nummer_105]  #
G_115=dalfa_dt_big[1]/  max(dalfa_dt_big[1])  #dalfa_dt_big[1][index_nummer_115]  #
G_125=dalfa_dt_big[2]/ max(dalfa_dt_big[2])  # dalfa_dt_big[2][index_nummer_125]   #
G_135=dalfa_dt_big[3]/     max(dalfa_dt_big[3]) #     dalfa_dt_big[3][index_nummer_135]    #



#now we need equal data points to do the least square fit so with every degree of cure

index_105=[]
G_105_equal=[]
alfa_105_equal=[]
punt=0.01
for i in range(len(alfa_big[0])):
   if alfa_big[0][i] >punt:
        index_105.append(i)
        punt=punt+0.01
        G_105_equal.append(G_105[i])
        alfa_105_equal.append(alfa_big[0][i])

index_115=[]
G_115_equal=[]
alfa_115_equal=[]
punt=0.01
for i in range(len(alfa_big[1])):
   if alfa_big[1][i] >punt:
        index_115.append(i)
        punt=punt+0.01
        G_115_equal.append(G_115[i])
        alfa_115_equal.append(alfa_big[1][i])

index_125=[]
G_125_equal=[]
alfa_125_equal=[]
punt=0.01
for i in range(len(alfa_big[2])):
   if alfa_big[2][i] >punt:
        index_125.append(i)
        punt=punt+0.01
        G_125_equal.append(G_125[i])
        alfa_125_equal.append(alfa_big[2][i])

index_135=[]
```

```
G_135_equal=[]
alfa_135_equal=[]
punt=0.01
for i in range(len(alfa_big[3])):
   if alfa_big[3][i] >punt:
        index_135.append(i)
        punt=punt+0.01
        G_135_equal.append(G_135[i])
        alfa_135_equal.append(alfa_big[3][i])


plot10=plt.figure(10)
plt.plot(alfa_105_equal,G_105_equal,label="Polynomial term G for 105$^oC$")
plt.plot(alfa_115_equal,G_115_equal,label="Polynomial term G for 115$^oC$")
plt.plot(alfa_125_equal,G_125_equal,label="Polynomial term G for 125$^oC$")
plt.plot(alfa_135_equal,G_135_equal,label="Polynomial term G for 135$^oC$")
plt.title('Polynomial term as function of the degree of cure \n for each isothermal curing temperature',fontsize=18)
plt.xlabel('Degree of cure',fontsize=18)
plt.ylabel('Polynomial term',fontsize=18)
plt.legend(bbox_to_anchor=(1.05, 1.0), loc='upper left',fontsize=12)
plt.tight_layout()
plt.show()



#make big lists to find the parameters for the polynomial
big_doc=[]
big_G=[]
big_dalpha=[]
big_K=[]
big_Tc=[]
big_alphamax=[]


#combine all list into bigger ones to get the data
big_doc=alfa_105_equal+alfa_115_equal+alfa_125_equal+alfa_135_equal
big_G=G_105_equal+G_115_equal+G_125_equal+G_135_equal

#big_doc=alfa_115_equal+alfa_125_equal+alfa_135_equal
#big_G=G_115_equal+G_125_equal+G_135_equal



# sort the lists
sorted_doc=sorted(big_doc)
sorted_G = [x for _,x in sorted(zip(big_doc,big_G))]

#poly fit to get the g1.....gn
plot11=plt.figure(11)
coef1 = np.polyfit(sorted_doc,sorted_G,number_poly)
poly1d_fn_g = np.poly1d(coef1)
# poly1d_fn is now a function which takes in x and returns an estimate for y
print("coef pol G", coef1)
print("poly",poly1d_fn_g)
plt.plot( sorted_doc, sorted_G, 'yo', label='Measured data points')
plt.plot(sorted_doc, poly1d_fn_g(sorted_doc), '--k',label='Polynomial function') #'--k'=black dashed line, 'yo' = yellow circle marker
plt.title('Polynominal function and the measured data points',fontsize=18)
plt.xlabel('Degree of cure',fontsize=18)
plt.ylabel('Value of G term for each degree of cure',fontsize=18)
plt.legend(bbox_to_anchor=(1.05, 1.0), loc='upper left',fontsize=12)
plt.show()



##########33
#alphamax formula

"""
inputTC=[105+273,115+273,125+273,135+273]
```

```
ab = np.polyfit(inputTC,[0.85,0.9,0.94,0.96],3)
lin = np.poly1d(ab)
"""



def lin(Tc):
    Tg_0=3.69   +273
    Tg_inf=273+138
    mu=0.5501

    DOC_max=(Tc-Tg_0) / ( (Tg_inf-Tg_0)*mu + (1-mu)*(Tc-Tg_0))


    if DOC_max > 1:
            DOC_max=1   # dit was eerst DOC_max[i], dus let erop als hier een error komt is het
                daardoor
    return DOC_max


# da_t= k_1*np.exp( - E_1 * (T_ref/T-1))  * poly1d_fn_g(alpha) *(alpha_max(T)-alpha)**n
# function that returns dy/dt
def model(y,t,T,k_1,E_1,T_ref,g,lin,n):
    T=T+273

    delta_alfa=(lin(T)-y)

    maxterm=(delta_alfa)**n


    if y > lin(T):
        maxterm=0.0000001
    dydt =  k_1*np.exp( - E_1 * (T_ref/T-1))  * g(y) *maxterm


    return dydt

# initial condition
y0 = 0
g=poly1d_fn_g

##############################3

n=np.linspace(0,0.5,100)
save=np.zeros(len(n))
T = 105
t1 = np.linspace(0,len(alfa_big[0]),len(alfa_big[0]))

# test

for i in range(len(n)):
    j=n[i]
    y1 = odeint(model,y0,t1,args=(T,k_1,E_1,T_ref,g,lin,j))
    save[i]=round(r2_score(alfa_big[0], y1),5)-1



minr2= max(save)
indexr2=np.argmax(save)
gebruikn105=n[indexr2]



print('print', minr2,indexr2,gebruikn105,save)


# actual run
n=-0.0164 *T + 2.163   # T in celcius

y1 = odeint(model,y0,t1,args=(T,k_1,E_1,T_ref,g,lin,n))
r2_BAIL_105=round(r2_score(alfa_big[0], y1),3)
```

```
281
282 ##########################
283 n=np.linspace(0,0.5,100)
284 save=np.zeros(len(n))
285
286 T=115
287 t2 = np.linspace(0,len(alfa_big[1]),len(alfa_big[1]))
288
289 for i in range(len(n)):
290     j=n[i]
291     y2 = odeint(model,y0,t2,args=(T,k_1,E_1,T_ref,g,lin,j))
292     save[i]=round(r2_score(alfa_big[1], y2),5)-1
293
294 minr2= max(save)
295 indexr2=np.argmax(save)
296 gebruikn115=n[indexr2]
297
298 print('print', minr2,indexr2,gebruikn115,save)
299
300 n=-0.0164 *T + 2.163   # T in celcius
301 y2 = odeint(model,y0,t2,args=(T,k_1,E_1,T_ref,g,lin,n))
302 r2_BAIL_115=round(r2_score(alfa_big[1], y2),3)
303
304
305 ############################################################
306 n=np.linspace(0,0.5,100)
307 save=np.zeros(len(n))
308
309 T = 125
310 t3 = np.linspace(0,len(alfa_big[2]),len(alfa_big[2]))
311
312 for i in range(len(n)):
313     j=n[i]
314     y3 = odeint(model,y0,t3,args=(T,k_1,E_1,T_ref,g,lin,j))
315     save[i]=round(r2_score(alfa_big[2], y3),5)-1
316
317 minr2= max(save)
318 indexr2=np.argmax(save)
319 gebruikn125=n[indexr2]
320
321 print('print', minr2,indexr2,gebruikn125,save)
322
323 n=-0.0164 *T + 2.163   # T in celcius
324 y3 = odeint(model,y0,t3,args=(T,k_1,E_1,T_ref,g,lin,n))
325 r2_BAIL_125=round(r2_score(alfa_big[2], y3),3)
326
327
328 ############################################################
329 n=np.linspace(0,0.5,100)
330 save=np.zeros(len(n))
331
332 T = 135
333 t4 = np.linspace(0,len(alfa_big[3]),len(alfa_big[3]))
334
335 for i in range(len(n)):
336     j=n[i]
337     y4 = odeint(model,y0,t4,args=(T,k_1,E_1,T_ref,g,lin,j))
338     save[i]=round(r2_score(alfa_big[3], y4),5)-1
339
340 minr2= max(save)
341 indexr2=np.argmax(save)
342 gebruikn135=n[indexr2]
343
344 print('print', minr2,indexr2,gebruikn135,save)
345
346
347 n=-0.0164 *T + 2.163   # T in celcius
348 y4 = odeint(model,y0,t4,args=(T,k_1,E_1,T_ref,g,lin,n))
349 r2_BAIL_135=round(r2_score(alfa_big[3], y4),3)
350
351   ############################################################
```

```
352
353 plot6 = plt.figure(6)
354 plt.plot(t1,y1,'r-.',linewidth=2,label='Bail model =105$^oC$, $R^2$:' +str(r2_BAIL_105))
355 plt.plot(t2,y2,'b-.',linewidth=2,label='Bail model =115$^oC$, $R^2$:' +str(r2_BAIL_115))
356 plt.plot(t3,y3,'g-.',linewidth=2,label='Bail model =125$^oC$, $R^2$:' +str(r2_BAIL_125))
357 plt.plot(t4,y4,'y-.',linewidth=2,label='Bail model =135$^oC$, $R^2$:' +str(r2_BAIL_135))
358 plt.title('Bailleul curing model versus experimental data, \u03B1 as function of time',fontsize='16
    ')
359 colours=['r','b','g','y']
360 #for x in range(4):
361 #    plt.plot(time_big[x], alfa_big[x], colours[x],label=names[x])
362
363 plt.xlabel('Time in seconds',fontsize=16)
364 plt.ylabel('y(t), Degree of cure \u03B1 ',fontsize=16)
365 plt.legend(loc=4, prop={'size': 14})
366 plt.show()
367
368
369 fig52=plt.figure(52)
370
371 plt.plot(np.linspace(0,1,100),g(np.linspace(0,1,100)))
372 plt.axvline(0.95, 0, 1, label='Assembly')
373 plt.show()
```

G.6. Kamal model graphical -analytical

G.7. Gel point

```
1  # -*- coding: utf-8 -*-
2  """
3  Created on Wed Oct 12 14:43:48 2022
4
5  @author: thomv
6  """
7  import numpy as np
8  from scipy import optimize
9  from matplotlib import pyplot as plt
10 from scipy.optimize import least_squares
11 from itertools import accumulate
12 from scipy.integrate import odeint
13 from IPython import get_ipython
14 import math
15 from numpy import log as ln
16 from sklearn.metrics import r2_score
17
18
19 get_ipython().magic('reset -sf')
20 plt.close('all')
21
22 H_ult=426
23
24
25
26 #final tool
27 # parameters KS
28
29 #"""
30 k1=767.1283
31 k2=0.49434
32 E1=5938
33 E2=1372
34 #"""
35
36
37 def m(x):
38     x=x+273
39     #return -0.02439 * x + 10.6
40     return -0.027 * x + 11.730
41
42 def n(x):
43     x=x+273
```

```
    #return -0.01894 *  x + 9.358
    return  -0.026 * x + 12.040




def alfamax(Tc):
    Tc=Tc+273
    Tg_0=3.69   +273
    Tg_inf=273+138
    mu=0.5501

    DOC_max=(Tc-Tg_0) / ( (Tg_inf-Tg_0)*mu + (1-mu)*(Tc-Tg_0))


    if DOC_max > 1:
            DOC_max=1


    return DOC_max



def T_g_dib(DOC):
    lam=0.59
    Tg_0=4.7+273
    Tg_inf=138+273
    T_g=Tg_0+ ( (Tg_inf-Tg_0)*DOC*lam ) / ( 1 - ( 1- lam) *DOC)
    return T_g

def model(y,t,T,k1,k2,E1,E2,n,m,alfamax):
    T=T+273

    K1 = k1*np.exp((-E1)/(T))
    K2 = k2*np.exp((-E2)/(T))
    da_t = ((K1 + K2*y**m)*((alfamax-y)**n))


    return da_t


def model_test(y,T,k1,k2,E1,E2,n,m,alfamax):
    T=T+273

    if alfamax >= 1:
        alfamax=1

    delta=alfamax-y




    if delta<0:
        delta=0



    K1 = k1*np.exp((-E1)/(T))
    K2 = k2*np.exp((-E2)/(T))


    da_t = ((K1 + K2*y**m)*((delta)**n))

    if y==1:
        da_t=0


    if   math.isinf(da_t):
        da_t=0
    return da_t
```

```
115
116
117
118
119 def timetocure(T_iso):
120     T_start=0
121     T_rampup=100           #rate           #temp in celcius
122     tijd_min=400    # in minuten
123     tijd_sec=tijd_min*60
124     T_rampdown=2000
125     T_end=5
126
127
128
129     lengte=(T_iso-T_start)/(T_rampup/60) +tijd_sec+ abs(T_iso-T_end)/(T_rampdown/60)
130
131     t2 = np.linspace(0,round(lengte),round(lengte))
132
133     T_test=np.zeros(len(t2))
134
135
136
137     test=np.zeros(len(t2))
138
139     count=0
140
141     T_test=np.zeros(len(t2))
142     for i in range(len(t2)):
143         if i == 0:
144             T_test[i]=T_start
145         if i>=1 and i<=(T_iso-T_start)/(T_rampup/60):
146             T_test[i]=T_start + T_rampup/60 * i
147         if i >= (T_iso-T_start)/(T_rampup/60) and i<= (T_iso-T_start)/(T_rampup/60) +tijd_sec:
148             T_test[i]= T_iso
149         if i >= (T_iso-T_start)/(T_rampup/60) +tijd_sec:
150             T_test[i]=T_iso -  (T_rampdown/60) * count
151             count=count+1
152
153
154
155     return(t2,T_test)
156
157
158 def findtime(t2,alfalim,temp):
159     DOC_test=np.zeros(len(t2))
160     dh_dt=np.zeros(len(t2))
161
162     for i in range(len(t2)):
163         T=T_test[i]
164         if i == 0 :
165             DOC_test[i]=0
166
167             dh_dt[i]=0
168         else :
169
170
171             DOC_test[i]=DOC_test[i-1]+   model_test(DOC_test[i-1],T,k1,k2,E1,E2,n(T), m(T),alfamax(
                    T))
172             dh_dt[i]= model_test(DOC_test[i-1],T,k1,k2,E1,E2,n(T), m(T),alfamax(T))    * H_ult
173
174
175
176
177
178         if DOC_test[i]>alfalim:
179             tijd=t2[i]
180             break
181         else:
182            tijd=0
183
184
```

```
185
186
187
188     return tijd,dh_dt
189
190 cures=np.linspace(0.2,0.4,6)
191 temp=[104,110,115,120,125,132,137]
192
193
194 x_save=np.zeros([len(temp),len(cures)])
195 y_save=np.zeros([len(temp),len(cures)])
196
197 #time_datasheet=[10,7.5,5,2.5]  # in minutes
198 #temperature_datasheet=[1/115,1/120,1/125,1/130]
199
200 time_datasheet=[ln(22),ln(14),ln(10),ln(7),ln(5),ln(3.5),ln(2.5)]
201 temperature_datasheet=[1/104,1/110,1/115,1/120,1/125,1/132,1/137]
202
203 #temperature_datasheet=[104,110,115,120,125,132,137]
204
205 for i in range(len(cures)):
206     for j in range(len(temp)):
207
208         t2,T_test=timetocure(temp[j])
209
210
211         tijd,dh_dt=findtime(t2,cures[i],temp[j])
212         y_save[j,i]=tijd/60      # in minutes
213         x_save[j,i]=1/temp[j]
214
215
216
217
218 for i in range(len(cures)):
219     store_y=[]
220     store_x=[]
221     for j in range(len(temp)):
222         if y_save[j,i] != 0:
223             store_y.append(ln(y_save[j,i]))
224             store_x.append(x_save[j,i])
225     globals()[f"save_y{i}"]=store_y
226     globals()[f"save_x{i}"]=store_x
227
228 figure1=plt.figure(1)
229 for i in range(len(cures)):
230
231     r2=round(r2_score(globals()[f"save_y{i}"], time_datasheet),5)
232     print(r2)
233     plt.plot(globals()[f"save_x{i}"],globals()[f"save_y{i}"], label='Degree of cure:'+str(  round(
        cures[i],2))+ 'R^2: '+str(r2) , linestyle='--' )
234
235
236 plt.xlabel('1/T, Temperature in Celcius',fontsize=18)
237 plt.ylabel('Time in minutes ',fontsize=18)
238
239
240
241
242 plt.plot(temperature_datasheet,time_datasheet, '-', color='red', label='DATASHEET')
243 plt.title('Geltime versus the inverse of the isothermal curing temperature',fontsize=18)
244
245 plt.legend()
246 plt.show()
```

```
1 # -*- coding: utf-8 -*-
2 """
3 Created on Thu Sep  8 12:45:59 2022
4
5 @author: thomv
6 """
7 import numpy as np
```

```
from scipy.optimize import least_squares
from definitions import *
from matplotlib import pyplot as plt
import matplotlib
from numpy import log as ln
from scipy.integrate import odeint
from runfile import T_ref,T_big,names ,max_alfa_big,alfa_big,dalfa_dt_big,time_big,K1_all,K2_all,
    n_all,m_all
from alpha_max import calc_DOC_max,mu,Tg_0,Tg_inf

from sklearn.metrics import r2_score



#make option for colour
colour=[]
for name, hex in matplotlib.colors.cnames.items():
    colour.append(name)


#create empty arrays for the temperatures
temperature_105=np.zeros(len(alfa_big[0]))
temperature_115=np.zeros(len(alfa_big[1]))
temperature_125=np.zeros(len(alfa_big[2]))
temperature_135=np.zeros(len(alfa_big[3]))


# fill the array with the temperatures
for i in range(len(alfa_big[0])):
    temperature_105[i]=105+273
for i in range(len(alfa_big[1])):
    temperature_115[i]=115+273
for i in range(len(alfa_big[2])):
    temperature_125[i]=125+273
for i in range(len(alfa_big[3])):
    temperature_135[i]=135+273



#Curve fitting for n and m
plot8=plt.figure(8)
coef_n=np.polyfit(T_big,n_all,1)
lijn_n=np.poly1d(coef_n)
plt.title('Temperature dependency n and m',fontsize='16')
plt.xlabel('Isothermal curing temperature [K]',fontsize='16')
plt.ylabel('Value n and m',fontsize='16')
plt.plot(T_big,n_all,'o',color='red',label='Measured data points')
plt.plot(T_big,lijn_n(T_big),'--', label='n',color='red')

coef_m=np.polyfit(T_big,m_all,1)
lijn_m=np.poly1d(coef_m)
plt.plot(T_big,m_all,'o', color='blue',label='Measured data points')
plt.plot(T_big,lijn_m(T_big),'--', label='m',color='blue')
plt.legend(loc=1, prop={'size': 10})
plt.show()

print('lijn_n:',lijn_n)
print('lijn_m:',lijn_m)
# combine the data into big arrays
T_combined=np.concatenate((temperature_105,temperature_115,temperature_125,temperature_135))
alfa_combined=np.concatenate((alfa_big[0],alfa_big[1],alfa_big[2],alfa_big[3]))
dalfa_dt_combined=np.concatenate((dalfa_dt_big[0],dalfa_dt_big[1],dalfa_dt_big[2],dalfa_dt_big[3]))


#use this when want to remove items to determine the numbers
T_big_use=T_big[:]
K1_all_use=K1_all[:]
K2_all_use=K2_all[:]



```

```
#make a lin fit
x_list=1/T_big_use
y_list=ln(K1_all_use)
coef = np.polyfit(x_list,y_list,1)
poly1d_fn = np.poly1d(coef)
# poly1d_fn is now a function which takes in x and returns an estimate for y
plot4=plt.figure(4)
plt.plot(x_list,y_list, 'yo', label='Fitted linear relationship ln(K1) with Tc')
plt.plot(x_list, poly1d_fn(x_list), '--y',label='K1 fit') #'--k'=black dashed line, 'yo' = yellow circle marker
plt.xlabel('1/T [1/K]',fontsize='16')
plt.ylabel('Ln(K)',fontsize='16')
plt.title('Fitted linear relationship ln(K) with Tc and experimental data',fontsize='16')
##plt.legend()
##plt.show()
print('coefk1',coef)
print('linek1',poly1d_fn)

k1=np.exp(coef[1]) #frequency factor
E1=-coef[0]  #activation energy no unit

print(k1,E1)



##############################################now k2
#make a lin fit
y_list=ln(K2_all_use)



##plot5=plt.figure(5)
coef = np.polyfit(x_list,y_list,1)
poly1d_fn = np.poly1d(coef)
# poly1d_fn is now a function which takes in x and returns an estimate for y
##plot5=plt.figure(5)
plt.plot(x_list,y_list, 'ro',label='ln(K2) measured')
plt.plot(x_list, poly1d_fn(x_list), '--r',label='Fitted linear relationship ln(K2) with Tc') #'--k'=black dashed line, 'yo' = yellow circle marker
##plt.xlabel('1/T')
##plt.ylabel('Ln(K2)')
#plt.title('Straight line characterizing K2(T)')

#plt.xlim([])
plt.ylim([-10,-2.5])
plt.legend( prop={'size': 12})
plt.show()

k2=np.exp(coef[1]) #frequency factor
E2=-coef[0]  #activation energy no unit



##########33
#alphamax formula
"""

inputTC=[105+273,115+273,125+273,135+273]
ab = np.polyfit(inputTC,[0.85,0.9,0.94,0.96],3)
lin = np.poly1d(ab)
"""



def lin(Tc):
    Tg_0=3.69   +273
    Tg_inf=273+138
    mu=0.5501

    DOC_max=(Tc-Tg_0) / ( (Tg_inf-Tg_0)*mu + (1-mu)*(Tc-Tg_0))

```

```
147
148     if DOC_max > 1:
149             DOC_max[i]=1
150     return DOC_max
151
152
153
154
155
156
157
158 # da_t= k_1*np.exp( - E_1 * (T_ref/T-1))  * poly1d_fn_g(alpha) *(alpha_max(T)-alpha)**n
159 # function that returns dy/dt
160 def model(y,t,T,k1,k2,E1,E2,n,m,lin):
161     T=T+273
162
163     K1 = k1*np.exp((-E1)/(T))
164     K2 = k2*np.exp((-E2)/(T))
165     da_t = ((K1 + K2*y**m)*((lin(T)-y)**n))
166
167
168     return da_t
169
170 # initial condition
171 y0 = 0
172
173
174
175
176 print("k1 all:",K1_all,", k2 all:",K2_all)
177 print("E1:",E1,",E2:",E2,",k1:",k1,",k2:",k2)
178
179 T = 105
180 t1 = np.linspace(0,len(alfa_big[0]),len(alfa_big[0]))
181 print(T,k1,k2,E1,E2,lijn_n(T_big[0]), lijn_m(T_big[0]),lin(T+273))
182 y1 = odeint(model,y0,t1,args=(T,k1,k2,E1,E2,lijn_n(T_big[0]), lijn_m(T_big[0]),lin))
183 r2_ks_105=round(r2_score(alfa_big[0], y1),3)
184
185 T=115
186 t2 = np.linspace(0,len(alfa_big[1]),len(alfa_big[1]))
187 y2 =  odeint(model,y0,t2,args=(T,k1,k2,E1,E2,lijn_n(T_big[1]), lijn_m(T_big[1]),lin))
188 r2_ks_115=round(r2_score(alfa_big[1], y2),3)
189
190 T = 125
191 t3 = np.linspace(0,len(alfa_big[2]),len(alfa_big[2]))
192 y3 =  odeint(model,y0,t3,args=(T,k1,k2,E1,E2,lijn_n(T_big[2]), lijn_m(T_big[2]),lin))
193 r2_ks_125=round(r2_score(alfa_big[2], y3),3)
194
195 T = 135
196 t4 = np.linspace(0,len(alfa_big[3]),len(alfa_big[3]))
197 y4 =  odeint(model,y0,t4,args=(T,k1,k2,E1,E2,lijn_n(T_big[3]), lijn_m(T_big[3]),lin))
198 r2_ks_135=round(r2_score(alfa_big[3], y4),3)
199
200
201
202
203 plot6 = plt.figure(6)
204 plt.plot(t1,y1,'r--',linewidth=2,label='Kamal model =105 $^oC$, R^2:' +str(r2_ks_105))
205 plt.plot(t2,y2,'b--',linewidth=2,label='Kamal model =115 $^oC$, R^2:' +str(r2_ks_115))
206 plt.plot(t3,y3,'g--',linewidth=2,label='Kamal model =125 $^oC$, R^2:' +str(r2_ks_125))
207 plt.plot(t4,y4,'y--',linewidth=2,label='Kamal model =135 $^oC$, R^2:' +str(r2_ks_135))
208
209 plt.title('Kamal curing model versus experimental data, \u03B1 as function of time. Graphical-
    analytical method',fontsize='16')
210
211 plt.xlabel('Time in seconds',fontsize=16)
212 plt.ylabel('y(t), Degree of cure \u03B1 ',fontsize=16)
213 plt.legend(loc=4, prop={'size': 14})
214 plt.show()
215
216
```

```
217
218
219 plot13=plt.figure(13)
220 plt.plot(time_big[0],dalfa_dt_big[0],color='r',label='Isothermal curing temperature = 105$^oC$')
221 plt.plot(time_big[0][0],dalfa_dt_big[0][0],"o",color='r',label='Initial reaction rate at = 105$^oC$
        ')
222 plt.plot(time_big[1],dalfa_dt_big[1],color='b',label='Isothermal curing temperature = 115$^oC$')
223 plt.plot(time_big[1][0],dalfa_dt_big[1][0],"o",color='b',label='Initial reaction rate at = 115$^oC$
        ')
224 plt.plot(time_big[2],dalfa_dt_big[2],color='g',label='Isothermal curing temperature = 125$^oC$')
225 plt.plot(time_big[2][0],dalfa_dt_big[2][0],"o",color='g',label='Initial reaction rate at = 125$^oC$
        ')
226 plt.plot(time_big[3],dalfa_dt_big[3],color='y',label='Isothermal curing temperature = 135$^oC$')
227 plt.plot(time_big[3][0],dalfa_dt_big[3][0],"o",color='y',label='Initial reaction rate at = 135$^oC$
        ')
228 plt.title('Isothermal DSC experiments at four different curing temperatures',fontsize=20)
229 plt.xlabel('Time [sec]',fontsize=20)
230 plt.ylabel('Reaction rate ',fontsize=20)
231 plt.legend(fontsize=14)
232 plt.show()
```